Uncertainty and Bias in Ground Motion Estimates from Ground Response Analyses

Jonathan P. Stewart

and

Mehmet B. Baturay

Department of Civil and Environmental Engineering
University of California, Los Angeles

A report on research sponsored by the Pacific Earthquake Engineering Research Center's Program of Applied Earthquake Engineering Research of Lifeline Systems.

PEER Report 2002/??
Pacific Earthquake Engineering Research Center
College of Engineering
University of California, Berkeley

September 2002

EXECUTIVE SUMMARY

Ground motions intensity measures (*IM*s) are typically estimated using probabilistic seismic hazard analyses (PSHA), which combine the effects of source, path, and site on the *IM*. Hazard analyses use attenuation relationships to define the probability density function (PDF) for *IM* conditioned on earthquake magnitude and site-source distance. These PDFs are log-normal, being defined by a median and standard deviation. When ground response analyses are performed to evaluate site effects in lieu of more approximate methods, it is with the expectation that the standard deviation would be reduced and any bias in the median would be removed. This study investigates the degree to which these benefits of ground response analyses are realized as a function of site condition, and outlines how ground response analyses can be implemented within PSHA.

Suites of input motions for ground response analyses were selected and scaled in a manner that accounts for magnitude, distance, and rupture directivity effects, while retaining natural aleatory uncertainty. Input motions were developed in this manner for ground response analyses for 68 sites having 134 recordings. *IM*s from recordings were compared to predictions from ground response, attenuation relations, and attenuation relations with amplification factors. Prediction residuals were evaluated using data from sites within categories to evaluate the models' bias and dispersion as well as the models' ability to capture spectral shape.

Spectral ordinates from ground response analyses are unbiased at low period ($T \leq \sim 1$ s), but underestimate long-period ($T \geq 1$ s) spectral ordinates from deep basin sites. At soft clay sites, ground response analyses reduce the dispersion in spectral accelerations at $T < 1$ s relative to alternative models. This dispersion reduction is not observed for stiff soil sites or at longer periods. Moreover, ground response analyses provide a more accurate estimate of spectral shape for soft clay sites than for stiff sites, and only for soft clay is spectral shape estimated more accurately than attenuation.

The results of the ground response analyses are interpreted to identify as a function of site category the combined uncertainties associated with the inaccurate physics of the site response model and unknown features of the input motions. This uncertainty can be combined with the standard error of the median to estimate the full dispersion. This dispersion can then be coupled with the median to define the PDF of the spectral ordinate for use in PSHA.

ACKNOWLEDGMENTS

This project was sponsored by the Pacific Earthquake Engineering Research Center's Program of Applied Earthquake Engineering Research of Lifeline Systems supported by the State Energy Resources Conservation and Development Commission and the Pacific Gas and Electric Company. This work made use of Earthquake Engineering Research Centers Shared Facilities supported by the National Science Foundation under Award #EEC-9701568. In addition, the support of the California Department of Transportation's PEARL program is acknowledged.

We would like to thank Drs. Norman Abrahamson, S.J. Chiou, Clifford Roblee, and Walter Silva for their helpful suggestions throughout the duration of this project. We also wish to thank several past and current UCLA students who assisted with project tasks, including James Chen, Ryan Bulatao, Onlei Kwok and Yoojoong Choi.

TABLE OF CONTENTS

LIST OF FIGURES

LIST OF TABLES

NOMENCLATURE

(partial list – additional variables used locally in the text)

A_{ij}	Median of spectral acceleration from attenuation prediction for site j in category i
AB_{ij}	Median of spectral acceleration from Basin amplification model for site j in category i
AS_{ij}	Median of spectral acceleration from NEHRP amplification model for site j in category i
$D_{a,5\text{-}75}$	5-75% significant duration as developed from Husid plot of acceleration waveform
$D_{a,5\text{-}95}$	5-95% significant duration as developed from Husid plot of acceleration waveform
D_b	Depth to base rock
$D_{v,5\text{-}75}$	5-75% significant duration as developed from Husid plot of velocity waveform
$D_{v,5\text{-}95}$	5-95% significant duration as developed from Husid plot of velocity waveform
e_{ij}	Misfit between observed spectral ordinate and scaled prediction, used for calculation of σ_e for site j in category i (Section 6.2.2)
F	Rupture mechanism parameter
f	Frequency
G	Shear modulus
G_{ij}	Median of output spectral acceleration from ground response analysis for site j in category i
G_{max}	Maximum shear modulus
HW	Hanging wall factor for dip-slip faults
IM	Ground motion Intensity Measure
I_a	Arias intensity
i_c	Critical angle (Figure 3.14)
m	Earthquake magnitude (generally moment magnitude unless indicated otherwise)
O_{ij}	Spectral acceleration of recorded motion for site j in category i
p	Significance level as calculated using F-distribution
PDF	Probability density function
PGA	Peak horizontal acceleration
PHA	Peak horizontal acceleration
PHA_r	Median peak horizontal acceleration from rock attenuation model
PHV	Peak horizontal velocity

PI	Plasticity index
R_{seis}	Distance to seismogenic rupture
RDI	Rupture directivity index (defined in Section 5.1.1)
RRS	Ratios of response spectral acceleration
$(RRS)_{ij}$	Median RRS across N_i input motions for site j in category i
r	Closest distance between site and seismic source
S	Site factor
S_a	Spectral acceleration
S_a^r	Reference motion amplitude
S_{hr}	Binary parameter for local site conditions
S_k	Response spectrum of individual time history k used as input for ground response analysis
S_{sr}	Binary parameter for local site conditions
se	Standard error
$(se_{g\text{-}out})_{ij}$	Standard error of median of output spectral acceleration from ground response analysis for site j in category i
$(\overline{se}_{g-out})_i$	Average standard error of median of output spectral acceleration from ground response analysis for category i
$(se_{RRS})_{ij}$	Standard error of ratio of response spectra for site j in category i
$(\overline{se}_{RRS})_i$	Average standard error of ratio of response spectra for category i
$(se_{\mu ra})_i$	Standard error of median of residuals from attenuation prediction for category i
$(se_{\mu rab})_i$	Standard error of median of residuals from Basin amplification model for category i
$(se_{\mu ras})_i$	Standard error of median of residuals from NEHRP amplification model for category i
$(se_{\mu rg})_i$	Standard error of median of residuals from output of ground response analysis for category i
$(se_{\sigma ra})_i$	Standard error of standard deviation of residuals from attenuation prediction for category i
$(se_{\sigma rab})_i$	Standard error of standard deviation of residuals from Basin amplification model for category i
$(se_{\sigma ras})_i$	Standard error of standard deviation of residuals from NEHRP amplification model for category i
$(se_{\sigma rg})_i$	Standard error of standard deviation of residuals from output of ground response analysis for category i
T	Period

T_m	Mean Period (defined in Section 4.2)
V_p	Pressure wave velocity
V_s	Small strain shear wave velocity
$V_{s\text{-}30}$	Averaged shear wave velocity in the upper 30 m (defined in Section 2.2)
X	Fraction of fault rupturing towards site, strike slip focal mechanism (Figure 5.1)
Y	Fraction of fault rupturing towards site, dip slip focal mechanism (Figure 5.1)
Z	Depth
Z_w	Depth of water table
β	Hysteretic soil damping
ε_1	Maximum 3m-average strain, considering the entire profile depth.
ε_2	Maximum 3m-average strain, considering only the top 30m
ε_3	Spatially averaged strain below the top low strain region
ε_4	Spatially average strain across entire profile
ε_5	Maximum strain at any location, considering the entire profile depth
ε_6	Maximum strain at any location, considering only the top 30m
γ	Shear strain within soil
μ	Median
μ_{be}	Median of target spectrum
$(\mu_{ra})_i$	Median of residuals from attenuation prediction across all sites in category i
$(\mu_{ra})_{ij}$	Residuals from attenuation prediction for site j in category i
$(\mu_{rab})_i$	Median of residuals from Basin amplification model across all sites in category i
$(\mu_{rab})_{ij}$	Residuals from Basin amplification model for site j in category i
$(\mu_{ras})_i$	Median of residuals from NEHRP amplification model across all sites in category i
$(\mu_{ras})_{ij}$	Residuals from NEHRP amplification model for site j in category i
$(\mu_{rg})_i$	Median of residuals from output of ground response analysis across all sites in category i
$(\mu_{rg})_{ij}$	Residuals from output of ground response analysis for site j in category i
μ_{sth}	Median spectra of the once-scaled time histories (Section 5.1.3)
μ_{th}	Median of the ensemble of unscaled time histories (Section 5.1.3)
μ_ε	Median of strain profiles
$(\mu_{\sigma e})_i$	Median of average shape misfit parameter for category i

ϕ	Offset azimuth of site from dip-slip fault (Figure 5.1)
ρ	Soil mass density
ρ_{ij}	Scale factor applied to Sa prediction during calculation of σ_e for site j in category i
σ	Standard error
$(\sigma_a)_{ij}$	Standard deviation of spectral acceleration from attenuation prediction for site j in category i
$(\sigma_{ab})_{ij}$	Standard deviation of spectral acceleration from Basin amplification model for site j in category i
$(\sigma_{as})_{ij}$	Standard deviation of spectral acceleration from NEHRP amplification model for site j in category i
$(\sigma_e)_{ij}$	Average shape misfit parameter across T = 0.05-2 s for site j in category i (Section 6.2.1)
σ_F	Dispersion of amplification model
σ_g	Approximate value of dispersion for use in ground motion hazard analysis
$(\sigma_{g\text{-}in})_{ij}$	Standard deviation of the input time history suite for site j in category i
$(\sigma_{g\text{-}net})_i$	Net dispersion associated with ground motion predictions from ground response calculations for category i
$(\sigma_{g\text{-}out})_{ij}$	Standard deviation of output spectral acceleration from ground response analysis for site j in category i
σ_m'	Mean effective confining pressure (Figure 3.7)
σ_r	Dispersion associated with the reference motion prediction
$(\sigma_{ra})_i$	Standard deviation of residuals from attenuation prediction for category i
$(\sigma_{rab})_i$	Standard deviation of residuals from Basin amplification model for category i
$(\sigma_{ras})_i$	Standard deviation of residuals from NEHRP amplification model for category i
$(\sigma_{rg})_i$	Standard deviation of residual from output of ground response analysis for category i
$(\sigma_{RRS})_{ij}$	Standard deviation of ratio of response spectra for site j in category i
σ_ε	Standard deviation of strain profiles
$(\sigma_{\sigma e})_i$	Standard deviation of average shape misfit parameter for category i
θ	Offset azimuth of site from strike-slip fault (Figure 5.1)

1 INTRODUCTION

1.1 STATEMENT OF THE PROBLEM

Earthquake ground motions are affected by source, path, and local site response effects. These effects are typically combined for implementation in engineering design practice using probabilistic seismic hazard analyses (PSHA). Hazard analyses typically use attenuation relations derived from strong motion recordings to define the probability density function for a ground motion parameter conditioned on the occurrence of an earthquake with a particular magnitude at a particular distance from the site. These relations are derived from statistical regression of observed ground motion parameters, and include site effects through a site term. The site term, in turn, is derived using data from all sites within broadly defined categories (e.g., rock and soil), and hence the site term represents a blended average site response effect from these sites.

Because of the broad range of site conditions within the "rock" and "soil" site categories used in attenuation relations, it is possible that for a particular site condition the predictions from attenuation relations are inaccurate. There are two meanings associated with this use of the word "inaccurate." First, the predictions could have a bias, or misfit, which is the difference between the medians of observed and calculated motions for the site condition. Second, the predictions could have an incorrect dispersion relative to observation. There are two common ways of accounting for local site effects to improve the accuracy of ground motion predictions: (1) adjustment of attenuation predictions through the use of amplification factors, and (2) site-specific geotechnical analysis of local ground response effects. Regional analyses of basin response effects are also possible. Note that our terminology distinguishes "site" effects from "ground response" effects. Site effects refer to the cumulative effects of ground response, basin response, and surface topography. Ground response refers to the influence of relatively shallow geologic materials on (nearly) vertically propagating body waves.

There is considerable cost and effort associated with performing ground response analyses in design practice, because such analyses require detailed site characterization and significant engineering time for analysis. Accordingly, if this expense is to be incurred, the

expectation is that the use of ground response analyses should improve the accuracy of predicted ground motions and decrease the level of uncertainty in these estimates relative to what would be obtained from an attenuation relationship or from site amplification factors. However, quantification of the improvement in ground motion predictions from site-specific ground response analyses compared to "blended" site effects in attenuation relations or amplification factors has to this point been anecdotal, and for practical purposes the benefits of ground response analyses are unknown. For the ground response effects modeled by such analyses to be of engineering significance, they must be distinguishable from the large data scatter associated with source/path variability.

Insight into the importance of ground response effects was provided by Lee and Anderson (2000), who examined the southern California strong motion inventory for soil and rock sites, and found that estimates from the Abrahamson and Silva (1997) attenuation relationship at short and intermediate periods are not systematically low or high for soil sites with multiple ground motion recordings. These results suggest that aleatory source/path variability more significantly influenced these soil site ground motions than the site response effect, which should be repeatable.

The results of Lee and Anderson (2000) contrast significantly with other research that has identified substantial site response effects on ground motions. Such research includes indirect evidence of ground response from variations in structural damage patterns with site condition (e.g., Seed et al., 1972; Seed et al., 1987; Seed et al., 1990; Chang et al., 1996; Rathje et al, 2000), and comparisons of instrumental recordings from nearby soil and rock sites (e.g., Seed and Idriss, 1971; Seed et al., 1987; Idriss, 1990; Seed and Dickenson 1996; Chang et al., 1996; Darragh and Idriss, 1997).

The disconnect between Lee and Anderson's findings and the significant site effects found in other empirical and analytical studies indicates a clear need to identify the site conditions where ground response effects cause motions to significantly and consistently differ from the predictions of empirical formulations such as attenuation relations. Resolution of this issue is the principal objective of this research. The approach taken is simple – we mimic the ground motion prediction process in a consistent, repeatable way for a large number of sites with strong motion recordings. The predictions are made knowing the magnitude, distance, and site-source azimuth (rupture directivity effect) associated with the recorded ground motion. The predictions are made using three analysis tools that require an increasing amount of site data: (1) attenuation relations, (2) attenuation relations adjusted with amplification factors, and (3) attenuation relations for a reference rock site condition coupled with 1-D ground response analyses with carefully selected

and scaled input motions representing the reference site condition. Details of these analysis procedures are provided subsequently in the report. The predictions are compared to the observed ground motions to identify median misfits (or residuals) and the dispersion of prediction residuals for individual sites and for multiple sites within categories. The results provide insight into the conditions for which costly site exploration and ground response studies are worthwhile in engineering design practice. The results also enable the development of recommendations for the construction of probability density functions from the results of ground response analyses for implementation in PSHA.

1.2 ORGANIZATION OF THE REPORT

The report begins in Chapter 2 with the description of several schemes for categorizing sites on the basis of geophysical, geologic or geotechnical data. Parameters used for the quantification of basin response effects are also described. In Chapter 3 we describe a suite of methods that can be used to account for site effects in ground motion prediction. Among the methods described are the site terms in soil attenuation relations, ground motion amplification factors, ground response analysis procedures, and basin response analysis procedures.

A critically important element of this study was the identification of a large number of sites for which ground motion predictions could be made for comparison to observation. Chapter 4 describes the criteria by which sites were selected, information on the geologic/geotechnical conditions at selected sites, and the parameter space covered by the ground motions at these sites. Innovative procedures for time history selection and scaling were developed in this study, which are described in Chapter 5. The time histories are selected and scaled such that each record represents a possible realization of the ground motion that could have been expected at the site for a firm rock site condition, while the ensemble median matches a target spectrum that is a function of the earthquake source and site-source distance and azimuth. Also described in Chapter 5 are several other protocols followed during the performance of 1D ground response analyses for this study.

We compare the predicted and observed ground motions in Chapter 6 and attempt to identify the categories of sites for which the benefits of performing ground response studies are significant from the standpoint of bias and/or dispersion reduction (relative to predictions from attenuation or attenuation/amplification factors). This analysis of benefit is performed for the ground motion intensity measures of spectral acceleration, Arias intensity, mean period, peak

velocity, and significant duration. Finally, in Chapter 7 we synthesize the principal findings of the study and provide recommendations for the application of ground response analysis for engineering hazard assessments.

2 SITE CLASSIFICATION SCHEMES

Site categorization schemes that have been used to differentiate ground conditions for strong motion studies include the following:

- Surface geology,
- Averaged shear wave velocity in the upper 30 m ($V_{s\text{-}30}$),
- Geotechnical data, including sediment stiffness, depth, and material type, and
- Basin geometric parameters including depth to basement rock and distance to basin edge.

In this chapter we present details on these methods of site categorization. Selected ground motion amplification factors defined on basis of these schemes are presented in Chapter 3.

2.1 SURFACE GEOLOGY

Geology-based classification schemes generally separate materials according to geologic age (e.g., Holocene-Pleistocene-Tertiary-Mesozoic). Separate categories are sometimes defined for granitic or volcanic rocks, or to subdivide Quaternary sediments. For example, Tinsley and Fumal (1985) categorized Los Angeles area Quaternary sediments according to age and texture, and these maps have been updated by Park and Elrick (1998). More detailed geologic data for southern California has recently become available through the Southern California Aerial Mapping Project (SCAMP), which provides for Quaternary materials information on sediment texture and depositional environment (e.g., Morton et al., 1999). In addition, the geology of the entire State of California is documented on 27 maps at 1:250,000 scale by the California Division of Mines and Geology (CDMG, 1959-1998). These maps distinguish Quaternary sediments based on age (Holocene-Pleistocene) and generalized descriptions of depositional environment. Given the availability of these data resources, Table 2.1 shows criteria that have been used for surface geologic classifications for general strong motion studies (Stewart et al., 2002).

Table 2.1. Criteria for surface geology classifications (modified from Stewart et al., 2002)

Age	Depositional Environment	Sediment Texture
Holocene	Fan alluvium	Coarse
Pleistocene	Valley alluvium	Fine
	Lacustrine/marine	Mixed
	Aeolian	
	Artificial Fill	
Tertiary		
Mesozoic + Igneous		

2.2 30-m SHEAR WAVE VELOCITY (V_{s-30})

Wave propagation theory suggests that ground motion amplitude should depend on the density and shear wave velocity of near-surface materials (e.g., Bullen, 1965; Aki and Richards, 1980). Density has relatively little variation with depth, and so shear wave velocity is the logical choice for representing site conditions. Two methods have been proposed for representing depth-dependent velocity profiles with a single representative value. The first takes the velocity over the depth range corresponding to one-quarter wavelength of the period of interest (Joyner et al., 1981), which produces frequency-dependent values. Fumal and Tinsley (1985) developed 1-Hz V_s maps for the Los Angeles region by relating quarter-wavelength velocities inferred from 33 boreholes to geologic units.

A practical problem with the quarter wavelength V_s parameter is that the associated depths are often deeper than can economically be reached with boreholes. The V_{s-30} parameter was proposed to overcome this difficulty and has found widespread use in practice. Parameter V_{s-30} is defined as the ratio of 30 m to the time for vertically propagating shear waves to travel from 30 m depth to the surface. Based on empirical studies by Borcherdt and Glassmoyer (1994), Borcherdt (1994) recommended V_{s-30} as a means of classifying sites for building codes, and similar site categories were selected for the NEHRP seismic design provisions for new buildings (Martin, 1994). The site classification scheme in the NEHRP provisions is presented in Table 2.2. The V_{s-30} parameter has been correlated with surface geology by Wills and Silva (1998), and this information has been used to generate state-wide maps of V_{s-30} by Wills et al. (2000).

Table 2.2. Site categories in NEHRP Provisions (Martin, 1994)

NEHRP Category	Description	Mean Shear Wave Velocity to 30 m
A	Hard Rock	> 1500 m/s
B	Firm to hard rock	760-1500 m/s
C	Dense soil, soft rock	360-760 m/s
D	Stiff soil	180-360 m/s
E	Soft clays	< 180 m/s
F	Special study soils, e.g., liquefiable soils, sensitive clays, organic soils, soft clays > 36 m thick	

2.3 SCHEMES BASED ON GEOTECHNICAL DATA

Geotechnical engineers have developed site classification schemes that can be used to estimate response spectra for soil sites. Early work on this topic is summarized in Seed and Idriss (1982), who recommended the following site classification scheme:

1. Rock sites
2. Stiff soil sites (< 60 m deep)
3. Deep cohesionless soil sites (> 75 m deep)
4. Sites underlain by soft to medium stiff clays

Response spectrum estimation procedures linked to this classification system were developed in which PHA on rock was first estimated from an attenuation relation, and then the ratio PHA_{soil} / PHA_{rock} and spectral shape were taken as a unique function of site condition (based on the work of Seed et al., 1976). Significant additional data gathered from the 1985 Mexico City, 1989 Loma Prieta, and 1994 Northridge earthquakes prompted revisions to the PHA rock-soil relations and spectral shapes, and the derivation of new site categories (e.g., Dickenson, 1994; Chang, 1996), which include information on sediment depth and near-surface shear wave velocity.

The most recent of the geotechnical classification schemes was proposed by Rodriguez-Marek et al. (2001) based on event-specific regressions of Loma Prieta and Northridge earthquake recordings. Data were grouped according to the categories in Table 2.3, and regressed using an attenuation function similar to that of Abrahamson and Silva (1997). Consistent trends were found for the Category D sites (deep stiff soil), as demonstrated by

error terms smaller than those for the overall data population. However, large intra-category dispersion was found for Category C sites (shallow stiff soil), indicating that further subdivision of this category may be appropriate. Rodriguez-Marek et al. (2001) recommend use of their classification scheme over the V_{s-30} scheme as intra-category standard error terms were reduced through use of the geotechnical scheme.

Table 2.3. Geotechnical site categories proposed by Rodriguez-Marek et al. (2001)

Site	Description	Site Period	Comments
A	Hard Rock	< 0.1 s	Hard, strong, intact rock; V_s > 1500 m/s
B	Rock	< 0.2 s	Most "unweathered" California rock cases (V_s > 760 m/s or < 6 m of soil)
C-1	Weathered/Soft Rock	< 0.4 s	Weathered zone > 6 m and < 30 m (V_s > 360 m/s increasing to 700 m/s).
C-2	Shallow Stiff Soil	< 0.5 s	Soil depth > 6 m and < 30 m
C-3	Intermediate Depth Stiff Soil	< 0.8 s	Soil depth > 30 m and < 60 m
D-1	Deep Stiff Holocene Soil, either S (Sand) or C (Clay)	< 1.4 s	Soil depth > 60 m and < 200 m. Sand has low fines content (< 15%) or nonplastic fines (PI < 5). Clay has high fines content (> 15%) and plastic fines (PI > 5).
D-2	Deep Stiff Pleistocene Soil, S (Sand) or C (Clay)	< 1.4 s	Soil depth > 60 m and < 200 m. See D-1 for S or C sub-categorization.
D-3	Very Deep Stiff Soil	< 2 s	Soil depth > 200 m
E-1	Medium Depth Soft Clay	< 0.7 s	Thickness of soft clay layer 3 m to 12 m
E-2	Deep Soft Clay Layer	< 1.4 s	Thickness of soft clay layer > 12 m
F	Special, e.g., Potentially Liquefiable Sand or Peat	= 1 s	Holocene loose sand with high water table (z_w < 6 m) or organic peat.

2.4 SITE PARAMETERS FOR BASIN EFFECTS

The site classification schemes presented above describe principally the characteristics of shallow sediments (i.e., at most, the upper few hundred meters). The dimensions of sedimentary basins can greatly exceed the dimensions of the sediment profiles considered in those schemes. Several measures of basin geometry have been proposed for site classification purposes. One is the depth to basement rock, which is typically defined as rock with a certain minimum shear wave velocity. Silva et al. (1999) took the “basement” shear wave velocity as 1000 m/s, whereas Steidl (2000), Lee and Anderson (2000), and Field (2000) took the basement velocity as 2500 m/s. Joyner evaluated basin effects using the distance from the site to the basin edge, measured

in the direction of the source-site wave propagation. Information on basin geometry is available for Los Angeles (Magistrale et al., 2000), the San Francisco Bay region (Brocher et al., 1998), Seattle (Frankel and Stephenson, 2000), the Kanto-Tokyo, Japan region (Sato et al., 1999), Kobe, Japan (Pitarka et al., 1998), and Taipei, Taiwan (Wen and Peng, 1998). An example of the type of data that can be retrieved from one of these basin models is presented in Figure 2.1, which shows the depth to the V_s = 2500 m/s isosurface in the Los Angeles basin.

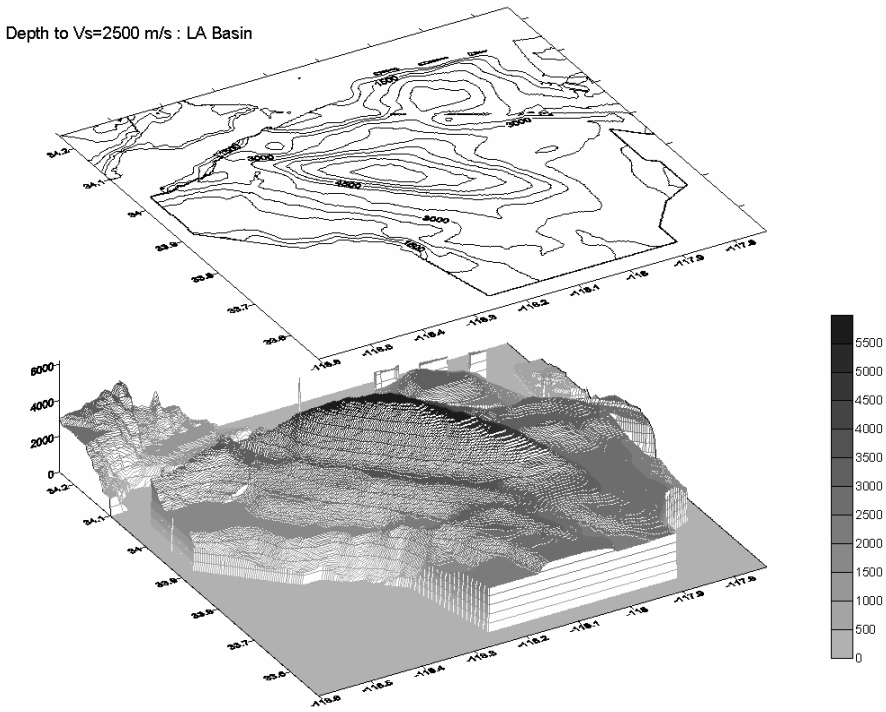

Fig. 2.1. Depth to V_s = 2500 m/s isosurface in Los Angeles basin, using basin model by Magistrale et al., 2000 (figure courtesy of Y. Choi)

3 MODELS FOR PREDICTION OF STRONG GROUND MOTION

3.1 INTRODUCTION

The subject of this chapter is models for prediction of earthquake ground motion intensity measures (*IM*s) given that an earthquake with particular characteristics has occurred. These characteristics include the moment magnitude (*m*), source rupture mechanism (e.g., strike slip, reverse, normal), and closest distance from source to site (*r*). A number of classes of models are available for predicting *IM*s at soil sites conditional on these source parameters. What distinguishes these models is the amount of information on site condition that is required as input and the form of the output. The classes of models considered herein are:

1. Attenuation relationships, which predict a probability density function (PDF) for *IM* conditional on source parameters for broadly defined site categories (e.g., rock and soil).
2. Amplification factors coupled with rock attenuation relations, which provide as output a conditional *IM* PDF (as was the case with attenuation relations). The distinction from attenuation is that the amplification factors allow more detailed information on site condition to be considered (e.g., a detailed description of surface geology).
3. Ground response analyses, which utilize detailed characteristics of shallow sediments in a wave propagation model that provides as output a transfer function between input (rock) motion and a calculated motion at the ground surface (soil), and
4. Basin response analyses, which utilize (a) a model for three-dimensional basin structure (3D distribution of sediment velocities) to evaluate waveforms across the ground surface given certain characteristics of the incoming wave field (from the source), or (b) statistical models for *IM* PDFs in basins using an amplification factor approach, in which

the input parameters for the models describe the local basin geometry (i.e., depth or distance to basin edge).

The following sections provide a review of the above classes of ground motion models, with an emphasis on those models selected for use in this study. Further information on these models can be found in Stewart et al. (2001).

3.2 ATTENUATION RELATIONSHIPS

Attenuation relationships are derived using regression analyses in which a ground motion *IM* is related to characteristics of the source, path, and site. The output of an attenuation model is a probabilistic distribution of *IM* that is typically log-normal, and hence is described by a median (μ) and standard error (σ). Commonly used *IM*s in earthquake engineering include spectral acceleration, duration, and mean period. The focus here is on spectral acceleration in tectonically active regions.

Attenuation functions for spectral acceleration have often had the following general form:

$$\ln IM = c_1 + c_2 m + c_3 m^{c_4} + c_5 \ln r + f(F) + f(HW) + f(S) \qquad (3.1)$$

where c_1 to c_5 are constants derived through regression analysis, *m* represents moment magnitude and *r* represents distance between source and site. *F* is a factor related to the source type (rupture mechanism), *HW* is a hanging wall factor for dip-slip faults, and *S* is a site factor. The principal focus of this section is on the manner in which site effects are represented in attenuation relations, and hence in the following we focus on alternative representations of *f(S)*.

Site term *f(S)* provides a value of amplification or de-amplification of ground motion as a function of site parameter *S*. The amplification/de-amplification is measured relative to a reference value of site parameter *S*, which usually corresponds to rock site conditions. Previous parameterizations of *S* include the following:

1. **S = 0 for rock and S = 1 for soil (Abrahamson and Silva, 1997; Sadigh et al., 1997). In these attenuation models, soil depth > 20 m is required for a soil site categorization.**
2. **$S = V_{s\text{-}30}$ (Boore et al., 1997; Spudich et al., 1999).**
3. **Multiple site parameters, including binary parameters S_{sr} and S_{hr} for local site conditions, and depth to basement rock, D_b (Campbell, 1997). The local site condition parameters are $S_{sr} = S_{hr} = 0$ for soil (>10 m depth), $S_{sr} = 1$ and $S_{hr} = 0$ for soft rock (Tertiary age and soft volcanic rocks), and $S_{sr} = 0$ and $S_{hr} = 1$ for hard rock (e.g., Cretaceous, metamorphic or crystalline rock, hard volcanic rocks). Parameter D_b is taken as depth to Cretaceous or older deposits with V_p (P-wave velocity) ≥ 5 km/s or $V_s \geq 3$ km/s.**

The analytical form of site factor $f(S)$ differs for the various attenuation relations. Abrahamson and Silva (1997) include the median peak acceleration on rock (i.e., median PHA from rock attenuation model, PHA_r) as an input parameter along with S, as follows,

$$f(S) = S\left(a_{10} + a_{11}\ln(PHA_r + c_5)\right) \tag{3.2}$$

where a_{10}, a_{11}, and c_5 are regression parameters. This formulation allows the amplification value $f(S)$ to vary with PHA_r, and hence the formulation can incorporate the effects of soil nonlinearity. Boore et al. (1997) take the site factor as the product of a period dependent constant and $V_{s\text{-}30}$,

$$f(S) = b_v\left(\ln(V_{s-30}/V_A)\right) \tag{3.3}$$

where b_v and V_A are regression parameters. With this model, amplification factor $f(S)$ is independent of the level of shaking. Campbell (1997) incorporates site-source distance (r) into the site term along with the S_{sr} and S_{hr} parameters as follows:

For PHA

$$f(S) = [0.440 - 0.171\ln(r)]S_{sr} + [0.405 - 0.222\ln(r)]S_{hr} \tag{3.4}$$

For S_a

$$f(S) = \ln(PHA) + 0.5c_6S_{sr} + c_6S_{hr} + c_7\tanh(c_8D)(1 - S_{hr}) \tag{3.5}$$

where c_6, c_7, and c_8 are regression parameters. Like Abrahamson and Silva (1997), this model allows amplification $f(S)$ values to be nonlinear (i.e., vary with the level of shaking).

Sadigh et al. (1997) do not use a site term, but perform the full regression separately for soil and rock sites.

The site terms *f(S)* for PHA and 1.0 s spectral acceleration from the aforementioned models are compared in Figure 3.1. The *f(S)* models by Abrahamson and Silva (1997) and Boore et al. (1997) are configured such that amplification is measured relative to a rock motion, whereas the *f(S)* model by Campbell (1997) provides amplification relative to soil. The inverse of *f(S)* from Campbell are shown in Figure 3.1 to illustrate the site terms in a manner consistent with the other models. Values of *f(S)* from the Abrahamson and Silva (1997) and Boore et al. (1997) relations are plotted in Figure 3.1 against PHA_r. Values of *f(S)* from the Campbell (1997) model are plotted against R_{seis}, the distance to seismogenic rupture. The R_{seis} and PHA_r axes were positioned relative to each other using the Campbell (1997) attenuation model for $m = 6.5$.

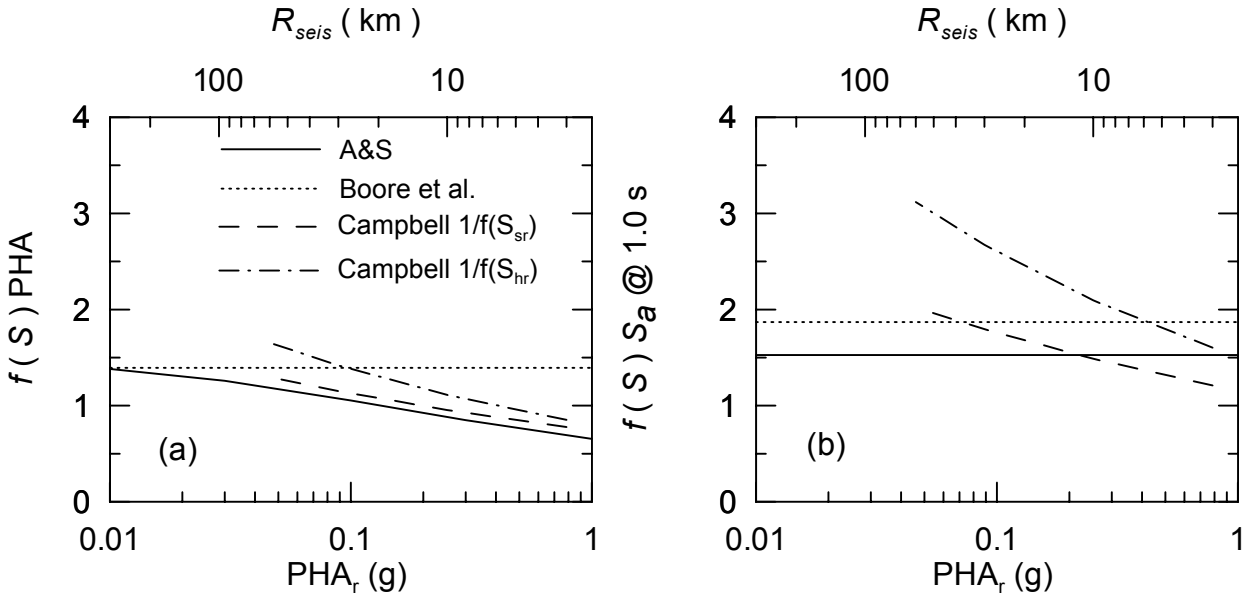

Fig. 3.1. Site terms f(S) from attenuation models for PHA and 1.0 s spectral acceleration

As shown in Figure 3.1, other than the Boore et al. (1997) relationship, which does not depend on PHA_r, the models predict PHA amplification for weak levels of motion (PHA_r < ~ 0.2 g) and de-amplification for stronger shaking. Values of *f(S)* from Abrahamson and Silva (1997) and soft-rock 1/*f(S)* from Campbell (1997) agree well, which is expected since the Abrahamson and Silva rock site condition corresponds to soft rock.

The Campbell (1997) 1/*f(S)* values for hard-rock indicate higher soil-rock amplification, as expected. As shown in Figure 3.1, *f(S)* values for spectral acceleration at 1.0 s are consistently larger than unity.

3.3 AMPLIFICATION FACTORS

3.3.1 Model Development and Formulation

Amplification factors represent the ratio of the expected value of a ground motion *IM* for a specified site condition (i.e., the site condition at the location of interest) to the expected value of the *IM* for a reference site condition. Amplification factors can only be applied in practice if a ground motion attenuation relationship is available for the reference site condition. Assuming such an attenuation relationship is available, an *IM* PDF is constructed by (1) defining the median as the product of the attenuation median (for the reference site condition) and the median amplification factor, and (2) identifying an appropriate value of dispersion for the site category. In the remainder of this section, we identify three techniques that have been used to evaluate amplification factors and describe the associated procedures by which the standard deviation (σ) of the PDFs can be obtained.

The three methods for evaluating site amplification factors that are presented herein are: (1) evaluations of amplification factors directly from strong ground motion data using so-called non reference site approaches (e.g., Stewart et al., 2002; Field, 2000; Steidl, 2000), (2) evaluations of amplification factors directly from strong ground motion data using a reference site approach (e.g., Borcherdt and Glassmoyer, 1994; Borcherdt, 2002), and (3) evaluation of amplification factors from wave propagation analyses (e.g., Silva et al., 1999; Silva et al., 2000).

A number of non-reference site approaches for evaluation of amplification factors are available, and are synthesized by Stewart et al. (2001). The non-reference site approach emphasized herein evaluates amplification using *IM* residuals between recorded data and reference motions evaluated from a rock attenuation relation. Several amplification models developed using this approach are presented in the sections that follow. When amplification factors are derived using this approach, the PDF σ value is simply the dispersion for the appropriate site category from the amplification model.

The evaluation of an amplification factor from a reference site approach requires two recorded motions from nearby sites, but different site conditions. The assumption inherent to reference site approaches is that the two motions are influenced by similar source and path characteristics, and that the difference between the motions can be attributed to variations in local site effects. When using such models, the appropriate PDF σ value is not the dispersion of the amplification model (σ_F). Rather, σ is calculated based on σ_F, the dispersion associated with the reference motion prediction (σ_r), and the functional relationship between amplification and reference motion amplitude. For example, suppose the amplification relationship is log-linear,

$$\ln(F) = a + b\ln\left(S_a^r\right) \tag{3.6}$$

where F = amplification factor, S_a^r = reference motion amplitude (usually taken as PHA_r), and a and b are regression parameters. The error term is then evaluated as (Bazzuro, 1998),

$$\sigma = \sqrt{(b+1)^2\sigma_r^2 + \sigma_F^2} \tag{3.7}$$

Note that σ can be larger or smaller than σ_r depending on the value of b and σ_F. Amplification models developed from a reference site approach are discussed as part of Section 3.3.2 below.

Amplification factors can be derived from the results of wave propagation analyses performed on a site-specific basis or for a site category. Amplification factors for geologic site categories have been derived by Silva et al. (1999) and for $V_{s\text{-}30}$-defined categories by Silva et al. (2000). These amplification factors were derived by performing 1D ground response calculations using randomized velocity profiles appropriate to the category, randomized modulus reduction and damping curves, and many input motions derived from a simulation procedure. Amplification factors derived using such an approach are described in Sections 3.3.2 and 3.3.4 below. The dispersion associated with these amplification factors (σ_F) is not equivalent to the *IM* PDF σ. Moreover, because the amplification models used by Silva et al. are not linear with respect to PHA_r (i.e., like Eq. 3.6 above), the relationship between reference motion dispersion (σ_r), σ_F, and σ is unknown. In fact, the general subject of how to evaluate σ when ground response analyses are performed has been a source of considerable controversy. In one study (Schneider et

al., 2000), the ground motion variance was conservatively taken as the sum of σ_r^2 and σ_F^2. In Section 6.4, we address the issue of dispersion estimation when ground response analyses are performed to estimate spectral accelerations.

3.3.2 Amplification Factors for Site Categories Defined on the Basis of V_{s-30}

Amplification factors defined on the basis of the V_{s-30}-defined categories introduced in Section 2.2 have been derived in the following studies:

Non-Reference Site Approach: Field (2000); Steidl (2000); Stewart et al. (2002)

Reference Site Approach: Borcherdt and Glassmoyer (1994); Borcherdt (2002)

Wave Propagation Analysis: Silva et al. (2000)

The models by Field (2000) and Steidl (2000) were derived using the southern California data set developed by Steidl and Lee (2000). Reference site conditions used in these studies are V_{s-30} = 760 m/s (Field) and a rock-average velocity for the Sadigh rock attenuation model (Steidl). Borehole compilations for western U.S. rock sites by Silva et al. (1997) and Boore et al. (1997) have found this rock-average velocity to be $V_{s-30} \approx$ 520 m/s and 620 m/s, respectively. The Stewart et al. (2002) model was developed using a data set for all tectonically active regions, and the reference site condition is again $V_{s-30} \approx$ 520 m/s — 620 m/s. The Borcherdt and Glassmoyer (1994) and Borcherdt (2002) models were developed using data from the 1989 Loma Prieta and 1994 Northridge earthquakes, respectively. The reference site conditions used for these studies are V_{s-30} = 1050 m/s (Loma Prieta) and 850 m/s (Northridge). The reference site condition used by Silva et al. is V_{s-30} = 760 m/s.

One of the major features observed from the above studies is the variation of spectral amplification levels with V_{s-30}. An example result illustrating a typical trend is shown in Figure 3.2 (Field, 2000). Amplification is seen to increase with decreasing V_{s-30}, with the gradient of decrease increasing with period. A somewhat atypical result is presented in Figure 3.3, which shows an increase of PHA amplification with increasing V_{s-30} (Steidl, 2000). This outcome was explained by Steidl as resulting from variable levels of nonlinearity, which can decrease amplification levels at high frequencies, particularly in softer sediments.

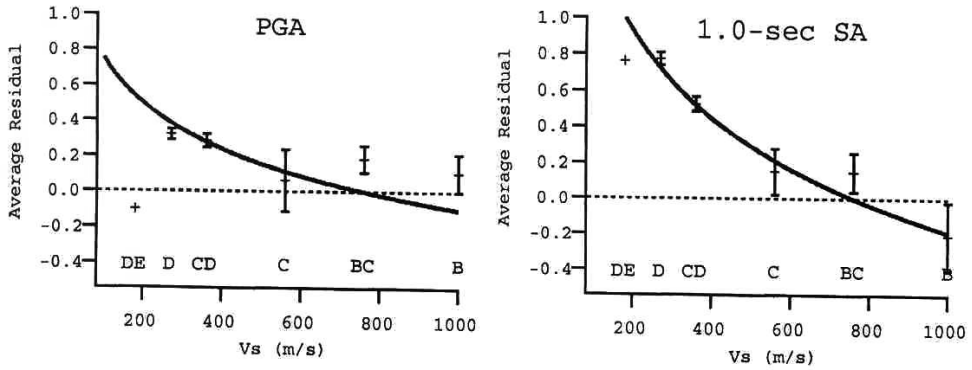

Fig. 3.2. Average residuals between southern California strong motion data and attenuation prediction for V_{s-30} = 760 m/s site condition as function of V_{s-30} (Field, 2000)

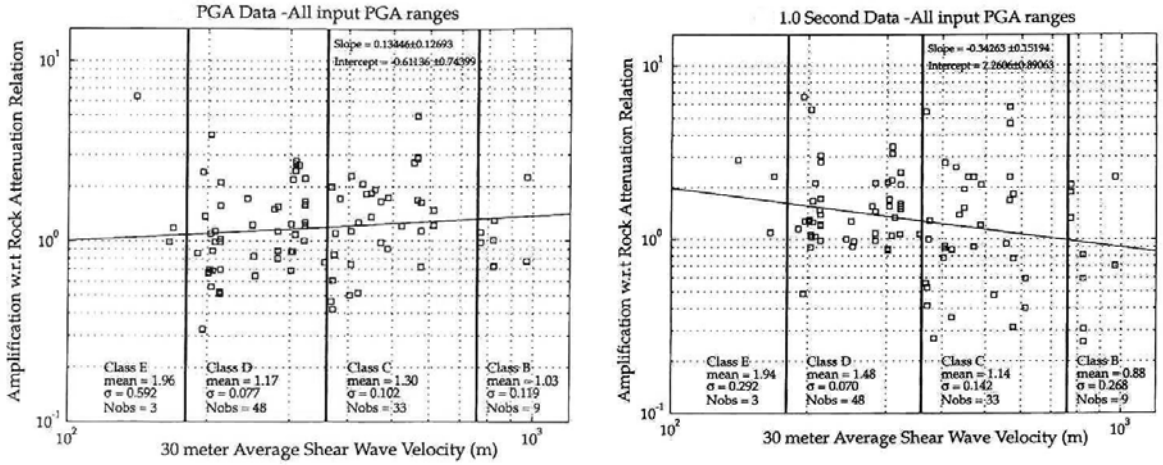

Fig. 3.3. Median amplification factors versus V_{s-30} (Steidl, 2000)

The variations with PHA_r (= PHA on reference site condition) of the median amplification factors for PHA and 1.0 s spectral acceleration predicted by the above models are presented in Figure 3.4. The amplification values apply for a V_{s-30} value mid-way between the NEHRP category boundaries (V_{s-30} = 1080, 520, and 250 m/s for NEHRP B, C, and D, respectively). Amplification models by Field (2000) and Borcherdt and Glassmoyer (1994) were developed primarily from low-amplitude motions, and are independent of PHA_r. For these relations, amplification values are plotted with symbols at PHA_r = 0.1 g. Steidl (2000) provided two models, one for PHA_r < 0.1g, and another for PHA_r as high as 0.3 to 0.8g. The Steidl amplification factors presented in Figure 3.4 are from the model that applies for all ground motion levels, and are plotted up to PHA_r = 0.3 g.

Silva et al. (2000) gave two sets of amplification factors that are derived from ground response analyses through the use of different nonlinear soil models (i.e., modulus reduction and damping curves). Results obtained using a soil model for the Los Angeles area are presented in Figure 3.4 as "LA," whereas results obtained using a nonlinear soil model for the San Francisco Bay area are presented as "SF." (these nonlinear soil models are discussed further in Section 3.4.1 below). It should be noted that the amplification factors by Silva et al. (2000) that are shown in Figure 3.4 for the B category were actually derived for a BC site condition.

A number of trends can be seen from the comparisons in Figure 3.4. Discussed in the following are (1) variations in amplification levels between categories, (2) the PHA_r-dependence of amplification factors, and (3) causes for variations of amplification levels within a category.

The models predict clearly differentiated amplification levels for Categories B, C, and D, with D exceeding C and C exceeding B. The only exception to this is the aforementioned Steidl (2000) study, for which PHA amplification increases with V_{s-30}. The V_{s-30}-dependence of amplification factors is larger for 1.0 s spectral acceleration than for PHA.

There are significant differences in the nonlinearity predicted by the models (i.e., decrease in amplification with increasing PHA_r). Models by Steidl, Field, and Borcherdt and Glassmoyer are linear. Models by Stewart et al. and Borcherdt show negligible PHA nonlinearity for Category B (trends shown in Figure 3.4 are statistically insignificant), but moderate PHA nonlinearity for Categories C and D. Nonlinearity for 1.0 s spectral acceleration is generally negligible. In each category, the highest levels of nonlinearity are predicted by the wave propagation model of Silva et al. (2000).

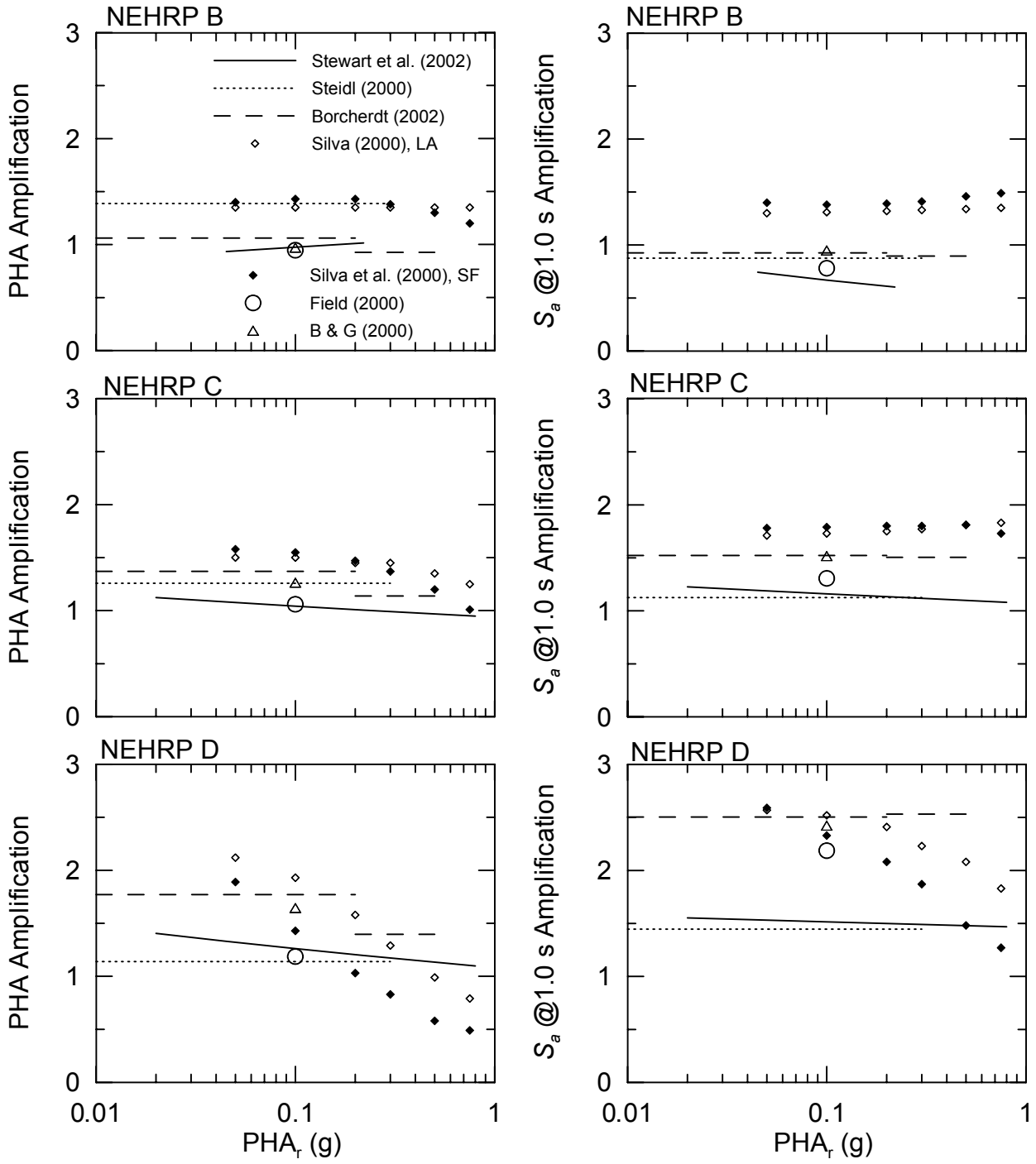

Fig. 3.4. Median amplification factors for PHA and 1.0 s S_a with respect to PHA_r for NEHRP categories

Within the various categories, there are significant differences in amplification levels at a given PHA_r, which in many cases may be attributed to variations in the reference site condition. In Categories C and D at low levels of shaking, amplification levels by Borcherdt and Glassmoyer, Borcherdt, and Silva et al. are significantly higher than those

by Steidl or Stewart et al. This difference is partially attributed to the use of rock-average reference site conditions in the Steidl and Stewart et al. studies (corresponding to $V_{s\text{-}30} \approx$ 520-620 m/s) and much firmer reference site conditions in the other studies ($V_{s\text{-}30} \geq 760$ m/s). These trends also generally hold for Category B. However, the site factors by Silva et al. (2000) for B are unusually high because they apply for a BC site condition.

3.3.3 Amplification Factors for Site Categories Defined on the Basis of Geotechnical Data

Classification schemes based on geotechnical data (i.e., sediment depth and stiffness) are discussed in Section 2.3. Amplification factors defined on the basis of the scheme proposed by Rodriguez-Marek et al. (2001) were derived by Stewart et al. (2002). The reference site condition used by Stewart et al. is the rock-average condition in active regions, which corresponds roughly to Geotechnical category C1 (Table 2.3). The variations with PHA_r of the median amplification factors predicted by these models are presented in Figure 3.5. Note that the amplification models for Categories C and D only differ significantly at long period, and that the amplification model for soft clay (Category E) exhibits much more nonlinearity and weak motion amplification than other categories.

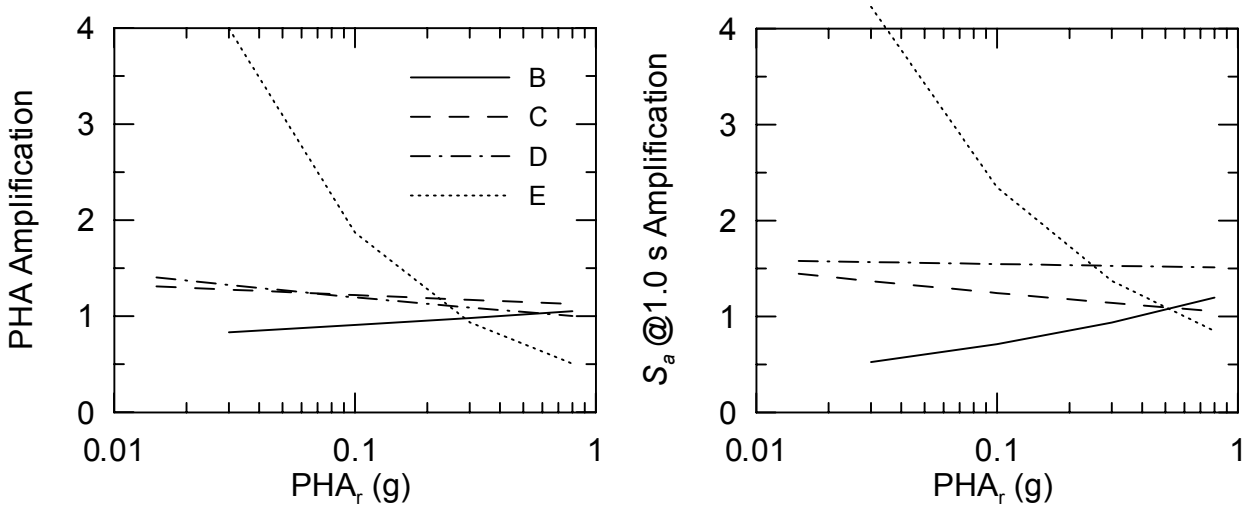

Fig. 3.5. Median amplification factors for PHA and 1.0 s S_a for geotechnical categories (Stewart et al., 2002).

3.3.4 Amplification Factors for Site Categories Defined on the Basis of Surface Geology

Site classification schemes based on surface geology are described in Section 2.1. Amplification factors derived on the basis of surface geology have been derived in the following studies:

Non-Reference Site Approach: Lee and Anderson (2000); Steidl (2000); Stewart et al. (2002)

Wave Propagation Analysis: Silva et al. (1999)

The models by Lee and Anderson (2000) and Steidl (2000) were derived using the southern California data set developed by Steidl and Lee (2000). Reference site conditions used in these studies are derived using the soil average site condition for active regions (Lee and Anderson) and the rock average for active regions (Steidl). The Stewart et al. (2002) model was developed using a data set for all active regions, and the reference site condition corresponds to rock average for active regions. The reference site condition used by Silva et al. is firm rock (Mesozoic or granitic rock).

The variations with PHA_r of the median amplification factors predicted by the Steidl, Stewart et al., and Silva et al. models are presented in Figure 3.6. The categories plotted are Holocene lacustrine/marine deposits (Hlm), Quaternary alluvium (Qa), Tertiary-age materials (T), and Mesozoic and Igneous materials (M+I). Steidl (2000) subdivided Quaternary (Q) class into younger Quaternary (Qy) and older Quaternary (Qo), with Tertiary added to the Qo class. Presented in Figure 3.6 are results for the cumulative category (Q).

Results for the Qa category (second row of Figure 3.6) show that the three models predict similar levels of PHA amplification, and similar levels of PHA nonlinearity. For 1.0 s spectral acceleration, the amplification factors from Silva et al. are larger than those derived from empirical data. In the T category (third row), the amplification models are again similar for PHA, but have significant deviations at long periods (with Silva et al. again providing the largest amplification factors). Results for the Hlm category (first row) are only available from the Stewart et al. and Silva et al. studies. Both demonstrate strong nonlinearity, particularly for PHA. As before, the models are generally consistent for PHA, but the Silva et al. amplification levels are significantly larger than those by Stewart et al. for 1.0 s spectral acceleration. Results for Category M (Figure 3.6) are only available from

empirical studies (Steidl, Stewart et al.), and show consistent levels of de-amplification. The apparent nonlinearity in these factors is not statistically significant.

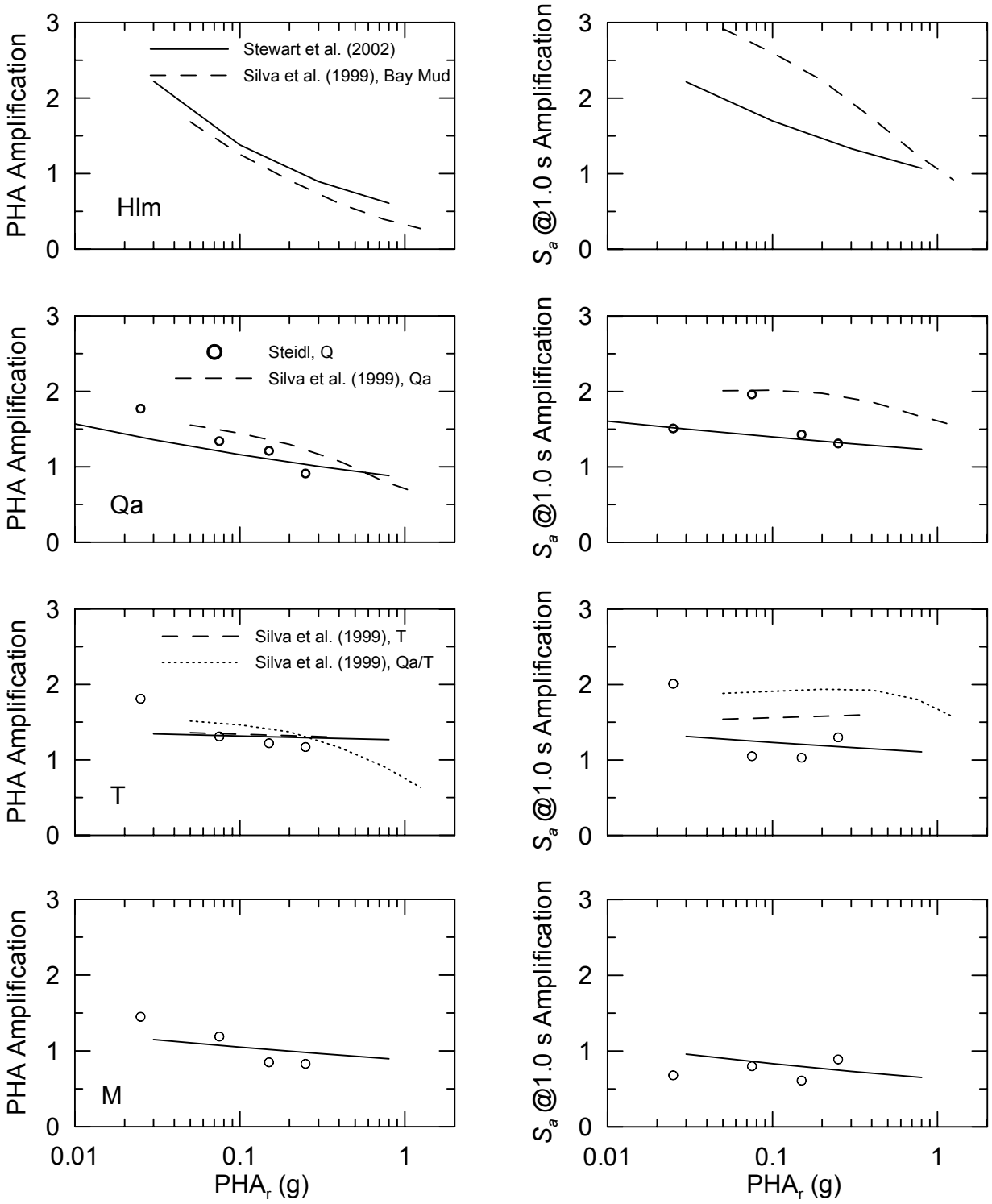

Fig. 3.6. Median amplification factors for PHA and 1.0 s S_a – comparison of results from studies by Steidl (2000), Stewart et al. (2002) and Silva et al. (1999).

3.4 GROUND RESPONSE ANALYSIS

Ground response analysis refers to the modification of vertically propagating body waves as they pass through shallow sediments. The analysis consists of numerical modeling of one-dimensional shear wave propagation through horizontal sediment layers. The analysis requires knowledge of ground motions at the base of the sediments. The following sections describe two crucial elements for ground response modeling: (1) the dynamic behavior of soil subject to cyclic excitation in shear, and (2) computational models for the nonlinear response of sediment layers to vertical wave propagation. A summary of previous verification studies for these analysis methods is presented in Section 5.3.2(d) of Stewart et al. (2001).

3.4.1 Soil Models

The properties of soil utilized in ground response analyses include a small strain shear wave velocity (V_s) profile, soil mass density (ρ), and relationships for the variation of normalized shear modulus (G/G_{max}) and hysteretic soil damping (β) with shear strain (γ) within the soil. Small strain shear wave velocity, V_s is related to maximum shear modulus as $G_{max} = V_s^2 \rho$.

Profiles of V_s are best obtained from in situ measurements by downhole, crosshole, or suspension logging techniques. Geophysical techniques such as spectral analysis of surface waves can also be effectively applied. Where in situ measurements are not available, V_s profiles can be estimated from correlations with other soil properties. The most accurate correlations are generally derived locally for specific soil formations [e.g., Dickenson (1994) for San Francisco Bay Mud]. More general correlations are available for clays (based on overconsolidation ratio and undrained shear strength, Weiler, 1988) and granular soils [based on penetration resistance and effective stress, Seed et al. (1986) for sand and Rollins et al. (1998) for gravel].

Modulus reduction, G/G_{max}, and damping, β, relations can be derived from material-specific testing, usually performed with simple shear (Dorourdian and Vucetic, 1995) or

torsional shear devices. The G/G_{max} and β curves are derived from backbone curves established from the first cycle of cyclic tests conducted at frequencies typically on the order of 1 Hz. The modulus, G corresponds to the secant modulus through the endpoints of the hysteresis loop, and damping ratio is proportional to the energy loss from a single cycle of shear deformation. For most applications, "standard" curves for various basic soil types and material properties are available. Site-specific curves can also be derived for particular materials [e.g., Bay Mud curves compiled by Sun et al. (1988)].

Modulus reduction and damping curves have generally been derived in one of two ways. First, laboratory-derived curves are available that are sensitive to soil plasticity for cohesive materials such as clays, and effective overburden stress for granular materials such as sands, low plasticity silts and clays, and gravels (e.g., Vucetic and Dobry, 1991; Seed et al., 1984; and EPRI, 1993). Second, curves can be derived from back analysis of regional ground motion records (Silva et al., 1997).

Modulus reduction and damping curves for cohesive soils with respect to plasticity index (PI) are shown in Figure 3.7 (Vucetic and Dobry, 1991). Also included in the figure are curves for low plasticity clays in the Los Angeles area at depths > 100 m and < 100 m as evaluated by Stokoe et al. (1999). It should be noted that low plasticity clays behave more linearly under higher confining pressures (large depth) than at shallow depths, which is a similar behavioral trend to granular soils. Curves for cohesionless soils are shown in Figure 3.8 (Seed et al., 1986; EPRI, 1993). The depth-dependent curves by EPRI (1993) show more linearity and less damping with increasing confinement. The upper bound of G/G_{max} and lower bound of β curves by Seed et al. (1986) agree well with EPRI (1993) curves at shallow depths (0- 37 m).

Material specific curves for Holocene soft clay deposits in the San Francisco Bay area (Bay Mud) have been presented by Sun et al. (1988). Representative curves for Bay Mud selected for subsequent use in this study are shown along with the Vucetic and Dobry curves for clays in Figure 3.9. The Bay Mud curves are comparable to the PI ≈ 50 curves.

A number of other material specific curves are available that can be used for specific sites (e.g., Hsu and Vucetic, 1999; Vucetic et al., 1998; KAJIMA, 2000). Presented below are several such curves used in this study. Modulus reduction and damping curves for the North Palm Springs, Desert Hot Springs, and El Centro Array #7 strong motion

recording sites were derived at several depths (KAJIMA, 2000). Curves for cohesionless soils at North Palm Springs and Desert Hot Springs sites are shown along with standard curves for granular soils in Figures 3.10 and 3.11. Curves for clayey soils at El Centro Array #7 site are shown along with standard curves that depend on plasticity index in Figure 3.12. The El Centro curves were derived from samples retrieved from several different depths. No significant depth dependence was observed in the curves, which are all similar to the Vucetic and Dobry PI = 30 curve.

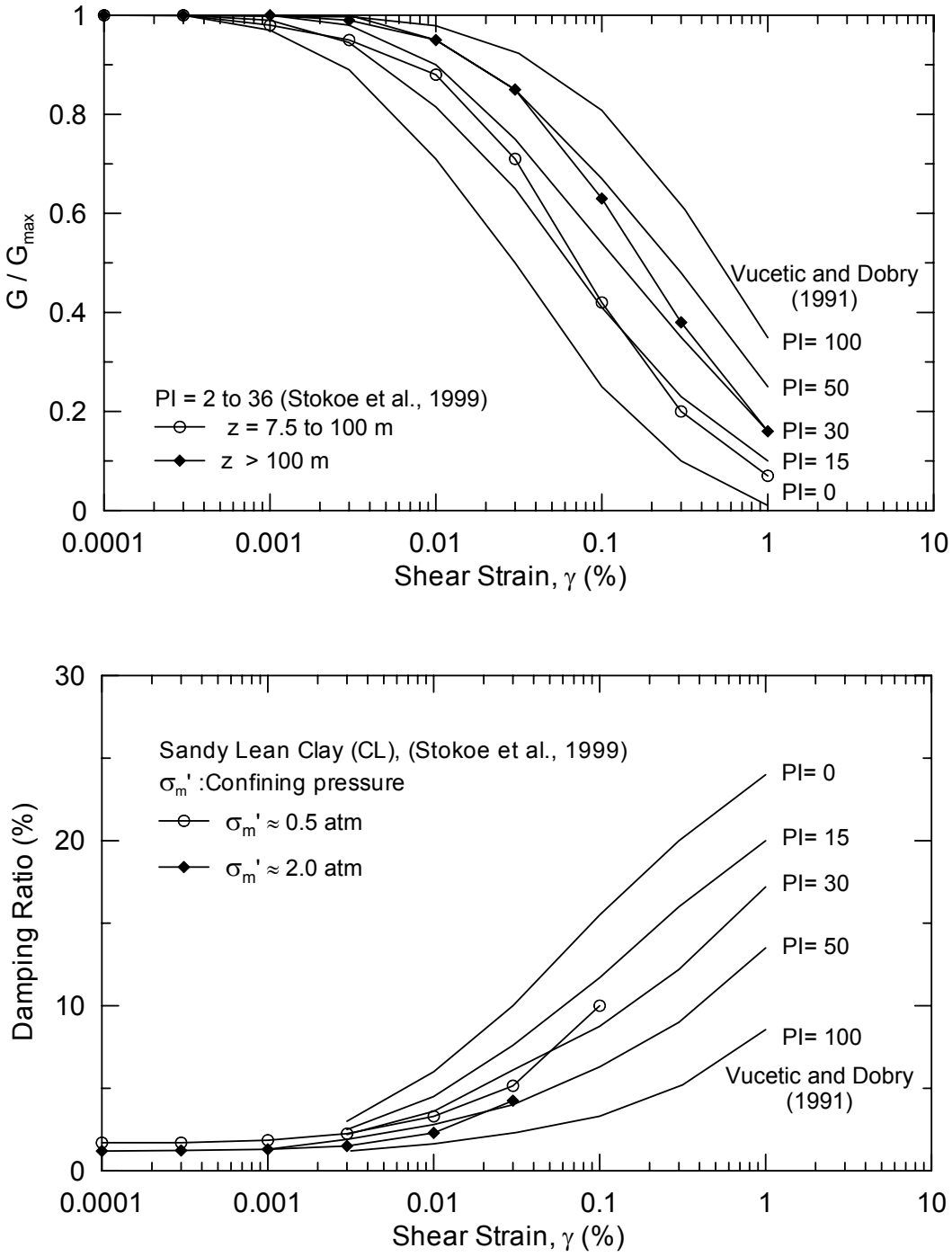

Fig. 3.7 Modulus reduction (G/Gmax) and damping ratio curves for cohesive soils with respect to plasticity index (Vucetic and Dobry, 1991); and PI=15 curves for sediments deeper than 100 m (Stokoe et al., 1999).

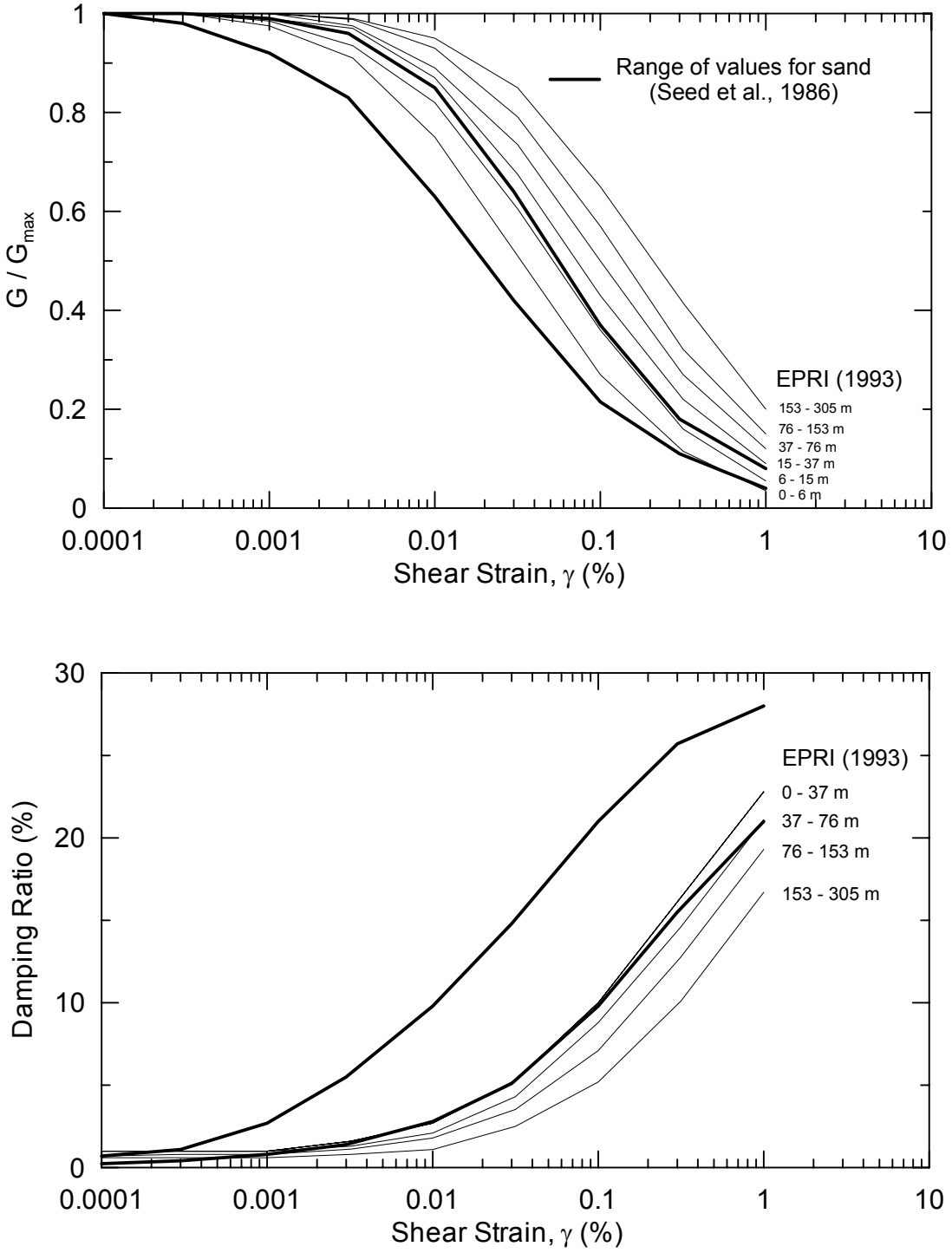

Fig. 3.8 Modulus reduction (G/Gmax) and damping ratio curves for cohesionless soils. Range of sand curves by Seed et al. (1986) and depth dependent curves by EPRI (1993).

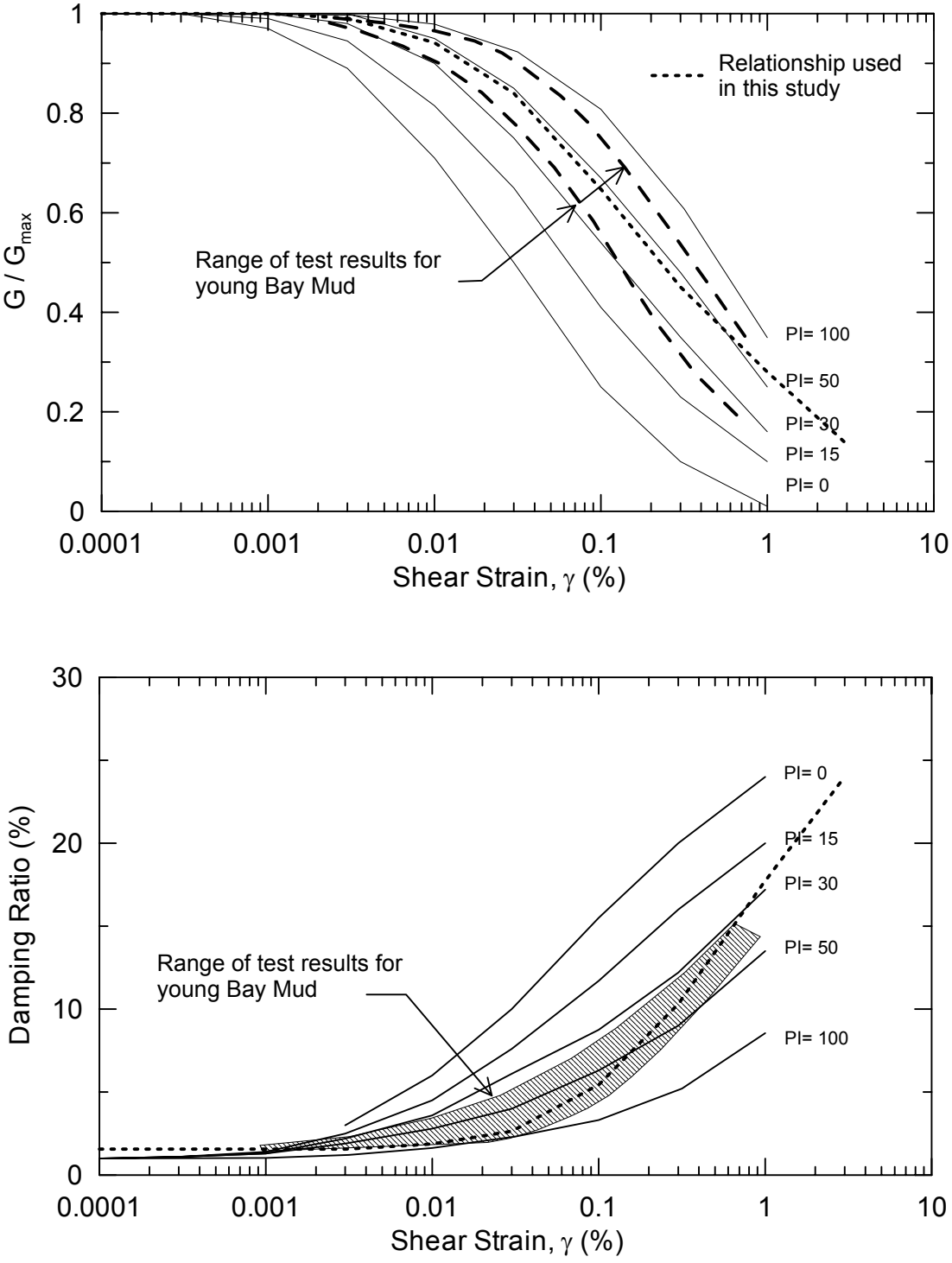

Fig. 3.9 Range of modulus reduction (G/Gmax) and damping ratio curves for Young Bay Mud (Sun et al., 1988), the curve selected for use in this study, and the Vucetic and Dobry (1991) curves for cohesive soils.

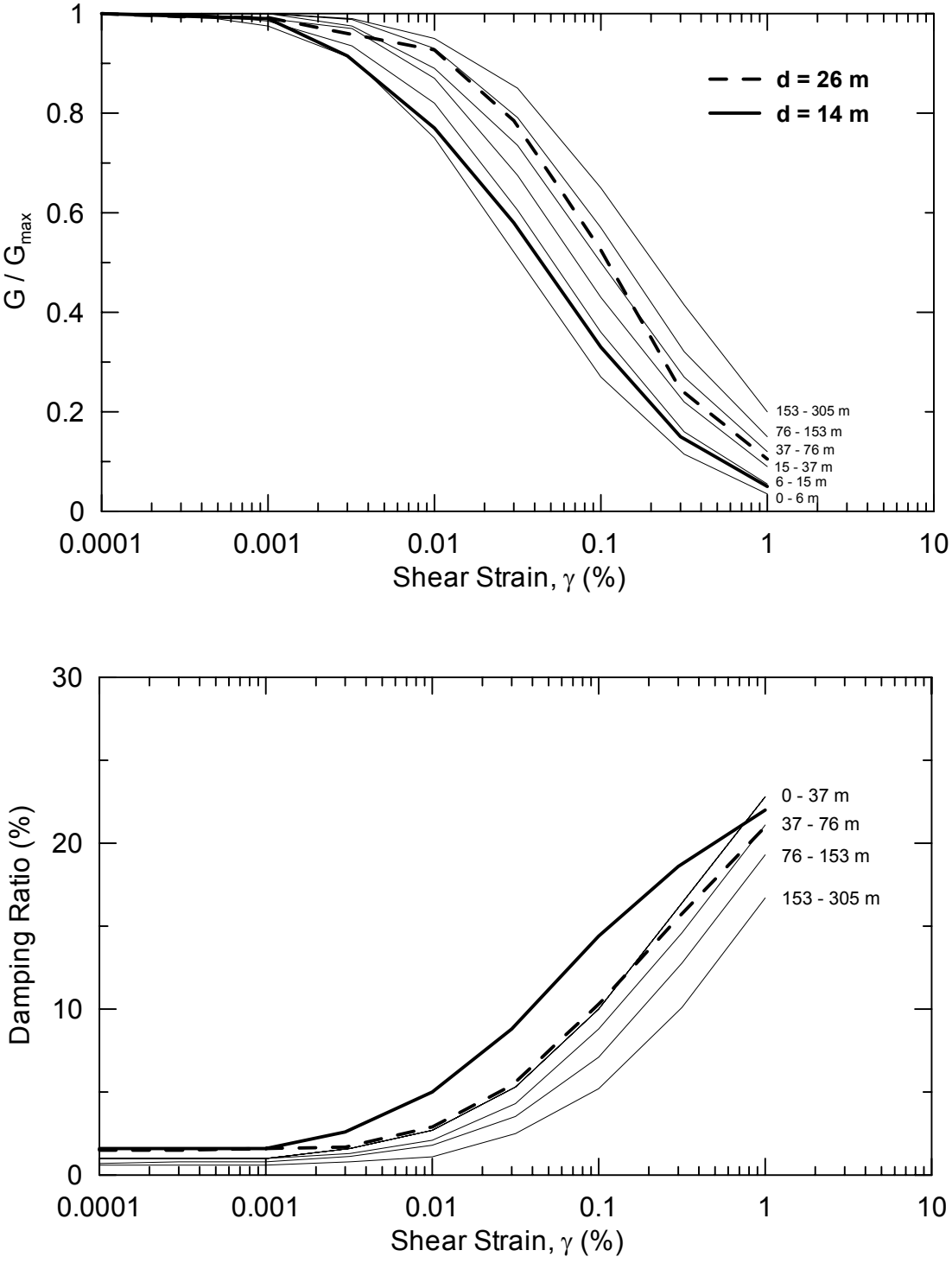

Fig. 3.10 Material specific modulus reduction (G/Gmax) and damping ratio curves for Desert Hot Springs strong motion recording site (KAJIMA, 2000).

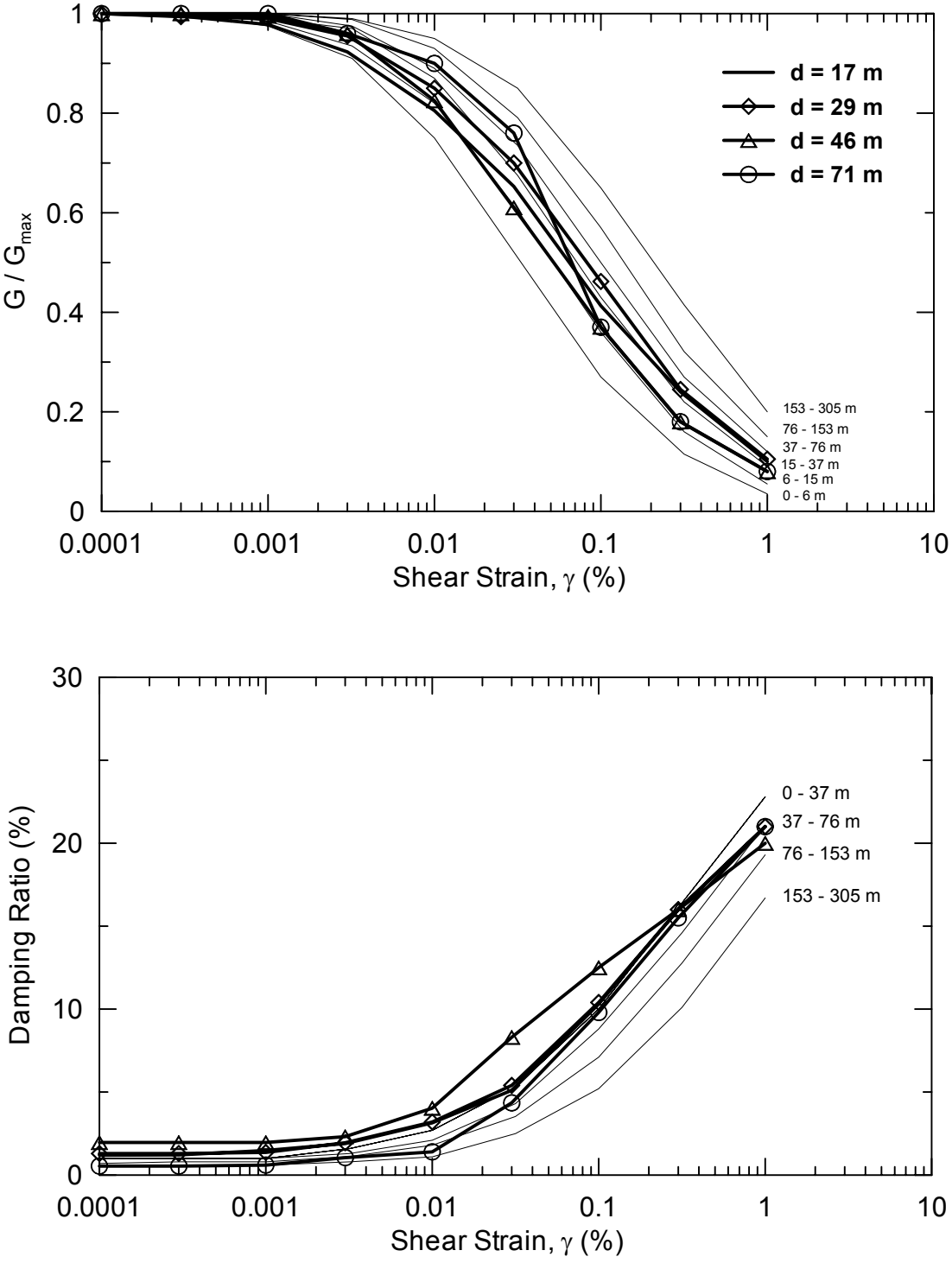

Fig. 3.11 Material specific modulus reduction (G/Gmax) and damping ratio curves for North Palm Springs strong motion recording site (KAJIMA, 2000).

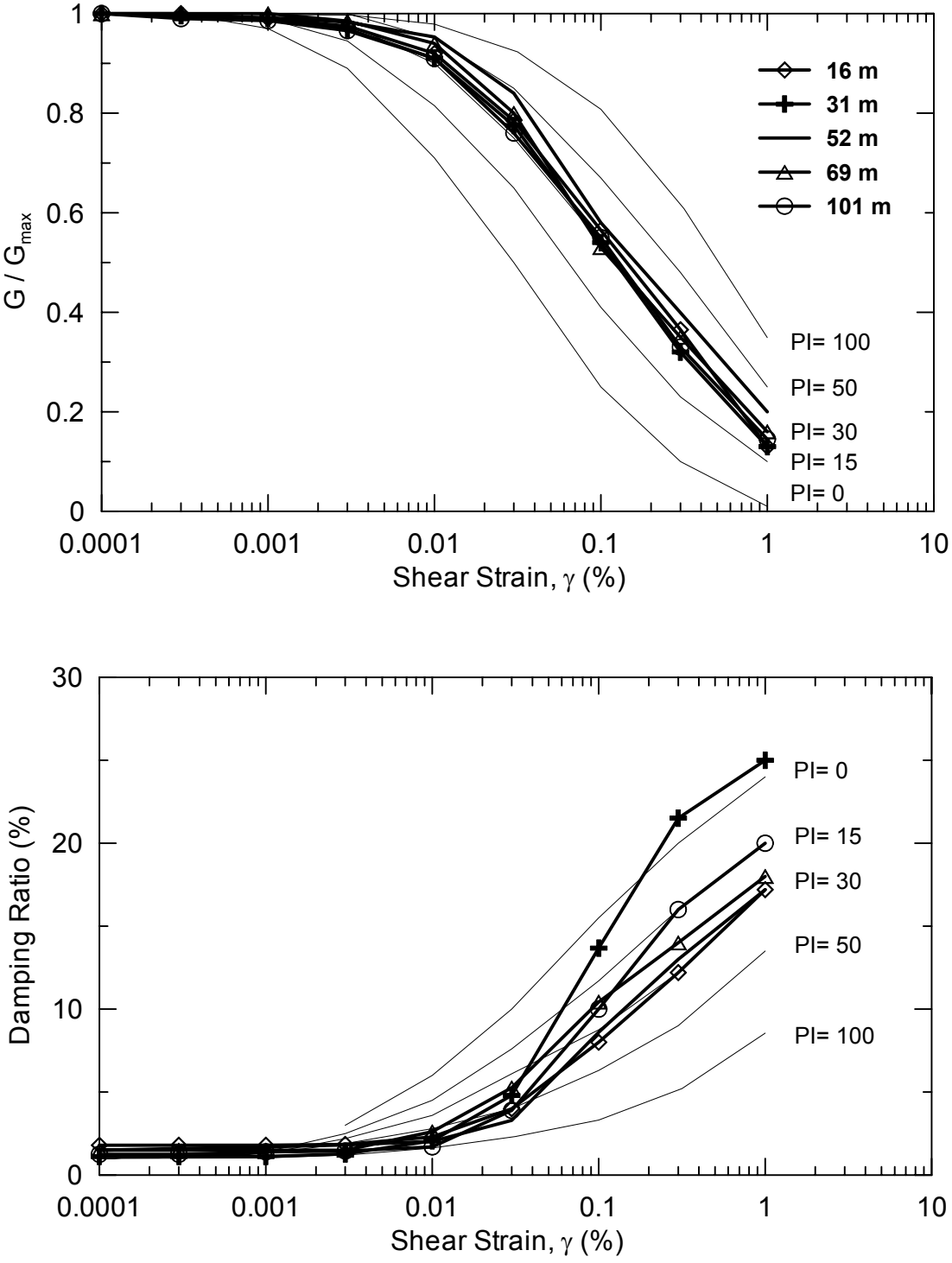

Fig. 3.12 Material specific modulus reduction (G/Gmax) and damping ratio curves for El Centro Array #7 strong motion recording site (KAJIMA, 2000)

Curves describing the variation of G/G_{max} and β with shear strain can also be derived from back analysis of regional strong motion data. Such an analysis was performed by Silva et al. (1997). In that study, ground motions were predicted using a stochastic finite fault model with site effects estimated through 1-D equivalent linear ground response calculations. Curves describing G/G_{max} and β variations with shear strain were adjusted to match the model predictions to the observed data. The results indicated that modulus reduction and damping curves for the Peninsular Range (e.g., Los Angeles area) should be more linear than suggested by standard curve sets (EPRI, 1993, curves). Silva et al. (1997) suggested the use of the following curves for the Peninsular Range:

Soils at 0 –15 m: use 15 – 37 m EPRI (1993) curves

Soils at > 15 m: use 153 – 305 m EPRI (1993) curves

Soils at > 153 m: use linear modulus reduction curve (no reduction) with 153 – 305 m EPRI (1993) damping curves.

Curves for other regions of California were also evaluated by Silva et al. (1997, 2000) using the same approach. Suggested curves for these regions are as follows:

1) **North Coast region (except soft clay sites around San Francisco Bay) and Mojave Desert region: Use EPRI (1993) curves down to 153 m depth and same curves as for Los Angeles region below 153 m.**
2) **San Francisco Bay area locations underlain by Bay Mud: Use EPRI (1993) curves for fill and alluvium and use Vucetic and Dobry (1991) PI = 30 curves for young and old Bay Mud. Use same curves as for the Los Angeles region below 153 m.**
3) **Imperial Valley region: For depths < 153 m, use more linear modulus curves than the Vucetic and Dobry (1991) curves for cohesive soils, as shown in Figure 3.13. Below 153 m depth, use linear modulus curves with the damping curve suggested for depths below 90 m (Figure 3.13).**

No formal consensus has been reached on standard curves that should be used for ground response analysis. The protocols for modulus reduction and damping curve selection for this study are presented in Chapter 5 (Table 5.2).

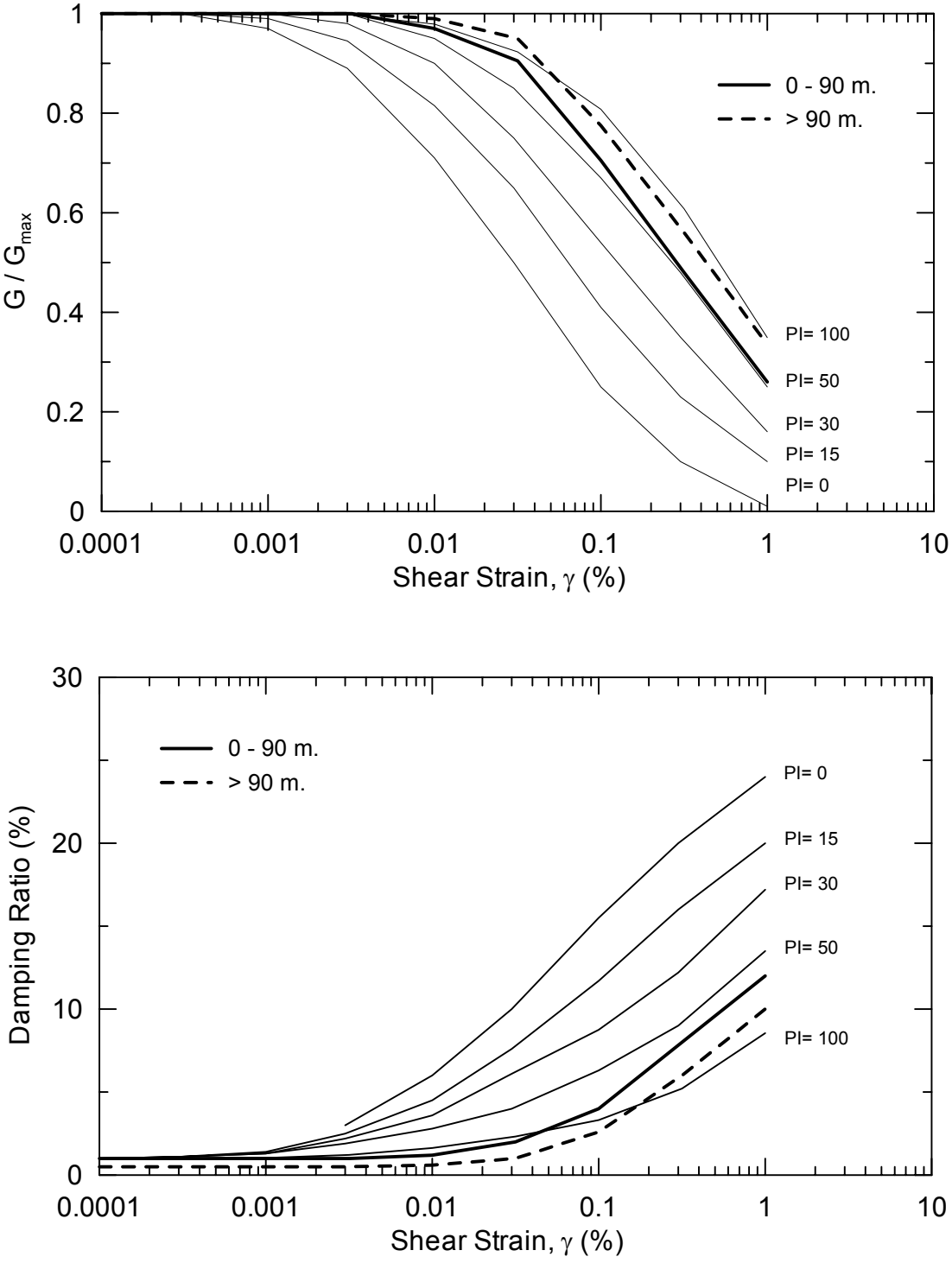

Fig. 3.13 The curves suggested by Silva et al. (1997) for use in ground response analysis at Imperial Valley sites. The curves are shown in comparison with Vucetic and Dobry (1991) curves for cohesive soils.

3.4.2 Computational Models

Ground response analysis models solve the one-dimensional wave propagation problem for a layered, nonlinear medium. The principal characteristic distinguishing various analysis routines is the manner in which nonlinear soil properties are modeled in the analysis. There are two general categories of models for representing nonlinear soil behavior in ground response analyses: equivalent-linear and fully-nonlinear models. The ground response analyses discussed subsequently in this thesis utilize an equivalent linear model, and hence this model is discussed below. Nonlinear models are not used herein, and hence are not discussed, although an overview can be found in Stewart et al. (2001).

The nonlinear behavior of soil can be modeled by an equivalent-linear characterization of dynamic soil properties (Seed and Idriss, 1970). The equivalent-linear method models the nonlinear variation of soil shear moduli and damping ratio as a function of shear strain. The hysteretic stress-strain behavior of soils under symmetrical loading is represented by an equivalent modulus, G, and an equivalent damping ratio, β, as introduced in Section 3.4.1. An iterative procedure, based on linear dynamic analysis, is performed to find the G and β corresponding to the computed shear strains. Initial estimates of the shear strains and corresponding estimates of G and β are provided for the first iteration. For the second and subsequent iterations, G and β values corresponding to an "effective" strain are determined. This "effective" strain is calculated as a fraction (n) of the maximum strain from the previous iteration. Idriss and Sun (1992) recommend that n be taken as a function of earthquake magnitude (m) as follows:

$$n = \frac{m-1}{10} \tag{3.8}$$

Iterations are repeated until estimated and computed values of G and β match within a specified level of tolerance.

The most widely used computer program currently utilizing this model is SHAKE91 (Idriss and Sun, 1992), which is a modified version of the program SHAKE (Schnabel et al., 1972). The program uses an equivalent-linear, total stress analysis procedure to compute the response of a one-dimensional, horizontally layered viscoelastic system subjected to vertically propagating shear waves. The program uses the exact continuum solution to the

wave equation adapted for use with transient motions through the Fast Fourier Transform algorithm. While SHAKE91 has some practical limits, such as maximum number of soil properties (13) and horizontal layers (50), other computer programs implementing the same method that have fewer limitations (e.g., EERA, 1998).

3.5 MODELS FOR BASIN RESPONSE

3.5.1 Introduction

A basin consists of alluvial deposits and sedimentary rocks that are geologically younger and have lower seismic wave velocities than the underlying rocks upon which they have been deposited (Stewart et al., 2001). These deposits may have thicknesses from hundreds of meters to tens of kilometers with lower seismic wave velocities than the underlying rock. For the purpose of this study, we distinguish basin response effects from ground response effects as follows. Local ground response refers to the influence of relatively shallow geologic materials on (nearly) vertically propagating waves. The term basin effects refers to the influence of two- or three-dimensional sedimentary basin structures on ground motions, including critical body wave reflections and surface wave generation at basin edges. The scale of numerical models for ground response and basin effects are different, ground response models being on the order of tens to perhaps hundreds of meters and basin models often being on the order of kilometers.

The physics associated with basin effects are shown in Figure 3.14. The left side of the figure shows a wave entering a horizontal soil layer (i.e., no basin effect), in which case motions are amplified only as a result of the impedance contrast between the underlying rock and the soil layer. The right side of the figure shows a basin model in which a wave is entering the basin in the direction of basin thickening. The wave can become trapped in the basin if post-critical incidence angles develop, which can in turn generate a surface wave that propagates across the basin. The net effect can be a significant increase in the amplitude and duration of ground motions in basins relative to what would occur on a flat layer. Based on analysis of recordings from a number of recent earthquakes (1971 San Fernando, 1994 Northridge, and 1995 Kobe earthquakes), the effect on amplitude is

typically concentrated at intermediate and low frequencies (i.e., f < ~1 Hz) (e.g., Graves et al., 1998; Kawase and Nagato, 2000; Boatwright et al., 2001).

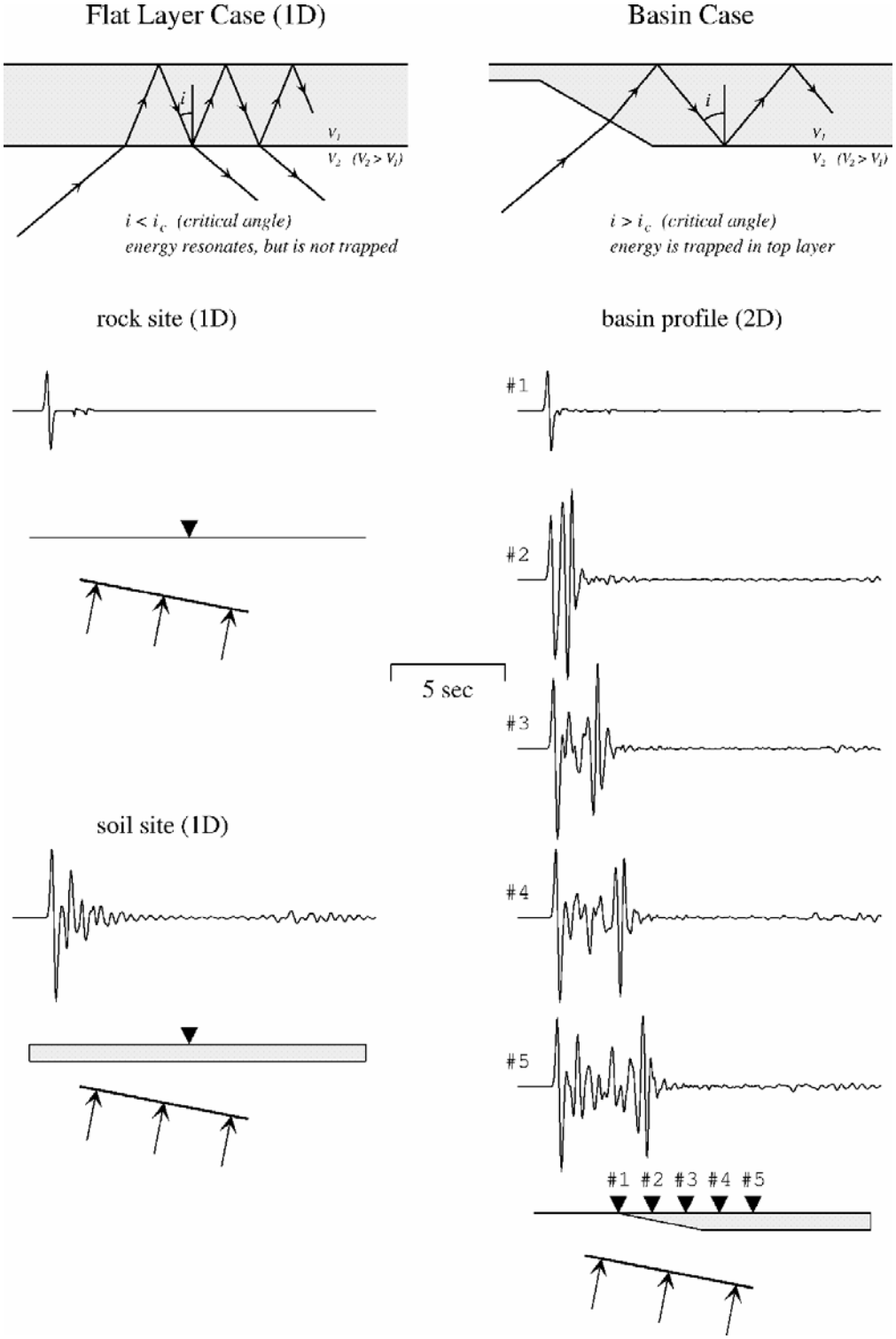

Fig. 3.14. Schematic diagram showing that seismic waves entering a sedimentary layer from below will resonate within the layer but escape if the layer is flat (left) but become trapped in the layer if it has varying thickness and the wave enters the layer through its edge (right). Source: Graves (1993).

Models for basin response effects can be categorized as (1) numerical models utilizing a finite difference or finite element discretization of a medium, which calculate the response of the basin to a specific input wave field, and (2) empirical models in which amplification factors are estimated as a function of basin geometric parameters. In this study, we utilize empirical basin models, which are described in the remainder of this section. Additional information on basin response effects can be found in Stewart et al. (2001).

3.5.2 Empirical Models for Basin Response

The most significant efforts to date to develop empirical models for basin response effects utilized the southern California strong motion database of Steidl and Lee (2000) and the Los Angeles area basin models of Magistrale et al. (2000). The objective of these studies was to develop amplification factors using a non-reference site approach (i.e., individual amplification factors taken as the residuals from an existing statistical ground motion model). These studies were performed jointly through the Southern California Earthquake Center by Field (2000), Steidl (2000), Lee and Anderson (2000), and Joyner (2000). The basin geometric parameters considered in these studies are as follows:

Depth: Field; Steidl; Lee and Anderson

Distance to basin edge: Joyner

The model by Field (2000) defines basin depth as the depth to the V_s = 2.5 km/s isosurface in the Magistrale et al. (2000) basin model. Field first derived regression parameters for the Boore et al. (1997) attenuation relationship, which incorporates V_{s-30} as a site parameter, using the southern California database of Steidl and Lee (2000). Residuals of this attenuation model (individual residuals being estimated using the appropriate site term in the attenuation model) were then evaluated with respect to basin depth. Shown in Figure 3.15 are the resulting relationships between basin depth and residuals for the ground motion parameters of PHA and spectral acceleration at 0.3, 1.0 and 3.0 s. The

dependence of residuals on basin depth was considered by Field to be significant at all periods. The substantial influence of basin effects can be illustrated by the best-fit line for 1.0 s spectral acceleration, which indicates twice the ground motion amplitude at 6 km depth as compared to 0 km depth.

Steidl (2000) utilized an approach similar to that of Field (2000), except that the residuals were calculated using amplification-adjusted predictions from a rock attenuation model. The attenuation model is the Sadigh et al. (1993) relation for rock sites in active regions. The amplification factors were derived as a function of age-based surface geology (Quaternary-Tertiary-Mesozoic classifications), and were presented previously in Section 3.3.4. The resulting relationship between residuals and basin depth are shown in Figure 3.16.

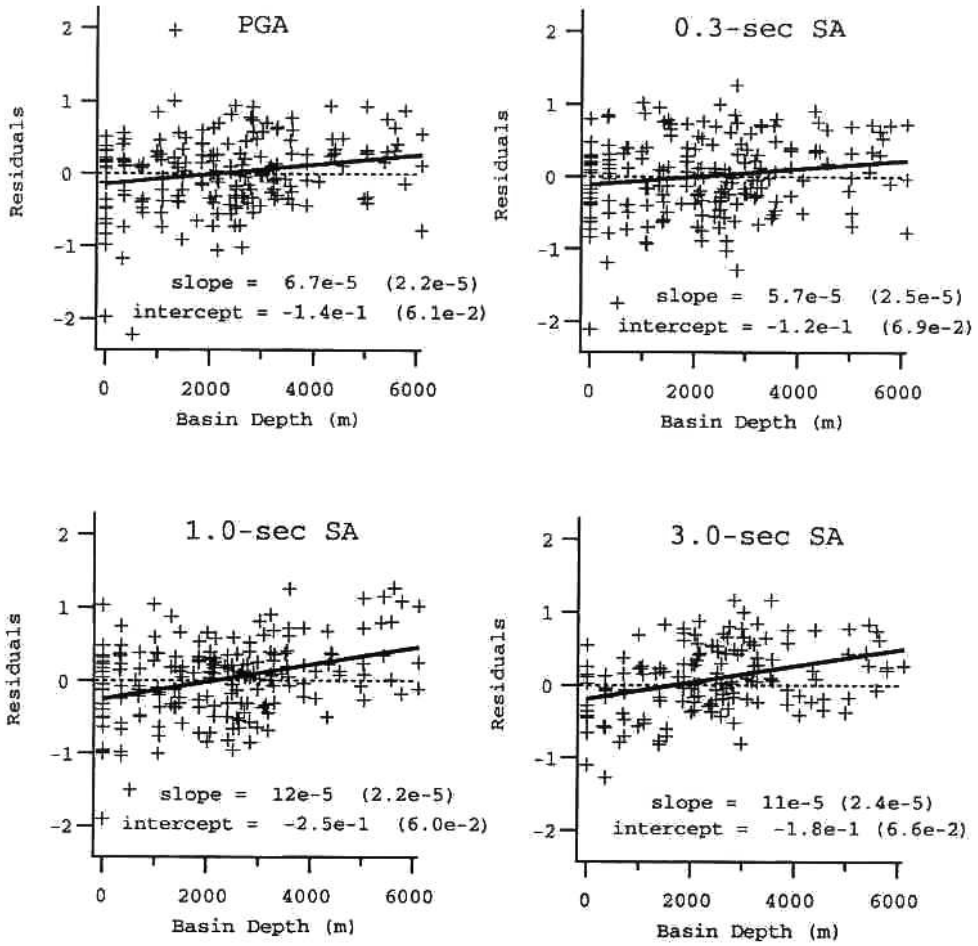

Figure 3.15. Inter-event corrected residuals versus basin depth (depth to V_s = 2.5 km/s isosurface). The values listed in parentheses are the one-sigma uncertainties (Field, 2000).

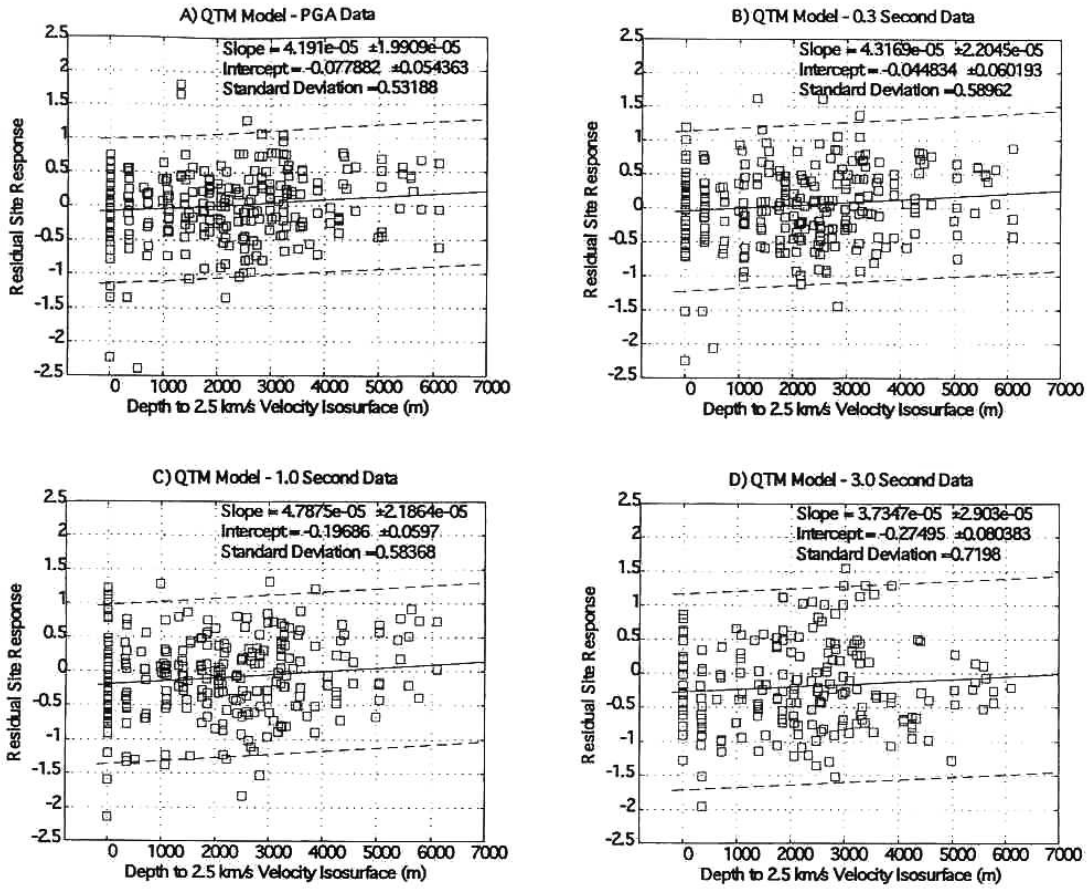

Figure 3.16. Residual site response with respect to the average QTM (Quaternary- Tertiary-Mesozoic) amplification factors plotted versus the basin depth. Least-squares fit to residuals plotted as solid line with slope and intercept shown. a) PGA, b) 0.3 sec period, c) 1.0 sec period, d) 3.0 sec period (Steidl, 2000).

The approach used by Lee and Anderson (2000) was similar to that of Field (2000), except that the Abrahamson and Silva (1997) soil attenuation relationship was used to calculate residuals. The dependence of these residuals on a number of parameters was then investigated, including depth to basement and 3D/1D amplification from theoretical models. However, since basin depth was found to be correlated to 3D/1D amplification, it was noted that there is no need to apply both corrections. Figure 3.17a shows the variation of residuals with basin depth, which shows trends similar to those found by Field (2000)

and Steidl (2000). Lee and Anderson performed a second phase of analysis in which residuals were adjusted using the basin depth model, and a new set of residuals was evaluated for comparison to other parameters (geology, weak motion amplification, and kappa from weak motion). Only surface geology had noticeable (although small) correlations to these residuals. The final form of the prediction equation for ground motion estimation was then given as,

$$\ln(SA_1) = \ln(SA_0) + (\alpha \times depth + \beta) + C_{geo}$$

(3.9)

where SA_1 is the adjusted median spectral acceleration, SA_0 is the median spectral acceleration determined by Abrahamson and Silva (1997) soil attenuation relationship, α is the slope of fitting line in Figure 3.17, β is the intercept of the line, and C_{geo} is the mean residual for each of the detailed geology categories after the basin depth adjustment, as listed in Table 3.1. The standard errors at four different periods before and after the basin depth and detailed geology corrections are summarized in Table 3.2. The relative contributions to the standard error ($\sigma_{depth/geology}$) is calculated using the following equation,

$$\sigma^2_{depth/geo\log y} = \sigma^2_{ori} - \sigma^2_{new}$$

(3.10)

where σ_{ori} is the standard error before adjustments, and σ_{new} is the standard error after the adjustments. It was noted that the adjustments result in a decrease in the total standard error, although the reduction is small.

The relationship between prediction residuals and basin depth from the above three models (Field, Steidl, Lee and Anderson) are compared in Figure 3.18. Both the slopes and values of the residuals at PHA and 0.3 s spectral acceleration are close to each other. At long periods, the residual values diverge significantly, with Steidl having the lowest residuals and Field the highest. Interestingly, at 3.0 s period, Steidl's residuals are negative across the full range of basin depths. The slopes of the residual curves from the Field and Lee and Anderson models are consistent, whereas the Steidl curves are flatter. In general, the slopes of the residual curves increases with increasing period, indicating the increasing importance of basin effects at long periods. With the Lee and Anderson and Field models, the residual ordinates are negative at depths less than ~2 km (which is

approximately the median of basin depths used with all three models), and positive at larger depths. This negative values at shallow depths and positive values at large depths suggest that the basin depth effect had been incorporated into the amplification factors for the "average" basin depth of approximately 2 km.

a)

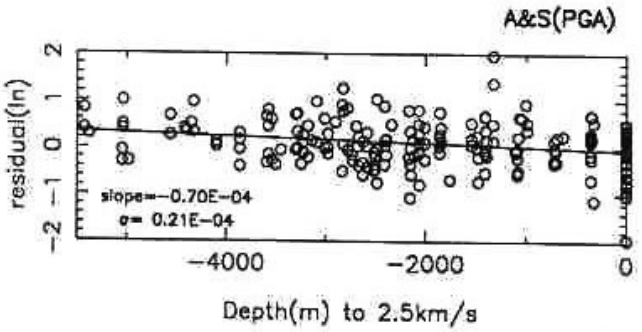

b)

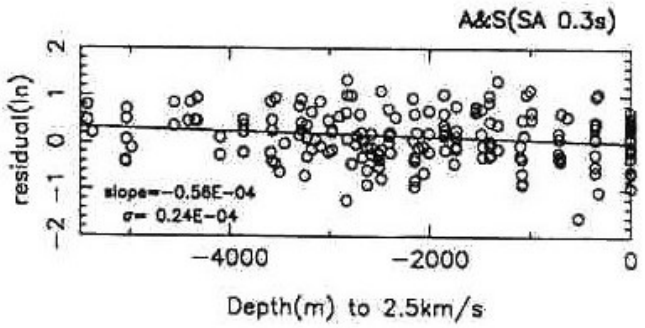

c)

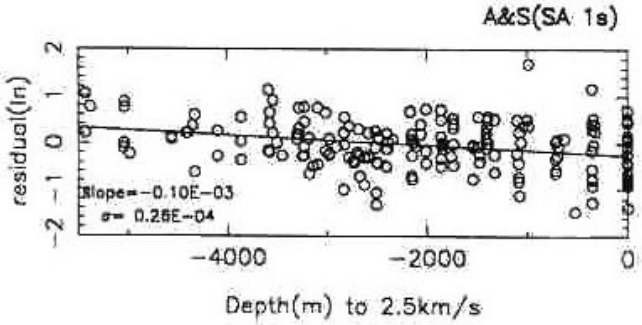

d)

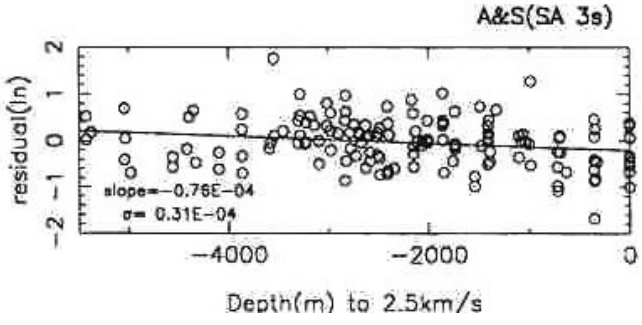

Figure 3.17. Correlation of the residuals from the Abrahamson and Silva (1997) attenuation relationship with depth (in m) to the 2.5 km/s V_s isosurface. The slope of the least-squares fit to residuals and the uncertainty on slope is given in the plot (Lee and Anderson, 2000).

Table 3.1 Statistical misfit parameters for recordings on selected types of surface geology in the Los Angeles Basin after residuals have been adjusted for the depth to basement (Lee and Anderson, 2000).

Peak Acceleration

	μ	σ_μ	σ	σ_σ	N
Qyf	0.00	0.17	0.71	0.24	17
Qym	-0.02	0.06	0.39	0.08	48
Qyc	0.03	0.09	0.40	0.12	21
Qof	-0.16	0.16	0.42	0.20	7
Qom	-0.01	0.09	0.49	0.12	32
Tss	0.23	0.18	0.81	0.24	21
Mxb	-0.21	0.17	0.55	0.22	11

SA at 0.3 s

	μ	σ_μ	σ	σ_σ	N
Qyf	-0.07	0.19	0.77	0.13	17
Qym	0.05	0.07	0.49	0.05	48
Qyc	0.01	0.10	0.45	0.07	21
Qof	-0.12	0.20	0.54	0.14	7
Qom	-0.09	0.08	0.46	0.06	32
Tss	0.42	0.18	0.84	0.13	21
Mxb	-0.10	0.17	0.57	0.12	11

SA at 1.0 s

	μ	σ_μ	σ	σ_σ	N
Qyf	-0.03	0.17	0.70	0.12	17
Qym	-0.05	0.06	0.44	0.04	48
Qyc	0.08	0.12	0.55	0.08	21
Qof	0.02	0.17	0.44	0.12	7
Qom	0.03	0.07	0.39	0.05	32
Tss	0.20	0.14	0.63	0.10	21
Mxb	0.12	0.21	0.66	0.15	11

SA at 3 s

	μ	σ_μ	σ	σ_σ	N
Qyf	0.03	0.12	0.45	0.08	15
Qym	-0.07	0.06	0.39	0.04	44
Qyc	-0.22	0.12	0.50	0.08	18
Qof	0.17	0.21	0.50	0.15	6
Qom	0.00	0.11	0.46	0.08	18
Tss	0.08	0.15	0.56	0.11	15
Mxb	0.15	0.18	0.49	0.13	7

Table 3.2 Comparison of reduction in the standard error after the basin depth and detailed geology adjustments (Lee and Anderson, 2000).

	σ_{subset}	bias	σ (after depth correction)	σ (after depth and geology correction)	$\sigma_{depth/geology}$
PGA	0.644	0.12	0.631	0.622	0.17
SA at 0.3 s	0.708	0.15	0.701	0.682	0.1
SA at 1.0 s	0.636	0.03	0.614	0.608	0.19
SA at 3.0 s	0.589	-0.05	0.583	0.574	0.13

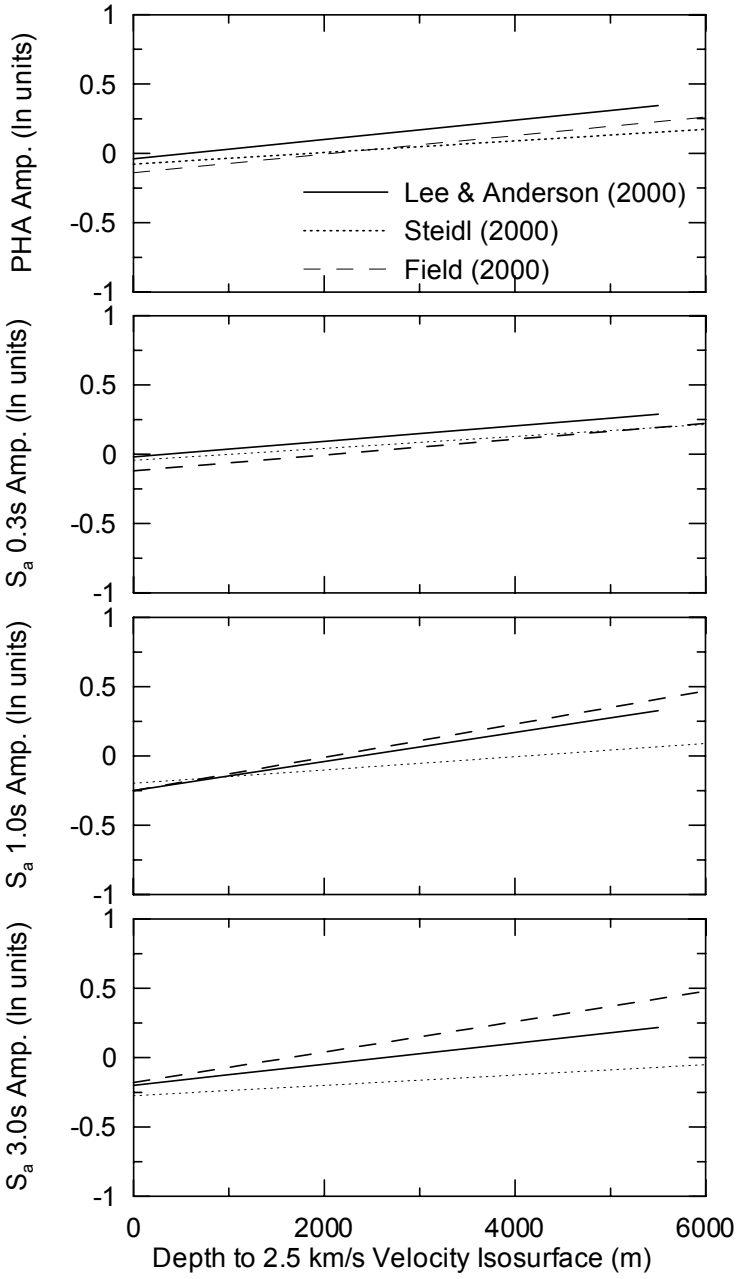

Figure 3.18. Median amplification factors from empirical basin models

4 SITE SELECTION

As noted in Chapter 1, the principal purpose of this study is to compare the residuals of ground motion predictions made using 1-D ground response analyses with those made using more simplified methods (such as an attenuation relationship or attenuation with amplification factors). Discussed in this chapter are the criteria by which the strong motion recording sites used to make these comparisons were selected. Also discussed are the ranges of site conditions present at the sites and the parameter space of ground motion intensity measures that is covered by the strong motion recordings at those sites.

4.1 SITE SELECTION CRITERIA

The principal criteria used for site selection were: (1) ground conditions must be well characterized, including in situ measurements of shear wave velocity and detailed descriptions of material type, and (2) at least one strong motion recording must be available.

An extensive effort was made in this study to compile information on soil conditions at strong motion accelerograph (SMA) stations. A GIS database was developed having the locations of both strong motion stations and boreholes in California. Each strong motion station location was checked with instrument owners (USGS and CSMIP), or against published reports (USC – Anderson et al., 1981), to optimize accuracy. Borehole locations were generally obtained from maps in reports. The borehole database is similar to that of Wills and Silva (1998), but also contains additional Caltrans boreholes, boreholes from selected consulting geotechnical engineers, and data compiled in the ROSRINE program (**http://geoinfo.usc.edu/rosrine/**). These databases were used to match boreholes with strong motion sites.

An SMA site was considered as matched to a borehole if the borehole-SMA separation distance is less than about 150 m and the two locations have the same surficial geology. Approximately 150 such sites were identified using the GIS database discussed above. A site

with a matched borehole was considered suitable for use in this study if (a) shear wave velocity measurements are available at the site (either from the borehole or from non-invasive surface wave techniques) and (b) the soil type descriptions and shear wave velocity profile extended to sufficient depths that a reasonable model of the soil profile can be developed for ground response analyses. The selected sites have profiles that extend to materials field-classified as bedrock (typically based on the physical structure of the material, and not necessarily the stiffness) or to a depth where measured shear wave velocities exceed about 600 m/s. In addition, some sites were selected that are underlain by very deep sediments that do not reach velocities > 600 m/s within the upper several hundred meters (these include sites in Imperial Valley and the Los Angeles basin). Our justification for use of these sites is that previous studies have found that details of the site profile below the upper 100 m do not significantly affect the results of ground response calculations (Roblee et al., 1996). Of the approximately 150 SMA sites matched to boreholes, the 68 sites listed in Table 4.1 were selected for use in this study.

It should be noted that at several sites, the borehole at the site was supplemented with available geological information to estimate the depth of the sediments and the shear wave velocity of the bedrock. These sites are Oakland Outer Harbor Wharf, Oakland 2-Story, Sunnyvale Colton Avenue, Alameda Naval Air Station, Apeel #1, Apeel #2, Emeryville, Foster City, and San Francisco Airport.

As listed in Table 4.1, the borehole data for the 68 selected sites were derived principally from: (1) the ROSRINE program initiated after the Northridge earthquake and recently extended to northern California and Imperial Valley (**http://geoinfo.usc.edu/rosrine/**); (2) the U.S. Geological Survey's post-Loma Prieta and post-Northridge SMA site investigation programs (published in USGS Open File Reports: 91-311, 92-287, 93-376, 93-502, 94-222, 94-552, 99-446); (3) the post-Loma Prieta site investigation program performed jointly by the Electrical Power Research Institute and California Universities for Research in Earthquake Engineering (Nigbor and Steller, 1993); and (4) a site characterization program conducted in the mid- to late-1970s for the Nuclear Regulatory Commission (Shannon and Wilson/Agbabian Associates, 1980).

Table 4.1. Strong motion station information

Station ID				Geology			30-m V_s and Geotechnical Data						
Location	**Station Name**	**Agency**	**Station #**	**Age**	**Dep. History**	**Reference[1]**	**V_{s-30} (m/s)**	**NEHRP**	**soil d. (m)[3]**	**Geot.**	**z_1 (m)**	**$z_{2.5}$ (m)**	**Reference[2]**
Agnew	Agnews Hospital	CSMIP	57066	Holocene	Alluvial Fan	DOC, GEOM	262	D	>70	D	758	2400	UJBLPE, N&S(1993)
Alameda	Naval Air Station	BYU	-	Holocene	Marine	boring	188	E	152	E1	222	2400	USGS OFR 92-287
Bear Valley	Callens Ranch	USGS	1474	Pleistocene	-	DOC	382	C	30	C2	829	3000	USGS OFR 94-552
Capitola	Fire Station	CSMIP	47125	Holocene	Alluvium	DOC	290	D	60	C3	63	853	USGS OFR 93-502, N&S(1993)
Corralitos	Eureka Canyon Road	CSMIP	57007	Tertiary	-	DOC, GEOM	458	C	28	C1	829	5066	USGS OFR 93-376
El Centro	El Centro Array #7	USGS	5028	Holocene	Lacustrine	DOC, GEOM	216	D	>104	DC	-	-	KAJIMA
El Centro	El Centro Array #9	USGS	117	Holocene	Lacustrine	DOC, GEOM	218	D	>240	D3	-	-	USGS OFR 84-562, SW/AA
El Centro	Meloland Overcrossing	CSMIP	5155	Holocene	Lacustrine	DOC, GEOM	195	E	>240	E1	-	-	ROSRINE
Emeryville	Pacific Park Plaza	USGS	1662	Holocene	Marine	DOC, GEOM	198	E	150	E1	222	2400	USGS OFR 94-222
Eureka FF	Myrtle & West Avenue	CSMIP	89509	Holocene	Marine	DOC, GEOM	274	D	>110	D	-	-	UCB/EERC-97/01
Foster City	Apeel #1	CSMIP	58375	Holocene	Marine	DOC, GEOM	114	E	190	E2	222	2400	USGS OFR 93-376
Foster City	Beach Park Boulevard	USGS	1001	Holocene	Marine	DOC, GEOM	126	E	110	E2	222	2400	USGS OFR 94-222
Fremont	Mission San Jose	CSMIP	57064	Pleistocene	Alluvium	DOC, GEOM	350	D	>77	D	829	2400	UJBLPE
Gilroy	Gilroy Array #7	CSMIP	57425	Holocene	Alluvial Fan	DOC, GEOM	337	D	17	C2	108	3000	USGS OFR 93-502, 93-376
Gilroy	Gavilan College	CSMIP	47006	Mesozoic	-	DOC, GEOM	744	C	12	C2	115	2400	SW/AA, USGS OFR 91-311
Gilroy	Gilroy Array #2	CSMIP	47380	Holocene	Alluvium	DOC	274	D	165	D1C	219	2400	USGS OFR 92-287, EPRI (1993)
Gilroy	Gilroy #3	CDMG	47381	Holocene	Alluvium	DOC, GEOM	291	D	140	D	556	2400	ROSRINE
Gilroy	Gilroy #6	CDMG	57383	Tertiary	-	DOC, GEOM	589	C	22	C1	534	2409	KAJIMA
Halls Valley	Halls Valley	CSMIP	57191	Holocene	-	DOC, GEOM	268	D	46	C3	97	3000	USGS OFR 93-502, N&S(1993)
Hollister	City Hall	USGS	1028	Holocene	-	DOC, GEOM	200	D	>105	D	829	3000	SW/AA, USGS OFR 91-311
Hollister	SAGO-South	CSMIP	47189	Mesozoic	-	DOC, GEOM	708	C	12	C1	104	1438	N&S(1993)/ UJBLPE
Imperial	Superstition Mtn. Top	USGS	286	Mesozoic	-	DOC	350	D	30	C1	-	-	ROSRINE
Joshua Tree	Fire Station	CDMG	22170	Holocene	-	GEOM	343	D	73	D	-	-	ROSRINE
Larkspur	Ferry Terminal	USGS	1590	Holocene	Marine	DOC	178	E	30	E2	117	2400	USGS OFR 94-222
Los Angeles	Dayton School	USC	90021	Holocene	Alluvial Valley	CDMG	314	D	36	C3	230	2113	ROSRINE
Los Angeles	ETEC, RD7	USGS	5108	Mesozoic	-	CDMG	707	C	12	C2	100	100	USGS OFR 00-470
Los Angeles	Rinaldi Receiving Stn.	LADWP	77, 5968	Pleistocene	Alluvial Fan	CDMG	327	D	13	C2	139	4537	USGS OFR 99-446
Los Angeles	Sylmar Converter West	LADWP	74	Holocene	Alluvial Fan	CDMG	251	D	>87	D	783	6155	USGS OFR 99-446
Los Angeles	Arleta Fire Station	CSMIP	24087	Holocene	Alluvial Fan	CDMG, GEOM	293	D	101	D1S	746	2175	ROSRINE
Los Angeles	Epiphany	USC	90053	Holocene	Alluvial Fan	CDMG	287	D	73	D2C	453	2840	USGS OFR 99-446
Los Angeles	Hollywood Storage Bldg.	CSMIP, CT	24303, 135	Holocene	Alluvial Valley	CDMG, GEOM	332	D	48	C3	220	2188	SW/AA
Los Angeles	Brentwood VA	USGS	638	Pleistocene	Alluvial Valley	CDMG	408	C	>100	D2S	285	1004	USGS OFR 00-470
Los Angeles	Obregon Park	CSMIP	24400	Holocene	Alluvial Valley	GEOM	453	C	>65	D	557	3315	ROSRINE, USGS OFR 00-470
Los Angeles	Wadsworth VA N.	USGS	5082	Pleistocene	Alluvial Valley	CDMG	427	C	>90	D	339	1292	ROSRINE
Los Angeles	White Oak Church	USC	90003	Pleistocene	Alluvial Fan	CDMG	280	D	81	D	560	3185	USGS OFR 99-446
Los Angeles	Baldwin Hills	CSMIP	24157	Holocene	Fill	CDMG, GEOM	291	D	>92	DS	540	3370	ROSRINE
Los Angeles	Bulk Mail	USGS	5129	Holocene	Alluvial Fan	CDMG, GEOM	303	D	98	D	913	3883	ROSRINE
Los Angeles	Saturn School	USC	90091	Holocene	Alluvial Valley	CDMG	303	D	>100	D	752	3341	ROSRINE
Los Angeles	Sepulveda VA	USGS	637	Pleistocene	Alluvial Fan	CDMG	370	C	>75	D2C	751	4100	USGS OFR 99-446
Los Angeles	Wadsworth VA S.	USGS	5082	Pleistocene	Alluvial Valley	CDMG	405	C	>90	D	468	1588	ROSRINE, USGS OFR 00-470
Los Angeles	Lake Hughes#9	CDMG(CIT)	24272(127)	Holocene		GEOM	638	C	9	C1	13	~50	ROSRINE
Los Angeles	Los Angeles Dam	LADWP(USGS)	2141 (0)	Tertiary	-	CDMG	630	C	25	C1	720	5105	USGS OFR 96-740
Los Angeles	Tarzana	CSMIP	24436	Tertiary	-	CDMG, GEOM	291	D	90	D	100	1028	ROSRINE

Table 4.1. Continued

Station ID				Geology			30-m V_s and Geotechnical Data						
Location	**Station Name**	**Agency**	**Station #**	**Age**	**Dep. History**	**Reference[1]**	**V_{s-30} (m/s)**	**NEHRP**	**soil d. (m)[3]**	**Geot.**	**z_1 (m)**	**$z_{2.5}$ (m)**	**Reference[2]**
Monterey	City Hall	CSMIP	47377	Mesozoic	-	DOC, GEOM	614	C	7	C2	163	853	N&S(1993), UJBLPE
Newhall	Fire Station	CSMIP	24279	Holocene	Alluvial Fan	CDMG	273	D	35-55	C3	725	1365	ROSRINE
Oakland	Title & Trust Bldg. (2-story)	CSMIP	58224	Holocene	Aeolian	DOC	302	D	140	D	222	2400	Guha et al. (1993), N&S(1993)
Oakland	Outer Harbor Wharf	CSMIP	58472	Holocene	Marine	DOC, GEOM	248	D	150	D1C	222	2400	USGS OFR 92-287
Pacoima	Pacoima Kagel Canyon	CSMIP	24088	Tertiary	-	CDMG, GEOM	502	C	7	C1	100	1349	ROSRINE
Palm Springs	Desert Hot Springs	CDMG	12149	Holocene	-	CDMG	384	C	52	C3	-	-	KAJIMA
Palm Springs	North Palm Springs	USGS	5070	Holocene	-	CDMG	394	C	73	D	-	-	KAJIMA
Palm Springs	Devers Hill Substation	SCE	5997	-	-	CDMG	482	C	30	C2	-	-	KAJIMA
Palo Alto	Palo Alto VA	USGS	1227	Pleistocene	-	GEOM	357	D	115	D	678	2400	USGS OFR 92-287
Petrolia	General Store	CDMG	1398, 89156	Holocene	-	DOC, GEOM	343	D	37	C3	-	-	SW/AA
Redwood City	Apeel #2	USGS	1002	Holocene	Marine	DOC, GEOM	136	E	86	E1	118	2400	USGS OFR 93-376
San Francisco	Diamond Heights	CSMIP	58130	Mesozoic	-	DOC	588	C	13	C1	105	2400	N&S(1993), UJBLPE
San Francisco	Yerba Buena Island	CSMIP	58163	Mesozoic	-	DOC	567	C	15	C1	116	2400	USGS OFR 92-287
San Francisco	International Airport	CSMIP	58223	Holocene	Marine	DOC	227	E	152	E1	118	2400	USGS OFR 92-287
Santa Barbara	Courthouse	USGS	283	Holocene	-	GEOM	392	C	98	D	-	-	SW/AA
Santa Clara	IBM Alm., Santa Teresa Hill	CDMG	57563	Mesozoic	-	DOC	629	C	6	C1	115	2400	ROSRINE
Santa Clarita	Potrero Canyon	USC	90056	Holocene	Alluvial Fan	CDMG	279	D	18	C2	322	3381	ROSRINE
Santa Cruz	UCSC Lick Observatory	CSMIP	58135	Mesozoic	-	DOC	700	C	8	C2	59	853	N&S(1993), USGS OFR 93-502
Simi Valley	Knolls School	USC	90055	Holocene	Alluvial Fan	CDMG	579	C	13	C2	100	100	USGS OFR 99-446, N&S(1993)
Sunnyvale	Colton	USGS	1695	Holocene	Alluvial Valley	DOC, GEOM	268	D	>120	D	520	2400	USGS OFR 94-222
Sylmar	Olive View Hospital	CDMG	24514	Holocene	Fill	CDMG, GEOM	357	D	80	D2	800	8945	USGS OFR 99-446
Sylmar	Converter Station East	DWP	75	Pleistocene	Alluvial Fan	CDMG, boring	366	C	>92	D	800	6522	USGS OFR 00-470
Sylmar	Jensen Gen. Bldg.	USGS	655	Pleistocene	Alluvial Fan	CDMG, boring	519	C	7	C1	780	5405	USGS OFR 99-446
Taft	Lincoln School	USGS	1095	-	-	-	386	C	42	C3	-	-	SW/AA
Yermo	Fire Station	CDMG	22074	Holocene	-	GEOM	340	D	>105	D	-	-	ROSRINE

[1] GEOM : Geomatrix (1993)
DOC : 1:500 000 scale geology maps by California Department of Mines and Geology
CDMG : Geology maps by Calilfornia Department of Mines and Geology

[2] N&S(1993) : Nigbor and Steller (1993)
SW/AA : Shannon & Wilson/Agbabian Associates (1980)
UJBLPE : Thiel and Schneider (1993)

[3] soil d.(m) : Soil depth to competent bedrock, the depth to a layer with Vs > 760 m/s, or the depth to a significant impedance contrast between surficial soil deposits and underlying harder material (Rodriguez-Marek et al., 2001)

4.2 PARAMETER SPACE SPANNED BY SELECTED SITES AND MOTIONS FROM THOSE SITES

Each of the strong motion sites selected for use in this study was classified based on the geologic, NEHRP ($V_{s\text{-}30}$), and geotechnical classification schemes described previously in Chapter 2. These classifications are provided in Table 4.1. Histograms showing the breakdown of sites (and the number of recordings from those sites) into the various categories are provided in Figure 4.1.

There are 134 recordings available from the 68 sites selected for this study. The earthquakes that generated those recordings and the corresponding intensity measures (*IM*s) are provided in Table 4.2. The *IM* parameter spaces covered by the data set are shown in Figures 4.2 (spectral accelerations), 4.3 (peak ground velocity) and 4.4 (Arias intensity, significant duration, and mean period). The 5- and 95-percentile limits on various *IM*s in the database are as follows:

PHA:	0.03g – 0.8g
S_a at 0.3s:	0.06g – 2.0g
S_a at 1.0s:	0.02g – 0.8g
S_a at 3.0s:	0.002g – 0.4g
PHV:	0.4 cm/s - 100 cm/s
Arias Intensity, I_a:	2 – 550 cm/s
5-75% significant duration, $D_{5\text{-}75}$:	1 – 25 s
5-95% significant duration, $D_{5\text{-}95}$:	5 – 40 s
Mean period, T_m:	0.2 – 1.2 s

The significant duration parameters are defined based on the time spanned between the indicated percentages of normalized Arias intensity. The mean period (T_m) is defined as (Rathje et al., 1998):

$$T_m = \frac{\sum C_i^2 \left(\frac{1}{f_i}\right)}{\sum C_i^2} \quad \text{for} \quad 0.25 \le f_i \le 20 \text{ Hz} \tag{4.1}$$

where C_i = Fourier amplitudes of the entire accelerogram, and f_i = discrete Fourier transform frequencies between 0.25 and 20 Hz.

Table 4.2 Recordings used in this study

Location	Station Name	Earthquake	m	r (km)	PHA (g)	S_a 0.3s (g)	S_a 1.0s (g)	S_a 3.0s (g)	PHV (cm/s)	I_a (cm/s)	D_{5-75} (s)	D_{5-95} (s)	T_m (s)
Agnew	Agnews Hospital	Loma Prieta 1989	6.9	28.2	0.17	0.45	0.16	0.111	21.4	40.3	7.8	19.7	0.78
		Morgan Hill 1984	6.2	29.4	0.03	0.09	0.09	0.030	5.2	5.1	22.5	38.1	1.09
Alameda	Naval Air Station	Loma Prieta 1989	6.9	75.2	0.24	0.27	0.45	0.044	30.6	40.3	2.8	5.3	0.93
Bear Valley	Callens Ranch	Loma Prieta 1989	6.9	49	0.07	0.20	0.10	0.039	9.5	9.0	11.3	19.2	0.75
Capitola	Fire Station	Loma Prieta 1989	6.9	14.5	0.48	1.27	0.40	0.056	32.7	334.1	5.6	13.0	0.48
		Morgan Hill 1984	6.2	38.1	0.12	0.31	0.07	0.010	6.3	19.7	4.9	15.0	0.37
Corralitos	Eureka Canyon Road	Morgan Hill 1984	6.2	22.7	0.10	0.19	0.15	0.008	1.5	7.8	4.1	10.2	0.58
		Loma Prieta 1989	6.9	5.1	0.50	1.65	0.51	0.071	10.1	288.4	3.6	7.4	0.53
El Centro	El Centro Array #7	Imperial Valley 1979	6.5	0.6	0.39	0.67	0.65	0.269	72.1	121.7	1.9	5.7	1.11
		Imperial Valley 1979, Aftershock	5.2	13.1	0.16	0.32	0.06	0.004	7.8	7.0	0.5	5.7	0.32
El Centro	El Centro Array #9	Imperial Valley 1940	7	8.3	0.24	0.55	0.36	0.101	30.0	142.8	14.1	24.0	0.55
El Centro	Meloland Overcrossing	Imperial Valley 1979	6.5	0.5	0.30	0.68	0.35	0.237	80.6	85.7	2.7	8.2	1.17
Emeryville	Pacific Park Plaza	Loma Prieta 1989	6.9	76.9	0.23	0.48	0.50	0.043	29.4	68.1	5.1	11.7	0.98
Eureka FF	Myrtle & West Avenue	Cape Mendocino 1992	7.1	44.6	0.17	0.37	0.18	0.064	23.9	31.7	7.7	20.3	0.89
Foster City	Apeel #1	Loma Prieta 1989	6.9	49	0.28	0.50	0.41	0.164	34.8	147.8	6.4	18.5	0.84
Foster City	Beach Park Boulevard	Loma Prieta 1989	6.9	51.2	0.11	0.31	0.19	0.070	20.5	26.1	5.6	14.5	0.92
Fremont	Mission San Jose	Livermore 1980	5.8	29.8	0.05	0.18	0.06	0.010	0.9	2.4	6.1	10.1	0.65
		Livermore 1980, Aftershock	5.4	29.8	0.04	0.07	0.06	0.004	0.6	1.2	2.7	7.8	0.64
		Morgan Hill 1984	6.2	31.4	0.02	0.06	0.04	0.008	0.9	1.4	16.5	27.3	0.72
		Loma Prieta 1989	6.9	43	0.14	0.30	0.12	0.025	4.6	25.2	7.9	17.3	0.49
Gilroy	Gilroy Array #7	Loma Prieta 1989	6.9	24.2	0.27	0.56	0.11	0.018	16.5	76.6	4.5	10.1	0.37
		Morgan Hill 1984	6.2	14	0.15	0.39	0.07	0.015	6.7	24.0	5.0	10.2	0.29
Gilroy	Gavilan College	Loma Prieta 1989	6.9	11.6	0.34	0.86	0.19	0.039	25.3	79.2	1.5	4.9	0.34
		Morgan Hill 1984	6.2	16.2	0.10	0.10	0.02	0.004	3.2	5.4	4.8	8.4	0.21
Gilroy	Gilroy Array #2	Coyote Lake 1979	5.7	7.5	0.27	0.67	0.24	0.025	16.5	38.4	1.4	5.6	0.44
		Loma Prieta 1989	6.9	12.7	0.19	1.01	0.40	0.061	35.9	116.4	2.5	10.7	0.60
		Morgan Hill 1984	6.2	15.1	0.34	0.39	0.09	0.011	8.0	20.1	6.0	13.9	0.38
Gilroy	Gilroy #3	Coyote Lake 1979	5.7	5.7	0.25	0.58	0.38	0.038	4.1	39.6	2.1	8.8	0.57
		Morgan Hill 1984	6.2	14.6	0.20	0.41	0.16	0.034	3.0	33.6	7.0	18.8	0.50
		Loma Prieta 1989	6.9	14.4	0.49	1.20	0.35	0.100	13.6	171.0	2.2	8.3	0.46
Gilroy	Gilroy #6	Coyote Lake 1979	5.7	3.1	0.37	0.89	0.32	0.033	5.4	72.6	0.9	3.4	0.51
		Morgan Hill 1984	6.2	11.8	0.28	0.55	0.29	0.021	3.4	57.5	3.6	7.1	0.45
		Loma Prieta 1989	6.9	19.9	0.17	0.55	0.27	0.031	4.0	32.6	4.5	12.1	0.47

Table 4.2 Continued

Location	Station Name	Earthquake	m	r (km)	PHA (g)	S_a 0.3s (g)	S_a 1.0s (g)	S_a 3.0s (g)	PHV (cm/s)	I_a (cm/s)	D_{5-75} (s)	D_{5-95} (s)	T_m (s)
Halls Valley	Halls Valley	Coyote Lake 1979	5.7	31.2	0.04	0.11	0.04	0.004	3.3	1.9	7.7	19.5	0.47
		Loma Prieta 1989	6.9	31.6	0.12	0.24	0.14	0.030	14.4	25.3	7.9	14.9	0.68
		Morgan Hill 1984	6.2	3.4	0.22	0.49	0.26	0.025	22.2	60.9	8.8	12.8	0.56
Hollister	City Hall	Hollister 1974	5.2	11.1	0.13	0.42	0.05	0.005	8.0	13.0	2.5	9.6	0.38
		Loma Prieta 1989	6.9	28.2	0.23	0.38	0.60	0.125	41.6	92.8	5.4	16.6	0.99
		Morgan Hill 1984	6.2	32.5	0.07	0.17	0.13	0.013	8.2	13.6	12.4	20.9	0.66
Hollister	SAGO-South	Hollister 1986	5.4	14.9	0.06	0.13	0.11	0.011	1.5	3.6	3.7	10.3	0.75
		Loma Prieta 1989	6.9	34.7	0.07	0.13	0.17	0.033	5.8	8.9	6.5	16.6	0.89
Imperial	Superstition Mtn. Top	Imperial Valley 1979	6.5	26	0.15	0.20	0.03	0.015	2.4	13.5	3.7	8.7	0.26
		Westmoreland 1981	5.8	26.5	0.09	0.13	0.04	0.002	0.3	5.5	3.6	9.5	0.29
		Superstition hills (B) 1987	6.7	4.3	0.82	1.40	0.43	0.060	5.9	480.9	8.8	12.2	0.35
Joshua Tree	Fire Station	Big Bear 1992	6.4	38	0.06	0.17	0.08	0.013	6.4	9.2	9.8	20.8	0.53
		Hector Mine 1999	7.1	27	0.17	0.38	0.31	0.047	20.1	46.8	6.9	13.0	0.66
		Landers 1992	7.3	11.6	0.28	0.70	0.47	0.072	34.5	196.5	21.3	26.6	0.76
		North Palm Springs 1986	6	29.8	0.06	0.14	0.06	0.005	3.8	5.0	5.9	12.8	0.48
Larkspur	Ferry Terminal	Loma Prieta 1989	6.9	99.2	0.11	0.23	0.43	0.024	16.6	35.3	6.2	10.5	0.86
Los Angeles	Dayton School	Landers 1992	7.3	159.2	0.04	0.14	0.04	0.015	3.8	5.1	15.8	23.1	0.56
		Northridge 1994	6.7	29	0.38	1.11	0.19	0.021	20.9	128.2	5.5	9.6	0.35
		Whittier Narrows 1987	6	16.6	0.21	0.41	0.09	0.005	7.8	34.8	2.7	7.4	0.26
Los Angeles	ETEC, RD7	Northridge 1994	6.7	19.3	0.28	0.75	0.22	0.039	19.6	97.8	3.9	7.7	0.36
Los Angeles	Rinaldi Receiving Stn.	Northridge 1994	6.7	7.1	0.63	1.86	1.40	0.227	110.1	564.3	3.8	7.2	0.68
Los Angeles	Sylmar Converter West	Northridge 1994	6.7	6.2	0.74	1.14	1.36	0.370	109.9	554.7	4.5	10.3	1.05
Los Angeles	Arleta Fire Station	Northridge 1994	6.7	9.2	0.33	0.69	0.41	0.092	30.7	130.5	6.2	13.4	0.58
		Whittier Narrows 1987	6	38.9	0.09	0.23	0.06	0.004	5.0	10.4	5.3	13.5	0.38
Los Angeles	Epiphany	Northridge 1994	6.7	15.8	0.39	0.96	0.40	0.118	44.2	233.4	6.3	11.2	0.59
		Whittier Narrows 1987	6	47.4	0.13	0.50	0.06	0.005	8.0	20.1	5.3	12.9	0.34
Los Angeles	Hollywood Storage Bldg.	Borrego Mountain 1968	6.8	217.4	0.01	0.02	0.02	0.009	2.6	0.5	17.9	26.0	1.27
		Kern County 1952	7.4	120.5	0.05	0.14	0.10	0.022	5.6	9.0	17.5	30.1	0.73
		Northridge 1994	6.7	25.5	0.29	0.57	0.32	0.036	22.4	137.0	6.1	11.3	0.42
		San Fernando 1971	6.6	21.2	0.19	0.43	0.18	0.069	16.8	53.0	5.0	10.7	0.46
Los Angeles	Brentwood VA	Northridge 1994	6.7	24.7	0.18	0.31	0.23	0.042	20.4	46.4	6.0	11.0	0.64

Table 4.2 Continued

Location	Station Name	Earthquake	m	r (km)	PHA (g)	S_a 0.3s (g)	S_a 1.0s (g)	S_a 3.0s (g)	PHV (cm/s)	I_a (cm/s)	$D_{5\text{-}75}$ (s)	$D_{5\text{-}95}$ (s)	T_m (s)
Los Angeles	Obregon Park	Hector Mine 1999	7.1	186.4	0.03	0.09	0.05	0.015	6.2	3.0	17.3	43.8	0.94
		Landers 1992	7.3	151.4	0.05	0.12	0.08	0.041	10.9	11.5	21.7	40.3	0.94
		Northridge 1994	6.7	37.9	0.45	0.93	0.17	0.010	20.2	124.6	5.6	11.1	0.29
		Northridge 1994, Aftershock	5.9	39.9	0.06	0.07	0.01	0.000	1.7	1.7	2.7	6.9	0.19
		Whittier Narrows 1987	6	13.9	0.42	0.63	0.24	0.014	19.2	115.3	2.8	7.6	0.26
		Whittier Narrows 1987, Aftershock	5.3	14.9	0.31	0.67	0.12	0.008	18.7	42.0	1.3	5.7	0.28
Los Angeles	Wadsworth VA N.	Northridge 1994	6.7	25.2	0.25	0.48	0.23	0.063	23.9	73.0	6.4	12.6	0.48
Los Angeles	White Oak Church	Landers 1992	7.3	176.5	0.04	0.08	0.07	0.044	13.9	8.6	27.6	35.4	1.29
		Northridge 1994	6.7	13.3	0.42	1.13	0.57	0.139	42.2	300.9	5.9	12.9	0.64
		Whittier Narrows 1987	6	39.8	0.14	0.33	0.06	0.007	6.6	19.6	6.9	18.0	0.36
Los Angeles	Baldwin Hills	Northridge 1994	6.7	31	0.22	0.50	0.17	0.051	16.2	64.2	7.8	17.0	0.52
		Northridge 1994, Aftershock	5.2	29.6	0.06	0.09	0.02	0.005	2.5	3.3	7.1	14.5	0.33
		Northridge 1994, Aftershock	5.9	33	0.07	0.15	0.02	0.001	2.5	1.8	3.6	10.5	0.31
		Whittier Narrows 1987	6	27	0.15	0.36	0.10	0.008	8.3	24.6	3.9	14.0	0.35
		Whittier Narrows 1987, Aftershock	5.3	27.6	0.09	0.18	0.09	0.006	8.3	6.3	2.8	8.9	0.51
Los Angeles	Bulk Mail	Northridge 1994	6.7	42.3	0.20	0.60	0.13	0.016	12.9	37.6	7.3	13.7	0.39
		Whittier Narrows 1987	6	12.9	0.39	0.94	0.23	0.013	21.8	99.0	1.9	6.3	0.38
Los Angeles	Saturn School	Northridge 1994	6.7	30	0.46	0.95	0.44	0.039	36.7	133.0	5.3	10.1	0.47
		Whittier Narrows 1987	6	20.8	0.12	0.23	0.05	0.008	5.2	12.5	3.6	11.7	0.26
Los Angeles	Sepulveda VA	Northridge 1994	6.7	8.9	0.84	2.05	0.81	0.184	80.6	564.0	4.4	7.9	0.51
Los Angeles	Wadsworth VA S.	Northridge 1994	6.7	25.56	0.33	0.59	0.31	0.073	26.0	94.1	5.3	10.4	0.48
Los Angeles	Lake Hughes#9	San Fernando 1971	6.6	23.6	0.15	0.19	0.04	0.006	1.2	12.7	2.8	10.5	0.21
		Northridge 1994	6.7	26.8	0.14	0.35	0.04	0.016	3.4	18.0	4.2	8.7	0.27
Los Angeles	Los Angeles Dam	Northridge 1994	6.7	2.6	0.49	0.84	0.57	0.193	17.9	154.6	3.8	6.5	0.81
Los Angeles	Tarzana	Whittier Narrows 1987	6	43	0.54	2.28	0.08	0.007	1.5	217.7	2.6	5.7	0.31
		Whittier Narrows 1987, Aftershock	5.3	42.7	0.09	0.14	0.01	0.001	0.3	4.8	6.4	11.8	0.25
		Landers 1992	7.3	175.6	0.05	0.15	0.07	0.016	4.2	9.9	20.5	37.2	0.63
		Northridge 1994	6.7	17.5	1.33	2.94	0.63	0.113	32.0	1948.6	6.8	11.5	0.38
		Northridge 1994, Aftershock	5.2	16.3	0.34	0.57	0.08	0.005	1.0	85.0	3.0	9.0	0.26
		Northridge 1994, Aftershock	5.9	15.2	0.27	0.55	0.09	0.006	1.1	44.5	1.6	9.2	0.27
Monterey	City Hall	Loma Prieta 1989	6.9	44.8	0.07	0.15	0.05	0.008	2.3	6.7	7.8	13.3	0.34
Newhall	Fire Station	Northridge 1994	6.7	7.1	0.59	2.19	0.78	0.154	85.7	479.7	3.0	5.9	0.57
		Whittier Narrows 1987	6	55.2	0.05	0.15	0.04	0.002	2.9	3.8	7.2	15.8	0.40
Oakland	Title & Trust Bldg. (2-story)	Loma Prieta 1989	6.9	77.4	0.22	0.53	0.44	0.042	26.8	51.0	4.7	12.0	0.80
Oakland	Outer Harbor Wharf	Loma Prieta 1989	6.9	72.1	0.28	0.53	0.59	0.080	41.5	84.5	3.4	7.8	0.86

Table 4.2 Continued

Location	Station Name	Earthquake	m	r (km)	PHA (g)	S_a 0.3s (g)	S_a 1.0s (g)	S_a 3.0s (g)	PHV (cm/s)	I_a (cm/s)	D_{5-75} (s)	D_{5-95} (s)	T_m (s)
Pacoima	Pacoima Kagel Canyon	Whittier Narrows 1987	6	37.9	0.16	0.40	0.07	0.005	0.8	16.1	4.0	10.6	0.37
		Northridge 1994	6.7	8.2	0.44	0.95	0.42	0.085	16.9	257.3	4.6	9.2	0.79
		Northridge 1994, Aftershock	5.2	14.1	0.19	0.52	0.06	0.005	0.9	18.9	2.5	7.6	0.37
		Northridge 1994, Aftershock	5.9	9.4	0.07	0.20	0.02	0.001	0.2	2.3	1.3	6.4	0.27
		Hector Mine 1999	7.1	196.5	0.03	0.07	0.08	0.012	3.7	3.0	28.1	41.7	0.82
Palm Springs	Desert Hot Springs	Hector Mine 1999	7.1	74.1	0.07	0.24	0.13	0.020	6.9	11.6	12.5	22.2	0.56
		Landers 1992	7.3	23.2	0.16	0.34	0.27	0.045	20.6	68.6	21.9	31.7	0.62
		North Palm Springs 1986	6	8	0.30	0.89	0.26	0.032	21.5	103.5	3.4	7.0	0.35
Palm Springs	North Palm Springs	Landers 1992	7.3	24.2	0.13	0.32	0.19	0.415	12.6	65.6	24.9	36.9	0.59
		North Palm Springs 1986	6	8.2	0.64	1.45	0.48	0.062	49.8	177.6	1.7	4.9	0.45
Palm Springs	Devers Hill Substation	North Palm Springs 1986	6	4.05	0.80	1.63	0.52	0.046	9.1	199.8	1.7	4.7	0.38
Palo Alto	Palo Alto VA	Loma Prieta 1989	6.9	26.1	0.37	0.98	0.35	0.171	29.9	79.0	3.4	13.4	0.81
Petrolia	General Store	Cape Mendocino 1992	7.1	9.5	0.62	1.01	0.82	0.174	65.9	361.2	4.2	16.9	0.60
Redwood City	Apeel #2	Loma Prieta 1989	6.9	47.9	0.25	0.33	0.78	0.065	42.9	92.5	3.3	9.9	0.95
San Francisco	International Airport	Loma Prieta 1989	6.9	64.4	0.28	1.05	0.37	0.041	26.7	87.9	4.6	11.0	0.55
		Morgan Hill 1984	6.2	71..2	0.05	0.18	0.05	0.003	2.9	3.2	10.7	14.3	0.39
San Francisco	Diamond Heights	Loma Prieta 1989	6.9	77	0.11	0.29	0.10	0.022	2.7	12.0	3.7	9.0	0.54
San Francisco	Yerba Buena Island	Loma Prieta 1989	6.9	80.6	0.04	0.12	0.06	0.017	2.2	2.5	4.2	10.8	0.73
Santa Barbara	Courthouse	Kern County 1952	7.4	87	0.11	0.21	0.25	0.030	13.7	23.2	11.8	29.7	0.89
		Santa Barbara 1978	6	14	0.14	0.41	0.12	0.020	11.0	14.0	2.8	5.9	0.52
Santa Clara	IBM Almaden, Santa Teresa H.	Loma Prieta 1989	6.9	14.4	0.24	0.41	0.22	0.029	5.9	114.5	6.2	10.1	0.33
Santa Clarita	Potrero Canyon	Whittier Narrows 1987	6	57.1	0.07	0.23	0.03	0.004	4.7	7.9	6.2	11.6	0.37
Santa Cruz	UCSC Lick Observatory	Loma Prieta 1989	6.9	17.9	0.46	1.10	0.20	0.022	4.5	221.8	6.0	9.5	0.26
		Morgan Hill 1984	6.2	44.1	0.05	0.16	0.03	0.003	0.4	4.4	4.5	7.7	0.30
Simi Valley	Knolls School	Northridge 1994	6.7	14.6	0.75	1.28	0.71	0.032	39.3	381.1	3.4	6.3	0.49
Sunnyvale	Colton	Loma Prieta 1989	6.9	28.8	0.21	0.47	0.27	0.280	36.6	69.9	10.3	20.6	1.32
Sylmar	Olive View Hospital	Northridge 1994	6.7	6.4	0.71	1.97	0.76	0.179	100.7	380.9	3.3	5.9	0.73
		Whittier Narrows 1987	6	47.7	0.06	0.14	0.03	0.004	3.8	5.8	6.3	14.3	0.37
Sylmar	Converter Station East	Northridge 1994	6.7	6.1	0.64	1.28	0.90	0.272	34.2	364.3	3.7	7.2	0.73
Sylmar	Jensen Gen. Bldg.	Hector Mine 1999	7.1	207.7	0.04	0.09	0.10	0.024	7.8	4.1	9.0	20.8	1.02
		Northridge 1994	6.7	6.24	0.74	1.69	0.83	0.233	35.9	436.7	3.9	6.7	0.68
Taft	Lincoln School	Kern County 1952	7.4	41	0.17	0.39	0.17	0.046	16.4	56.3	10.5	29.5	0.54
		Parkfield 1966	6.1	126.5	0.10	0.02	0.02	0.007	2.2	0.3	16.8	38.9	1.05
Yermo	Fire Station	Big Bear 1992	6.4	68	0.05	0.11	0.07	0.018	4.3	7.1	14.7	27.3	0.57
		Landers 1992	7.3	24.9	0.19	0.46	0.41	0.108	39.1	80.0	8.5	18.1	0.80

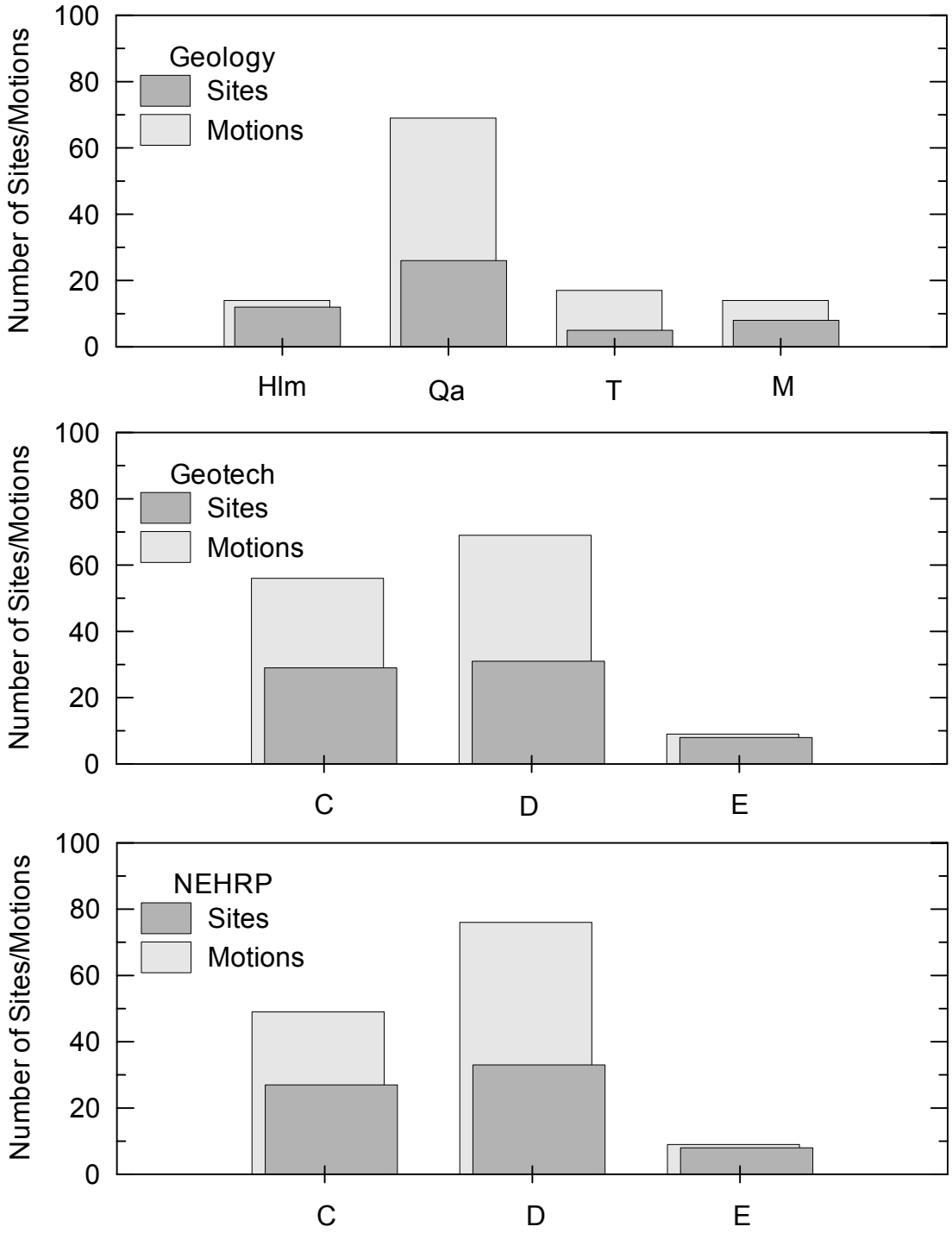

Fig. 4.1. Data breakdown for Geology, Geotechnical (Rodriguez-Marek et al.,2001) and $V_{s\text{-}30}$ (NEHRP) classification schemes

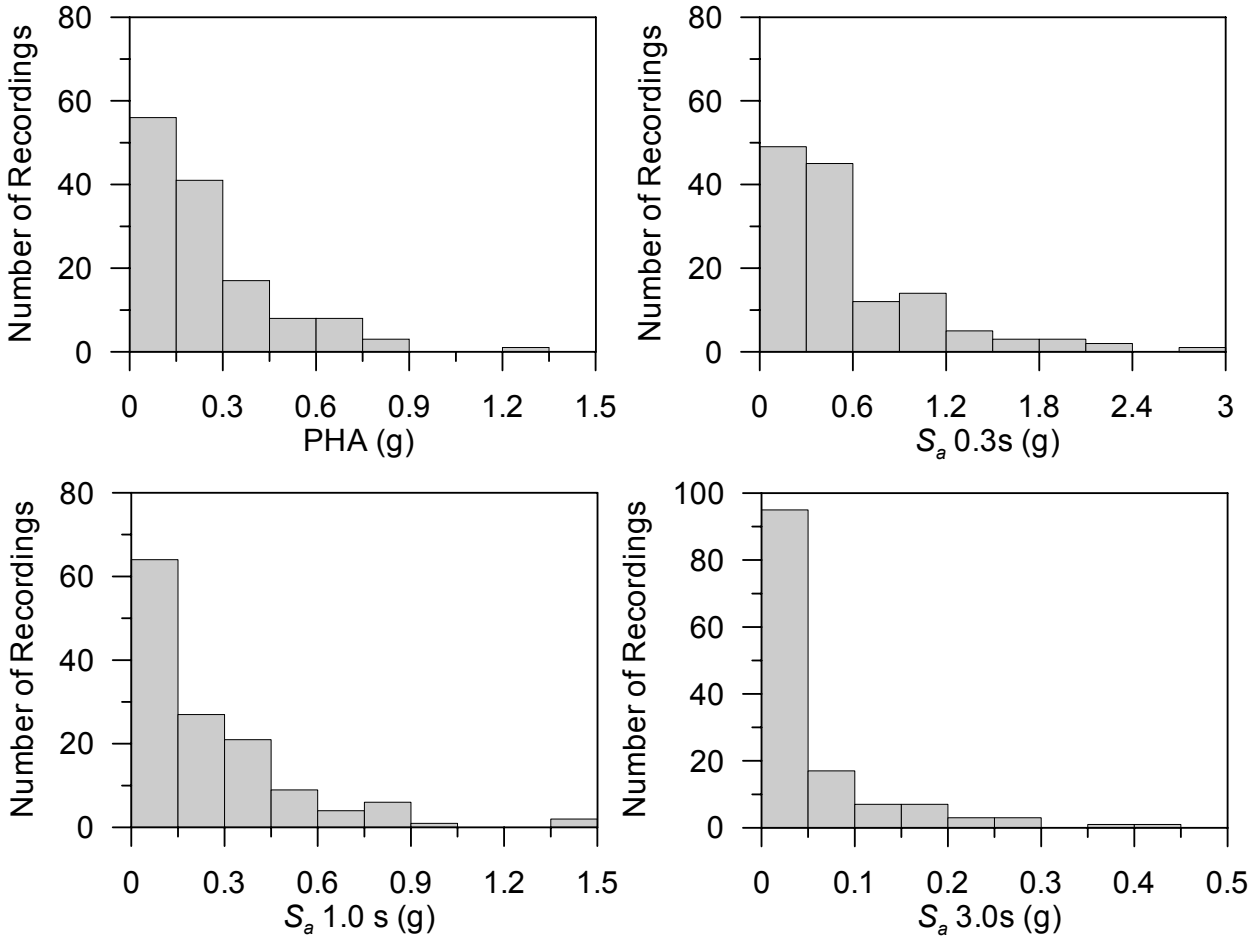

Fig. 4.2. Histograms of 5% damped spectral acceleration at various periods for strong motion data set used in this study

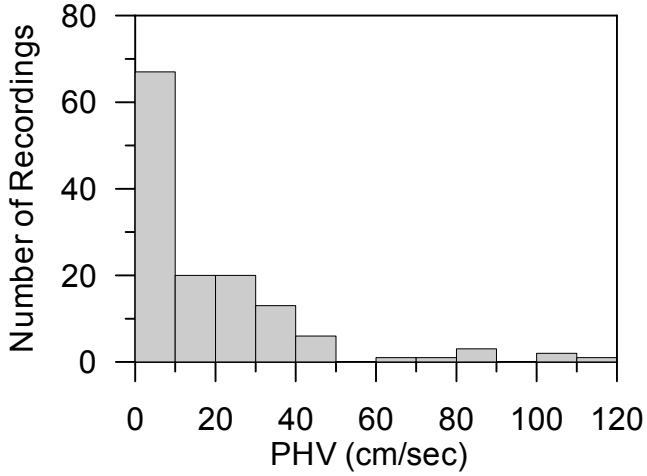

Fig. 4.3. Histogram of peak ground velocities for strong motion data set used in this study

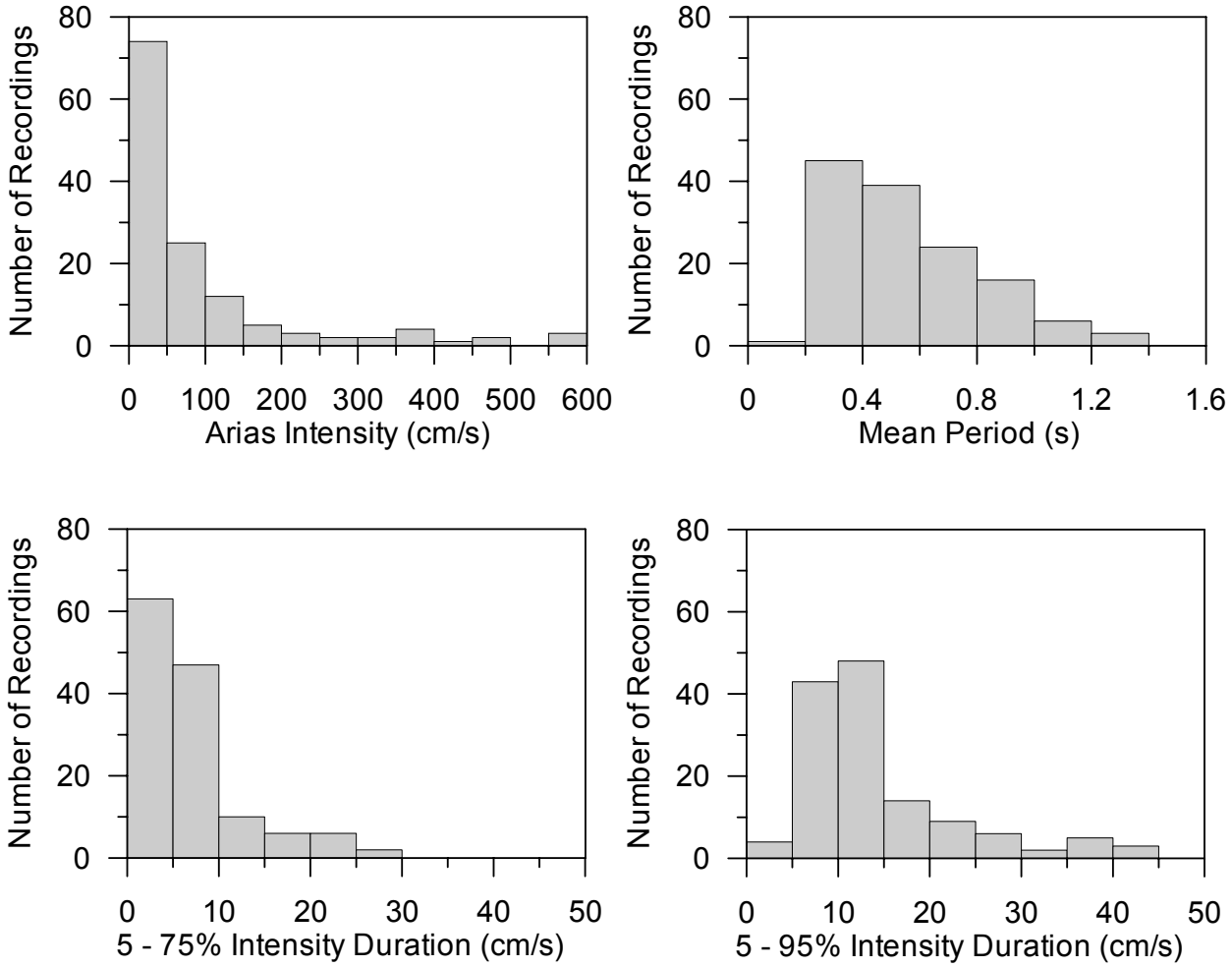

Fig. 4.4. Histograms of various IM parameters for strong motion data set used in this study (The plot for Arias Intensity does not show the data for the recording from 1994 Northridge Earthquake at Tarzana site which is 1959 cm/s)

As shown in the histograms, many of the recordings correspond to relatively weak shaking conditions. For example, only 18% have peak horizontal accelerations (PHA) in excess of 0.4 g. In order to gain preliminary insight into the level of soil nonlinearity that would be expected in the ground at these levels of shaking, we compile values of the strain factor parameter at the selected sites. This parameter is defined by Trifunac and Todorovska (1996) as the ratio of peak velocity to small-strain shear wave velocity at the site, and provides a crude, lower-bound indicator of shear strain in the ground. Many parameterizations of shear wave velocity at a given site can be used to define the strain factor. Parameterizations considered here are the smallest value of shear wave velocity that extends across at least a 3 m depth range, and $V_{s\text{-}30}$. Using these definitions of shear wave velocity, histograms of strain factor are presented in Figure 4.5 and the

distributions of strain factor within NEHRP categories C-E are presented in Figure 4.6. As shown in Figure 4.5, the strain factor for most recordings is less than 0.1 %. Almost 60% of the strain factors are less than 0.05% and only 3% of them are larger than 0.5%. Accordingly, it would appear from this preliminary evaluation that relatively few of the recordings are sufficiently strong to induce strongly nonlinear soil behavior at the selected sites. This topic is revisited subsequently in the report using calculated ground strains from ground response analyses (Section 6.5).

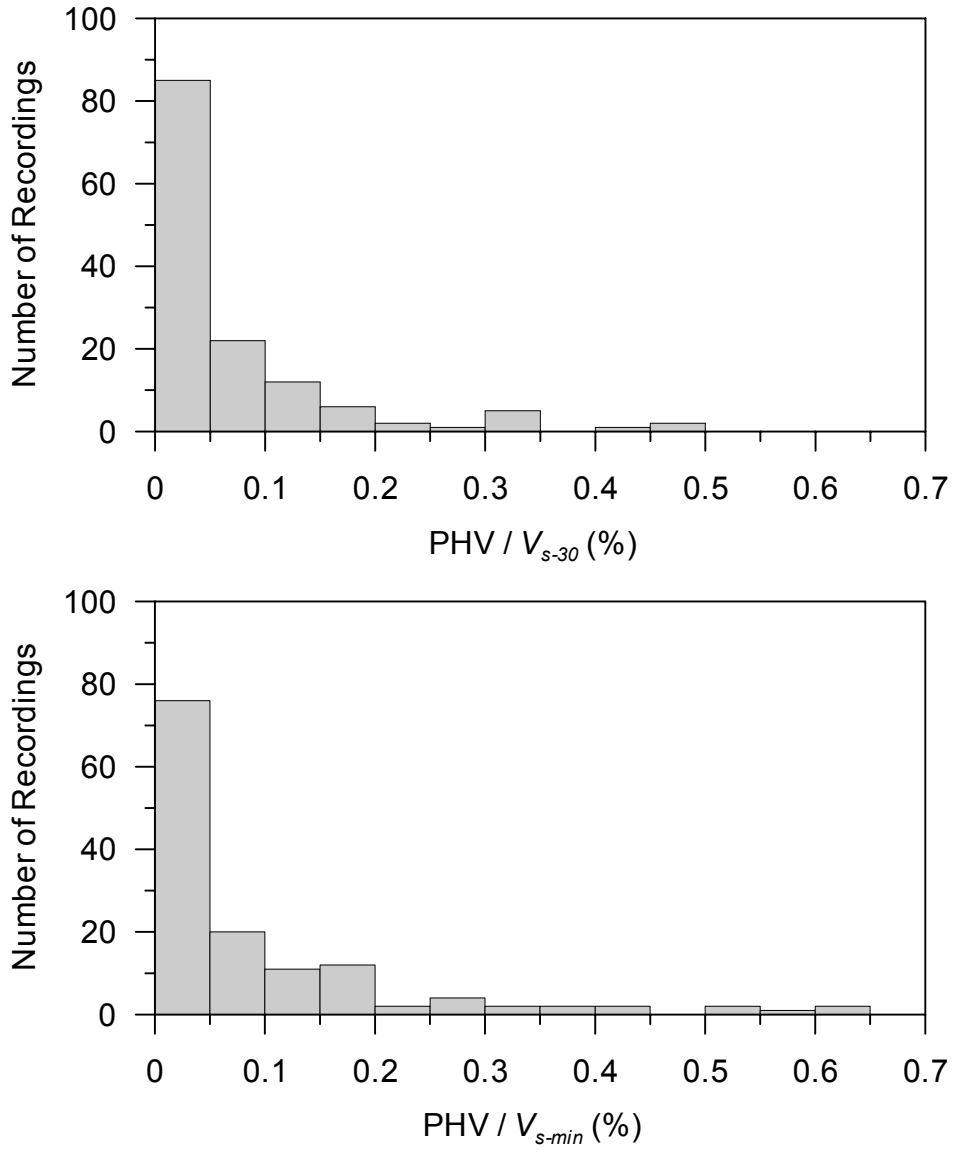

Fig. 4.5. Histograms of strain factors for strong motion data set used in this study

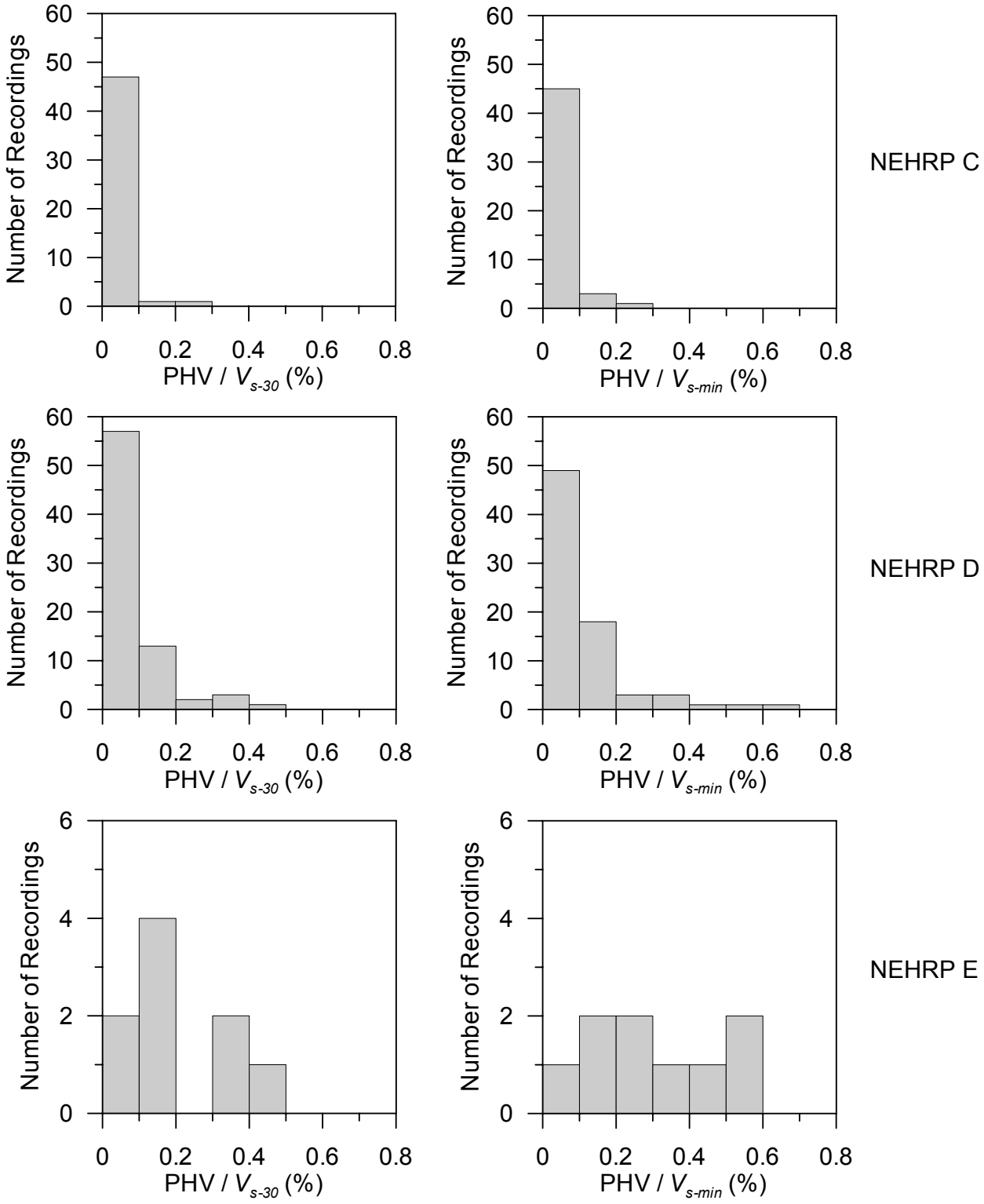

Fig. 4.6. Histograms of strain factors showing the breakdown in each NEHRP category

5 PROTOCOLS FOR TIME HISTORY SELECTION AND GROUND RESPONSE ANALYSES

This chapter describes the procedures used to select and scale time histories to be used as input for ground response analyses. Also described are several detailed protocols associated with performing ground response calculations at the selected sites.

5.1 DEVELOPMENT OF INPUT MOTIONS

5.1.1 Strong Motion Database

A database of time histories was developed to serve as a library from which input motions could be selected. Database development began with the PEER strong motion database for shallow crustal earthquakes in active tectonic regions (available at http://peer.berkeley.edu**). The database was augmented with (1) selected free-field motions, and (2) recordings from the ground level of building structures selected per the criteria set forth in Stewart (2000).**

Each time history in the database was assigned a series of seismological parameters that describe the source, path, and site effects that would be expected to have influenced the characteristics of the recordings. These variables include the following:

- **Moment magnitude of causative earthquake, m**
- **Closest distance from source to site, r**
- **Focal mechanism index to distinguish strike-slip, normal, and thrust earthquakes**
- **Parameters that describe the likely influence of rupture directivity (i.e., source-site azimuthal effects) on the recordings (see below).**

Rupture directivity effects were assumed to be negligible for moment magnitudes, $m \leq 6.0$, and site-source distances, $r > 60$ km (Abrahamson, 2000). For motions with $m > 6.0$ and $r < 60$ km, the geometric rupture directivity parameters defined in Figure 5.1 were obtained from a previous compilation (N. Smith, 1999, *personal communication*), and for sites missing in this compilation, were measured based on published fault rupture models. As shown in Figure 5.1, recordings triggered by dip-slip earthquakes but made at sites located

off the ends of the fault were assumed to have no rupture directivity effect. Based on the above data, the rupture directivity model for spectral acceleration by Somerville et al. (1997) and modified by Abrahamson (2000) was used to evaluate the expected rupture directivity effect for each site in the database. These effects were expressed using a Rupture Directivity Index (RDI), defined as the amplification/de-amplification of the geometric mean of 3.0 s period spectral acceleration due to rupture directivity effects as computed by the Somerville/Abrahamson model. A site experiencing no rupture directivity effect has RDI = 1.0. For strike-slip faults, RDI varies from 1.48 (forward directivity) to 0.55 (backward directivity). The range for dip slip faults is 1.16 to 0.72.

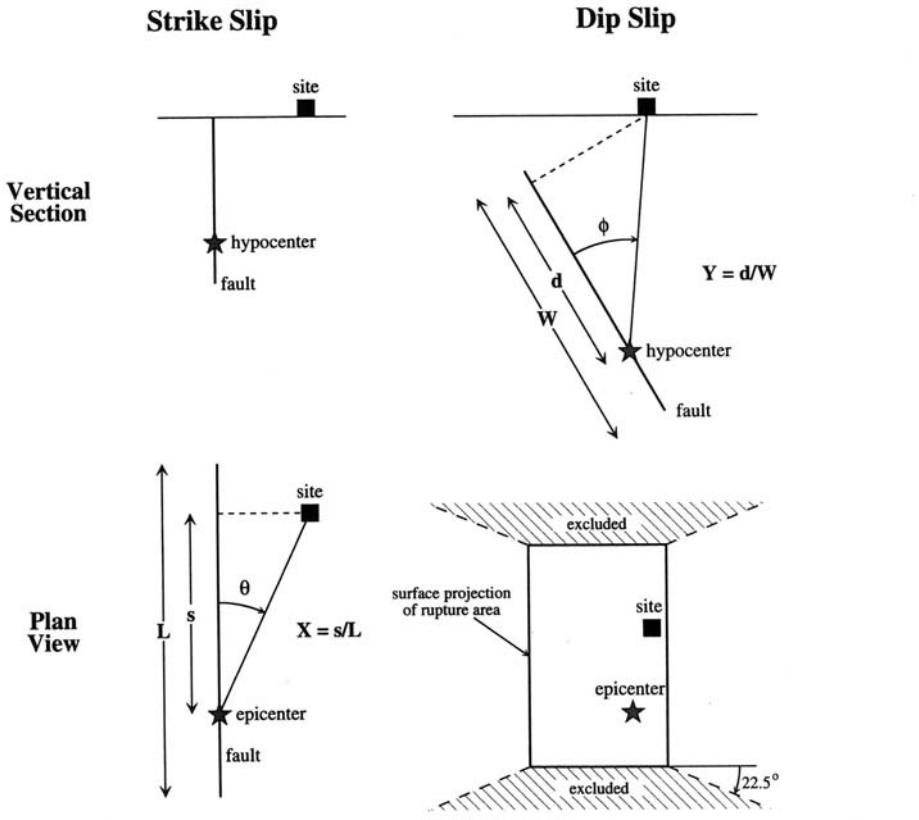

Fig. 5.1. Definition of rupture directivity parameters θ and X for strike-slip faults, and ϕ and Y for dip-slip faults, and region off the end of dip-slip faults excluded from the model (Somerville et al., 1997)

5.1.2 Time History Selection Criteria

The database described in Section 5.1.1 was used to select specific time histories representing possible realizations of the motion that would have been expected at the site had the geologic condition been the rock-average site condition for active tectonic regions. This site condition corresponds to soft, weathered rock having a median shear wave velocity that has been estimated as $V_{s\text{-}30} \approx$ 520 m/s – 620 m/s (Silva et al., 1997; Boore et al., 1997). The selected time histories were scaled as described in Section 5.1.3, and then used as input for ground response analyses for the sites selected in Chapter 4.

The seismological criteria by which these rock time histories were selected are as follows, where the term "target" refers to a characteristic of the causative earthquake for the subject site:

1) **Magnitude: Selected recordings must have been triggered by an event with a magnitude within ± 0.5 of the target.**
2) **Amplitude: Time histories were sought that had a PHA within a factor of two to four of the target PHA on rock (evaluation of target PHA on rock is described in Section 5.1.3).**
3) **Site Condition: Time histories were selected from sites underlain by geologic rock or with a thin (< 20 m) layer of soil overlying rock.**
4) **Rupture Directivity: Time histories should have RDI's that are similar to the target RDI. Target RDI is based on site location relative to the fault plane, not deviations of the recorded motion from an attenuation model.**

The target values of magnitude, amplitude, and RDI for each site/earthquake in the database are presented in Table 5.1.

The orientation of the input time histories that were used in analysis were selected as follows:

- **For sites that have RDI = 1.0 because $m \leq 6.0$ or $r > 60$ km, a single random horizontal component of each time history was selected.**
- **For sites with RDI ≠ 1.0 and angle θ (strike-slip) or ϕ (dip-slip) < 45 degrees, the model of Somerville et al. (1997) suggests that there is a motion orientation effect associated with the near-fault wave pattern. Accordingly, time histories are rotated into fault normal and fault parallel components for separate ground response analyses for these two orientations.**

- **For sites with RDI ≠ 1.0, and angle θ (strike-slip) or ϕ (dip-slip) > 45 degrees, the Somerville et al. model suggests no significant motion orientation effect. We attempted to select input motions from sites having similar θ or ϕ angles, but this was not always possible due to sparse data. Accordingly, some time histories were selected with RDI ≠ 1.0 and θ or ϕ < 45 degrees, and for these recordings the orientation effect was eliminated by using the geometric mean. This was accomplished by performing the ground response analyses using both horizontal components of the input, and then taking the geometric mean of the computed response as the result.**
- **For sites with RDI = 1.0 because the site is located off the end wall, the Somerville model suggests that motion orientation effects can be present (provided θ, ϕ < 45 degrees) despite the absence of rupture directivity effects. Hence, time histories are rotated into separate fault normal and fault parallel components.**

We did not consider rupture mechanism or hanging wall effects in time history selection. The specific motions selected for each site are presented in Appendix B.

Table 5.1 Target values of magnitude, amplitude, and RDI for each site/earthquake

Location	Station Name	Earthquake	m	r (km)	PHA (g)	RDI	Orientation Effect
Agnew	Agnews Hospital	Loma Prieta 1989	6.9	28.2	0.17	1.37	Yes
		Morgan Hill 1984	6.2	29.4	0.03	0.79	No
Alameda	Naval Air Station	Loma Prieta 1989	6.9	75.2	0.24	1.00	No
Bear Valley	Callens Ranch	Loma Prieta 1989	6.9	49	0.07	1.16	Yes
Capitola	Fire Station	Loma Prieta 1989	6.9	14.5	0.48	0.55	No
		Morgan Hill 1984	6.2	38.1	0.12	1.12	Yes
Corralitos	Eureka Canyon Road	Morgan Hill 1984	6.2	22.7	0.10	1.17	Yes
		Loma Prieta 1989	6.9	5.1	0.50	0.68	No
El Centro	El Centro Array #7	Imperial Valley 1979	6.5	0.6	0.39	1.48	Yes
		Imperial Valley 1979, Aftershock	5.2	13.1	0.16	1.00	No
El Centro	El Centro Array #9	Imperial Valley 1940	7	8.3	0.24	0.78	Yes
El Centro	Meloland Overcrossing	Imperial Valley 1979	6.5	0.5	0.30	1.48	Yes
Emeryville	Pacific Park Plaza	Loma Prieta 1989	6.9	76.9	0.23	1.00	No
Eureka FF	Myrtle & West Avenue	Cape Mendocino 1992	7.1	44.6	0.17	0.85	No
Foster City	Apeel #1	Loma Prieta 1989	6.9	49	0.28	1.15	Yes
Foster City	Beach Park Boulevard	Loma Prieta 1989	6.9	51.2	0.11	1.12	Yes
Fremont	Mission San Jose	Livermore 1980	5.8	29.8	0.05	1.00	No
		Livermore 1980, Aftershock	5.4	29.8	0.04	1.00	No
		Morgan Hill 1984	6.2	31.4	0.02	0.79	Yes
		Loma Prieta 1989	6.9	43	0.14	1.14	No
Gilroy	Gilroy Array #7	Loma Prieta 1989	6.9	24.2	0.27	1.48	Yes
		Morgan Hill 1984	6.2	14	0.15	1.17	Yes
Gilroy	Gavilan College	Loma Prieta 1989	6.9	11.6	0.34	1.48	Yes
		Morgan Hill 1984	6.2	16.2	0.10	1.17	Yes
Gilroy	Gilroy Array #2	Coyote Lake 1979	5.7	7.5	0.27	1.00	No
		Loma Prieta 1989	6.9	12.7	0.19	1.48	Yes
		Morgan Hill 1984	6.2	15.1	0.34	1.17	Yes
Gilroy	Gilroy #3	Coyote Lake 1979	5.7	5.7	0.25	1.00	No
		Morgan Hill 1984	6.2	14.6	0.20	1.17	Yes
		Loma Prieta 1989	6.9	14.4	0.49	1.48	Yes
Gilroy	Gilroy #6	Coyote Lake 1979	5.7	3.1	0.37	1.00	No
		Morgan Hill 1984	6.2	11.8	0.28	1.17	Yes
		Loma Prieta 1989	6.9	19.9	0.17	1.48	Yes

Table 5.1 Continued

Location	Station Name	Earthquake	m	r (km)	PHA (g)	RDI	Orientation Effect
Halls Valley	Halls Valley	Coyote Lake 1979	5.7	31.2	0.04	1.00	No
		Loma Prieta 1989	6.9	31.6	0.12	0.64	No
		Morgan Hill 1984	6.2	3.4	0.22	0.83	Yes
Hollister	City Hall	Hollister 1974	5.2	11.1	0.13	1.00	No
		Loma Prieta 1989	6.9	28.2	0.23	1.48	Yes
		Morgan Hill 1984	6.2	32.5	0.07	1.16	Yes
Hollister	SAGO-South	Hollister 1986	5.4	14.9	0.06	1.00	No
		Loma Prieta 1989	6.9	34.7	0.07	1.48	Yes
Imperial	Superstition Mtn. Top	Imperial Valley 1979	6.5	26	0.15	1.48	Yes
		Westmoreland 1981	5.8	26.5	0.09	1.00	No
		Superstition hills (B) 1987	6.7	4.3	0.82	0.82	Yes
Joshua Tree	Fire Station	Big Bear 1992	6.4	38	0.06	1.05	No
		Hector Mine 1999	7.1	27	0.17	1.48	Yes
		Landers 1992	7.3	11.6	0.28	0.65	No
		North Palm Springs 1986	6	29.8	0.06	1.00	No
Larkspur	Ferry Terminal	Loma Prieta 1989	6.9	99.2	0.11	1.00	No
Los Angeles	Dayton School	Landers 1992	7.3	159.2	0.04	1.00	No
		Northridge 1994	6.7	29	0.38	1.00	No
		Whittier Narrows 1987	6	16.6	0.21	1.00	No
Los Angeles	ETEC, RD7	Northridge 1994	6.7	19.3	0.28	1.00	No
Los Angeles	Rinaldi Receiving Stn.	Northridge 1994	6.7	7.1	0.63	1.13	Yes
Los Angeles	Sylmar Converter West	Northridge 1994	6.7	6.2	0.74	1.14	Yes
Los Angeles	Arleta Fire Station	Northridge 1994	6.7	9.2	0.33	1.00	Yes
		Whittier Narrows 1987	6	38.9	0.09	1.00	No
Los Angeles	Epiphany	Northridge 1994	6.7	15.8	0.39	0.80	No
		Whittier Narrows 1987	6	47.4	0.13	1.00	No
Los Angeles	Hollywood Storage Bldg.	Borrego Mountain 1968	6.8	217.4	0.01	1.00	No
		Kern County 1952	7.4	120.5	0.05	1.00	No
		Northridge 1994	6.7	25.5	0.29	1.00	No
		San Fernando 1971	6.6	21.2	0.19	1.06	Yes
Los Angeles	Brentwood VA	Northridge 1994	6.7	24.7	0.18	0.73	No

Table 5.1 Continued

Location	Station Name	Earthquake	m	r (km)	PHA (g)	RDI	Orientation Effect
Los Angeles	Obregon Park	Hector Mine 1999	7.1	186.4	0.03	1.00	No
		Landers 1992	7.3	151.4	0.05	1.00	No
		Northridge 1994	6.7	37.9	0.45	1.00	No
		Northridge 1994, Aftershock	5.9	39.9	0.06	1.00	No
		Whittier Narrows 1987	6	13.9	0.42	1.00	No
		Whittier Narrows 1987, Aftershock	5.3	14.9	0.31	1.00	No
Los Angeles	Wadsworth VA N.	Northridge 1994	6.7	25.2	0.25	0.73	No
Los Angeles	White Oak Church	Landers 1992	7.3	176.5	0.04	1.00	No
		Northridge 1994	6.7	13.3	0.42	0.90	No
		Whittier Narrows 1987	6	39.8	0.14	1.00	No
Los Angeles	Baldwin Hills	Northridge 1994	6.7	31	0.22	0.74	No
		Northridge 1994, Aftershock	5.2	29.6	0.06	1.00	No
		Northridge 1994, Aftershock	5.9	33	0.07	1.00	No
		Whittier Narrows 1987	6	27	0.15	1.00	No
		Whittier Narrows 1987, Aftershock	5.3	27.6	0.09	1.00	No
Los Angeles	Bulk Mail	Northridge 1994	6.7	42.3	0.20	1.00	No
		Whittier Narrows 1987	6	12.9	0.39	1.00	No
Los Angeles	Saturn School	Northridge 1994	6.7	30	0.46	0.95	No
		Whittier Narrows 1987	6	20.8	0.12	1.00	No
Los Angeles	Sepulveda VA	Northridge 1994	6.7	8.9	0.84	1.06	Yes
Los Angeles	Wadsworth VA S.	Northridge 1994	6.7	25.56	0.33	0.73	No
Los Angeles	Lake Hughes#9	San Fernando 1971	6.6	23.6	0.15	1.00	No
		Northridge 1994	6.7	26.8	0.14	1.14	Yes
Los Angeles	Los Angeles Dam	Northridge 1994	6.7	2.6	0.49	1.14	Yes
Los Angeles	Tarzana	Whittier Narrows 1987	6	43	0.54	1.00	No
		Whittier Narrows 1987, Aftershock	5.3	42.7	0.09	1.00	No
		Landers 1992	7.3	175.6	0.05	1.00	No
		Northridge 1994	6.7	17.5	1.33	0.79	No
		Northridge 1994, Aftershock	5.2	16.3	0.34	1.00	No
		Northridge 1994, Aftershock	5.9	15.2	0.27	1.00	No
Monterey	City Hall	Loma Prieta 1989	6.9	44.8	0.07	1.07	No
Newhall	Fire Station	Northridge 1994	6.7	7.1	0.59	1.16	Yes
		Whittier Narrows 1987	6	55.2	0.05	1.00	No
Oakland	Title & Trust Bldg. (2-story)	Loma Prieta 1989	6.9	77.4	0.22	1.00	No
Oakland	Outer Harbor Wharf	Loma Prieta 1989	6.9	72.1	0.28	1.00	No

Table 5.1 Continued

Location	Station Name	Earthquake	m	r (km)	PHA (g)	RDI	Orientation Effect
Halls Valley	Halls Valley	Coyote Lake 1979	5.7	31.2	0.04	1.00	No
		Loma Prieta 1989	6.9	31.6	0.12	0.64	No
		Morgan Hill 1984	6.2	3.4	0.22	0.83	Yes
Hollister	City Hall	Hollister 1974	5.2	11.1	0.13	1.00	No
		Loma Prieta 1989	6.9	28.2	0.23	1.48	Yes
		Morgan Hill 1984	6.2	32.5	0.07	1.16	Yes
Hollister	SAGO-South	Hollister 1980	5.4	14.9	0.06	1.00	No
		Loma Prieta 1989	6.9	34.7	0.07	1.48	Yes
Imperial	Superstition Mtn. Top	Imperial Valley 1979	6.5	26	0.15	1.48	Yes
		Westmoreland 1981	5.8	26.5	0.09	1.00	No
		Superstition hills (B) 1987	6.7	4.3	0.82	0.82	Yes
Joshua Tree	Fire Station	Big Bear 1992	6.4	38	0.06	1.05	No
		Hector Mine 1999	7.1	27	0.17	1.48	Yes
		Landers 1992	7.3	11.6	0.28	0.65	No
		North Palm Springs 1986	6	29.8	0.06	1.00	No
Larkspur	Ferry Terminal	Loma Prieta 1989	6.9	99.2	0.11	1.00	No
Los Angeles	Dayton School	Landers 1992	7.3	159.2	0.04	1.00	No
		Northridge 1994	6.7	29	0.38	1.00	No
		Whittier Narrows 1987	6	16.6	0.21	1.00	No
Los Angeles	ETEC, RD7	Northridge 1994	6.7	19.3	0.28	1.00	No
Los Angeles	Rinaldi Receiving Stn.	Northridge 1994	6.7	7.1	0.63	1.13	Yes
Los Angeles	Sylmar Converter West	Northridge 1994	6.7	6.2	0.74	1.14	Yes
Los Angeles	Arleta Fire Station	Northridge 1994	6.7	9.2	0.33	1.00	Yes
		Whittier Narrows 1987	6	38.9	0.09	1.00	No
Los Angeles	Epiphany	Northridge 1994	6.7	15.8	0.39	0.80	No
		Whittier Narrows 1987	6	47.4	0.13	1.00	No
Los Angeles	Hollywood Storage Bldg.	Borrego Mountain 1968	6.8	217.4	0.01	1.00	No
		Kern County 1952	7.4	120.5	0.05	1.00	No
		Northridge 1994	6.7	25.5	0.29	1.00	No
		San Fernando 1971	6.6	21.2	0.19	1.06	Yes
Los Angeles	Brentwood VA	Northridge 1994	6.7	24.7	0.18	0.73	No

5.1.3 Scaling of Input

The time histories selected according to the criteria in Section 5.1.2 were scaled prior their use in ground response analyses. The intent of the scaling was to provide an ensemble of time histories with median spectral ordinates matching the "best estimate" soft rock spectrum for the subject event and site, while retaining the inherent variability of the time history suite.

The best estimate spectrum is taken as median 5% damped response spectral ordinates from the Abrahamson and Silva (1997) rock attenuation relation, with the following modifications:

1) **Addition of period dependent event terms (in natural log units) provided by Abrahamson (1999, *personal communication*), which quantify event-specific deviations from the Abrahamson and Silva (1997) attenuation model.**
2) **Addition of median rupture directivity effects and motion orientation effects (in natural log units) as computed by the models of Somerville et al. (1997) and Abrahamson (2000).**
3) **Removal of near-surface amplification effects at weathered soft rock sites using firm-to-soft rock ratios of response spectra (RRS) developed by Idriss (1999). The RRS used for this purpose is plotted as a function of period in Figure 5.2. The application of this RRS to the soft rock spectrum is intended to more nearly approximate the spectrum for less weathered rock profiles, such as might occur at depth beneath sediments.**

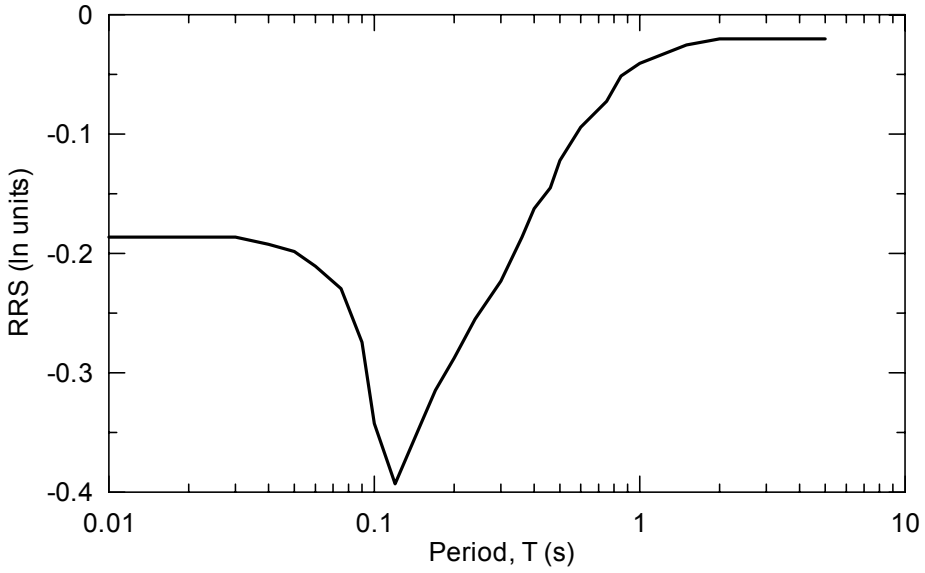

Fig. 5.2. Firm-to-soft rock ratios of response spectra (RRS) developed by Idriss (1999)

The best estimate spectrum obtained by these procedures represents the median ground motion that would have been expected at the site had the geologic condition been rock. At a particular period, T, this median spectral acceleration is denoted $\mu_{be}(T)$. The objective of the time history scaling is to adjust the median of the time history ensemble, $\mu_{th}(T)$, to match $\mu_{be}(T)$.

The scaling of the time histories is effectively performed in two stages. First, individual time history k is scaled up or down by factor $(F_1)_k$ so that its response spectrum, $S_k(T)$, matches $\mu_{be}(T)$ in an average sense over the range T = 0 – 1.0 s. Denoting the median spectra of the scaled time histories as $\mu_{sth}(T)$ [i.e., $\mu_{sth}(T)$ is the median of $S_k(T) \times (F_1)_k$ across all k], a second set of period-dependent scaling factors are defined as:

$$F_2(T) = \frac{\mu_{be}(T)}{\mu_{sth}(T)} \qquad \textbf{(5.1)}$$

The second scaling consists of time domain response spectral matching of each individual time history k to a target spectrum that is $S_k(T) \times (F_1)_k \times F_2(T)$. The time domain response spectral matching is performed with the program RSPMATCH (Abrahamson, 1998).

The above procedure ensures that the median spectral ordinates of the twice-scaled time histories nearly match the best estimate spectrum, $\mu_{be}(T)$. Further, the inherent variability across the time histories is preserved. The two-step scaling procedure is

illustrated in Figure 5.3 for an example recording. From the bottom frame, it is seen that the match between the median rock time histories and best estimate spectrum is excellent, although the scatter of the motions at long periods is accentuated by the second scaling (this is because the amount of the F_2 scaling at long periods was large for this site). For each site/earthquake in Table 5.1, the best estimate spectrum (from modified attenuation) along with the median and median ± one standard error of the twice-scaled input rock motions (assuming log-normal distribution) are presented in Appendix B.

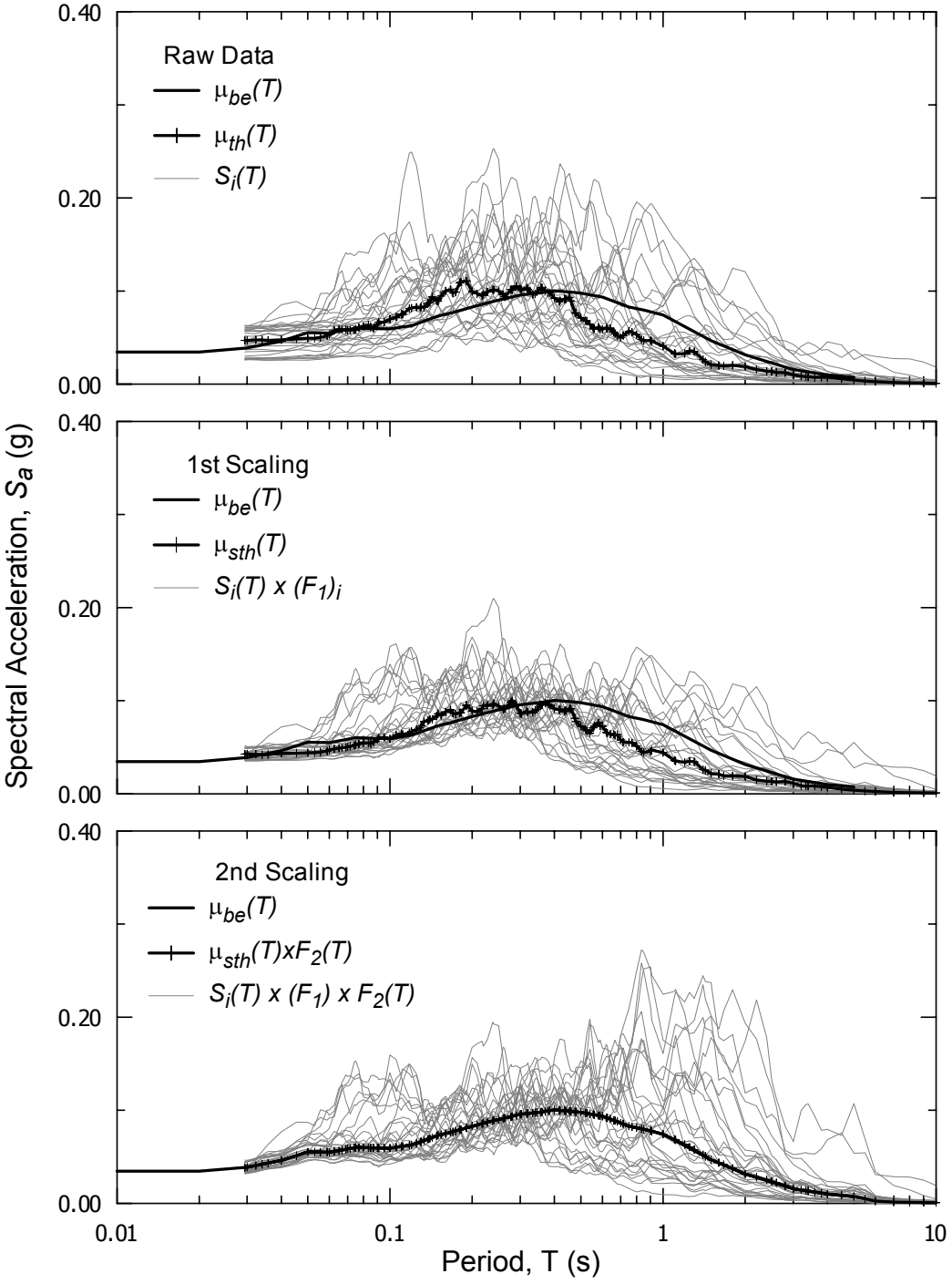

Fig. 5.3. Illustration of scaling procedure to match median acceleration response spectra of recordings to target. Data shown is for input motions for Larkspur Ferry Terminal site, 1989 Loma Prieta earthquake. The top frame shows spectra for the selected input motions before scaling, their median value (μ_{th}), and the target spectrum (μ_{be}); middle frame shows spectra for the once-scaled records, the median of these spectra (μ_{sth}), and the target; bottom frame shows spectra for the twice scaled records, and the match between this median spectrum and the target.

5.2 PROTOCOLS FOR GROUND RESPONSE MODELING

Ground response modeling was performed using the program SHAKE91 (Idriss and Sun, 1992), which performs equivalent linear modeling of 1-D ground response, as described in Chapter 3.

5.2.1 Dynamic Soil Properties

The characterization of soil conditions for each site consists of specifying: (1) a profile of small strain shear wave velocity (V_s) and mass density (ρ), and (2) relationships between normalized shear modulus (G/G_{max}) and hysteretic soil damping (β) and shear strain (γ). For each of the selected sites, V_s profiles were available from in situ measurements either by suspension logging, downhole or SASW techniques. Modulus reduction and damping curves were specified on the basis of soil type as indicated in Table 5.2. However, material specific curves were used where available (i.e., North Palm Springs, Desert Hot Springs, and El Centro Array #7). As described further in Chapter 6, limited additional analyses were performed using the more linear set of curves recommended by Silva et al. (1997) and presented in Section 3.4.1. It should be noted that the shear wave velocity profiles at the subject sites were assumed to be fixed at the measured values, and no variability in shear wave velocity was considered. The effect of dynamic soil property variability on the dispersion of estimated soil site ground motions has been investigated by others (Roblee et al., 1996; EPRI, 1993). The effects are most pronounced at $T < 1$ s, and increase in significance with the level of uncertainty in soil properties (i.e., these effects are less significant for well characterized sites, such as the sites considered in this study).

Table 5.2. Criteria used in this study for selecting modulus reduction and damping curves

Soil Type	Condition[1]	Reference
Sand and silty sand	Z < 100 m	Seed et al. (1986), upper bound sand G/G_{max} and lower bound β
	Z > 100 m	EPRI (1993): Z=76-173 m
Clays, silty clays, loams	PI=15 & Z<100m	Vucetic and Dobry (1991), PI=15[2]
	PI=15 & Z>100m	Stokoe et al. (1999), CL curve, Z = 100-250 m
	PI >= 30	Vucetic and Dobry (1991)
	Bay Mud	Sun et al. (1988)
	Old Bay Clay	Vucetic and Dobry (1991), PI=30[3]
Bedrock	V_S < 900 m/s	Soil curves for appropriate material type and depth
	V_S > 900 m/s	Schnabel (1973)

[1] Z=depth, PI = plasticity index

[2] Consistent with Stokoe et al. (1999), CL curve, Z < 100 m

[3] Consistent with Guha et al. (1993) material testing

5.2.2 Location of Control (Input) Motion

As described in Section 5.1.2, time histories were selected from rock sites for use as input in ground response analyses. Accordingly, control motions were entered into soil profile models at or slightly below the soil-bedrock interface for sites where this location is known or could be estimated. However, for several sites in the San Fernando, Imperial, and Santa Clara basins, bedrock occurs at depths beyond the practical limits of geotechnical subsurface exploration, and hence little data exists from which to estimate dynamic soil properties at depth. For these sites, the base of the ground response model is in soil, and the site condition that should be used to represent the input motion is not clear. If rock site motions are used, the motions would lack long-period energy content associated with ground response effects related to the deep basin structure and 2-D/3-D basin response effects. If soil motions are used, these effects would be included in the input in an average sense.

Since the objective in this study is to evaluate the effect of detailed modeling of 1-D ground response through shallow sediment layers (scale of tens of meters to several hundred meters), it was considered inappropriate to use soil recordings as input motions because these recordings already have a 1-D soil ground response effect "built-in" to them that would be double-counted by performing ground response analyses with these recordings as input. Accordingly, rock site motions are used as input even for sites where the soil profiles do not extend to rock. It is acknowledged that this practice may underpredict ground motions on soil at long periods. We accept this because we are

principally interested in characteristics of short-period ground motions (T < ~1.0 s) affected by the shallow sediment structure.

5.2.3 Analysis of Strain-Dependent Soil Properties

SHAKE91 analyses are performed for one direction of shaking, hence consideration must be given to which ground motion component is used to calculate equivalent linear soil properties when both horizontal components of shaking are considered for sites subject to near-fault motion orientation effects from rupture directivity. For these sites, fault normal motions generally exceed fault parallel motions at long periods, hence dynamic soil properties are estimated based on ground response analysis results for the fault normal direction. These same properties are applied for the calculation of fault parallel ground response (for which the calculated shear strains would otherwise be smaller).

For sites subject to near-fault effects but for which no motion orientation effect is expected based on the Somerville et al. (1997) model, the geometric mean of the calculated response from the two horizontal components was used. In these cases, dynamic soil properties were separately evaluated for the two horizontal directions. For non near-fault sites, only one randomly oriented horizontal component of input motions was used.

6 ANALYSIS AND INTERPRETATION OF RESULTS

In this chapter, we present and interpret the results of ground motion analyses performed using the procedures outlined in Chapter 3. We begin by synthesizing in Section 6.1 the ground motion prediction models for S_a utilized in the analyses. Example results for selected individual sites are presented in Section 6.2, while a synthesis of results across site categories is presented in Section 6.3. In Section 6.4 dispersion levels from ground response analyses are evaluated. Section 6.5 investigates the bias in the ground motion predictions with strain level. The chapter is concluded in Section 6.6 with a discussion of results for intensity measures (*IM*s) other than S_a.

6.1 GROUND MOTION PREDICTION MODELS UTILIZED

Ground motion predictions for sites presented in Chapter 4 were performed using several different models that were introduced in Chapter 3. The models used for prediction of 5% damped response spectral acceleration (S_a) are listed below:

1. Modified Abrahamson and Silva (1997) attenuation model for rock or soil site condition
2. Modified Abrahamson and Silva (1997) rock attenuation model with site amplification factors model by Stewart et al. (2002). These amplification factors are available for NEHRP, surface geology, and geotechnical-based site categorization schemes.
3. Modified Abrahamson and Silva (1997) soil/rock attenuation model with amplification factors for basin depth by Lee and Anderson (2000)
4. Ground response analysis performed according to the procedures in Section 5.1.3. Predictions of median S_a from ground response analyses were developed directly from computed time histories and as the product of the input median spectrum μ_{be} and the

median calculated Ratio of Response Spectrum (RRS = ratio of calculated surface spectrum to input spectrum).

The modifications to the Abrahamson and Silva (1997) attenuation model consisted of the addition of event terms and rupture directivity effects as described in Section 5.1.3.

The attenuation models that are used for prediction of *IM* parameters other than spectral acceleration are:

1. Travasarou et al. (2002) for Arias Intensity, I_a: The predictions depend on moment magnitude m; rupture mechanism; closest distance, r; and site category (Geotechnical B-D, as defined in Table 2.3).
2. Abrahamson and Silva (1996) for 5-75 and 5-95% acceleration significant duration, $D_{a,5-75}$, D_{a5-95}: The predictions depend on m, r, and site factor S (zero for rock, one for soil).
3. Rathje et al. (1998) for mean period, T_m: The predictions depend on the same parameters (m, r, and S) as the significant duration model.
4. Campbell (1997, 2000, 2001) for Peak Horizontal Velocity, PHV: The predictions depend on, m; the closest distance to seismogenic rupture on the fault, R_{seis}; the fault mechanism; site factors, S_{sr} and S_{hr}; and depth to basement, D_b (defined in Section 3.2).

6.2 RESULTS FOR SELECTED INDIVIDUAL SITES

6.2.1 Overview and Notation

In this section, we present for two recordings at each of three sites S_a predictions by the four models listed in Section 6.1. These sites are selected as representative examples of three distinct site conditions - shallow stiff soil, deep stiff soil, and soft clay. Soil profiles of the three sites are shown in Figures 6.1-6.3. At least two motions have been recorded at each site, and we consider here one relatively weak and one relatively strong recording, which are listed in Table 6.1.

Table 6.1. Sites used to illustrate S_a prediction routines

Location	Station Name	Earthquake	m	r (km)	PHA (g)	V_{s-30} (m/s)[1]	soil d. (m)[2]
Capitola	Fire Station	Loma Prieta 1989	6.9	14.5	0.48	290	60
		Morgan Hill 1984	6.2	38.1	0.12	290	60
Los Angeles	Saturn School	Northridge 1994	6.7	30	0.46	303	752
		Whittier Narrows 1987	6	20.8	0.12	303	752
San Francisco	Int. Airport	Loma Prieta 1989	6.9	64.4	0.28	227	152
		Morgan Hill 1984	6.2	71.2	0.05	227	152

[1] V_{s-30} = average shear wave velocity for upper 30 m of site

[2] Soil depth to competent bedrock, defined as layer with V_s > 760 m/s [approximated for Saturn site as depth to 1.0 km/s isosurface from Magistrale et al. (2000) basin model]

Notation for the S_a of the recorded motion and the S_a predictions for site *j* in category *i* is listed below. All of the terms have a functional dependence on period.

Observation (recorded motion): O_{ij}

Predictions:	Median	Std. Dev.	Standard Error (*se*) of Median
Model 1: Attenuation	A_{ij}	$(\sigma_a)_{ij}$	*n/a*
Model 2: NEHRP Factors	AS_{ij}	$(\sigma_{as})_{ij}$	*n/a*
Model 3: Basin Factors	AB_{ij}	$(\sigma_{ab})_{ij}$	*n/a*
Model 4: GR Output	G_{ij}	$(\sigma_{g\text{-}out})_{ij}$	$(se_{g\text{-}out})_{ij}$

All of these median and standard deviation quantities are in natural log units. The term $(se_{g\text{-}out})_{ij}$ denotes the standard error of G_{ij}, and is estimated as:

$$(se_{g-out})_{ij}^2 = (\sigma_{g-out})_{ij}^2 / N_j \qquad \textbf{(6.1)}$$

where N_j = number of input motions for Site *j*. Additional nomenclature for Model 4 includes:

Calculated S_a from input motion *k*: $(G_{ij})_k$

Std. dev. of input S_a across N_j input motions: $(\sigma_{g\text{-}in})_{ij}$

Median *RRS* across N_j input motions: RRS_{ij}

Std. dev. *RRS* across N_j input motions: $(\sigma_{RRS})_{ij}$

In order to quantify the degree to which a ground motion prediction (e.g., G_{ij}) captures the shape of the observed spectrum (i.e., O_{ij}), a shape misfit parameter is defined as follows:

1. **The average misfit between O_{ij} and G_{ij} is removed over the period range T = 0.05-2 s. This is accomplished by applying a single scale factor ρ_{ij} to G_{ij} that causes it to**

match O_{ij} in an average sense over the above period range [i.e., $\rho_{ij} \times (G_{ij})_{avg,T=0.05\text{-}2s} = (O_{ij})_{avg,T=0.05\text{-}2s}$].

2. **The misfit at each period T between O_{ij} and $\rho_{ij} \times G_{ij}$ is calculated as follows**

$$e_{ij}(T) = O_{ij}(T) - \rho_{ij} G_{ij}(T) \qquad \textbf{(6.2a)}$$

3. **An average shape misfit parameter $(\sigma_e)_{ij}$ is defined across T = 0.05-2 s as**

$$(\sigma_e)_{ij} = \sqrt{\frac{\sum_{1}^{t} e_{ij}^2}{t-1}} \qquad \textbf{(6.2b)}$$

where t = 116, the number of period ordinates for which e_{ij} is evaluated.

All of the above can be repeated for other ground motion prediction methods such as attenuation.

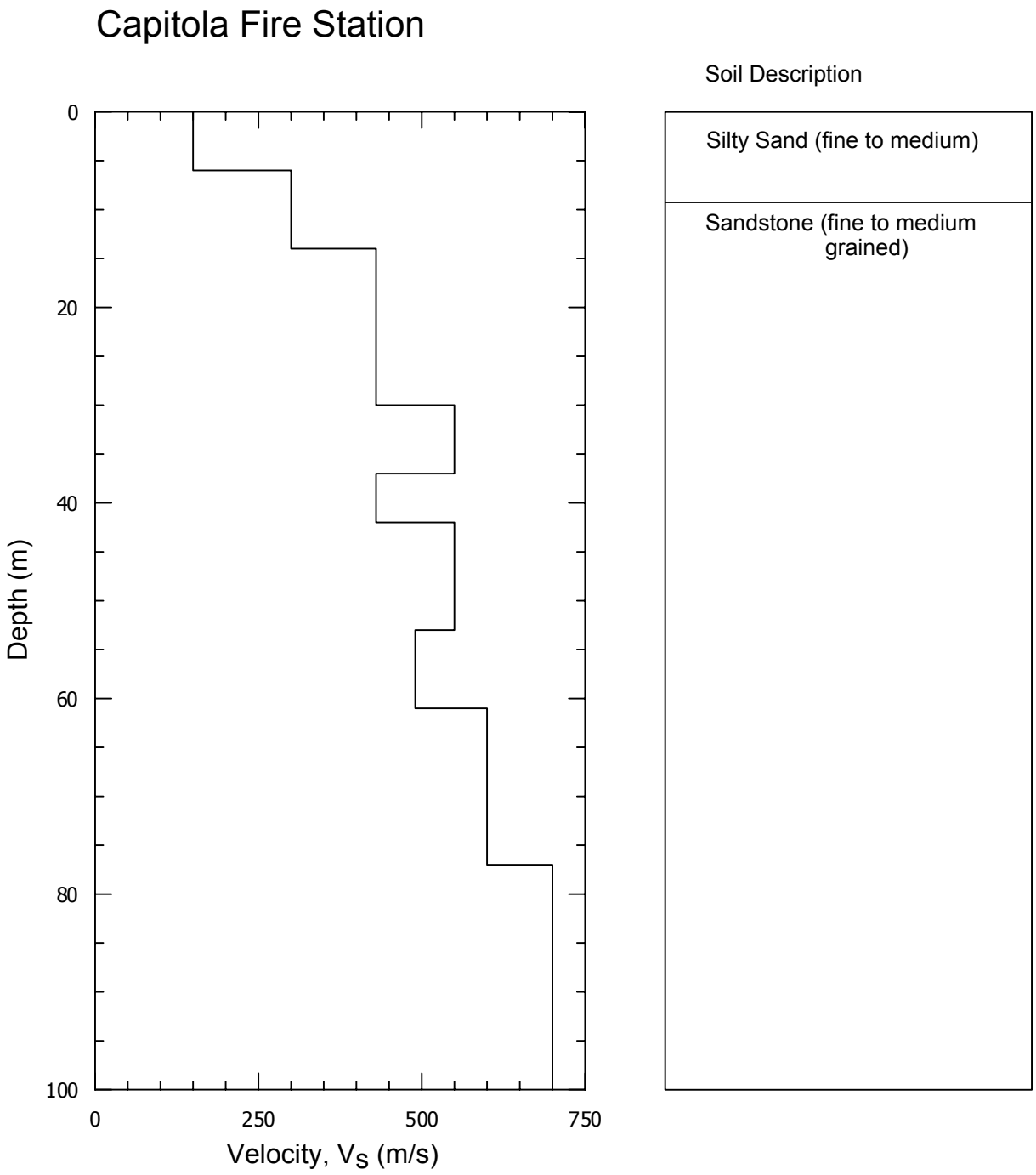

Data Source: Nigbor and Steller, 1993 (velocities); Powers and Fumal, 1993 (geologic log)

Fig. 6.1. Shear wave velocity and schematic soil profiles for Capitola Fire Station site

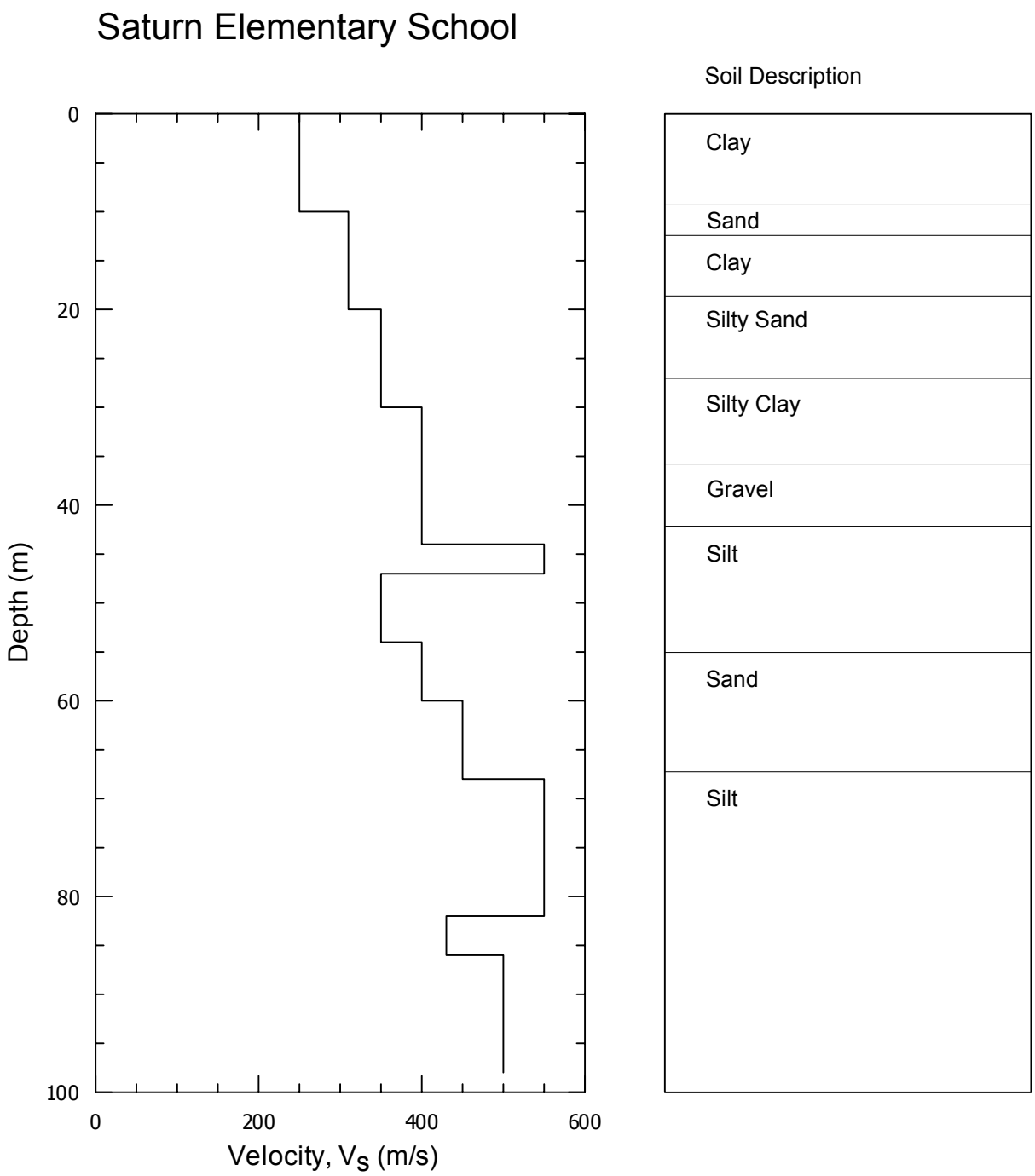

Fig. 6.2. Shear wave velocity and schematic soil profiles for Saturn Elementary School site

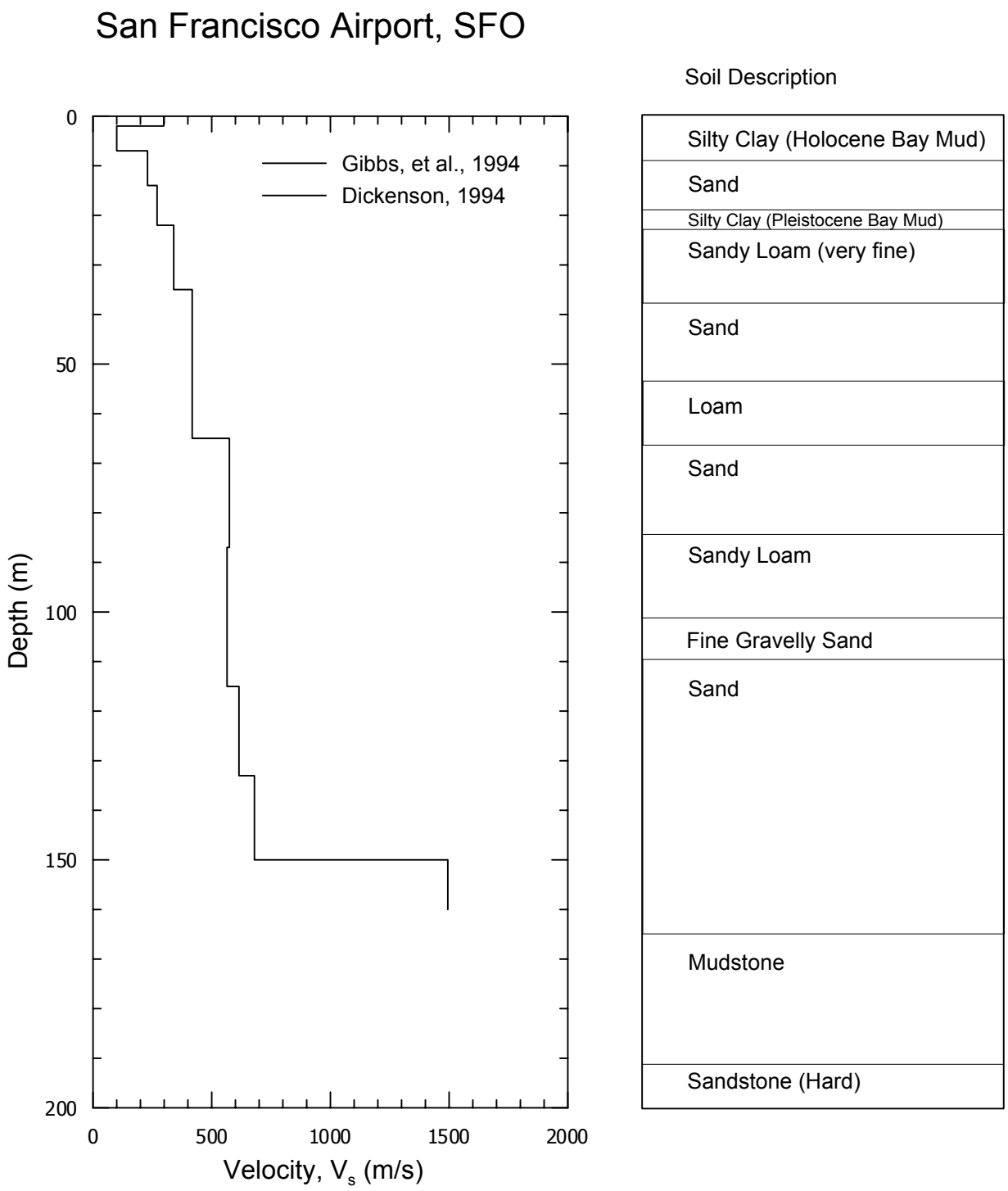

Data Source: Gibbs, et al., 1992 (velocities and geologic log); Dickenson, 1994 (velocities)

Fig. 6.3. Shear wave velocity and schematic soil profiles for San Francisco Airport, SFO, site

6.2.2 Evaluation of Results

The median and standard deviation of S_a predictions at the three subject sites are shown in Figures 6.4 to 6.6 with log scales. The ground response results are repeated in Figure 6.7 with linear vertical scales.

The modified soil attenuation relationship generally underestimates the observed spectral accelerations at these three sites. Many of the 134 motions used in this study show such a bias as discussed subsequently in Section 6.3. This bias is associated with the criterion for site selection that sites must be well characterized; the bias arises because the sites selected for detailed geotechnical characterization often have recorded anomalously high ground motions.

The ground response results appear qualitatively to provide a better fit to the observed spectral shape for the Capitola and SFO sites than for the Saturn site. Ground response analyses for SFO capture several specific peaks in the recording successfully, suggesting that shallow ground response effects are responsible for significant features of the recorded spectra and these features are captured by the analyses. Conversely, while the spectral prediction for Capitola matches the general shape of the observed spectra, it fails to capture detailed features. For the Saturn site, the ground response analyses fail to capture either the general shape or detailed features of the observed spectrum. As shown in Figure 6.7 for all three sites, median predicted spectra of the direct ground response output match the median spectrum obtained by use of RRS values. Accordingly, in future discussions, only the median spectrum computed directly from ground response output is reported.

The NEHRP amplification model does not significantly affect predicted spectral ordinates for the Capitola or Saturn sites, but does noticeably improve predictions for the SFO site. The Capitola and Saturn sites are on stiff soils for which the amplification factors are nearly unity; the SFO site is on soft soils for which the amplification factors are large.

The amplification model for basin depth does not significantly affect the predicted spectra for the Capitola site compared to soil attenuation predictions due to its shallow basin depth (depth to 2.5 km/s isosurface, $z_{2.5}$ = 0.9 km). The model has a small effect on the predicted spectra at small T for the SFO and Saturn sites, which are located on deeper basin structure ($z_{2.5}$ = 2.4 and 3.3 km, respectively), but no significant effect at longer periods.

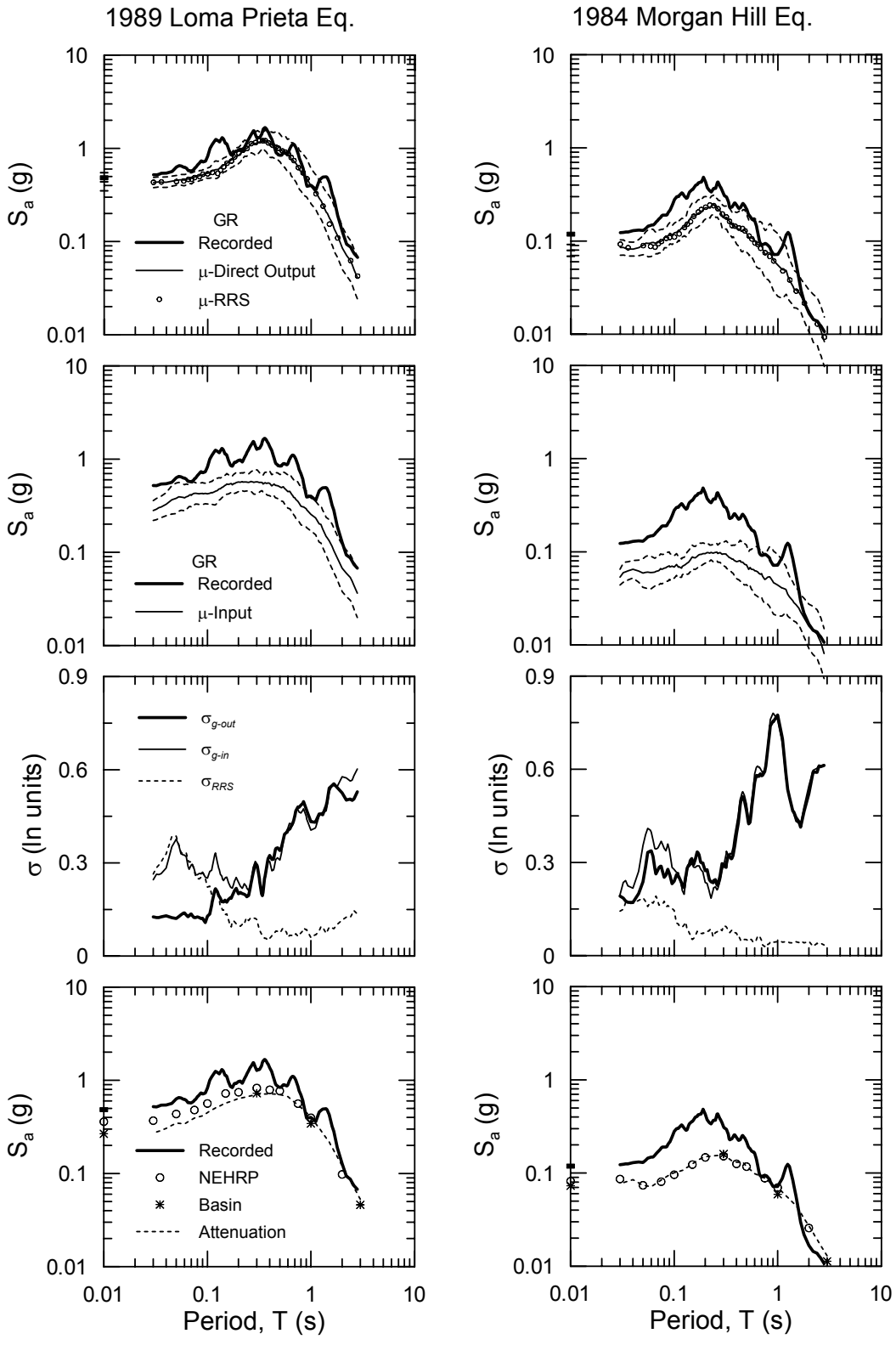

Fig. 6.4. The median and standard error of predictions at Capitola Fire Station site

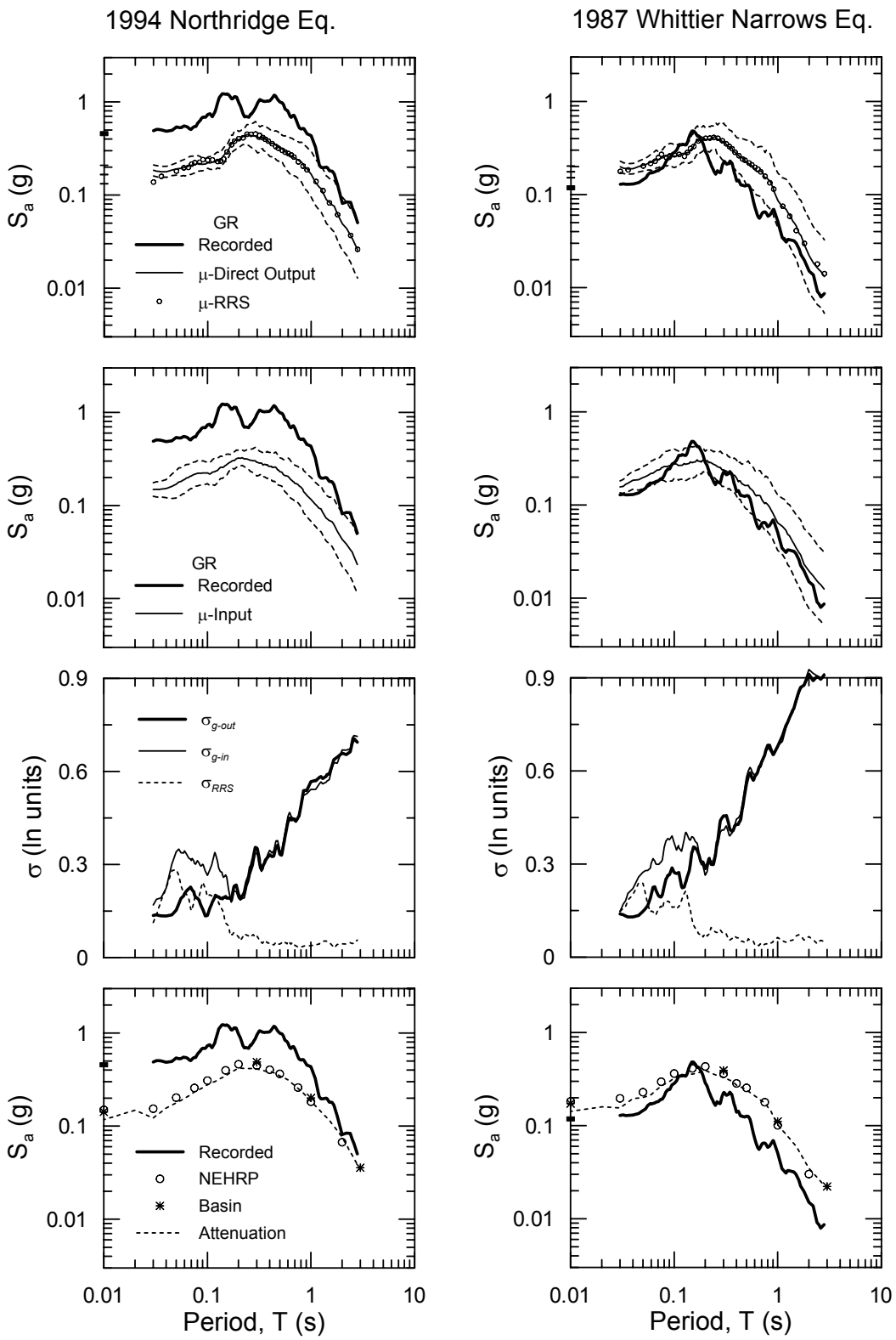

Fig. 6.5. The median and standard error of predictions at Saturn Elementary School site

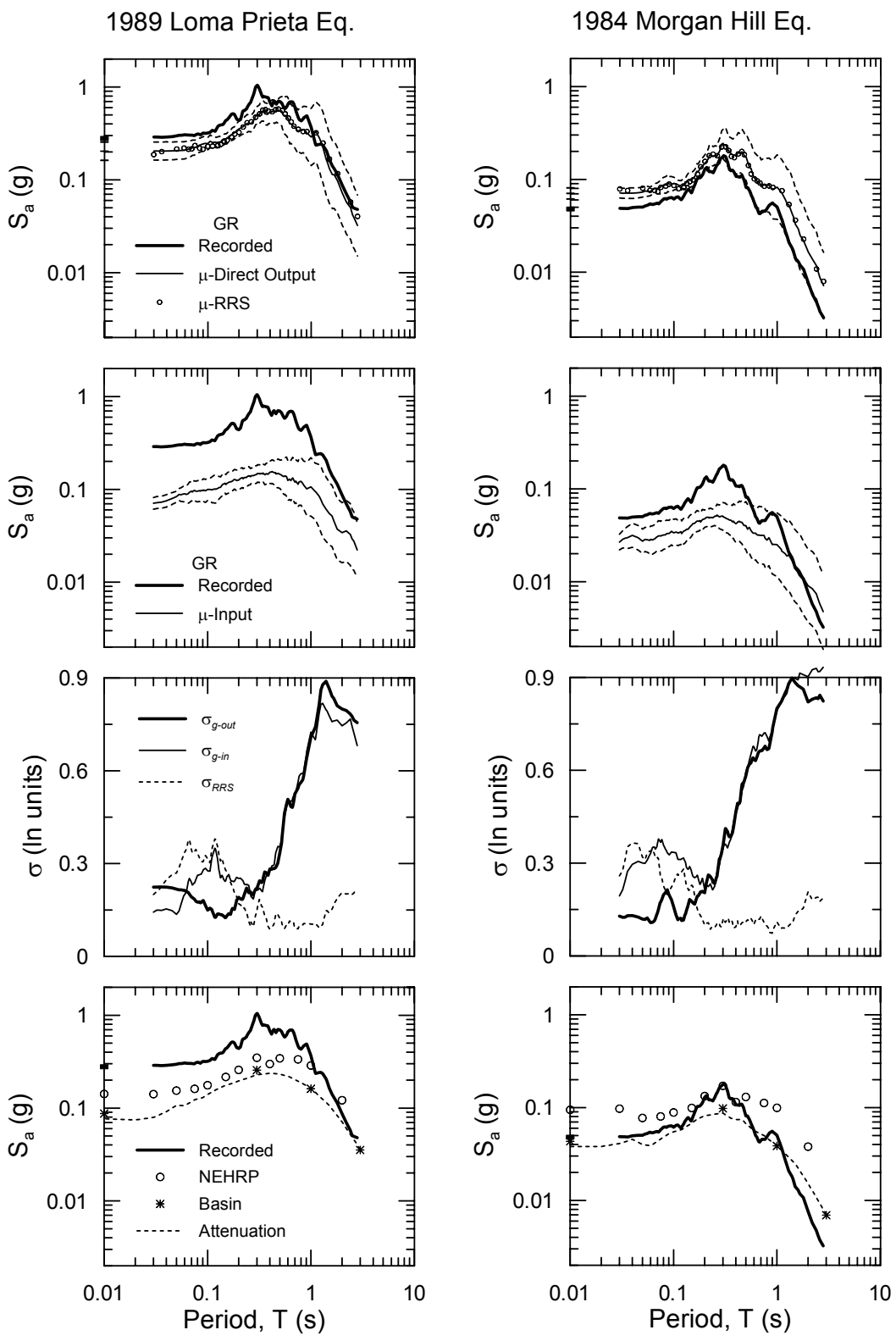

Fig. 6.6. The median and standard error of predictions at San Francisco Airport, SFO, site

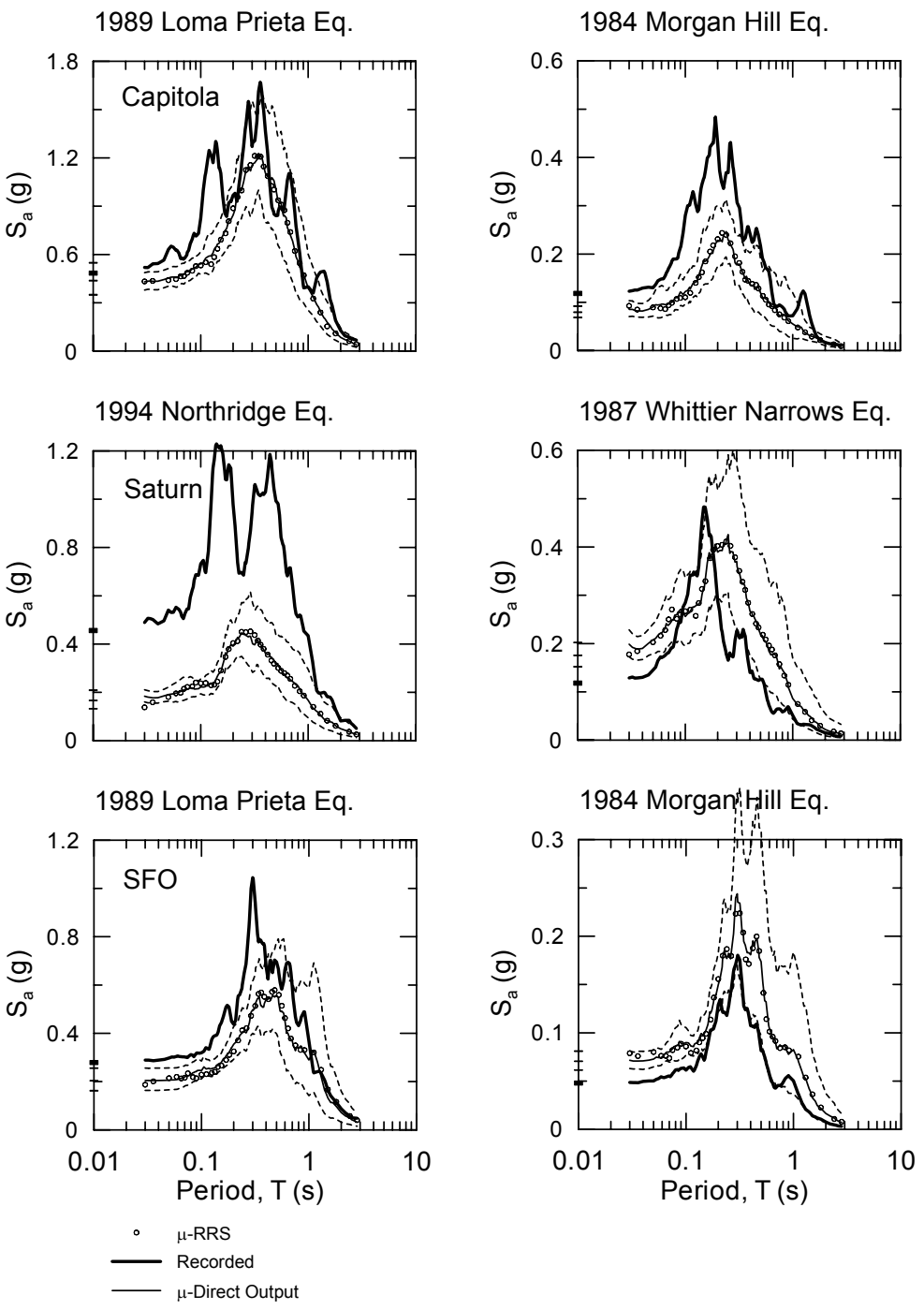

Fig. 6.7. Median ground response analysis predictions at the selected sites: Capitola Fire Station (shallow stiff soil), Saturn Elementary School (deep stiff soil), and San Francisco Airport, SFO (soft clay)

To help visualize the calculation of shape misfit parameter σ_e, the spectral shape represented by $\rho_{ij} \times G_{ij}(T)$ and $\rho_{ij} \times A_{ij}(T)$ are compared to O_{ij} for the three example sites in Figure 6.8. Values of σ_e for these sites are given in Table 6.2 for these models as well as the amplification factor model. The results support the qualitative observations made previously that ground response captures spectral shape for SFO better than for Saturn and Capitola. Moreover, ground response fits the spectral shape better than amplification and attenuation models for SFO, but not for the other sites.

Table 6.2. The average misfit value, σ_e for the sample recordings

	σ_e		
Recording	**Ground Response**	**NEHRP Amp. Factors**	**Attenuation**
Capitola, 1989 Loma Prieta	0.25	0.21	0.25
Saturn, 1994 Northridge	0.25	0.21	0.26
SFO, 1989 Loma Prieta	0.17	0.32	0.26

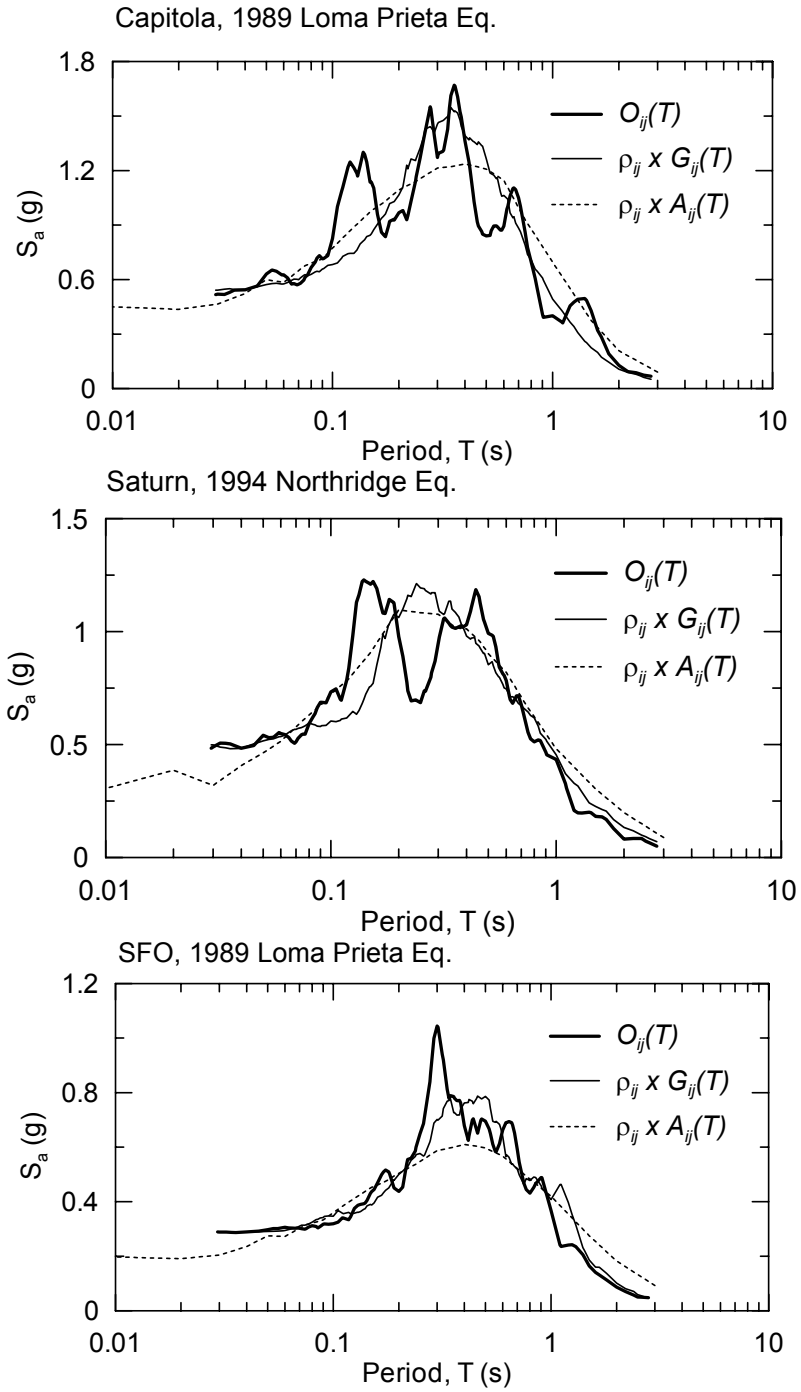

Fig. 6.8. The scaled spectral shapes predictions from ground response analyses and soil attenuation model at the selected sites: Capitola Fire Station, Saturn Elementary School, and San Francisco Airport, SFO

6.2.3 Propagation of Uncertainties Through Ground Response Analyses

The overall uncertainty in predicted spectra from ground response analyses can be thought of as arising from the following sources:

1. **Input Motions: There are two principle sources of uncertainty associated with the input motions. The first relates to the shape of the target rock spectrum (derived as explained in Section 5.1.3). This spectrum would ideally represent the spectral shape that would have occurred at the site had the site condition been firm rock. Our estimate from a modified attenuation relationship averages essentially random source/path effects from many sites, and would obviously be expected to misfit any particular site, with the amount of misfit being unknown and non-quantifiable. The second source of uncertainty relates to the time histories scaled to match the target spectrum in an average sense. This can be thought of as a time history uncertainty that is conditional on the assumed target spectral ordinates. The uncertainty is derived from (a) the random amplitude of the time history suite around the target and (b) the random phasing of the time histories. Since both amplitude and phasing affect response spectral ordinates, the second (time history) uncertainty can be quantified for ground motion *j* in category *i* by the period dependent standard deviation of the time history suite [$(\sigma_{g\text{-}in})_{ij}$].**
2. **Site Response Physics: Factors other than the response of shallow sediments to nearly vertically propagating waves influence the "site effects" inherent to ground motion recordings. These factors may include basin effects, surface waves, relatively deep ground response effects, and topographic effects. Since these factors are not included in our modeling of the site response, epistemic uncertainty is introduced as a result of the incomplete model of the site response physics. The magnitude of this uncertainty is unknown.**
3. **Ground Response Analysis: The modification of an input motion by the ground response analysis model depends on input motion characteristics such as phasing and amplitude. These variable input motion characteristics produce variable levels of non-linearity, the standard deviation of which is quantified by $(\sigma_{RRS})_{ij}$, which is calculated for each site. Note that $(\sigma_{RRS})_{ij}$ could be generalized to also incorporate**

response uncertainty from aleatory uncertainty in soil properties. This uncertainty has not been considered in the analyses reported herein.

The complete uncertainty associated with the above three sources could only be quantified if many recordings at a given site were available from which residuals could be defined based on ground response results. The uncertainty beyond $(\sigma_{g\text{-}out})_{ij}$ would be that associated with the unknown sources identified above (input spectrum + site response physics).

If the ground response model was linear, the variance of output motions, $(\sigma_{g-out})_{ij}^2$, would be equal to the sum of the variances of input and system response (Ang and Tang, 1975, p97).

$$(\sigma_{g-out})_{ij}^2 = (\sigma_{g-in})_{ij}^2 + (\sigma_{RRS})_{ij}^2 \text{: linear system} \quad (6.3)$$

The equality in Eq. 6.3 does not apply, and as seen in Figures 6.4 to 6.6, the standard deviation of ground response output, $(\sigma_{g-out})_{ij}$, is in fact lower at short periods than the standard deviation of input motions, $(\sigma_{g-in})_{ij}$. This reduction is the result of non-linearity in the sediment response, which effectively correlates RRS to the input amplitude. For example, an unusually small input amplitude produces a relatively linear response, and hence produces a relatively large output due to low damping. Conversely, a large input creates large non-linearity with large damping, which reduces the output at low periods. The net effect is that the input and response counter-act each other in such a way as to reduce the output motion dispersion at low periods.

The main contribution to $(\sigma_{g-out})_{ij}$ comes from $(\sigma_{g-in})_{ij}$ for $T > 0.3$ s., as can be seen from Figures 6.4 to 6.6. At lower periods, $(\sigma_{g-out})_{ij}$ is heavily influenced by both uncertainty in the site response $(\sigma_{RRS})_{ij}$ and $(\sigma_{g-in})_{ij}$.

6.2.4 Sensitivity of Ground Response Results to Non-linear Soil Model

The sensitivity of the ground response analysis results for the three subject sites to alternative non-linear soil models was tested by comparing the above results (obtained using the lab-based nonlinear soil models in Table 5.2) to a second set of results obtained using the recommended set of curves by Silva et al. (1997). The recommended nonlinear

soil models by Silva et al. (1997) are described in Section 3.4.1. For southern California sites (i.e., Saturn), the Silva models are significantly more linear at large strains than the lab-based models. For Bay Area sites not on Bay Mud, the Silva models are generally more nonlinear at shallow depths and more linear at depth. For Bay Mud soils, there are no significant differences between the Silva model and the lab-based model.

The ground response analysis results obtained through the use of both sets of nonlinear soil models are presented in Figure 6.9. Median strain profiles at each site from ground response analyses for both recordings are shown in Figure 6.10. Results obtained from the two models for weak levels of shaking (e.g., SFO-Morgan Hill, and Capitola-Morgan Hill recordings) show little difference. The levels of shear strain induced by the relatively weak input motions at these sites are generally less than 0.02%. Differences in computed spectra begin to become significant when shear strains approach 0.1-0.5% (i.e., Saturn site and Loma Prieta motion at Capitola site). For the Saturn site, the effect of the more linear model is to shift the spectrum up and to the left (i.e., shifting the energy to lower periods). For the Capitola site, the effect of the more nonlinear model at shallow depths is to shift of spectrum down and to the left. For the SFO site, the two models produce essentially identical results because of the nearly identical modeling of the Bay Mud nonlinear properties.

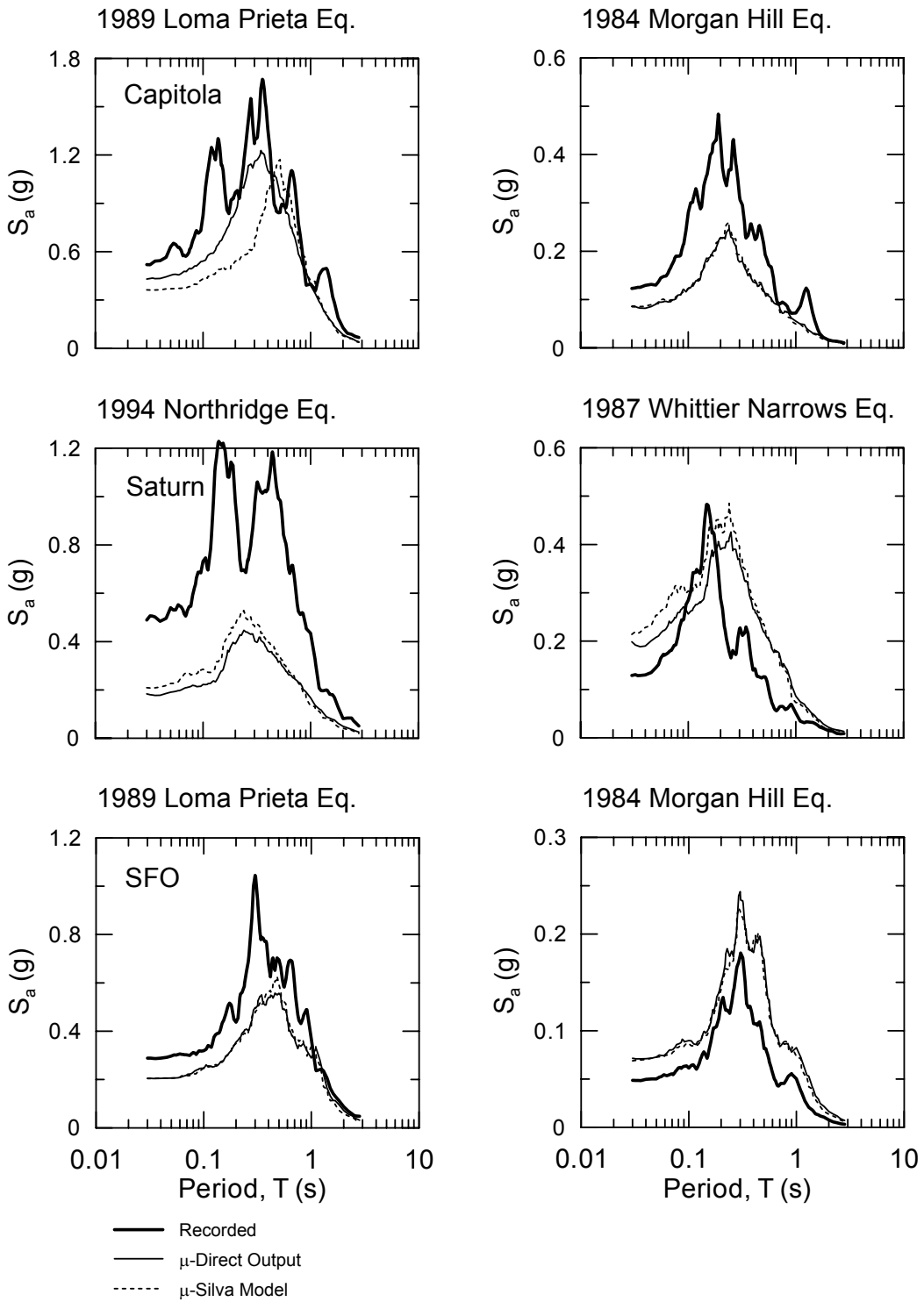

Fig. 6.9. The ground response analysis results by soil model recommended by Silva et al. (1997) along with the original results at the selected sites

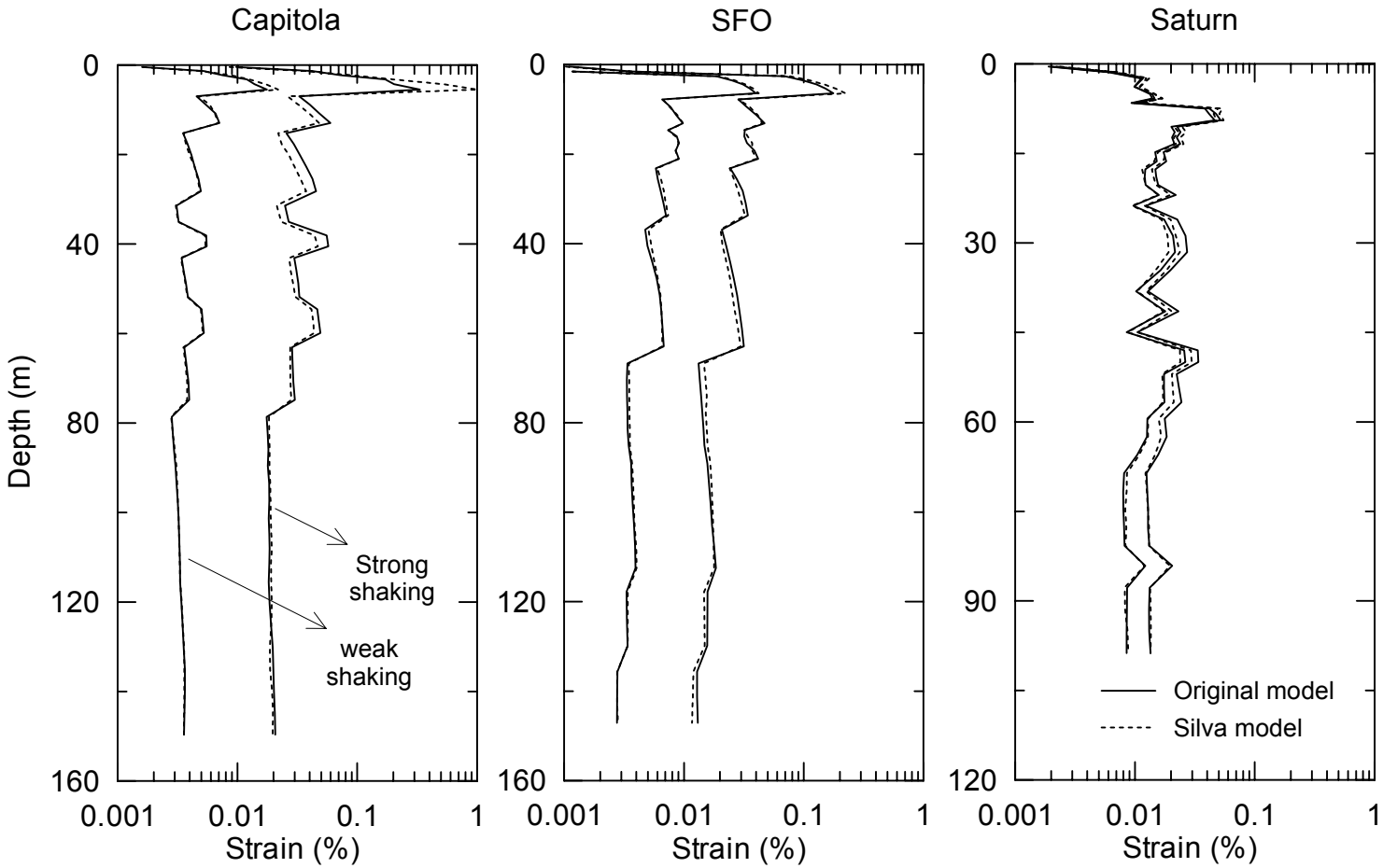

Fig. 6.10. The strain profiles for same motion with different soil models

6.3 COMPILATION OF CATEGORY STATISTICS

6.3.1 Objectives and Notation

In this section, we compile together analysis results for collections of sites sharing common characteristics (i.e., sites within a category) to elucidate the benefits of performing ground response analyses relative to other, more simplified procedures for ground motion estimation. In this context, benefits of ground response analysis are considered to be reductions in the bias or dispersion of prediction residuals relative to the residuals obtained from the more simplified procedures and/or improved predictions of spectral shape. To more clearly illustrate bias and dispersion trends, prediction residuals are also compiled as a function of real valued site parameters ($V_{s\text{-}30}$ and depth to V_s = 1 km/s $\equiv z_1$).

The notation defined in Section 6.2.1 is retained here, but a few additional terms related to the definition of residuals are introduced. Denoting the natural logarithm of a recorded, or "observed", ground motion parameter at soil site *j* in category *i* as O_{ij}, residuals between the estimated median S_a values and O_{ij} are taken as:

$(\mu_{ra})_{ij} = O_{ij}, - A_{ij}$: **residual of attenuation estimate**

$(\mu_{ras})_{ij} = O_{ij}, - AS_{ij}$: **residual of estimate from attenuation + site amplification factor**

$(\mu_{rab})_{ij} = O_{ij}, - AB_{ij}$: **residual of estimate from attenuation + basin amplification factor**

$(\mu_{rg})_{ij} = O_{ij}, - G_{ij}$: **residual of ground response estimate**

Each of these residuals is evaluated across a range of spectral periods. For each period, the medians, standard deviations of residuals, standard errors of median quantities, and standard errors of standard deviation quantities within category *i* are evaluated across the *j*=1 to M_i sites (denoting the number of sites in category *i* as M_i). The standard errors of medians are calculated as (Ang and Tang, 1975, p 232)

$$(se_{\mu ra})_i^2 = (\sigma_{ra})_i^2 / M_i \qquad \textbf{(6.4)}$$

where $(se_{\mu ra})_i$ denotes the standard error of the estimate of $(\mu_{ra})_i$. The standard errors of standard deviations are calculated by Eqn. 6.5, which is valid for large M_i (Lee and Anderson, 2000)

$$(se_{\sigma ra})_i = (\sigma_{ra})_i / \sqrt{2M_i} \quad \textbf{(6.5)}$$

Similar definitions apply for the other median quantities considered. Notation for the four statistical quantities evaluated from the residuals of each prediction method is as follows:

	Median	Std. Dev.	*se* of Median	*se* of Std. Dev.
Attenuation	$(\mu_{ra})_i$	$(\sigma_{ra})_i$	$(se_{\mu ra})_i$	$(se_{\sigma ra})_i$
NEHRP Amp. Factors	$(\mu_{ras})_i$	$(\sigma_{ras})_i$	$(se_{\mu ras})_i$	$(se_{\sigma ras})_i$
Basin Amp. Factors	$(\mu_{rab})_i$	$(\sigma_{rab})_i$	$(se_{\mu rab})_i$	$(se_{\sigma rab})_i$
GR Output	$(\mu_{rg})_i$	$(\sigma_{rg})_i$	$(se_{\mu rg})_i$	$(se_{\sigma rg})_i$

Hereafter, the attenuation + site amplification factors model will be referred to by the type of site factors used (i.e., the "NEHRP amplification" model, "surface geology amplification" model, or "geotechnical amplification" model). Likewise, the attenuation + basin amplification factor model will be referred to as the "basin" model.

It is important to emphasize that the quantities given above are statistics computed using median prediction residuals for all sites within category *i*. Two other quantities are also of interest, which are statistics computed using the standard error of predictions for all sites within a category. These are $(\overline{se}_{g-out})_i$, which defines the average uncertainty in the location of the median residual, and $(\overline{se}_{RRS})_i$, which defines the average standard error in the RRS. These quantities are computed as

$$(\overline{se}_{g-out})_i = average(se_{g-out})_{ij} \quad \textbf{(6.6a)}$$

$$(\overline{se}_{RRS})_i = average(se_{RRS})_{ij} \quad \textbf{(6.6b)}$$

Note that $(\overline{se}_{RRS})_i$ is a contributor to $(\overline{se}_{g-out})_i$.

As noted above, statistical analysis of residuals as a function of real-valued site parameters such as V_{s-30} or z_1 are also performed. In these cases, regression analyses are performed in lieu of simple calculations of the median within a category. Standard errors

are then calculated from the misfits between the data and regression using standard statistical techniques. Notation associated with specific regression analyses is introduced at the location in the report where the analyses are presented.

6.3.2 Results for NEHRP Categories

Compiled in Figures 6.11-6.13 are the category statistics defined above for NEHRP Categories C-E. The top frames of each figure relate to the ground response results, showing on the top-left side the period-dependence of the median residual (μ_{rg}) along with the error bounds on the median (i.e., $\mu_{rg} \pm se_{\mu rg}$), and showing on the top-right side the standard deviation of the residuals (σ_{rg}) along with their error bounds (i.e., $\sigma_{rg} \pm se_{\sigma rg}$) and the additional error terms defined in Eq. 6.6. One of these additional error terms, $(\overline{se}_{g-out})_i$, defines the average uncertainty in the location of the median residual, and represents one contribution to σ_{rg} (as discussed in Section 6.2.3, the other contributions to σ_{rg} are input target spectrum and modeling errors). The bottom-left frames of each figure show the median predictions and their error bounds from attenuation alone (plotted with continuous lines) and attenuation modified with NEHRP and basin amplification factors (plotted with circles at discrete periods). The bottom right frames show the standard deviation of the residuals and the corresponding error bounds for each estimation procedure.

It should be noted that the statistics shown in Figures 6.11-6.13 for the basin model are based on subsets of sites due to missing data. This model was used for 39 motions at 22 C sites, 62 motions at 26 D sites, and eight motions at seven E sites.

The NEHRP amplification model provides a convenient baseline set of results against which to compare the results of other models. This is because the NEHRP model represents an empirical customization of the Abrahamson and Silva attenuation relation for specific site categories, and hence the results obtained through use of the amplification model represent the expected median for each NEHRP category. Accordingly, when median residuals from the NEHRP amplification model are non-zero, the sub-set of sites within the category is biased with respect to the category as a whole. Statistically significant bias is considered to occur when zero is not within the range of $\mu_{ras} \pm se_{ras}$. As shown in Figure 6.12, this bias is generally not observed for Category D, but is observed at all periods for C and near PHA and 1.0 s for E. This bias results from the process by which sites are selected for detailed geotechnical ground characterization work – i.e., sites with unusually large ground motions are disproportionately selected. It is important to consider this bias, which is inherent to the site selection, when interpreting the bias reported for a particular prediction method such as ground response.

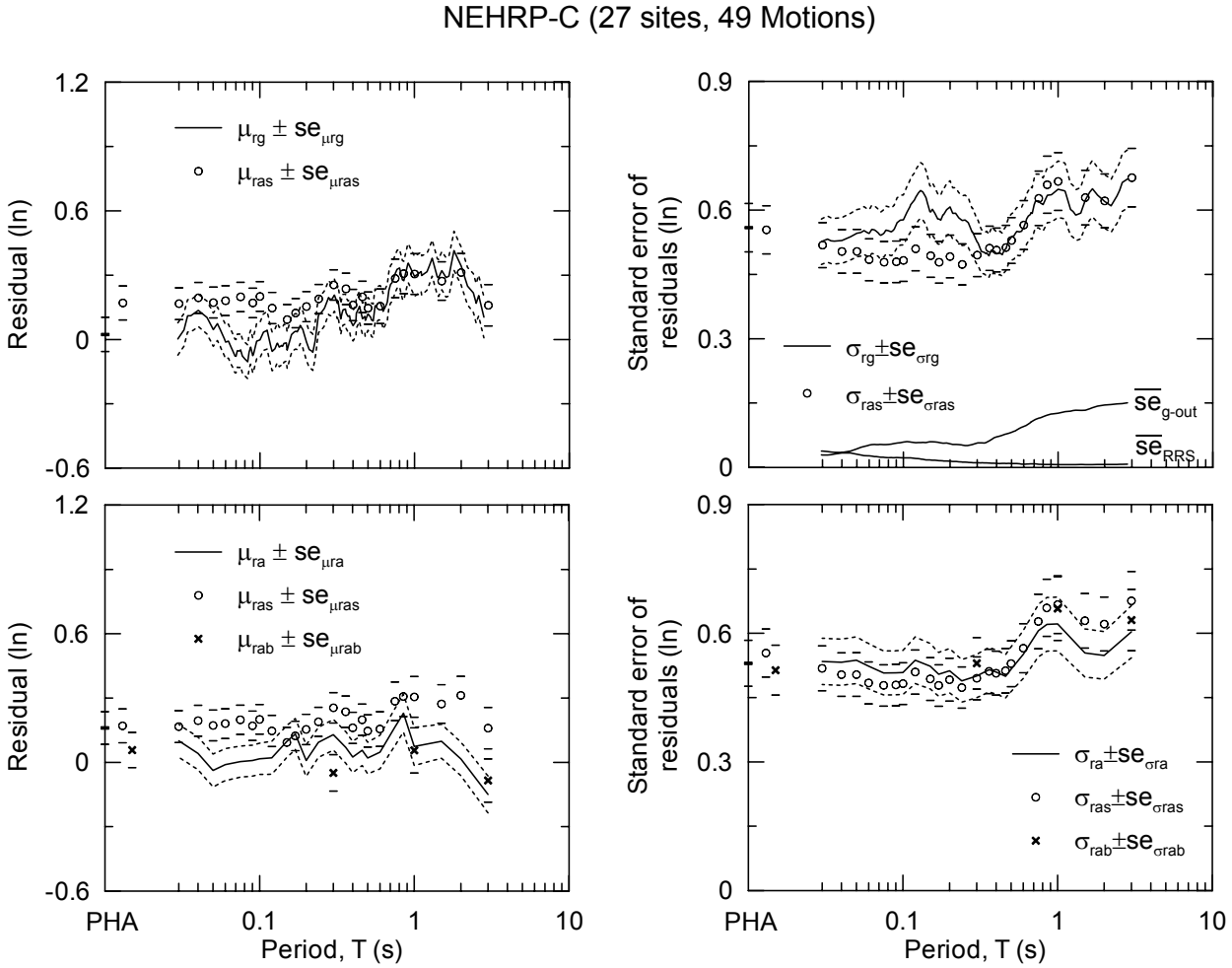

Fig. 6.11. Category residuals for NEHRP C sites

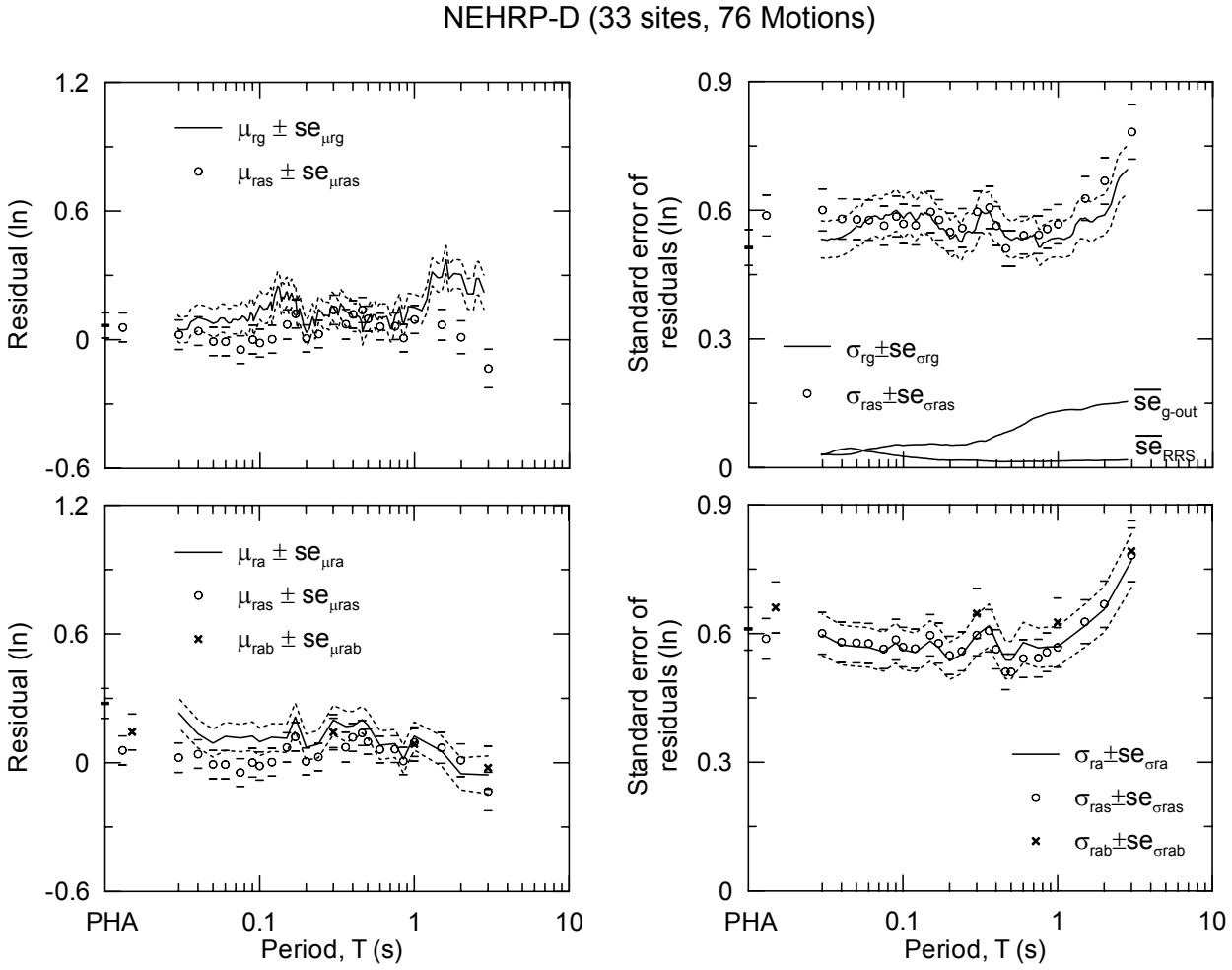

Fig. 6.12. Category residuals for NEHRP D sites

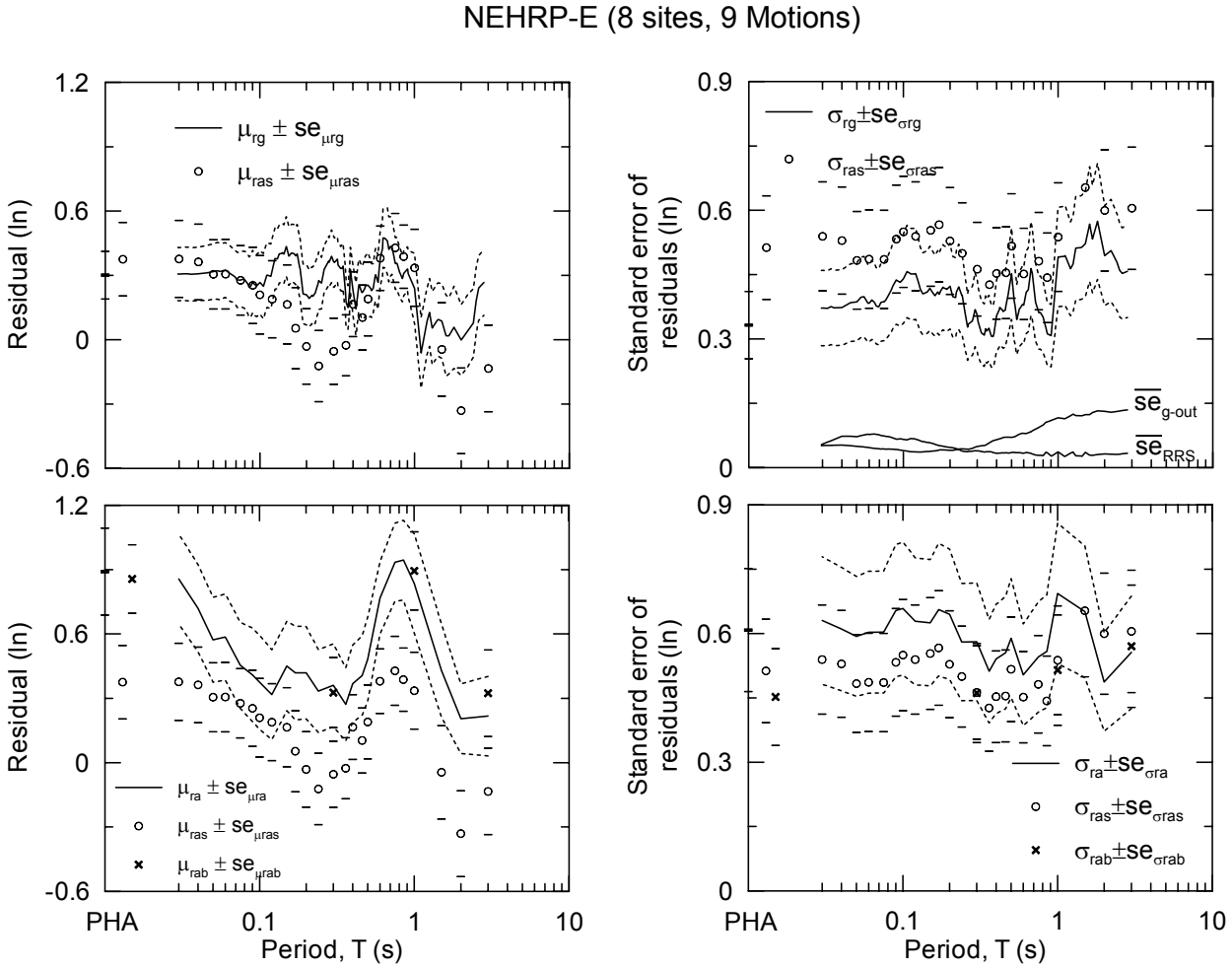

Fig. 6.13. Category residuals for NEHRP E sites

The first potential benefit of ground response analyses that is investigated is bias reduction relative to alternative models. Initial inspection of Figures 6.11-6.12 suggests significant positive bias in ground response results (i.e., $\mu_{rg} > 0$) across all periods for NEHRP C (Figure 6.11) and at mid-periods for D (Figure 6.12). However, in many cases the amount of this bias nearly matches the bias from the amplification factors, suggesting that the ground response analysis results themselves are *not* biased. This is confirmed by hypothesis testing in which sample 't' statistics are compiled to test the null hypothesis that $(\mu_{rg})_i - (\mu_{ras})_i = 0$. This statistical testing provides a significance level = α that the null hypothesis cannot be rejected. For clarity of expression, we tabulate in Table 6.3 values of 1-α, which we refer to as a rejection confidence for the null hypothesis. Large rejection confidence levels (i.e., > ~95%) suggest significant bias. As shown in Table 6.3, actual rejection confidence values are generally small for Categories C and D, suggesting the lack of a statistically significant bias. Results are mixed for E (Figure 6.13), with significant bias relative to amplification at some periods (0.3 and 3.0 s) but not at others (PHA and 1.0 s). Moreover, bias for E sites is sometimes positive and sometimes negative, suggesting no systematic trend towards under- or over-prediction. Overall, our results do not suggest systematic bias in predictions of spectral acceleration from ground response analyses.

Table 6.3. Rejection confidence levels (in percent) for the hypothesis that $\mu_{rg} - \mu_{ras}=0$

T(s)	ALL (134 mtns)	C (49 mtns)	D (76 mtns)	E (9 mtns)
PHA	38	81	9	28
0.3	42	39	10	95
1	72	7	47	30
3	97	25	100	92

A second potential benefit of ground response that can be investigated is the reduction of dispersion relative to alternative prediction methods. As shown in Figures 6.11-6.12, $\sigma_{rg} \approx \sigma_{ras}$ for Categories C-D across the period range considered, whereas $\sigma_{rg} < \sigma_{ras}$ for Category E at $T <$ 0.5 s. A statistical test for the degree to which these dispersion values are distinct is performed using the *Two-Sample F Test* (Ayyub and McCuen, 1997, p 226). This test compares the normalized residual sum-of-squares for two alternative models fit to the same data. These sum-of-squares are represented by category variance terms, which are used to calculate an F-statistic as follows for the example of the ground response and NEHRP amplification factor models:

$$F = \sigma_{ras}^2 \big/ \sigma_{rg}^2 \tag{6.7}$$

This F statistic can be compared to the F distribution to evaluate a significance level (p) for the test. Values of p serve as an indicator of the distinction in dispersion levels, with smaller p values indicating greater distinction. A consensus does not exist on what value of p corresponds to "significant" distinction, although values on the order of 0.05 to 0.15 have been used as benchmarks (Stewart et al., 2002). For Categories C-D, p values are generally on the order of 0.3 to 0.5, which are sufficiently high to clearly indicate that σ_{rg} and σ_{ras} are not significantly distinct.

Table 6.4. F-statistics indicating distinction between residual dispersion levels for ground response (σ_{rg}) and NEHRP amplification models (σ_{ras})

	ALL (134 mtns)		C (49 mtns)		D (76 mtns)		E (9 mtns)	
T(s)	F	p	F	p	F	p	F	p
PHA	1.20	0.15	1.02	0.48	1.31	0.12	2.38	0.11
0.3	1.03	0.43	1.13	0.34	1.09	0.35	1.69	0.22
1	1.09	0.30	1.06	0.42	1.12	0.31	1.20	0.40
3	1.21	0.14	1.01	0.48	1.23	0.18	1.95	0.17

Examining the dispersion results in Figure 6.13 and Table 6.4 for Category E, the NEHRP and ground response dispersion levels are seen to be qualitatively different at low periods (e.g., PHA and 0.3 s period), and the F values are larger than for the other categories at all periods. The difference is such that the ground response dispersion is smaller than the NEHRP amplification dispersion, although the statistical significance of the difference based on the F test is only moderate for PHA and insignificant for longer periods. However, these results should be interpreted with caution, because the 9 ground motions used to establish the E statistics represent a large fraction of motions used to develop the E amplification factors (18 motions were used to establish these factors in Stewart et al. 2002, including all 9 from this study). Given the redundancy of the data sets, one would expect the amplification factors to provide a good fit to the observed spectra. More meaningful statistics are enabled when one expands the E category to Hlm, because Hlm amplification factors are established from a much larger, and less redundant data set. Further discussion of Hlm category results is presented in Section 6.3.4.

The final benefit of ground response predictions that is investigated is the degree to which the predictions are able to capture spectral shape, as measured for an individual site by $(\sigma_e)_{ij}$. We compile shape misfit parameters for all sites within NEHRP categories using the ground response, amplification factors, and attenuation models. These values are used to calculate the median and standard deviation of σ_e [$(\mu_{\sigma e})_i$ and $(\sigma_{\sigma e})_i$, respectively] across all sites in Category i, with the results shown in Table 6.5. The ground response median shape misfit parameters are seen to be much smaller for E (0.19) than for C-D (~0.3), indicating that ground response analyses are more successful at capturing spectral shape for soft soil sites than for stiffer materials. Moreover, ground response $\mu_{\sigma e}$ for E is much smaller than the corresponding $\mu_{\sigma e}$ from the amplification and attenuation models, whereas for C-D the ground response, amplification, and attenuation $\mu_{\sigma e}$ values are nearly equal. This indicates that ground response analyses are able to significantly improve upon spectral shape estimates from the amplification or attenuation models only for soft soil (E) sites.

Table 6.5. The median ($\mu_{\sigma e}$) and standard deviation ($\sigma_{\sigma e}$) of the average misfit values for NEHRP categories

Category		Ground Response	Amp. Factors	Attenuation
ALL 134 mtns	$\mu_{\sigma e}$	0.29	0.28	0.29
	$\sigma_{\sigma e}$	0.12	0.13	0.12
C 49 mtns	$\mu_{\sigma e}$	0.30	0.28	0.31
	$\sigma_{\sigma e}$	0.12	0.14	0.14
D 76 mtns	$\mu_{\sigma e}$	0.29	0.28	0.28
	$\sigma_{\sigma e}$	0.12	0.13	0.11
E 9 mtns	$\mu_{\sigma e}$	0.19	0.30	0.32
	$\sigma_{\sigma e}$	0.08	0.10	0.06

Ground response results can of course also be compared to predictions from other models such as attenuation alone or attenuation with basin amplification factors. With respect to attenuation, one can qualitatively observe in Figures 6.11-6.13 bias levels different from ground response within Categories C and E at specific periods (e.g., 3.0 s for C, 1.0 s for E), which is also borne out by high rejection confidence values for the null hypothesis that the bias values are equal (Table 6.6). For mid-periods, Category D generally does not show distinct bias levels, which is expected because the data set used to develop the soil attenuation model is dominated by class D sites. At $T > 1$ s, significant differences exist between attenuation and ground

response for Categories C-D. These differences at long period result from positive ground response bias and nearly zero attenuation bias. This may be a result of basin response effects, which are not simulated by the ground response modeling, but which are present in an average sense in the attenuation relations. The results of F tests comparing standard deviations between models are presented in Table 6.7, and confirm what can be qualitatively observed from Figures 6.11-6.13 that dispersion levels between ground response and attenuation are moderately to significantly distinct at small periods (T < 1.0 s) within category E, but are generally not significantly distinct for other site categories.

Table 6.6 Rejection confidence levels (in percent) for the hypothesis that μ_{rg} - μ_{ra}=0

T(s)	ALL (134 mtns)	C (49 mtns)	D (76 mtns)	E (9 mtns)
PHA	98	78	98	98
0.3	16	51	39	1
1	84	91	23	95
3	100	99	99	36

Table 6.7. F-statistics indicating distinction between residual dispersion levels for ground response (σ_{rg}) and attenuation models (σ_{ra})

	ALL (134 mtns)		C (49 mtns)		D (76 mtns)		E (9 mtns)	
T(s)	F	p	F	p	F	p	F	p
PHA	1.30	0.07	1.11	0.36	1.42	0.07	3.35	0.04
0.3	1.10	0.29	1.10	0.37	1.09	0.35	2.66	0.08
1	1.13	0.24	1.09	0.38	1.13	0.30	1.99	0.16
3	1.07	0.35	1.24	0.23	1.19	0.22	1.65	0.23

Qualitative results for the basin amplification model for Categories C and D (Figures 6.11-6.12) suggest that the basin model bias is slightly reduced from that obtained by attenuation at all periods considered, although the difference is not statistically significant. Dispersion values are generally also slightly reduced. For NEHRP E (Figure 6.13), the bias values are again not significantly different from attenuation, although the dispersions are smaller.

All of the above discussion focused on prediction residuals grouped within NEHRP site categories. Also of interest is the trend in these residuals with $V_{s\text{-}30}$, which is presented in Figures 6.14. To help illustrate the trends in these data, also plotted in Figures 6.14 are the results of regression analyses performed according to the following equation:

$$\ln(\mu_{ra})_j = a + b\ln(V_{s-30})_j \tag{6.8}$$

where $(\mu_{ra})_j$ is the median residual for site j, $(V_{s\text{-}30})_j$ is the velocity for that site, and a and b are regression coefficients. Confidence intervals (±95%) are also presented on the plots. Of interest is the degree to which a trend exists in the regression lines, which is investigated using sample 't' statistics to test the null hypothesis that $b = 0$ and a = overall data median. This statistical testing provides a significance level = α that the null hypothesis cannot be rejected. For ease of interpretation, tabulated in Table 6.8 are the values of 1-α, which is here referred to as a "rejection confidence for a b=0 model". Large rejection confidence levels (i.e., >95%) suggest significant $V_{s\text{-}30}$ dependence in residuals.

Table 6.8 Regression coefficients for residuals vs. $V_{s\text{-}30}$

Category	T(s)	a	b	σ	Rejection confidence for b=0 model (%)
Ground Response	PHA	1.11 ± 0.51	-0.17 ± 0.09	0.52	95
	0.3	1.27 ± 0.53	-0.19 ± 0.09	0.54	96
	1	0.72 ± 0.57	-0.09 ± 0.10	0.58	67
	3	2.48 ± 0.65	-0.39 ± 0.11	0.66	100
NEHRP	PHA	0.30 ± 0.56	-0.03 ± 0.10	0.57	27
	0.3	0.28 ± 0.54	-0.02 ± 0.09	0.55	19
	1	1.68 ± 0.59	-0.27 ± 0.10	0.60	99
	3	0.37 ± 0.73	-0.06 ± 0.13	0.75	39
Attenuation	PHA	2.42 ± 0.57	-0.36 ± 0.10	0.58	100
	0.3	1.85 ± 0.55	-0.28 ± 0.09	0.56	100
	1	2.51 ± 0.59	-0.40 ± 0.10	0.60	100
	3	1.57 ± 0.68	-0.28 ± 0.12	0.69	98
Basin	PHA	2.67 ± 0.62	-0.42 ± 0.10	0.60	100
	0.3	2.19 ± 0.61	-0.35 ± 0.10	0.60	100
	1	2.76 ± 0.66	-0.44 ± 0.11	0.64	100
	3	1.56 ± 0.74	-0.27 ± 0.13	0.72	97

As shown in Figures 6.14 and Table 6.8, the NEHRP model residuals generally do not have a significant trend with $V_{s\text{-}30}$. Ground response analysis residuals have a statistically significant trend at small periods (PHA and 0.3 s), although the slope is small. The residuals from the attenuation and basin amplification models both have relatively large and significant trends with $V_{s\text{-}30}$ at all periods. Based on these results, it appears that ground motion predictions obtained from the attenuation or basin models can be significantly biased for small $V_{s\text{-}30}$ values (the amplification at small $V_{s\text{-}30}$ controls the trends depicted in Figures 6.14), but that this bias is

significantly reduced or removed by performing ground response analyses or applying NEHRP amplification factors.

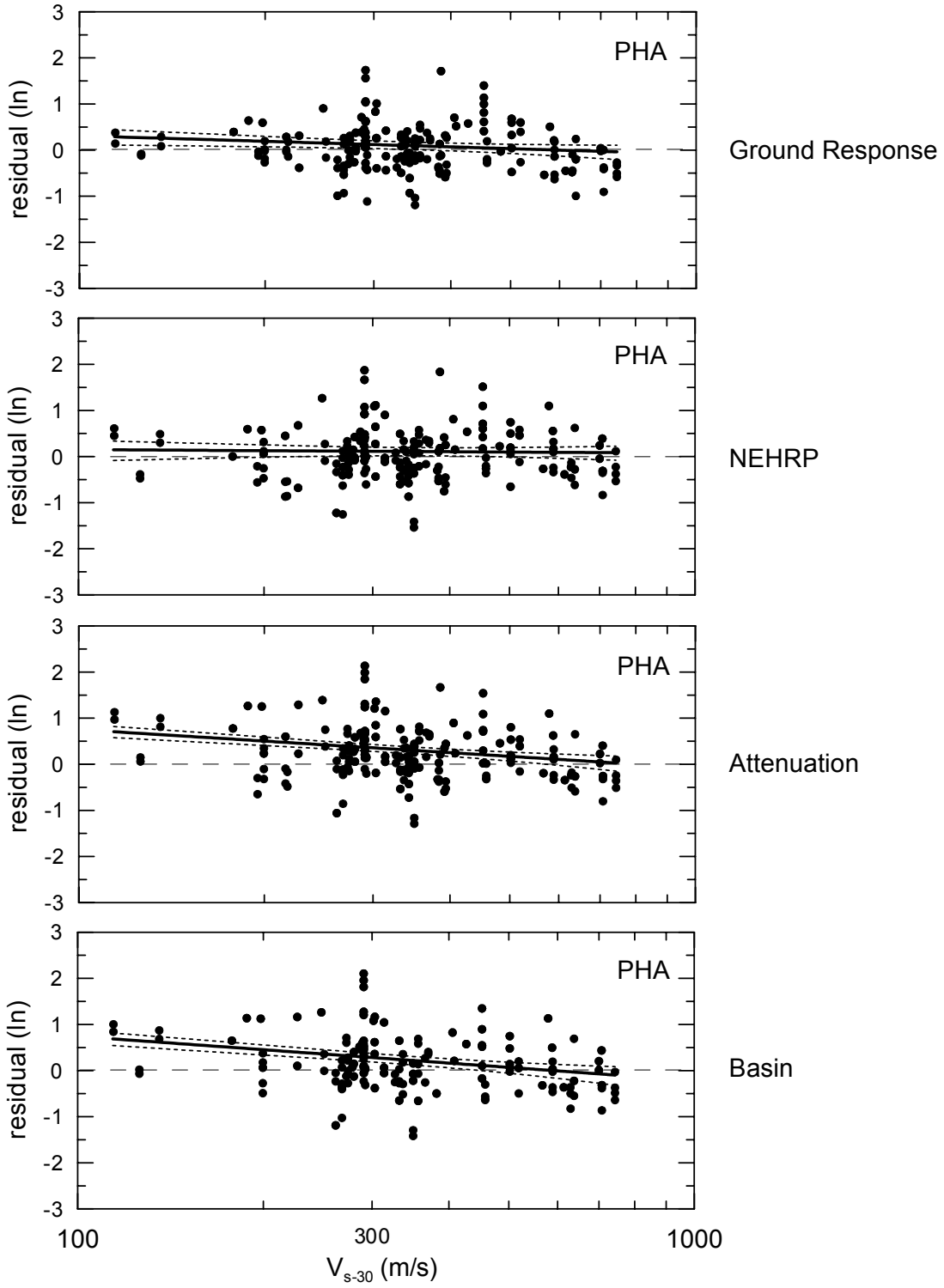

Fig. 6.14 (a). The variation of PHA residuals with respect to V_{s-}

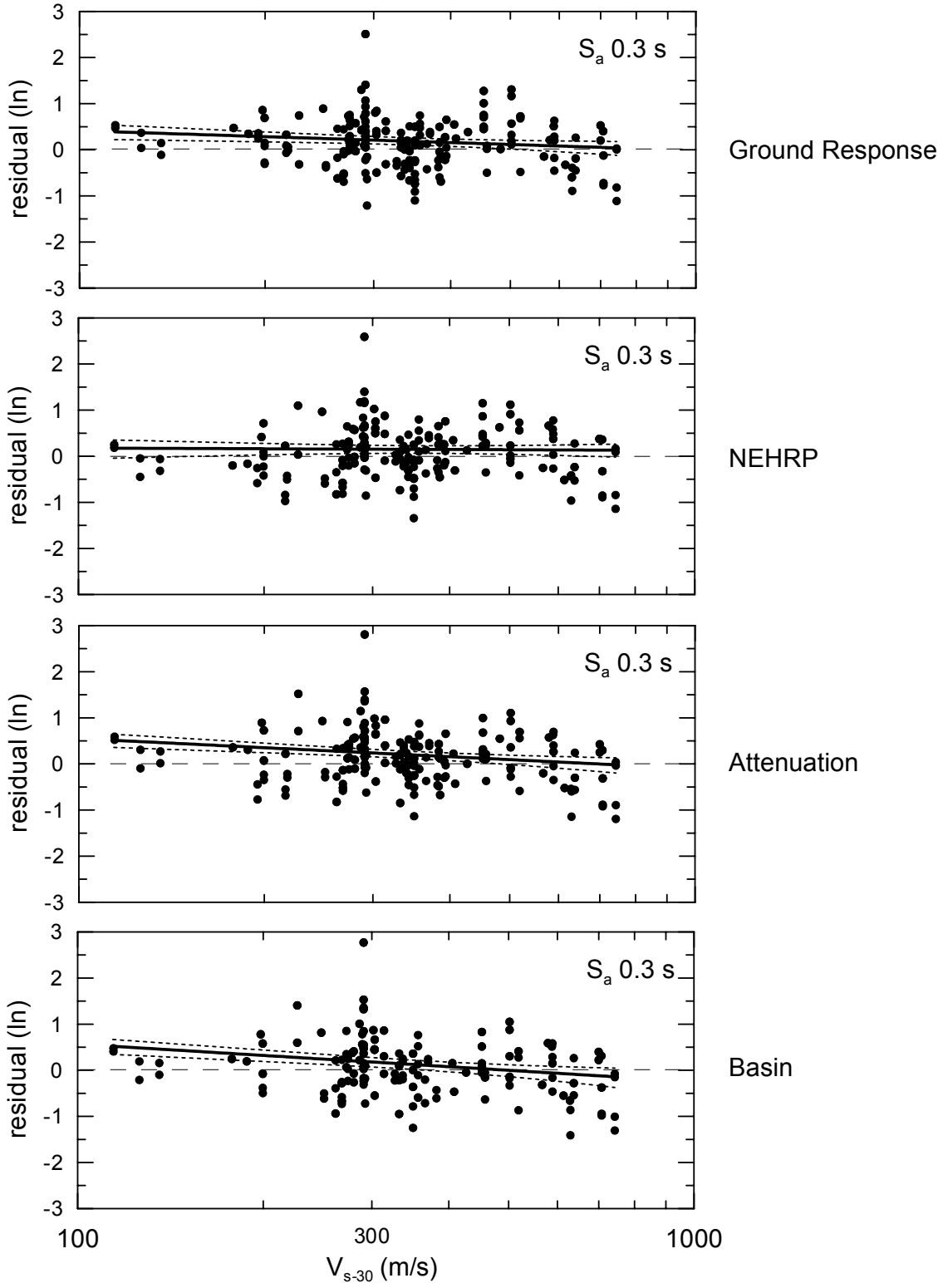

Fig. 6.14 (b). The variation of S_a 0.3 s residuals with respect to V_{s-30}

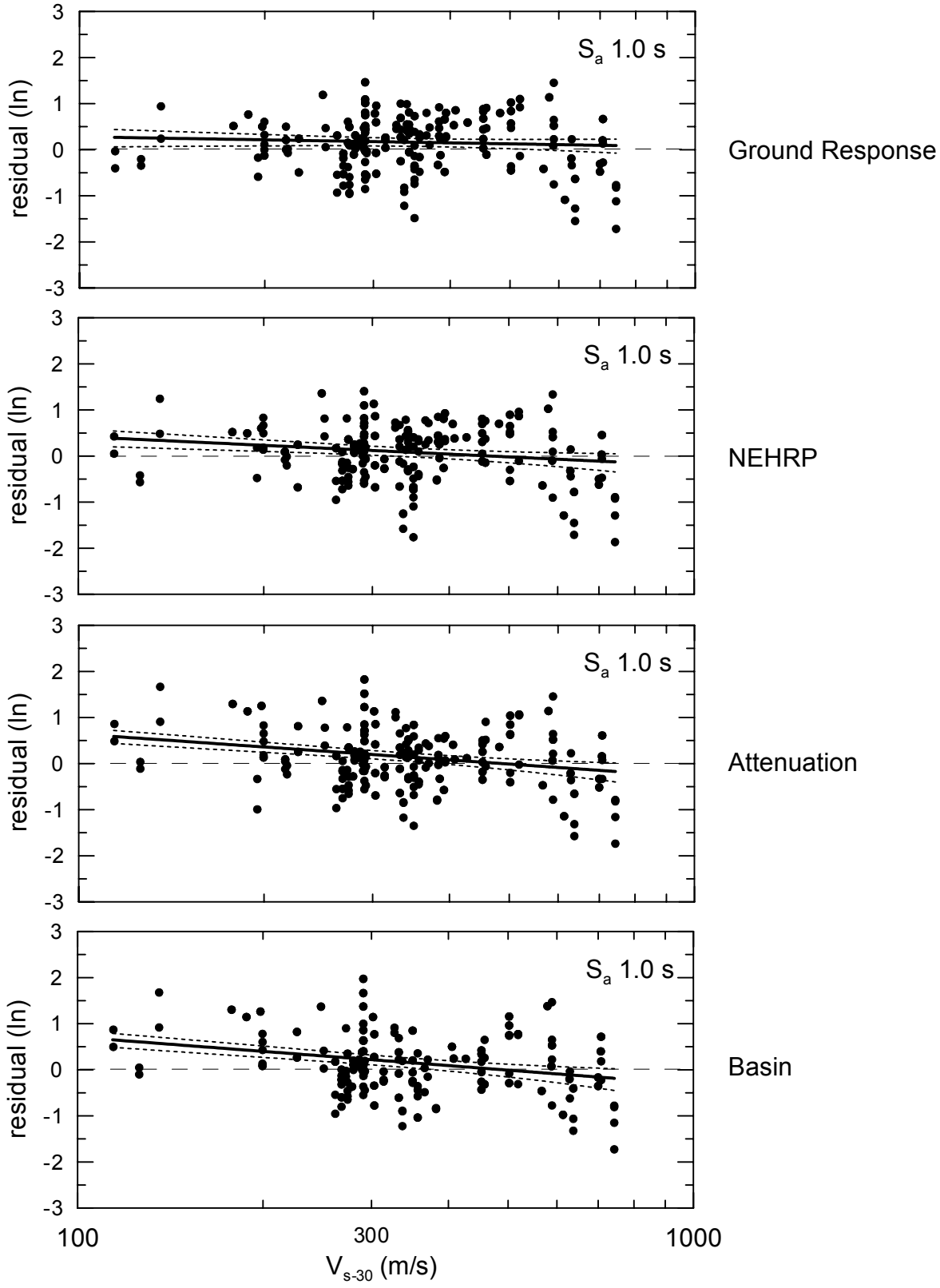

Fig. 6.14 (c). The variation of S_a 1.0 s residuals with respect to V_{s-30}

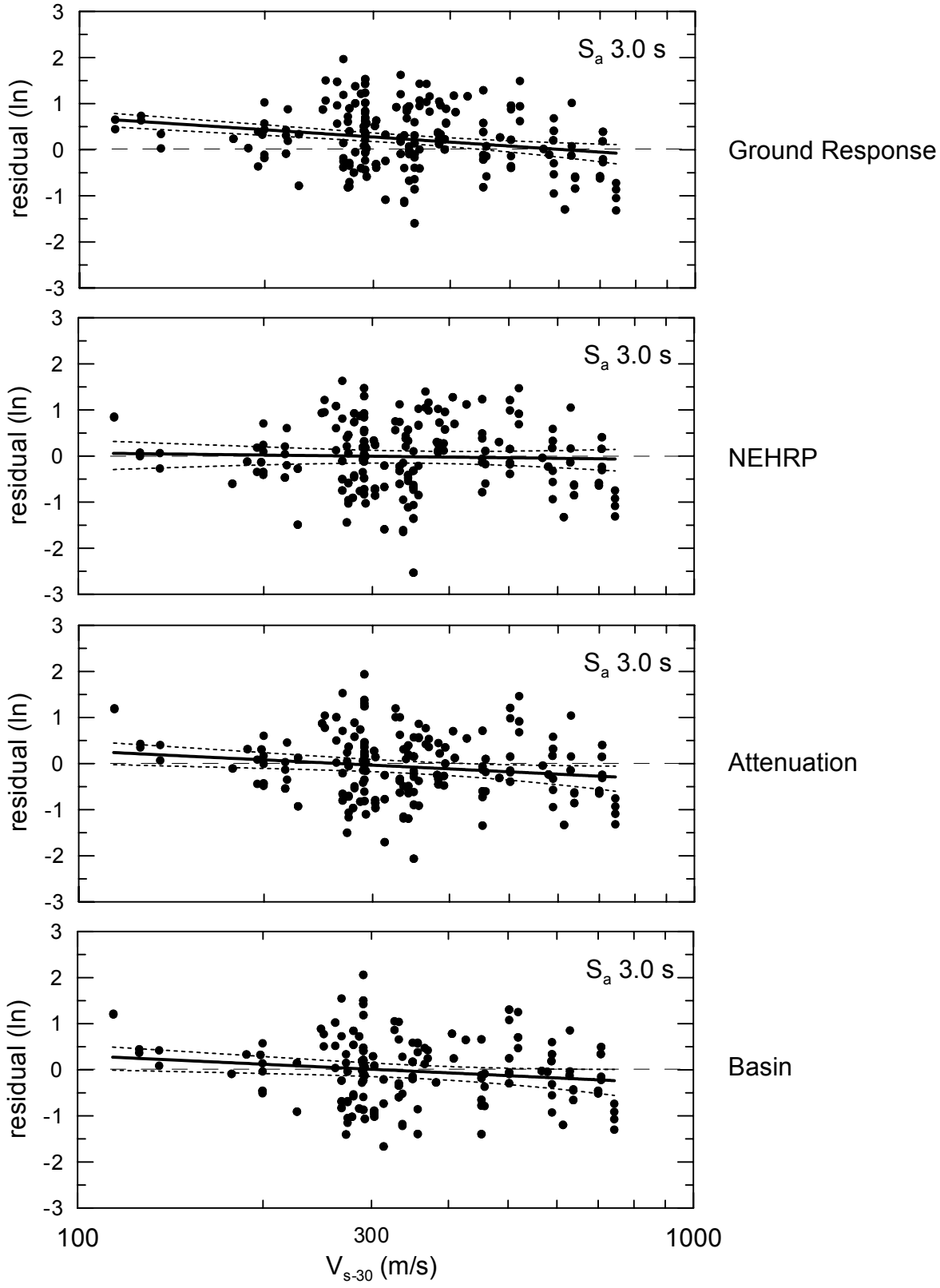

Fig. 6.14 (d). The variation of S_a 3.0 s residuals with respect to V_{s-30}

6.3.3 Results for Geotechnical Categories

Compiled in Figures 6.15-6.17 are the category statistics for Geotechnical Categories C-E, which are defined in Table 2.3. As with the NEHRP amplification model used in the previous section, spectral accelerations derived using the geotechnical amplification model can be taken as baseline results because these predictions represent the expected category medians. As shown in Figure 6.15, the amplification factor model (denoted as $\mu_{as} \pm se_{as}$ in the legend) has for Category C a statistically significant over-prediction bias (negative residuals) at short periods ($T \leq 0.2$ s), but no apparent bias at longer periods. This implies that the selected time histories in Category C tend to have lower spectral amplitudes than the category median at short periods. For Category D (Figure 6.16), a small but statistically significant under-prediction bias (positive residuals) exists across the full period range, indicating that selected motions for Category D are larger than the category median. Results for Category E (Figure 6.17) are mixed, with an under-prediction bias being present at most periods, but with no significant bias for $T \approx 0.1$-0.5 s and $T > 1.5$ s. It should be noted that the sites in Category E are the same as those in NEHRP E.

As shown in the top-left frames of Figures 6.15 to 6.17, the ground response median results (denoted as $\mu_{rg} \pm se_{\mu rg}$) have for Category C a negative bias at short periods ($T < 0.3$ s) but no significant bias at long periods, for Category D a positive bias at all periods, and for Category E a positive bias for $T < 1.0$ s. Qualitative examination of Figures 6.15 to 6.17 suggests that the ground response bias is similar to the amplification model bias for Category C at most periods. For Category D, the ground response residuals exceed those from the amplification model, with the offset increasing with T. The ground response under-prediction for Category D is especially large for $T > 1.0$ s, which is likely due to basin effects at these deep sites that are not captured by ground response analyses. For Category E, ground response and amplification model residuals differ for $T \approx 0.1$-0.5 s (amplification bias is smaller). These trends for Categories C-E are confirmed by tests for the rejection confidence of the null hypothesis that the two models have the same median residuals (Table 6.9). Statistically significant differences between the models are only found for Category D ($T \geq 1.0$ s) and Category E at $T = 0.3$ s. The systematic under-prediction of spectral acceleration for sites having deep profiles (Category D) is of some concern. This may result from basin effects or the nonlinear soil models having excessive damping at depths.

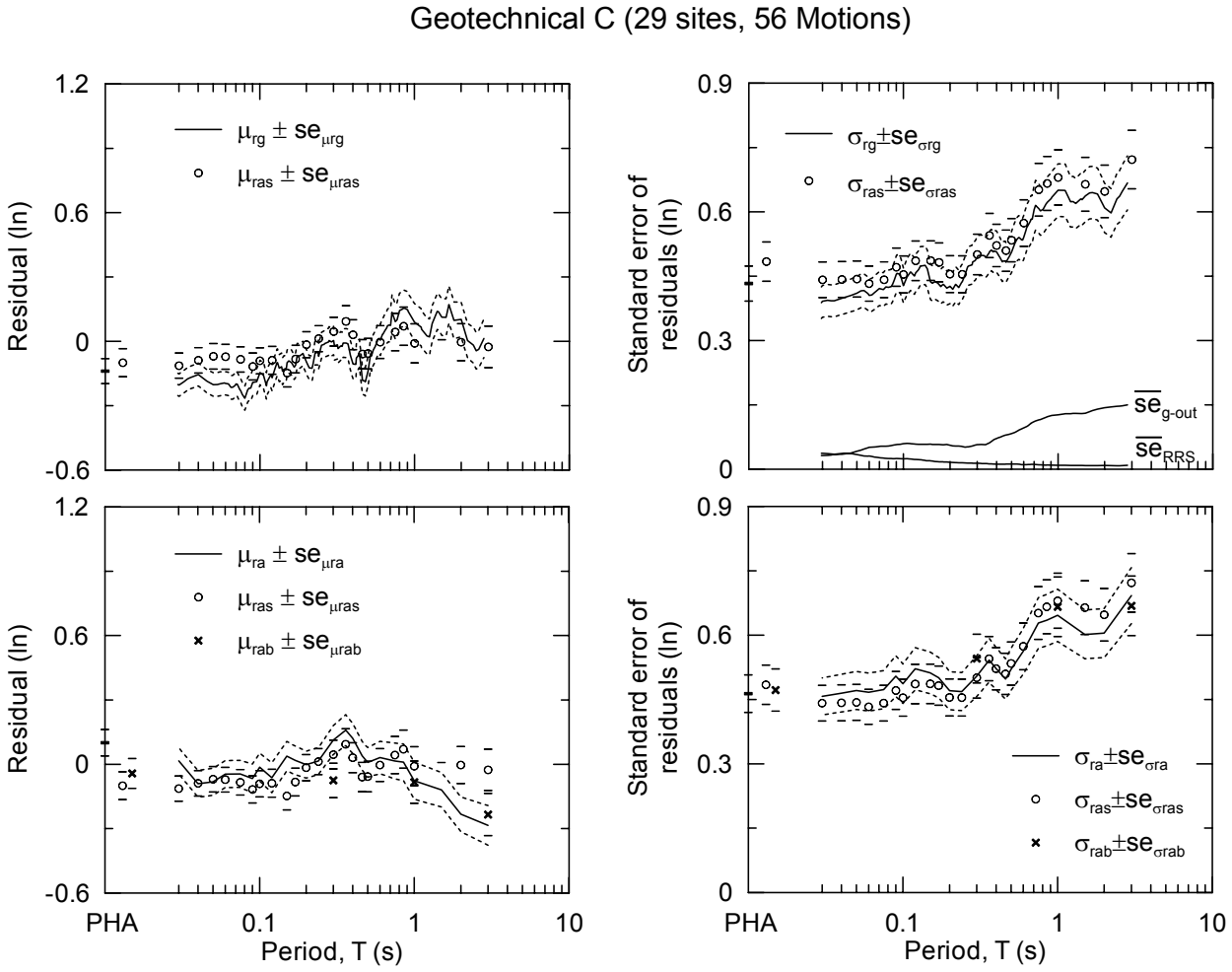

Fig. 6.15. Category residuals for Geotechnical C sites

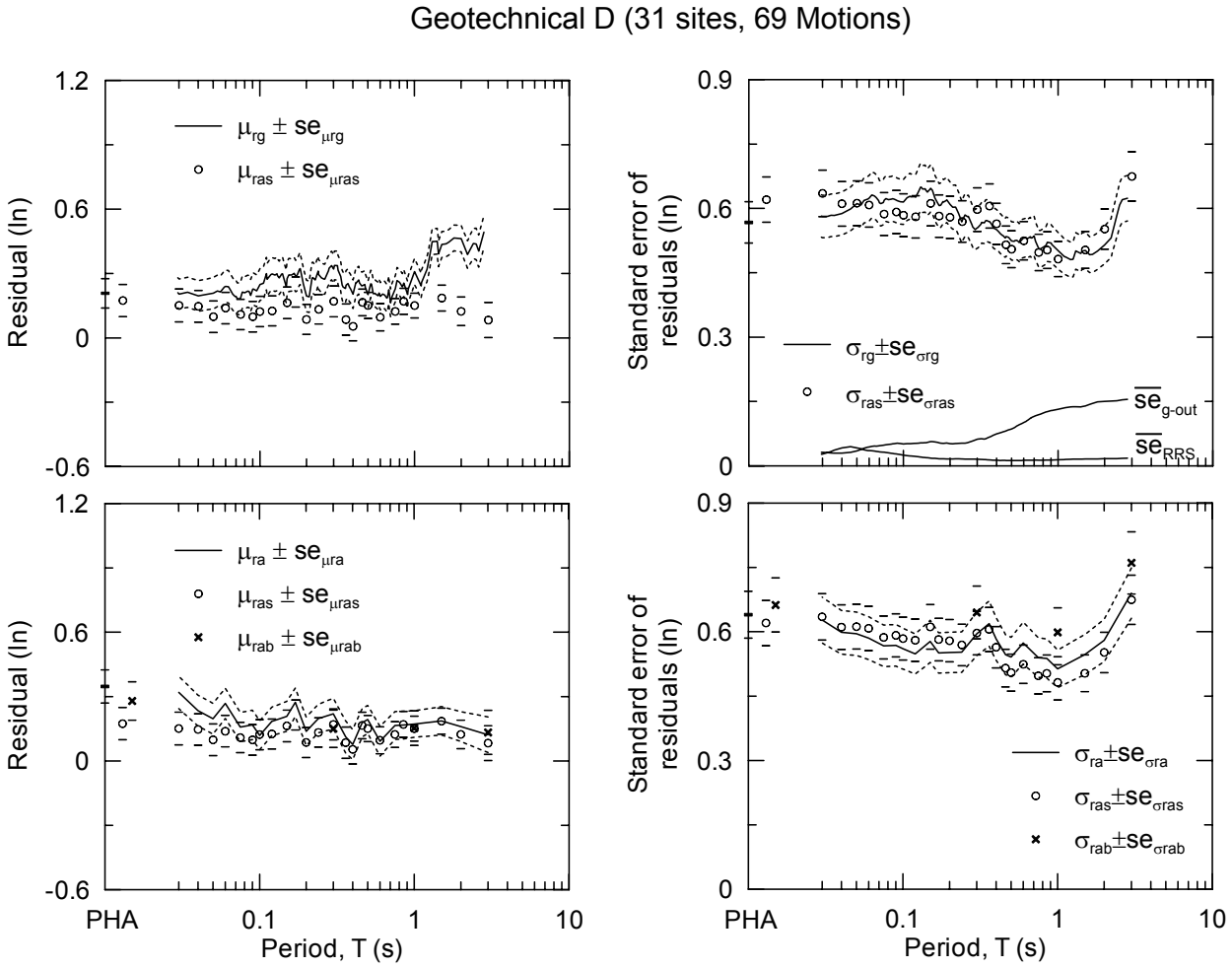

Fig. 6.16. Category residuals for Geotechnical D sites

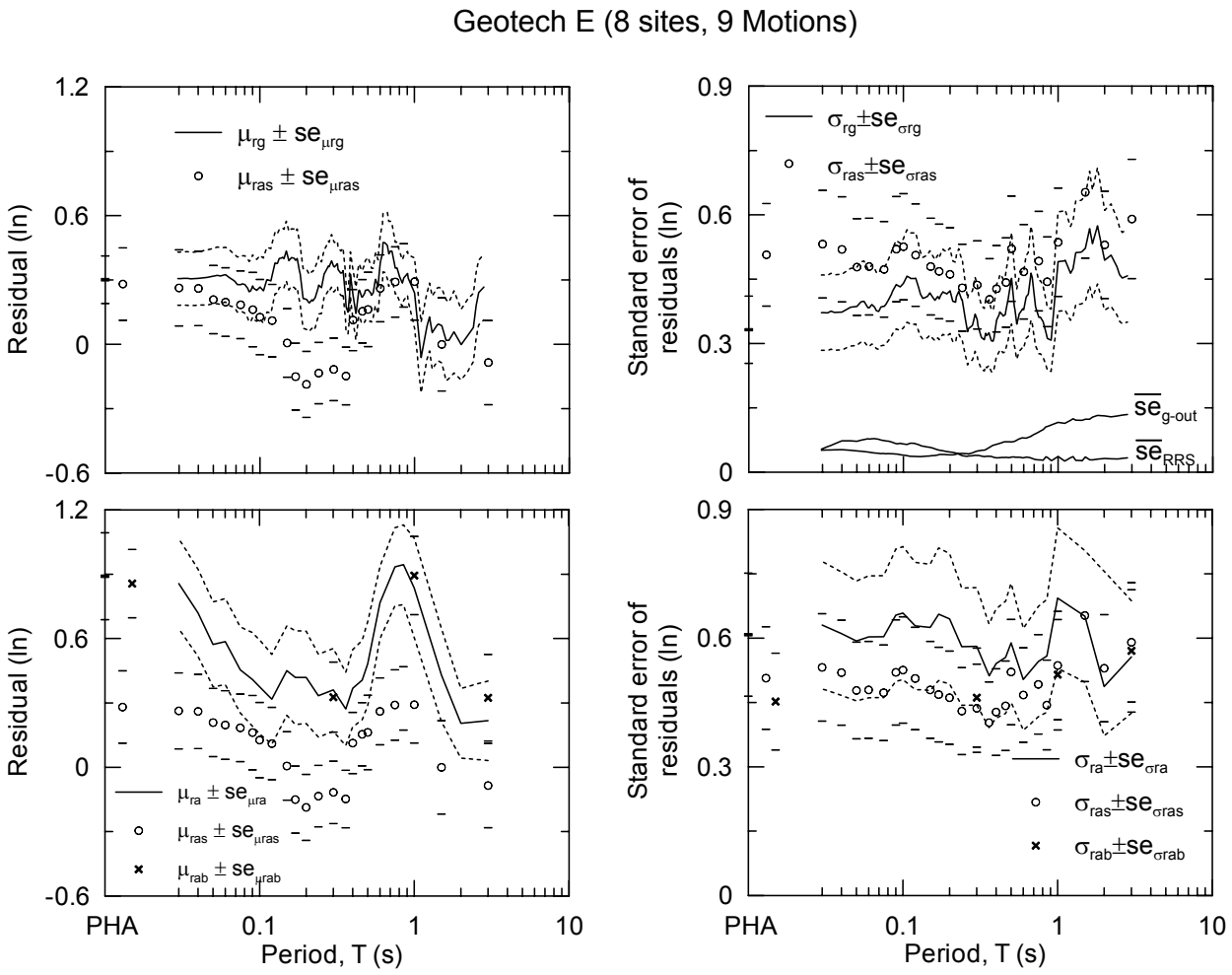

Fig. 6.17. Category residuals for Geotechnical E sites

Table 6.9. Rejection confidence levels (in percent) for the hypothesis that $\mu_{rg} - \mu_{ras}=0$

T(s)	ALL (134 mtns)	C (56 mtns)	D (69 mtns)	E (9 mtns)
PHA	19	35	26	8
0.3	79	34	87	98
1	91	56	94	17
3	99	56	100	89

Variations in dispersion levels between ground response and amplification factor predictions (quantified by σ_{rg} and σ_{ras}, respectively) are shown in the upper-right frames of Figures 6.15-6.17. For Categories C-D, the standard deviation values are generally similar, which is verified by the results of statistical F tests, as reported in Table 6.10. These tests show high *p* values, which suggest the lack of a statistically significant variation in the models' dispersion levels. For Category E the ground response dispersion is smaller than the amplification model dispersion at all periods, although the difference is moderate to insignificant per the F tests. As noted in Section 6.3.2, our measurements of the variations in dispersion for Category E may be questionable because of the similarity of the data sets used to derive the amplification models and the ground response results.

Table 6.10. F-statistics indicating distinction between residual dispersion levels for ground response (σ_{rg}) and geotechnical amplification models (σ_{ras})

	ALL (134 mtns)		C (56 mtns)		D (69 mtns)		E (9 mtns)	
T(s)	F	p	F	p	F	p	F	p
PHA	1.21	0.14	1.25	0.20	1.20	0.23	2.33	0.11
0.3	1.06	0.37	1.03	0.46	1.16	0.27	1.50	0.28
1	1.02	0.45	1.09	0.37	1.08	0.37	1.19	0.40
3	1.04	0.40	1.14	0.31	1.13	0.31	1.86	0.19

Ground motion predictions from the attenuation model are presented in the lower frames of Figures 6.15-6.17 (denoted $\mu_{ra} \pm se_{\mu ra}$ in the legend). For Category D, the attenuation and amplification factor predictions are very similar in both median residuals and dispersions, which is expected since D sites comprise a large fraction of the database used in the development of the soil attenuation relations. Differences in the median residuals are observed for Categories C and E, with the amplification factor residuals generally being closer to zero. A comparison of the distinction between attenuation median residuals and those from ground response is made in Table 6.11, in which we test the null hypothesis that the median predictions are identical. The null hypothesis can be rejected with moderate to high confidence for most of the categories and

periods. These rejection confidence levels are generally similar to or larger than those in Table 6.9, indicating generally larger distinction between ground response-attenuation than ground response-amplification factors. Standard error terms for the two models are not significantly different for C or D, but σ_{ras} is significantly less than σ_{ra} for Category E at small periods ($T < 1.0$ s). The results of F tests comparing σ_{ra} and σ_{rg} values are presented in Table 6.12, and confirm the qualitative trends that dispersion levels are generally similar with the exception of Category E at short periods ($T \leq 1.0$ s.), for which the σ_{rg} is moderately to significantly distinct from σ_{ra}.

Table 6.11. Rejection confidence levels (in percent) for the hypothesis that $\mu_{rg} - \mu_{ra}=0$

T(s)	ALL (134 mtns)	C (56 mtns)	D (69 mtns)	E (9 mtns)
PHA	98	99	82	98
0.3	16	75	69	1
1	84	82	89	95
3	100	99	99	36

Table 6.12. F-statistics indicating distinction between residual dispersion levels for ground response (σ_{rg}) and attenuation models (σ_{ra})

	ALL (134 mtns)		C (56 mtns)		D (69 mtns)		E (9 mtns)	
T(s)	F	p	F	p	F	p	F	p
PHA	1.30	0.07	1.15	0.31	1.27	0.16	3.35	0.04
0.3	1.10	0.29	1.04	0.44	1.15	0.28	2.66	0.08
1	1.13	0.24	1.01	0.48	1.05	0.42	1.99	0.16
3	1.07	0.35	1.05	0.43	1.18	0.25	1.65	0.23

The ground response shape misfit parameters for Geotechnical categories are evaluated, as was done previously in Section 6.3.2 for NEHRP categories. Both the median and standard deviation ($\mu_{\sigma e}$ and $\sigma_{\sigma e}$, respectively) of σ_e are similar between Categories C and D, but are significantly lower for Category E (Table 6.13). Moreover, the ground response shape misfit parameters are similar to attenuation for all categories except E, for which $\mu_{\sigma e}$ from ground response is significantly smaller than $\mu_{\sigma e}$ from attenuation, indicating that ground response provides a more accurate estimate of spectral shape.

Table 6.13. The median ($\mu_{\sigma e}$) and standard deviation ($\sigma_{\sigma e}$) of the average misfit values among Geotechnical categories

Category		Ground Response	Attenuation
ALL 134 mtns	$\mu_{\sigma e}$	0.29	0.29
	$\sigma_{\sigma e}$	0.12	0.12
C 56 mtns	$\mu_{\sigma e}$	0.31	0.32
	$\sigma_{\sigma e}$	0.12	0.13
D 69 mtns	$\mu_{\sigma e}$	0.28	0.27
	$\sigma_{\sigma e}$	0.11	0.11
E 9 mtns	$\mu_{\sigma e}$	0.19	0.32
	$\sigma_{\sigma e}$	0.08	0.06

Prediction residuals and dispersion values for the basin amplification model (μ_{rab} and σ_{rab}, respectively) are presented in the bottom frames of Figures 6.15 to 6.17. This model was implemented for a partial data set consisting of 46 motions at 24 C sites, 55 motions at 24 D sites, and eight motions at seven E sites. For Categories C and D (Figures 6.15-6.16), μ_{rab} matches or is slightly smaller than μ_{ra}. For E sites (Figure 6.17), the bias values are not significantly affected by the basin factors, although the dispersion values (σ_{rab}) are smaller.

6.3.4 Results for Surface Geology Categories

Compiled in Figures 6.18 - 6.21 are category statistics for surface geology categories Hlm (Holocene lacustrine and marine soils), Qa (Quaternary alluvium), T (Tertiary), and M+I (Mesozoic + Igneous). As above, the predictions of spectral acceleration derived using the surface geology amplification factor model can be taken as a baseline set of results because these predictions represent the expected category medians. As shown in Figures 6.18-6.21, the amplification factor model (denoted as $\mu_{as} \pm se_{as}$ in the legend) has for both Qa and Hlm a statistically significant under-prediction bias (positive residuals) over most of the period range considered (the only exception is that Qa has negative residuals for $T = 3$ s). An underprediction bias is also present for Category T at mid-periods ($T = 0.2 - 2$ s). The amplification factor model does not have significant bias for Category M. These results indicate that the selected motions for Qa, Hlm, and T are generally larger than the respective category medians.

As shown in the top-left frames of Figures 6.18-6.20, the ground response median residuals (denoted as $\mu_{rg} \pm se_{\mu rg}$ in the legend) for Categories Qa, Hlm, and T generally do not differ significantly from those derived from amplification factors. These trends are confirmed by tests for the rejection confidence of the null hypothesis that the two models have the same median residuals (Table 6.14). In Figure 6.21, the ground response median for Category M+I is clearly

smaller than the attenuation median, although the differences are generally not found to be statistically significant from hypothesis testing. The results of F tests comparing σ_{ras} and σ_{rg} values are presented in Table 6.15, and confirm the qualitative trends from Figures 6.18-6.19 that dispersion levels are generally similar for Qa, T, and M+I, but that for Hlm σ_{rg} is smaller than σ_{ra} for $T < \sim 1$ s at significance level (p) that is notably smaller than aforementioned E sites.

Table 6.14. Rejection confidence levels (in percent) for the hypothesis that $\mu_{rg} - \mu_{ras}=0$

T(s)	ALL (114 mtns)	Hlm (14 mtns)	Qa (69 mtns)	T (17 mtns)	M+I (14 mtns)
PHA	42	4	23	75	82
0.3	4	39	23	51	1
1	24	48	40	23	54
3	99	87	100	52	95

Table 6.15. F-statistics indicating distinction between residual dispersion levels for ground response (σ_{rg}) and surface geology amplification models (σ_{ras})

	ALL (114 mtns)		Hlm (14 mtns)		Qa (69 mtns)		T (17 mtns)		M+I (14 mtns)	
T(s)	F	p	F	p	F	p	F	p	F	p
PHA	1.13	0.25	2.39	0.06	1.05	0.42	1.36	0.27	1.60	0.19
0.3	1.03	0.43	2.27	0.07	1.16	0.27	1.23	0.33	1.02	0.49
1	1.06	0.37	1.22	0.36	1.11	0.34	1.15	0.39	1.01	0.49
3	1.08	0.33	1.62	0.19	1.19	0.24	1.41	0.24	1.35	0.29

Ground motion predictions from the soil attenuation model are presented in the lower frames of Figures 6.18 to 6.21 (denoted $\mu_{ra} \pm se_{\mu ra}$ in the legend). Generally the soil attenuation and amplification factor predictions are very similar in both median residuals and dispersions. A comparison of the distinction between soil attenuation results and those from ground response is made in Table 6.16, in which we test the null hypothesis that the median predictions are identical. The null hypothesis cannot be rejected with confidence for any of the categories (except Qa at $T = 3$ s), indicating the lack of a statistically significant deviation between the median residuals. The results of F tests comparing σ_{ra} and σ_{rg} values are presented in Table 6.17, and confirm the qualitative trends from Figures 6.18-6.21 that dispersion levels are similar for Qa, T, and M+I, but that for Hlm σ_{rg} is moderately to significantly smaller than σ_{ra} for $T \leq 1.0$ s.

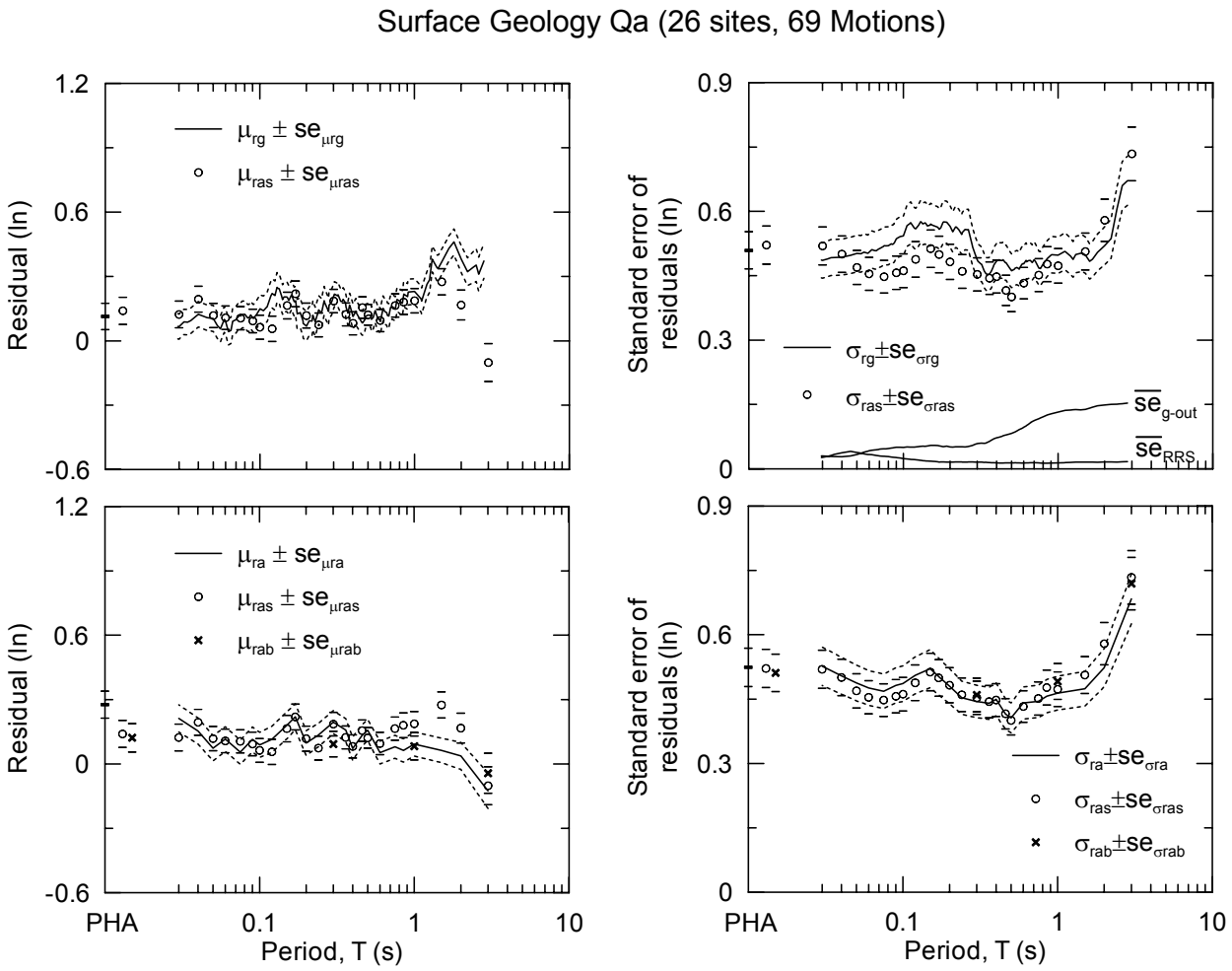

Fig. 6.18. Category residuals for Surface Geology Qa sites

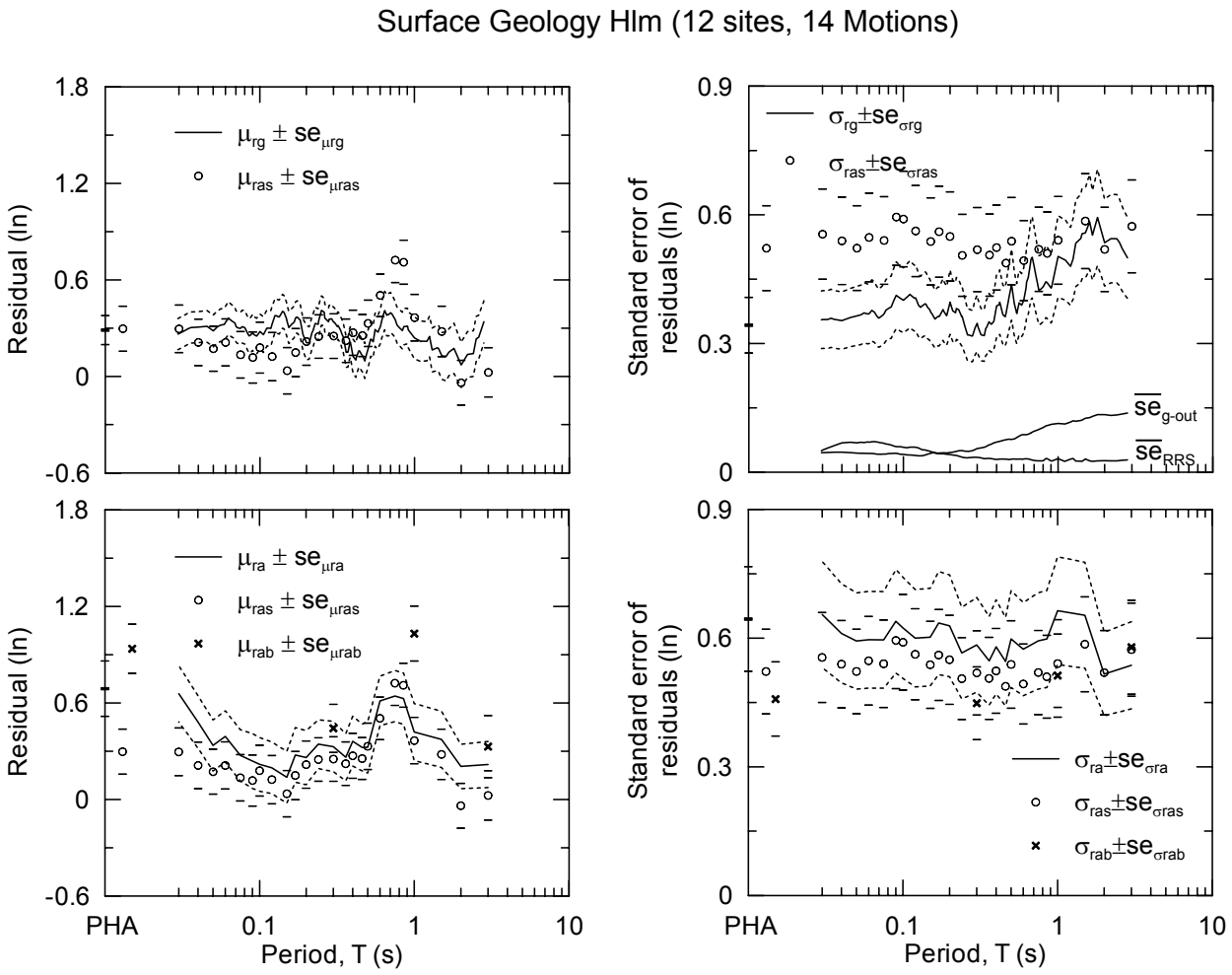

Fig. 6.19. Category residuals for Surface Geology Hlm sites

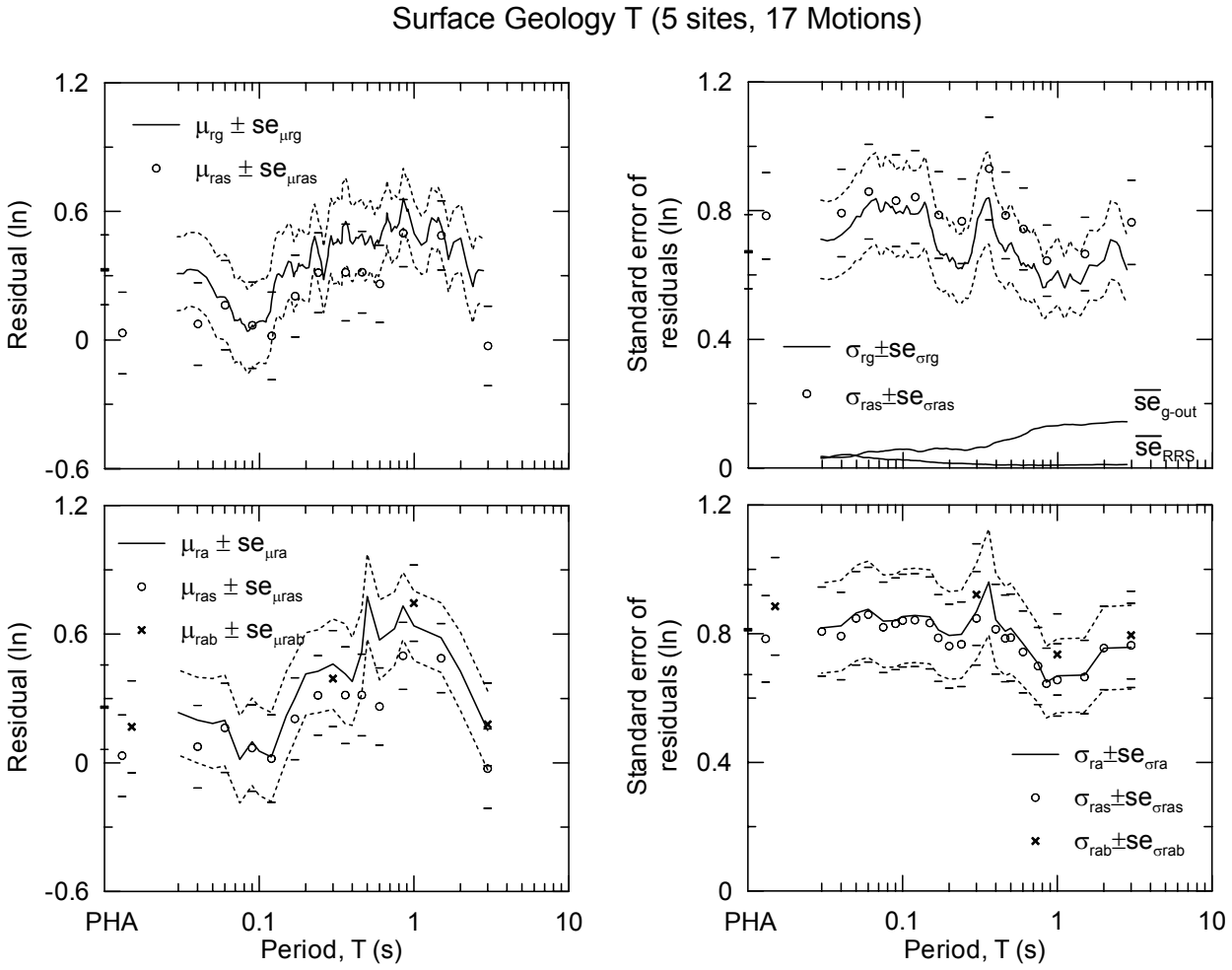

Fig. 6.20. Category residuals for Surface Geology T sites

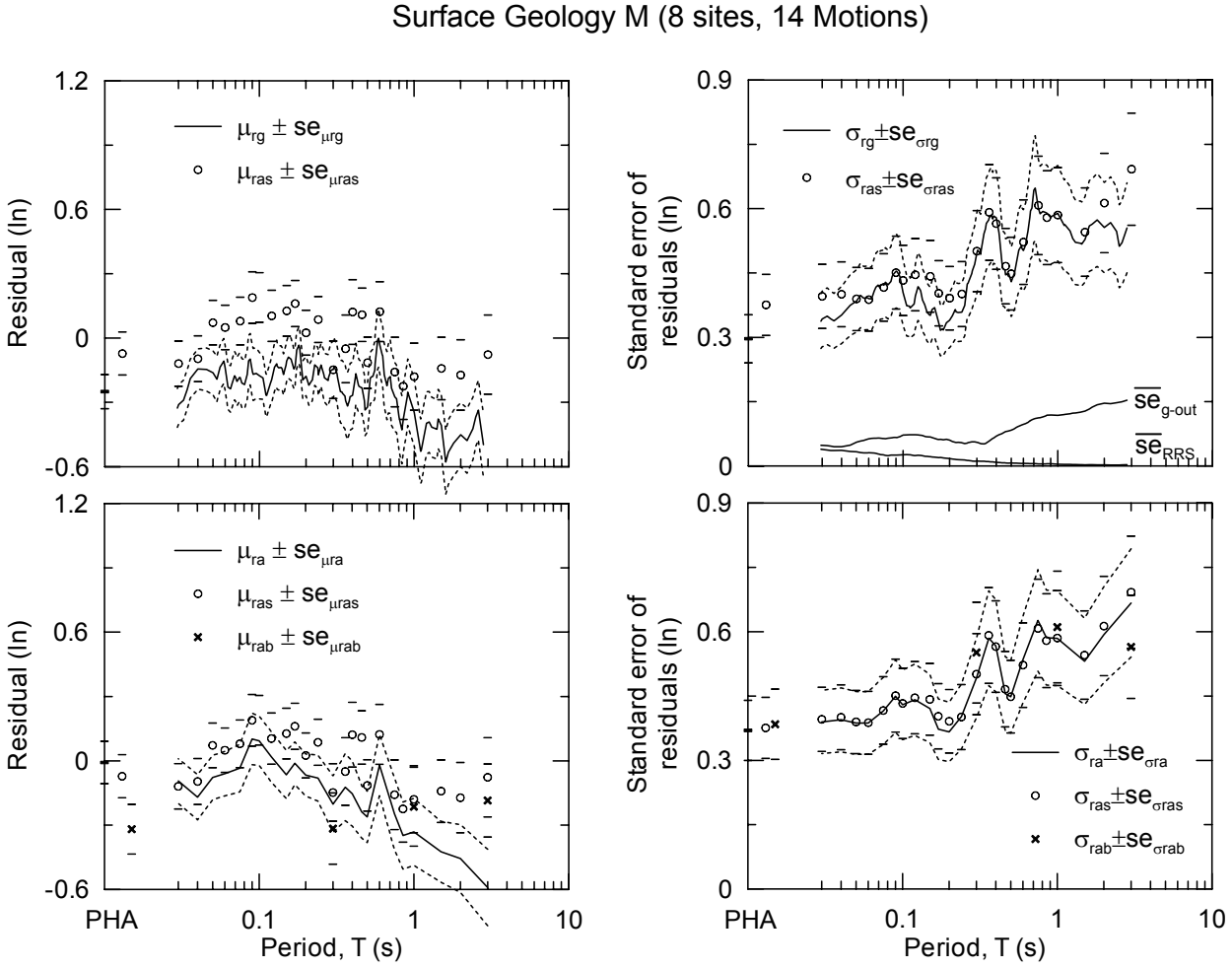

Fig. 6.21. Category residuals for Surface Geology M+I sites

Table 6.16. Rejection confidence levels (in percent) for the hypothesis that μ_{rg} - μ_{ra}=0

T(s)	ALL (114 mtns)	Hlm (14 mtns)	Qa (69 mtns)	T (17 mtns)	M+I (14 mtns)
PHA	97	95	93	21	93
0.3	11	4	14	4	23
1	80	58	90	48	5
3	100	46	100	2	5

Table 6.17. F-statistics indicating distinction between residual dispersion levels for ground response (σ_{rg}) and attenuation models (σ_{ra})

	ALL (114 mtns)		Hlm (14 mtns)		Qa (69 mtns)		T (17 mtns)		M+I (14 mtns)	
T(s)	F	p	F	p	F	p	F	p	F	p
PHA	1.31	0.07	3.64	0.01	1.06	0.40	1.46	0.22	1.56	0.21
0.3	1.08	0.33	2.88	0.03	1.20	0.22	1.30	0.30	1.02	0.48
1	1.15	0.22	1.83	0.13	1.15	0.28	1.19	0.36	1.02	0.49
3	1.08	0.34	1.42	0.26	1.03	0.45	1.39	0.25	1.25	0.34

Ground response shape misfit parameters for surface geology categories are presented in Table 6.18. The median and standard deviation of σ_e are lower for the Hlm category than for the Qa, T, and M+I categories, i.e. spectral shape is captured better (i.e., lower $\mu_{\sigma e}$) and more consistently (i.e., lower $\sigma_{\sigma e}$) for Hlm sites than the others. Values of $\mu_{\sigma e}$ from the ground response model match those from attenuation for Qa, T and M+I, but are significantly smaller for Hlm, indicating that ground response analyses provide a better estimate of spectral shape.

Table 6.18. The median ($\mu_{\sigma e}$) and standard deviation ($\sigma_{\sigma e}$) of the average misfit values among surface geology categories

Category		Ground Response	Attenuation
ALL 114 mtns	$\mu_{\sigma e}$	0.29	0.31
	$\sigma_{\sigma e}$	0.12	0.12
Hlm 14 mtns	$\mu_{\sigma e}$	0.19	0.27
	$\sigma_{\sigma e}$	0.07	0.07
Qa 69 mtns	$\mu_{\sigma e}$	0.29	0.29
	$\sigma_{\sigma e}$	0.12	0.12
T 17 mtns	$\mu_{\sigma e}$	0.30	0.35
	$\sigma_{\sigma e}$	0.12	0.12
M+I 14 mtns	$\mu_{\sigma e}$	0.36	0.38
	$\sigma_{\sigma e}$	0.10	0.14

Prediction residuals and dispersion values for the basin amplification model (μ_{rab} and σ_{rab}, respectively) are presented in the bottom frames of Figures 6.18-6.21. The basin amplification model was implemented for a subset of 59 motions at 28 Qa sites, 9 motions at 8 Hlm sites, 17

motions at 5 T sites, and 11 motions at 7 M+I sites. For Qa and T, $\mu_{rab} \approx \mu_{ra}$, whereas for Hlm $\mu_{rab} > \mu_{ra}$ at mid-periods (0.3, 1.0 s). Values of μ_{ra} and μ_{rab} also differ for M+I sites. For dispersion, $\sigma_{rab} \approx \sigma_{ra}$ for Qa, T, and M+I, but for Hlm $\sigma_{rab} < \sigma_{ra}$ for $T \leq 1.0$ s.

6.3.5 Effect on Residuals of Depth to V_s= 1 km/s (z_1) and Magnitude (m)

The residuals of spectral acceleration predictions are examined with respect to a depth to engineering rock parameter, z_1 (defined as depth to V_s= 1 km/s) and moment magnitude (m) of causative earthquake.

The prediction residuals are plotted as a function of z_1 in Figures 6.22 for periods of PHA, 0.3 s, 1.0 s, and 3.0 s. Also plotted in Figures 6.22 are the results of regression analyses performed according to the following equation:

$$\ln(\mu_{ra})_j = c + d \ln(z_1)_j \qquad (6.9)$$

where $(\mu_{ra})_j$ is the median residual for site j (for the example of the attenuation ground motion estimate – the analyses are performed for other prediction methods as well), $(z_1)_j$ is the depth to V_s= 1 km/s for that site, and c and d are regression coefficients. Confidence intervals (±95%) are also presented on the plots. The statistical significance of the slope of regression lines is evaluated with hypothesis testing similar to that discussed in Section 6.3.2 for $V_{s\text{-}30}$ data. Tabulated in Table 6.19 are the values of 1-α, which is here referred to as a "rejection confidence for a d=0 model". Large rejection confidence levels (i.e., >95%) suggest significant z_1 dependence in residuals.

Table 6.19 Regression coefficients for residuals vs. z_1 (depth to V_s= 1km/s)

Category	T(s)	c	d	σ	Rejection confidence for d=0 model (%)
Ground Response	PHA	0.19 ± 0.21	-0.01 ± 0.04	0.52	26
	0.3	0.44 ± 0.23	-0.03 ± 0.04	0.56	62
	1	-0.55 ± 0.24	0.12 ± 0.04	0.58	100
	3	-0.95 ± 0.27	0.21 ± 0.05	0.66	100
NEHRP	PHA	0.40 ± 0.23	-0.04 ± 0.04	0.56	71
	0.3	0.45 ± 0.23	-0.05 ± 0.04	0.57	74
	1	-0.74 ± 0.24	0.14 ± 0.04	0.60	100
	3	-1.00 ± 0.29	0.18 ± 0.05	0.72	100
Attenuation	PHA	0.67 ± 0.24	-0.05 ± 0.04	0.60	80
	0.3	0.63 ± 0.24	-0.07 ± 0.04	0.59	89
	1	-0.10 ± 0.26	0.05 ± 0.05	0.64	70
	3	-0.44 ± 0.29	0.07 ± 0.05	0.72	84
Basin	PHA	0.90 ± 0.25	-0.12 ± 0.04	0.61	99
	0.3	0.80 ± 0.24	-0.12 ± 0.04	0.60	99
	1	0.41 ± 0.27	-0.05 ± 0.05	0.66	68
	3	-0.04 ± 0.29	0.00 ± 0.05	0.73	2

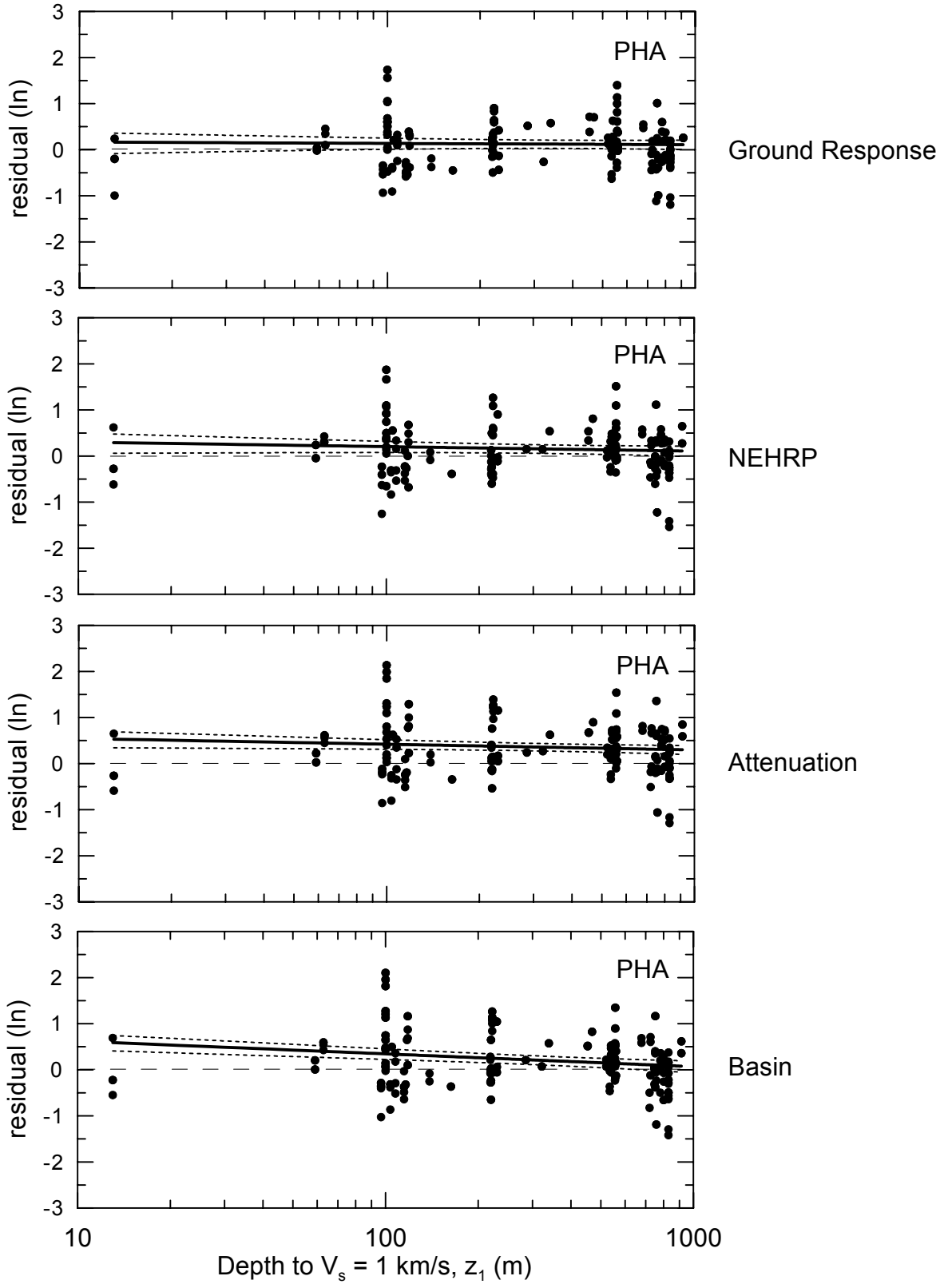

Fig. 6.22 (a). The variation of PHA residuals with respect to z_1

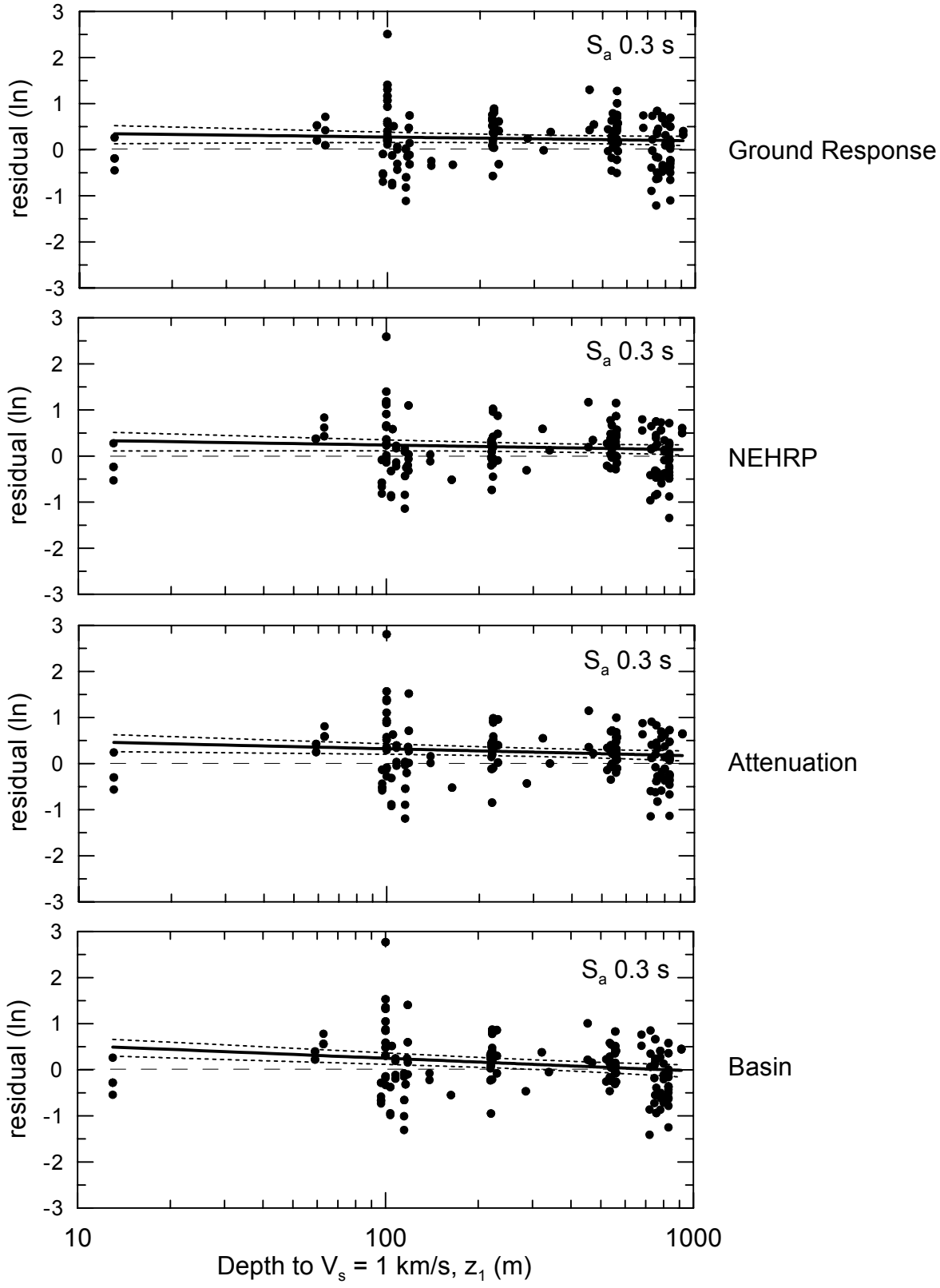

Fig. 6.22 (b). The variation of S_a 0.3 s residuals with respect to z_1

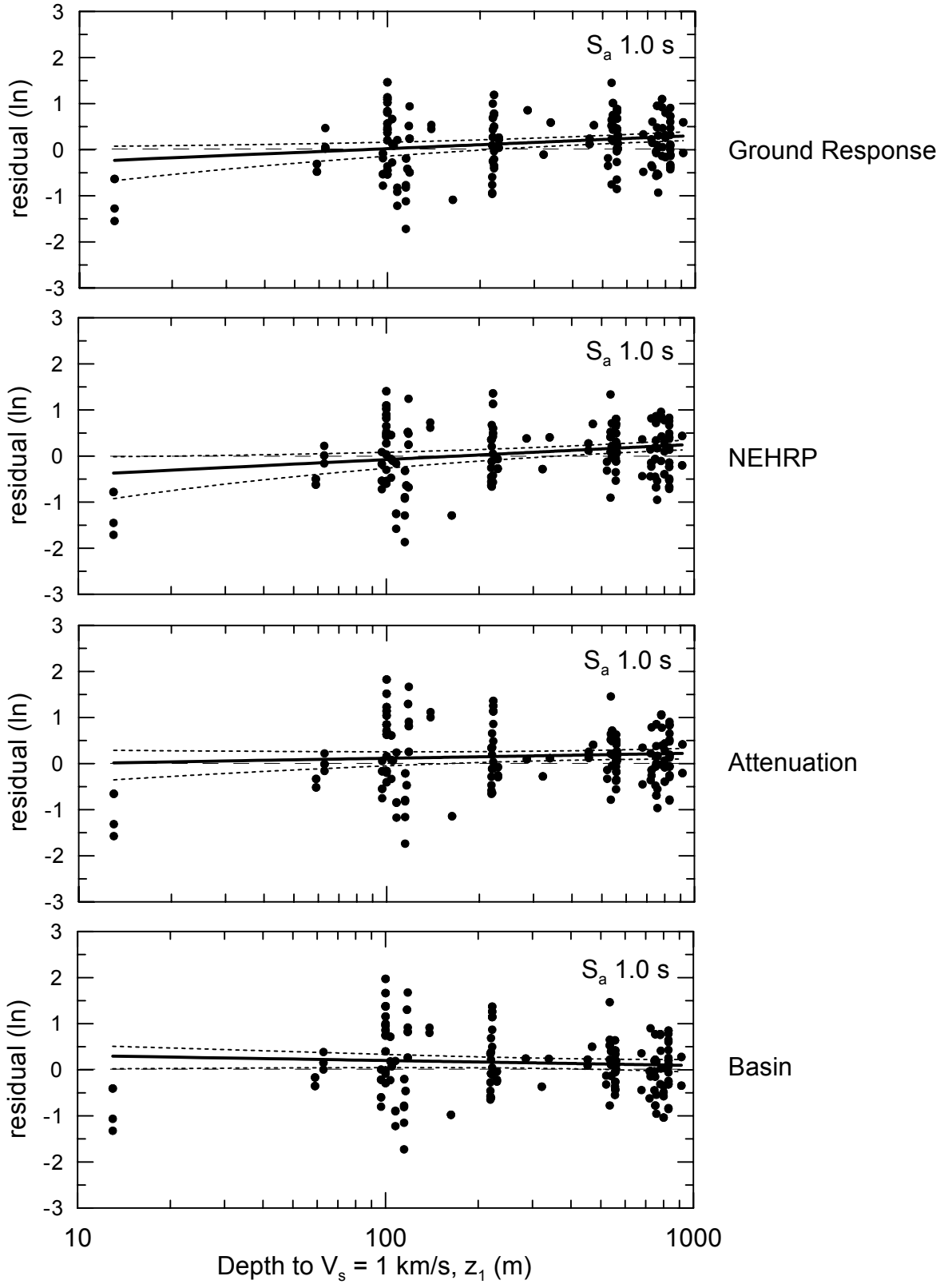

Fig. 6.22 (c). The variation of S_a 1.0 s residuals with respect to z_1

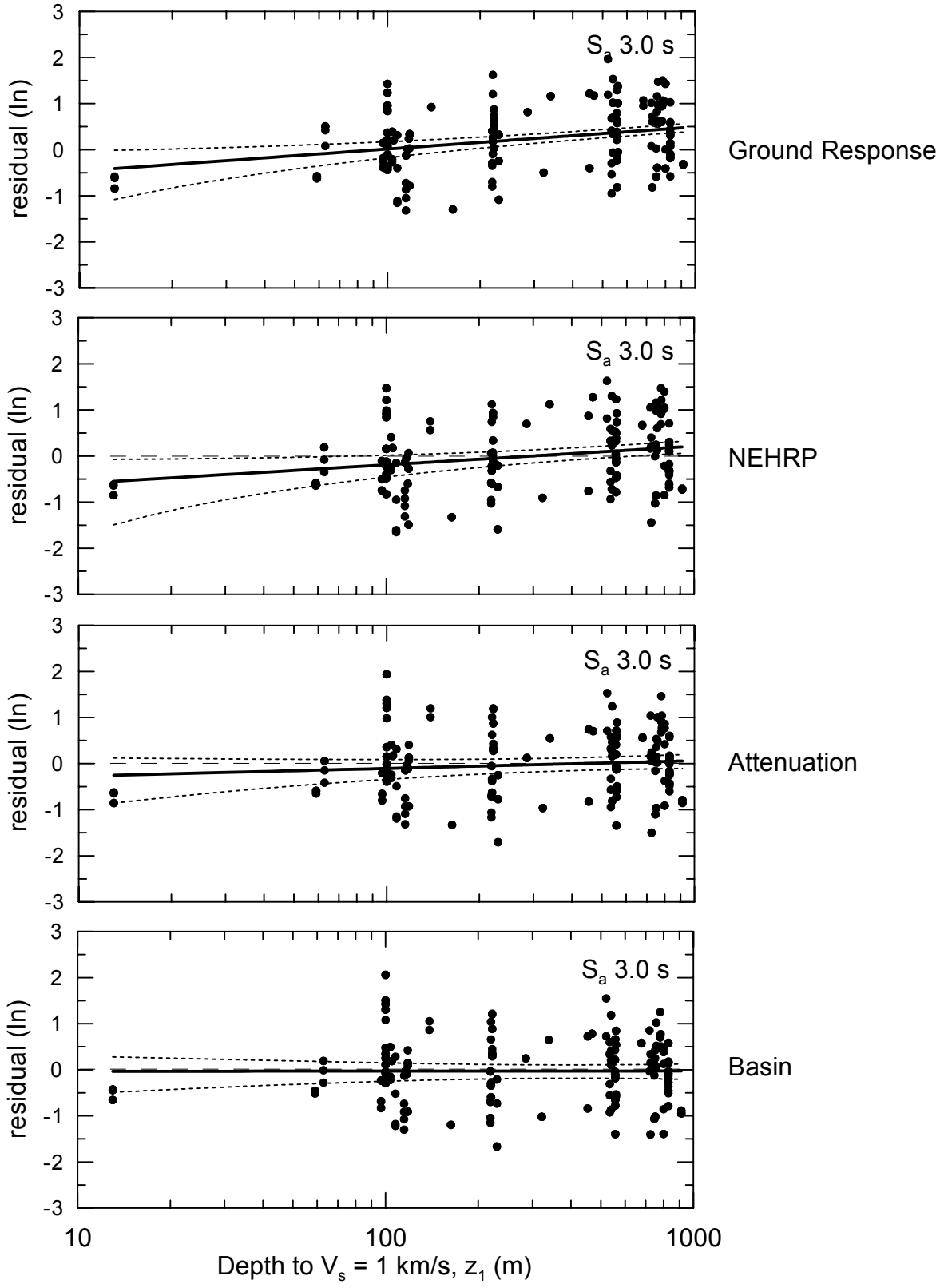

Fig. 6.22 (d). The variation of S_a 3.0 s residuals with respect to z_1

As can be seen from Figures 6.22 and Table 6.19, the NEHRP and ground response residuals have a significant trend with z_1 at intermediate and long periods (T = 1.0 and 3.0 s), but lack any significant trend at short periods ($T \leq 0.3$ s). The trend at long periods is towards increasing residuals, and hence increasing observed ground motions, with z_1. This trend is suggestive of long-period amplification associated with deep basin structure. Residuals from the soil attenuation model do not show statistically significant trends with z_1. Residuals from the basin model have significant trends with z_1 at small periods ($T \leq 0.3$ s), but no significant trend at longer periods. The trend is towards decreasing residuals (and hence increasing ground motion predictions) with increasing z_1. This trend, coupled with the lack of trend for the soil attenuation model, suggests that the basin amplification model is over-correcting for basin response effects at small periods for the sites considered in this study.

The prediction residuals are plotted as a function of magnitude in Figures 6.23. Most of the recordings used in this study are from earthquakes with $m \approx 6$ to 7.5. To help visualize any trends in the data, median residuals and 95% confidence intervals on the median are superimposed in Figures 6.23 on top of the data within each magnitude bin. For each period considered, the results from all the models generally show the smallest residuals in the middle magnitude range (6-6.5) and slightly larger residuals at smaller and larger magnitudes. Overall, there appears to be no significant trend between median residual and magnitude.

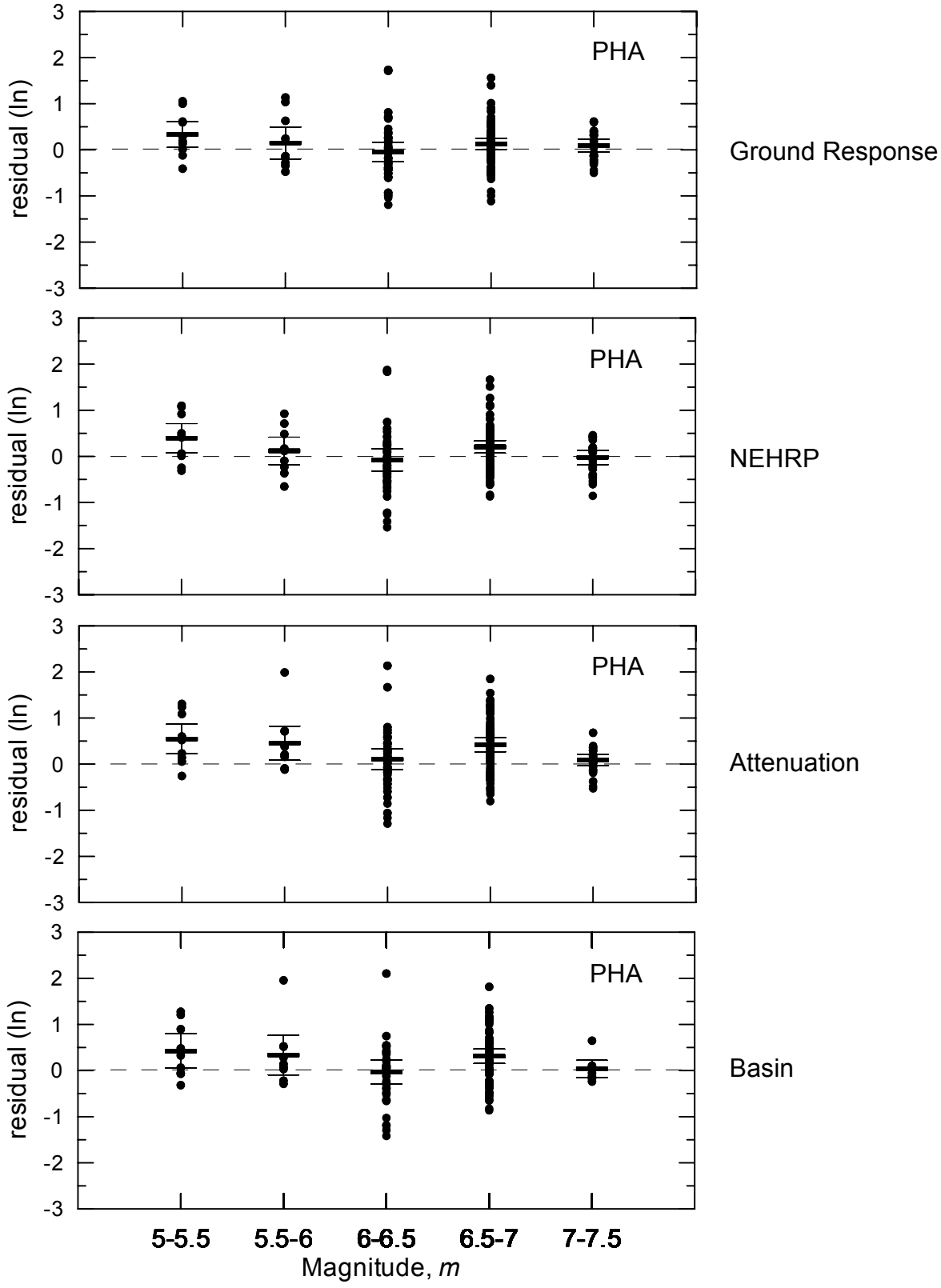

Fig. 6.23 (a) The variation of PHA residuals with respect to *m*

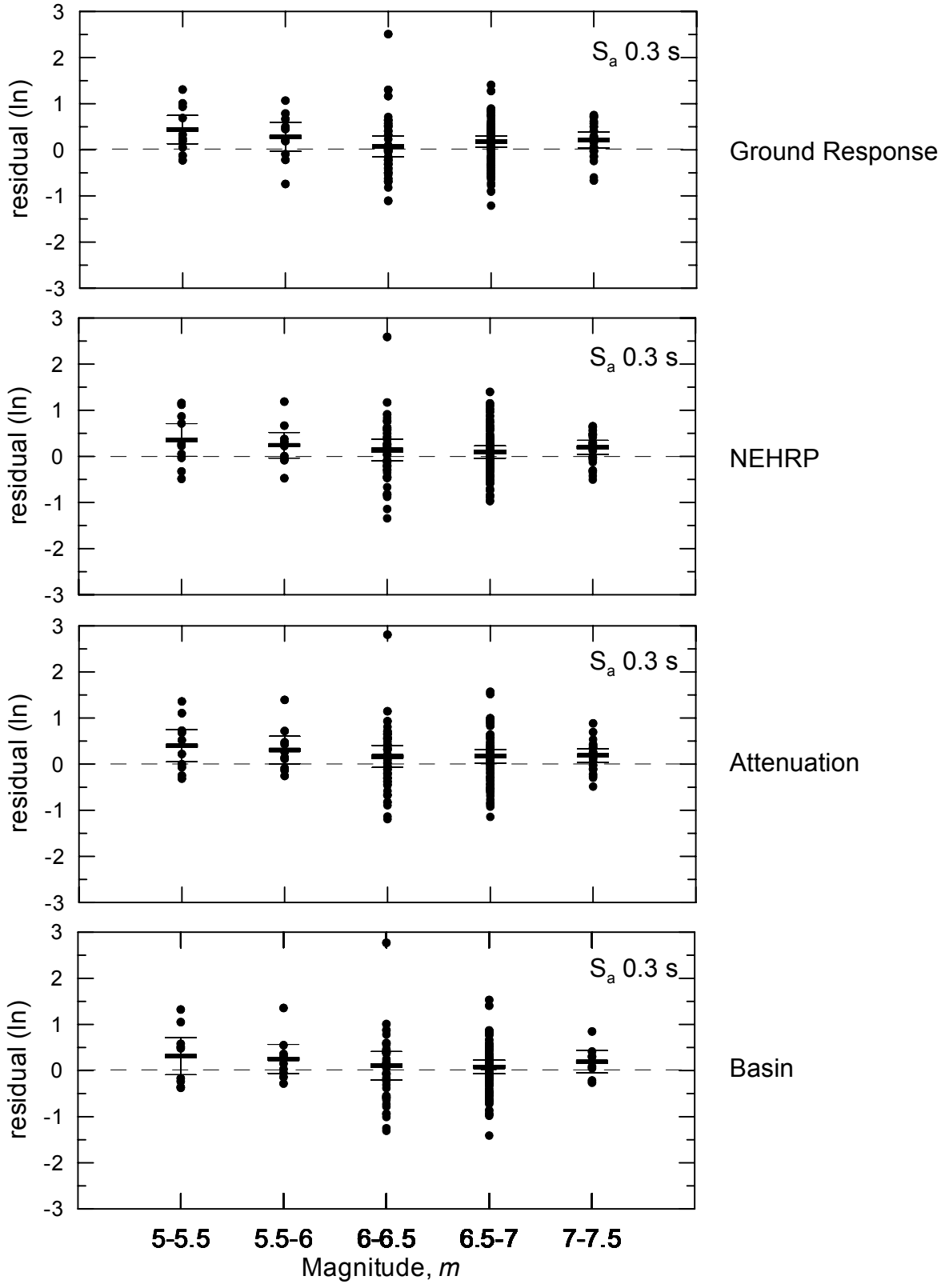

Fig. 6.23 (b) The variation of S_a 0.3 s residuals with respect to m

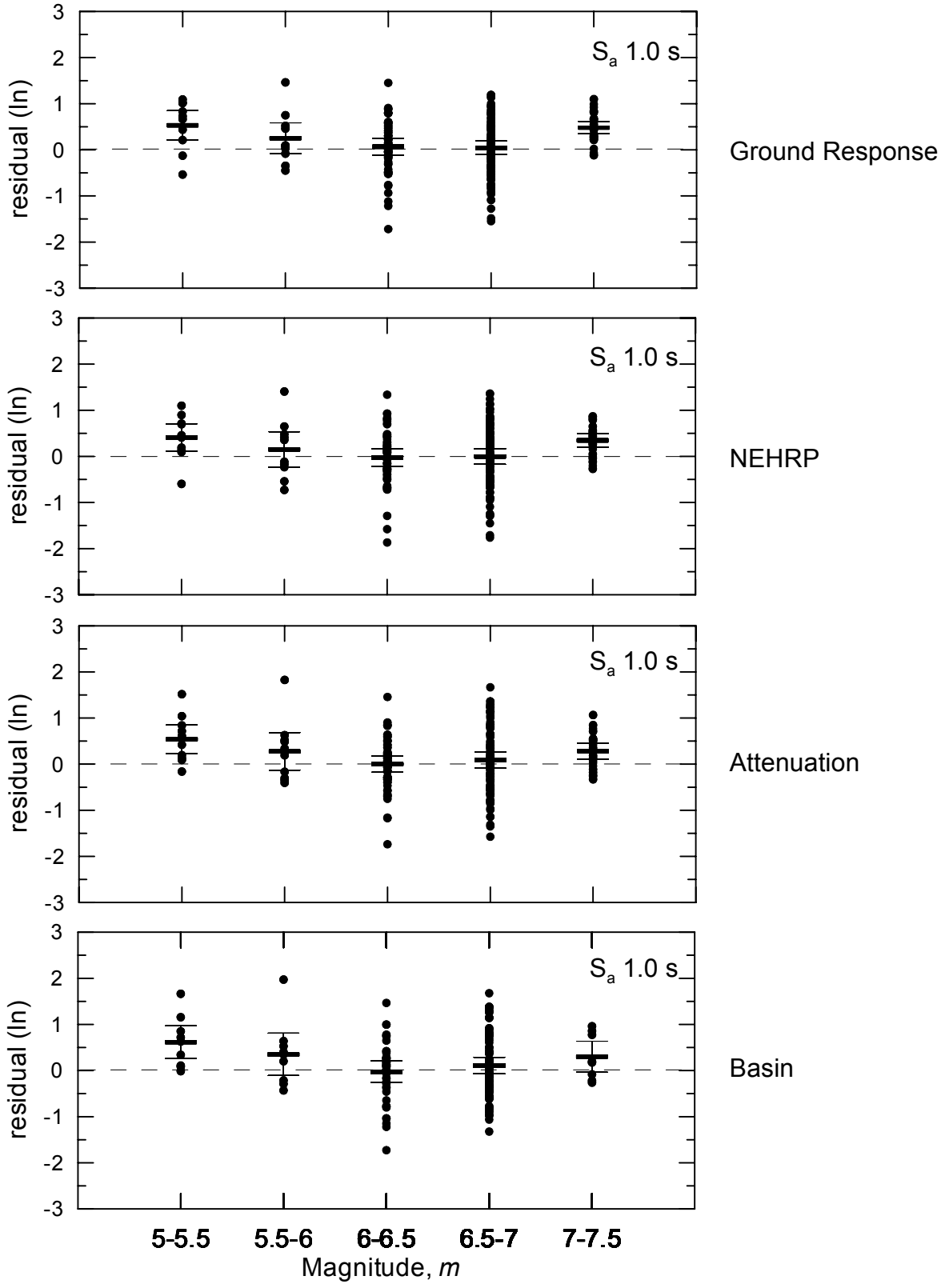

Fig. 6.23 (c) The variation of S_a 1.0 s residuals with respect to m

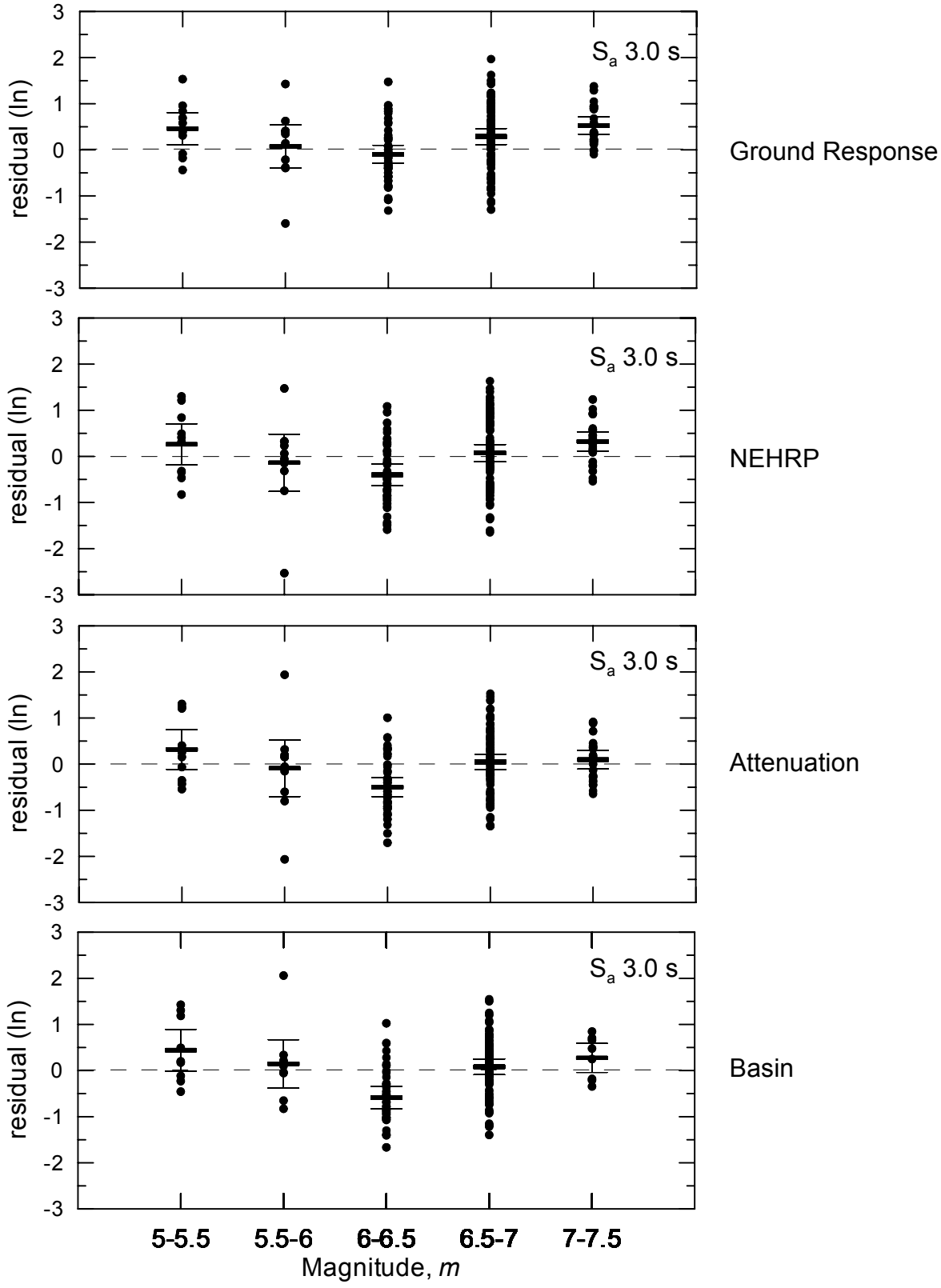

Fig. 6.23 (d) The variation of S_a 3.0 s residuals with respect to *m*

6.4 ESTIMATION OF DISPERSION IN GROUND RESPONSE PREDICTIONS FOR USE IN GROUND MOTION HAZARD ANALYSES

A topic of significant practical interest for probabilistic seismic hazard analysis is the dispersion associated with ground motion predictions from ground response calculations. An initial estimate of this dispersion is provided by the σ_{rg} values reported above for specific site categories (e.g., Figures 6.11-6.13 for NEHRP categories). As discussed in Section 6.2.3, several factors contribute to this dispersion, some of which can be quantified as part of the ground response calculations, and others of which are unknown. An uncertainty that can be estimated is the uncertainty in the location of the median ground motion estimate for each site $(se_{g\text{-}out})_{ij}$, and the average value of this uncertainty for all sites within a category, $(\overline{se}_{g-out})_i$. The latter represents one contribution to the overall uncertainty for the category $(\sigma_{rg})_i$, the other contributions being modeling errors whose individual magnitudes are unknown. However, the net variance associated with these other factors $(\sigma_{g\text{-}net})_i^2$ can be estimated from the difference between the total category variance and the variance associated with median ground response prediction,

$$(\sigma_{g-net})_i^2 = (\sigma_{rg})_i^2 - (\overline{se}_{g-out})_i^2 \tag{6.10}$$

This net dispersion is plotted for NEHRP categories in Figure 6.24, and represents an estimate of the dispersion from ground response modeling errors as a function of site category. The results suggest similar levels of dispersion for Categories C and D, but a much lower level of dispersion for E at low periods (T < 1 s). For T > 1 s, dispersion levels among the three categories are approximately equal. For practical application, the following values can be used to approximate the results from Figure 6.24:

Category	**Approximate** σ_{g-net}
C (T < 1 s)	0.56
D (T < 1 s)	0.56
E (T < 1 s)	0.38
All (T > 1 s)	Use σ from site factors or attenuation

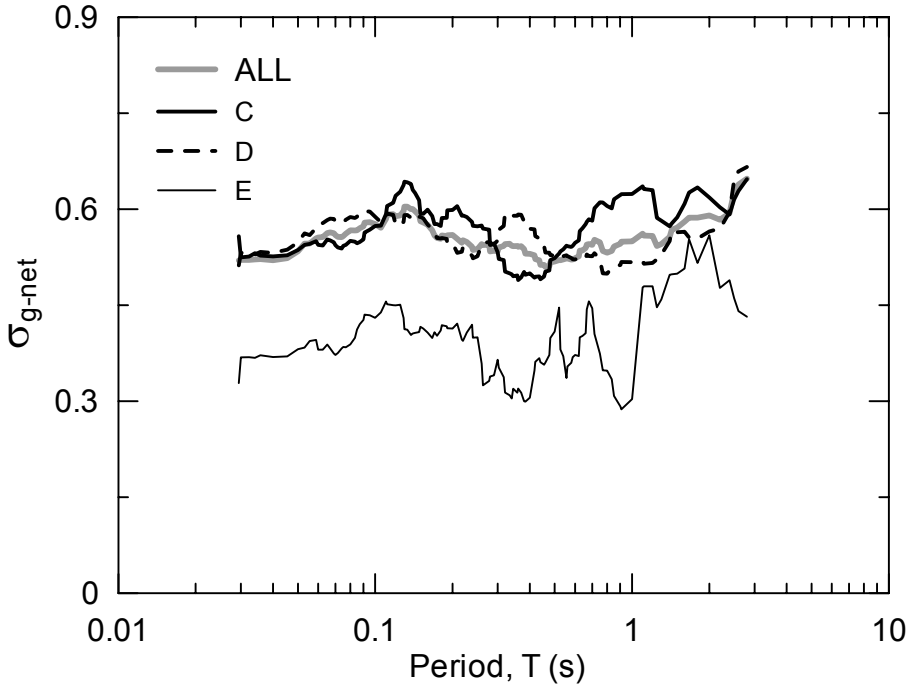

Fig. 6.24. Variation with period of dispersion in ground response predictions associated with factors other than the ground response model estimation error for NEHRP categories C-E

These values of σ_{g-net} are of interest because the variance of S_a that should be used in a forward analysis of ground motions [$(\sigma_g)^2$] is the sum of the above-listed variances and the variance of the median from forward ground response analyses $(se_{g-out})^2$,

$$(\sigma_g)^2 = (\sigma_{g-net})^2 + (se_{g-out})^2 \tag{6.11}$$

The quantity σ_g from Eq. 6.11 is the appropriate value of dispersion for use in ground motion hazard analyses.

The net dispersion values compiled above for NEHRP categories can be re-compiled for Geotechnical and Surface Geology categories, the results of which are presented in Figures 6.25 and 6.26. The distinction between low-period dispersion levels across categories is not as significant for the Geotechnical scheme (Figure 6.25) as for the NEHRP scheme (Figure 6.24). Geotechnical Categories C and E both have low dispersion at small periods, with D dispersion being significantly larger. Distinct levels of dispersion are observed between Surface Geology Categories for T < ~1.0 s, with T dispersion being highest, Qa being intermediate, and Hlm and M+I being the lowest. It should be noted that the results for the rock categories (T and M+I) are based on a small number of recordings, and may not be reliable. For T > 1 s, dispersion levels

across the various categories in the Geotechnical and Surface Geology schemes are approximately equal. The approximate σ_{g-net} values for those classification schemes can be taken as:

Geotechnical Category	**Approximate σ_{g-net}**
C ($T < 1$ s)	0.47
D ($T < 1$ s)	0.58
E ($T < 1$ s)	0.38
All ($T > 1$ s)	Use σ from site factors or attenuation

Surface Geology Category	**Approximate σ_{g-net}**
Hlm ($T < 1$ s)	0.38
Qa ($T < 1$ s)	0.51
T ($T < 1$ s)	0.72
M+I ($T < 1$ s)	0.44
All ($T > 1$ s)	Use σ from site factors or attenuation

An examination of the results for σ_{g-net} presented above indicates that soft soil site categories (i.e., NEHRP E, Geotechnical E and Surface Geology Hlm) have significantly lower levels of dispersion than other categories at small period. Deep stiff soil sites (i.e., NEHRP D, Geotechnical D, and Surface Geology Qa) have much larger dispersion at low periods. Interestingly, shallow stiff soil and weathered rock sites (Geotechnical C) appear to have smaller dispersion than deep stiff sites at low periods. The above results for σ_{g-net} can be used in Eq. 6.11 to assign dispersion levels to the results of ground response analyses for use in ground motion hazard analyses.

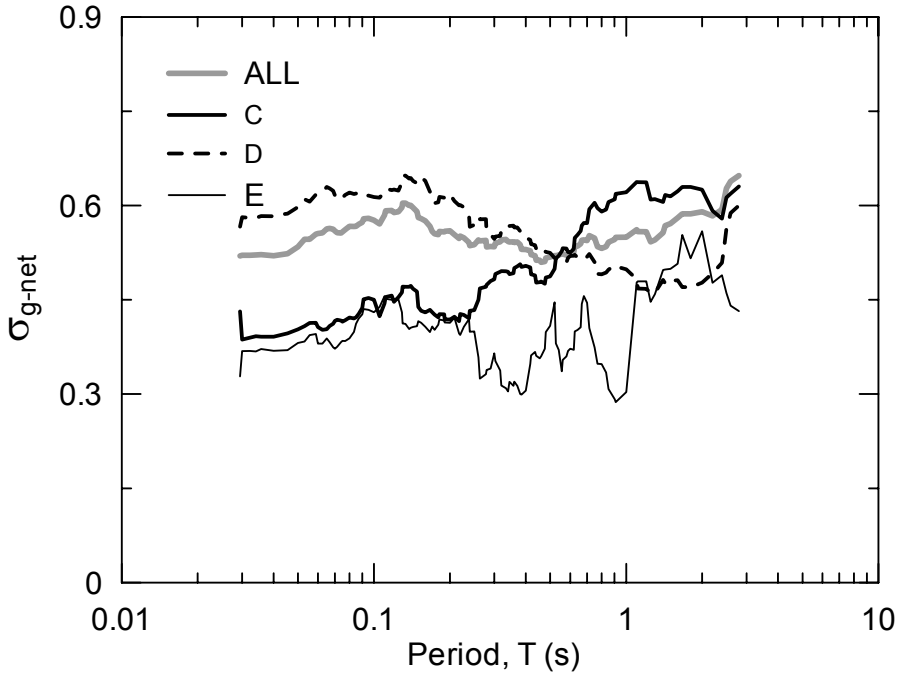

Fig. 6.25. Variation with period of dispersion in ground response predictions associated with factors other than the ground response model estimation error for Geotechnical Categories C-E

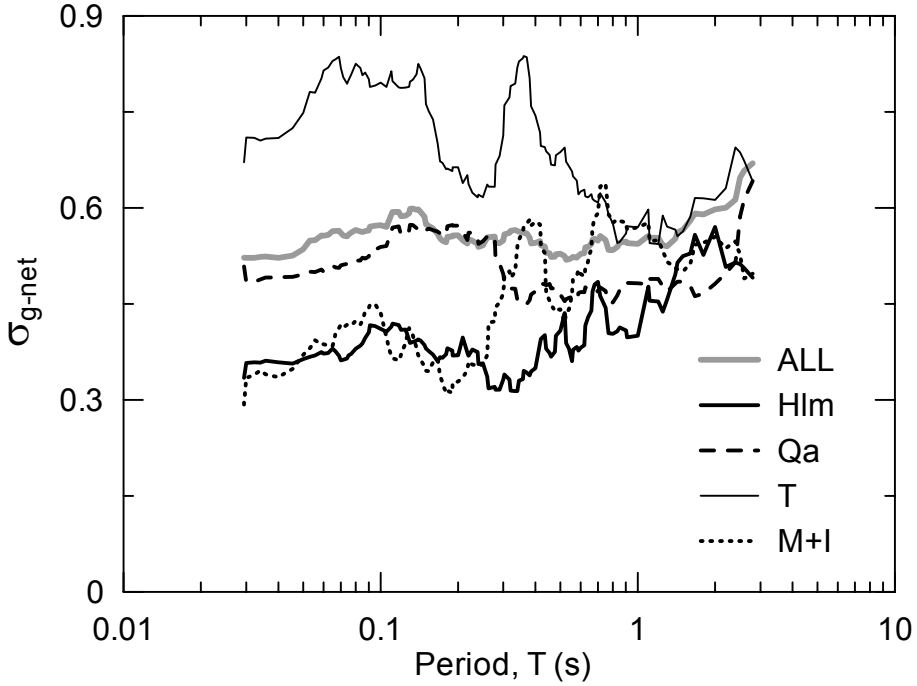

Fig. 6.26. Variation with period of dispersion in ground response predictions associated with factors other than the ground response model estimation error for Surface Geology Categories Qa and Hlm

6.5 ESTIMATED SHEAR STRAINS AT SITES

6.5.1 Parameterization of Shear Strain

We seek to parameterize the depth-dependent strain profile at each of the site/motion pairs using a single strain parameter. There are two factors to consider. First, since we have calculated not a single profile of strain, but a statistical distribution of strains at each depth in the site profiles, at issue is the percentile value of calculated strain that should be taken as an estimate of the actual strains in the ground. The distribution of calculated strains is associated with the multiple input motions utilized in the ground response analyses. The distribution of calculated shear strains with depth for an example site is represented by the black lines in Figure 6.27, which show median (μ_ε) and median ± one standard deviation ($\mu_\varepsilon \pm \sigma_\varepsilon$) strain profiles.

The second consideration associated with the selection of a strain parameter is the representation of a depth-dependant strain profile by a single strain parameter. The strain parameters we have considered are:

- ε_1: Maximum 3m-average strain, considering the entire profile depth.
- ε_2: Maximum 3m-average strain, considering only the top 30m.
- ε_3: Spatially averaged strain below the top low strain region.
- ε_4: Spatially average strain across entire profile.
- ε_5: Maximum strain at any location, considering the entire profile depth.
- ε_6: Maximum strain at any location, considering only the top 30m.

Parameters ε_5 and ε_6 are intended to capture the large strains that can occur in soft layers with any thickness, whereas parameters ε_1 and ε_2 are similarly defined but average the strains over a 3 m interval to filter out large strains within very thin layers. Parameters ε_3 and ε_4 represent averaged strains across the profile depth (ε_3 omitting the top low strain region). Each of these strain parameters can be compiled for a given profile of strain. In Figure 6.27, we apply these definitions to the μ_ε profile.

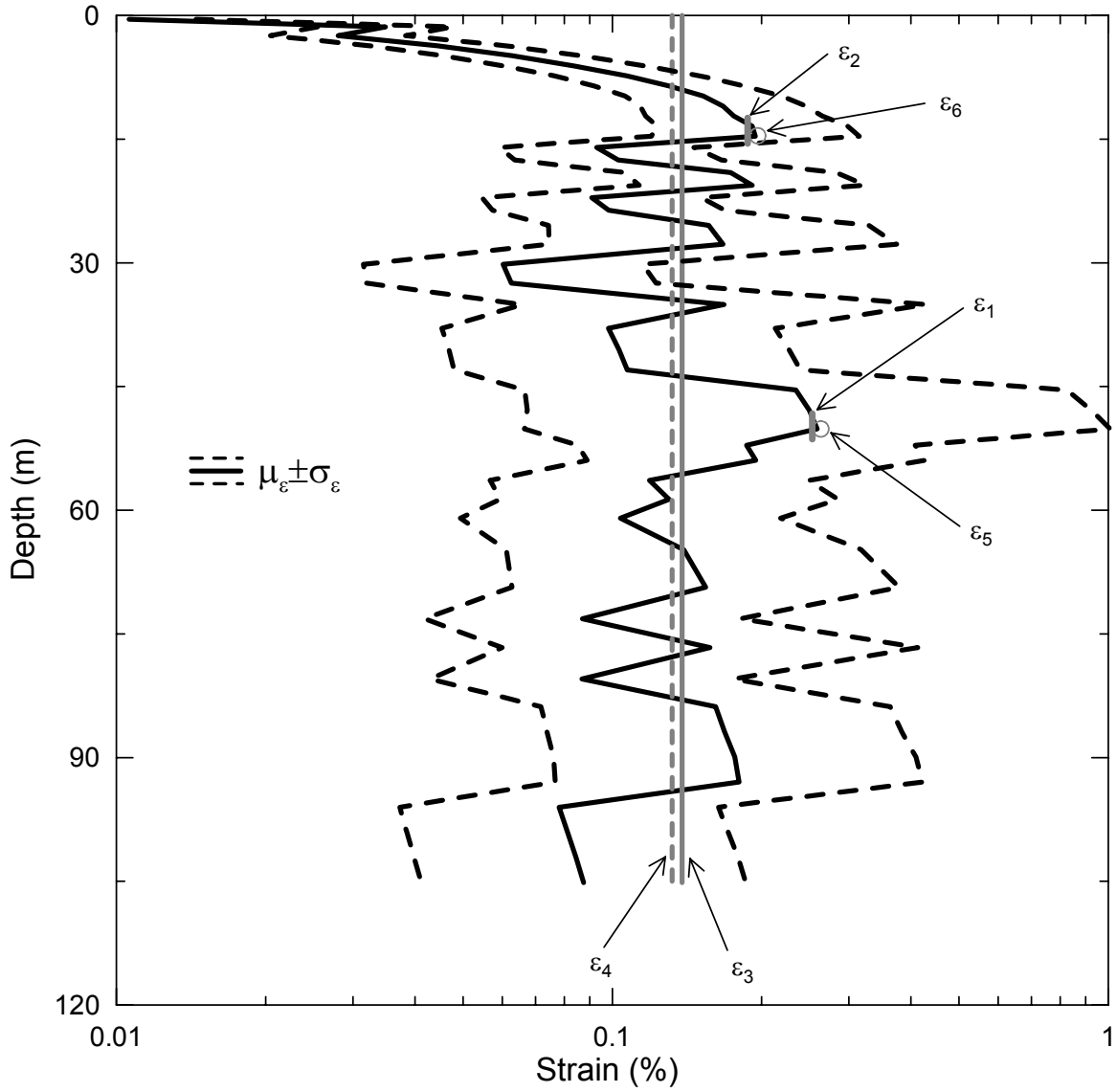

Fig. 6.27. Calculated Strain Profile by SHAKE and representative strain values of the profile for the El Centro #7 Site, 1979 Imperial Valley Earthquake recording

6.5.2 Compilation of Strain Parameters Across Sites

The strain parameters defined in the previous section were calculated as part of the ground response analyses performed for each site. Median + one-half sigma strain parameters are compiled in Figure 6.28 within NEHRP site categories. Our opinion is that the $\mu_\varepsilon + 0.5\sigma_\varepsilon$ strain profiles are generally good estimates of actual strain profiles because on average our ground motion predictions are biased low by about one-half of a standard deviation.

Strain parameters are seen to be higher for E sites than D, and higher for D than C, which is expected given the increase of V_s from E to D to C. The following parameter pairs are seen to be

essentially identical: ε_1 - ε_2, ε_3 - ε_4, and ε_5 - ε_6. For Category C, the calculated strains are generally less than 0.1%, and hence the soil response for sites within these categories would not be expected to be significantly nonlinear. For Categories D and E, the strain values for some sites are sufficiently large (> ~ 0.5%) that significantly nonlinear soil response would be expected.

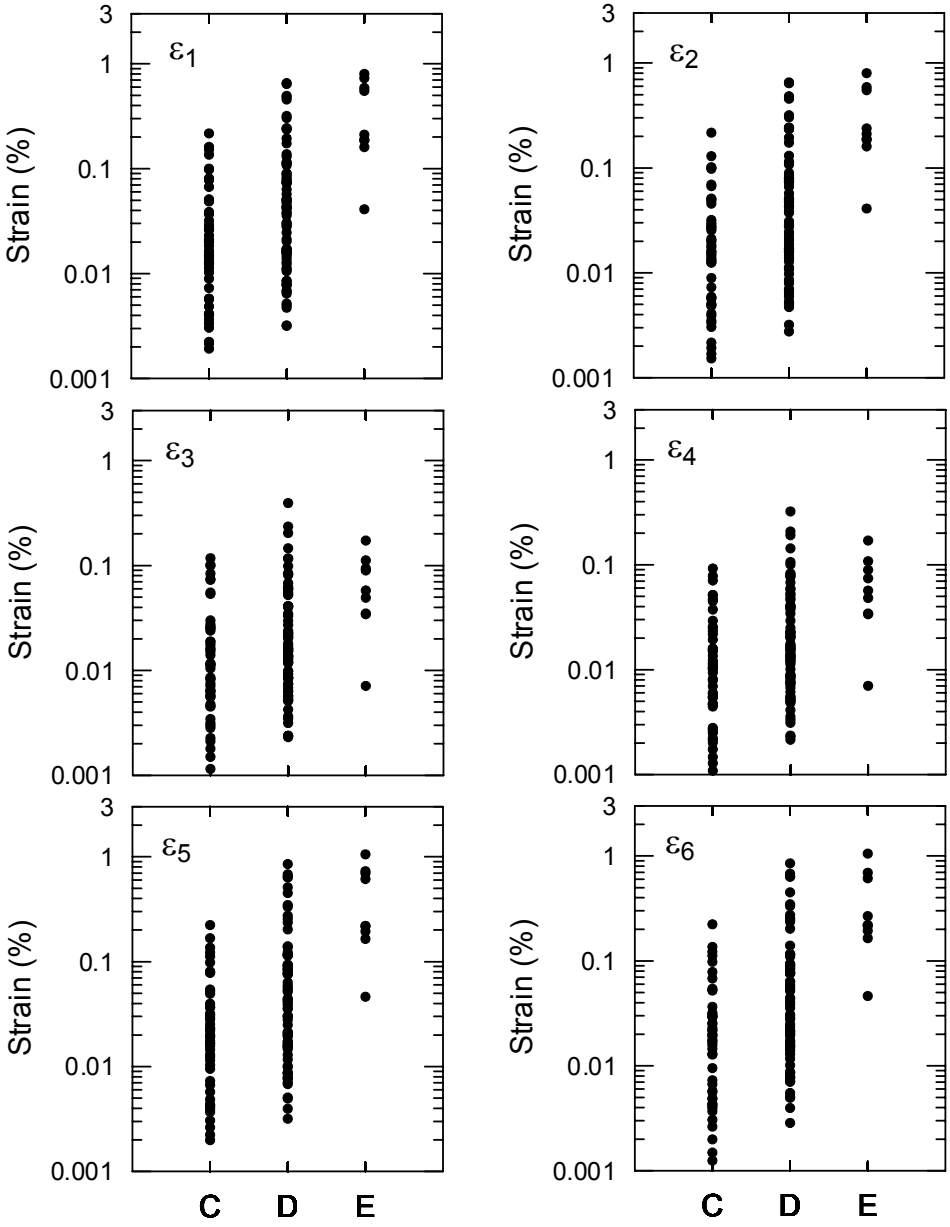

Fig. 6.28. Profiles of $\mu_\varepsilon + 0.5\sigma_\varepsilon$ strain for NEHRP categories

6.5.3 Dependence of Residuals on Shear Strains

It is of interest to investigate whether the ground response analysis results compiled in this report show a trend with respect to the strain parameters defined above. A statistically significant trend would indicate errors in the nonlinear model. For example, if the residuals were significantly larger for large strains than small strains, one could infer that the nonlinear soil model is over-softening the soil response at large strains, which would increase the soil damping and correspondingly decrease the predicted motions and hence increase the residuals.

We perform linear regression analyses according to the following equation to elucidate trends in the residuals with strain,

$$\ln(\mu_{rg})_j = e + f \ln(\varepsilon_n)_j \tag{6.12}$$

where $(\mu_{rg})_j$ is the median residual for site j, $(\varepsilon_n)_j$ is strain parameter n for that site (n = 1-6), and e and f are regression coefficients which are tabulated in Table 6.20. These regression lines are plotted against the data in Figures 6.29 for strain parameters ε_1, ε_3, and ε_5 along with confidence intervals (±95%) around the fit line. Of interest is the degree to which a trend exists in the regression lines, which is tested using sample 't' statistics to test the null hypothesis that $f = 0$ and e = overall data median. This statistical testing provides a significance level = α that the null hypothesis cannot be rejected. For ease of interpretation, tabulated in Table 6.20 are the values of 1-α, which is referred to as a "rejection confidence for a f=0 model". Large rejection confidence levels (i.e., >95%) would suggest significant strain-dependence of residuals.

The regression fits shown in Figures 6.29 and tabulated in Table 6.20 indicate for $T \leq 1.0$ s a weak trend of decreasing residual with strain parameter (i.e., less underprediction as strain increases). However, the values of slope parameters f are generally small, as reflected by rejection confidence levels for the zero slope null hypotheses that are low. Accordingly, we cannot conclude on the basis of these analyses that the laboratory-based nonlinear soil model utilized in our ground response analyses (and listed in Table 5.2) contains a bias toward over- or under-prediction of soil nonlinearity.

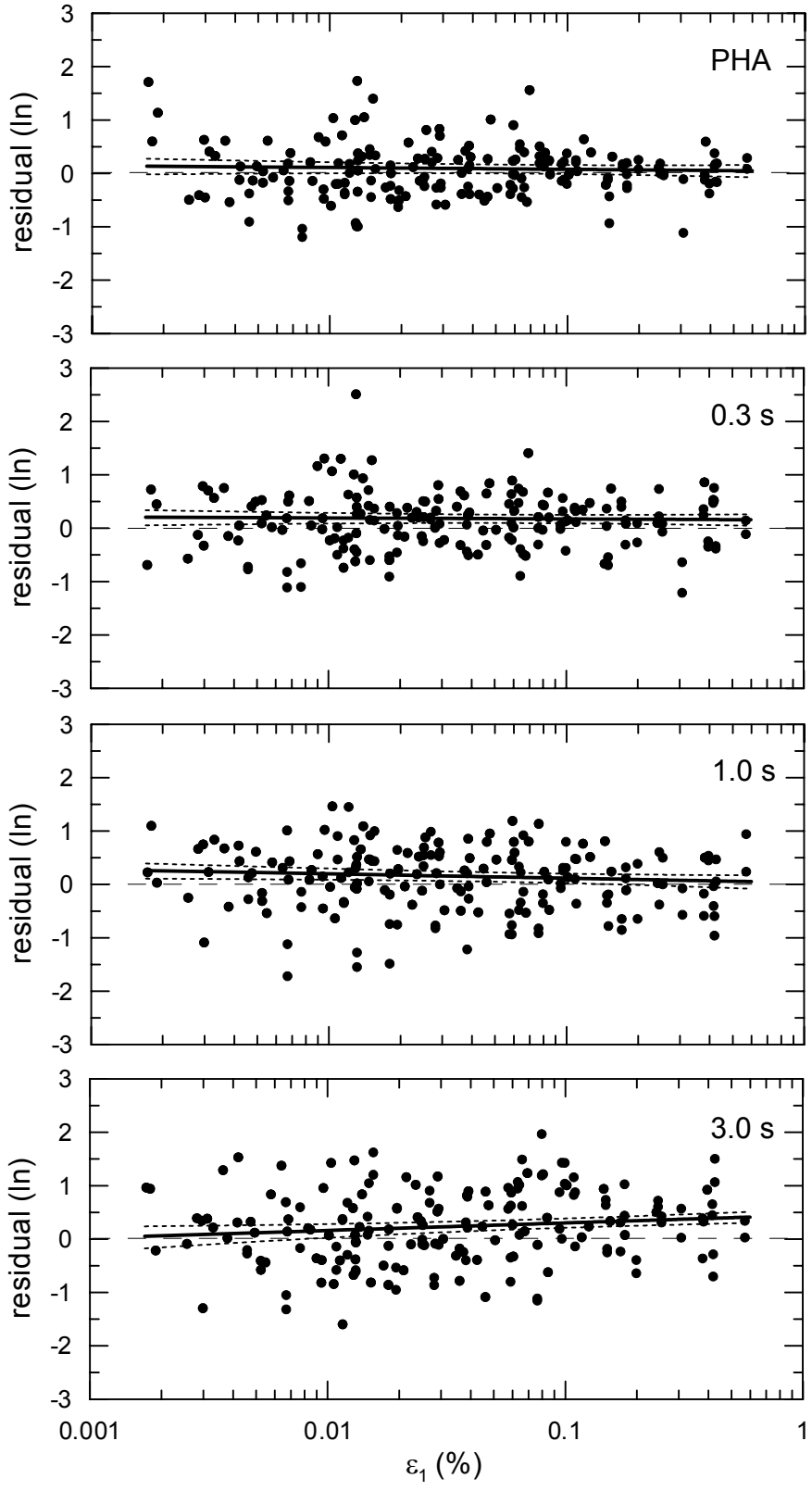

Fig. 6.29(a). The variation of residuals with strain parameter ε_1

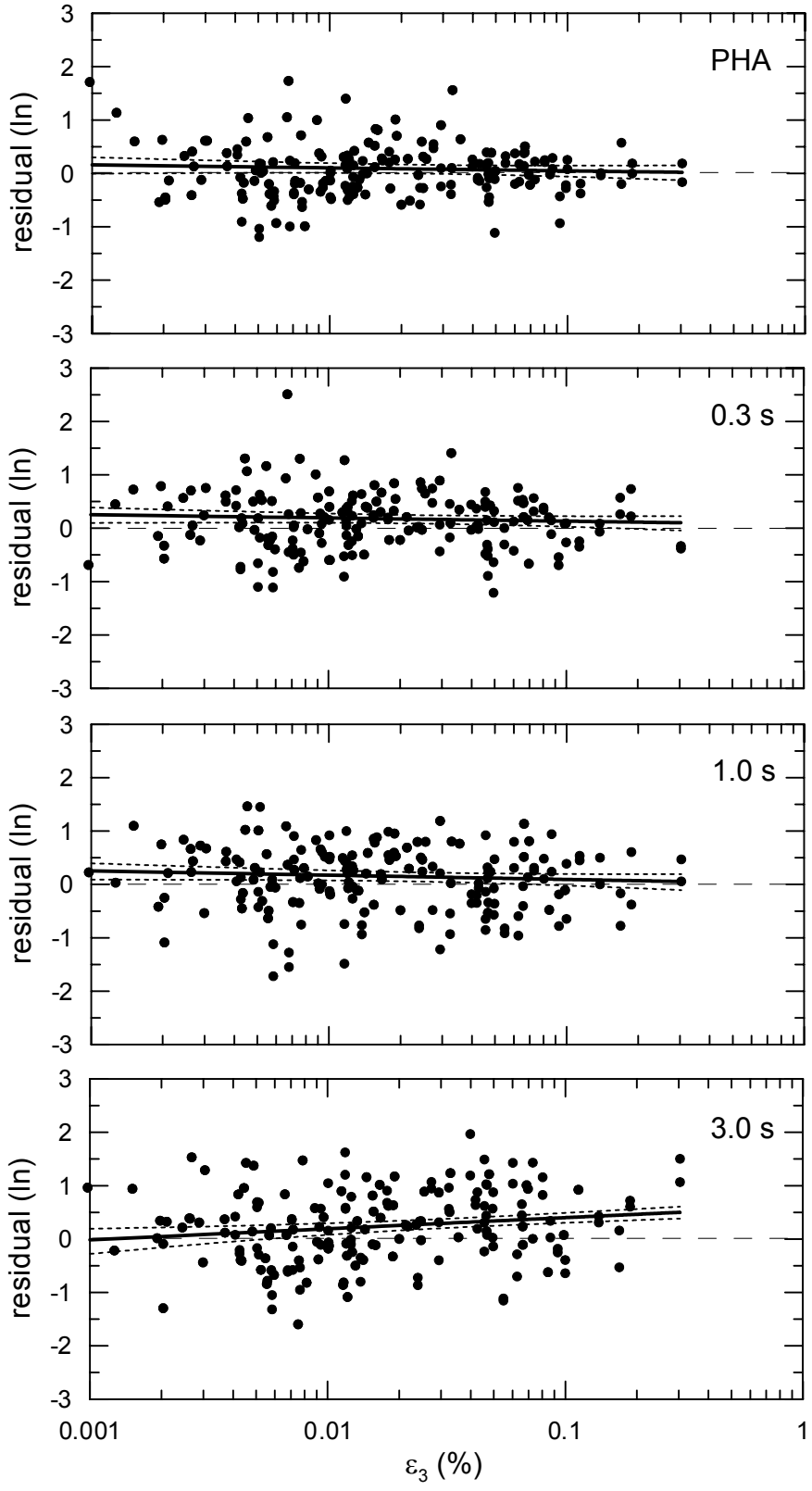

Fig. 6.29(b). The variation of residuals with strain parameter ε_3

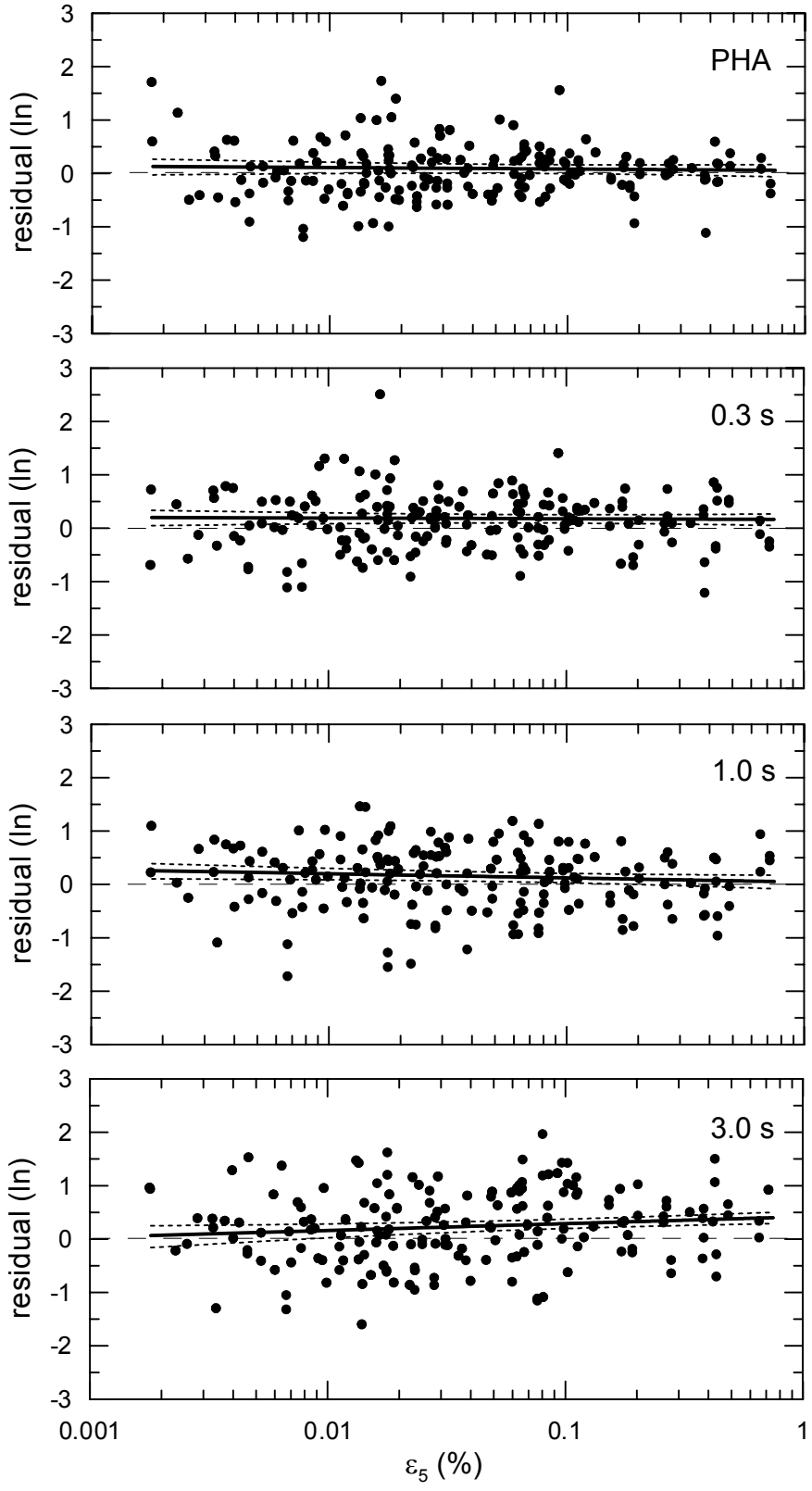

Fig. 6.29(c). The variation of residuals with strain parameter ε_5

Table 6.20. Coefficients of linear regression analyses relating residuals to strain parameters

Strain	T(s)	e	f	σ	Rejection confidence for f=0 model (%)
ε_1	PHA	0.04 ± 0.09	-0.02 ± 0.02	0.52	49
	0.3	0.16 ± 0.09	-0.01 ± 0.02	0.54	26
	1	0.04 ± 0.10	-0.04 ± 0.03	0.58	83
	3	0.44 ± 0.12	0.06 ± 0.03	0.67	96
ε_3	PHA	-0.01 ± 0.12	-0.02 ± 0.03	0.52	63
	0.3	0.07 ± 0.13	-0.03 ± 0.03	0.54	65
	1	0.01 ± 0.13	-0.03 ± 0.03	0.58	75
	3	0.61 ± 0.16	0.09 ± 0.03	0.67	99
ε_5	PHA	0.05 ± 0.09	-0.01 ± 0.02	0.52	40
	0.3	0.16 ± 0.09	-0.01 ± 0.02	0.54	20
	1	0.05 ± 0.09	-0.03 ± 0.03	0.58	82
	3	0.42 ± 0.11	0.06 ± 0.03	0.67	94

6.6 INTENSITY MEASURES OTHER THAN SPECTRAL ACCELERATION

In this section, predictions of *IM*s other than S_a are presented and compared to observation. The *IM*s considered here are:

1. **Peak horizontal velocity (*PHV*). Predictions from ground response and attenuation (Campbell, 1997, 2000, 2001).**
2. **Arias intensity (I_a). Predictions from ground response and attenuation (Travasarou et al., 2002).**
3. **Significant duration as developed from Husid plot of acceleration waveform ($D_{a,5\text{-}75}$, $D_{a,5\text{-}95}$). Predictions from ground response and attenuation (Abrahamson and Silva, 1996).**
4. **Significant duration as developed from Husid plot of velocity waveform ($D_{v,5\text{-}75}$, $D_{v,5\text{-}95}$). Predictions from ground response only.**
5. **Mean period (T_m). Predictions from ground response and attenuation (Rathje et al., 1998).**

Ground response predictions for Site *j* are developed using the computed waveform at the ground surface for each input motion *k*. The median *IM* in natural log units calculated across the $k = 1..N_j$ waveforms for Site *j* is calculated for comparison to the observed *IM* for Site *j*. Where available, predictions from attenuation are also compiled, the prediction

again being taken as the median estimate in natural log units. Prediction residuals for all sites *j* within Category *i* are compiled, from which category medians (μ_{rg}, μ_{ra}), 95% confidence intervals on the medians, and category standard deviations (σ_{rg}, σ_{ra}) are computed. The categorization scheme used here to define the site categories is NEHRP (Table 2.2).

Prediction residuals from ground response and attenuation for each individual Site *j* within the NEHRP categories are shown with dots and open circles, respectively, in Figures 6.30 – 6.32. Shown with dashes in the figures are the category median residuals and the ±95% confidence intervals on the median. The category standard deviations are also listed in the figures.

Figure 6.30 shows results for *IM*s related to the amplitude of the ground motions, *PHV* and I_a. The ground response results for *PHV* have a significant positive bias for C, D, and E sites, but not for I_a. The difference between median residuals for the ground response and attenuation prediction models is generally small for Category D, but is large for C and E for parameter *PHV*, with the absolute value of the ground response bias generally being smaller than the attenuation bias. For parameter *PHV*, standard deviations from ground response are smaller than attenuation for all categories, with the difference being especially significant for Category E. For parameter I_a, the standard deviations from these two models are not significantly different.

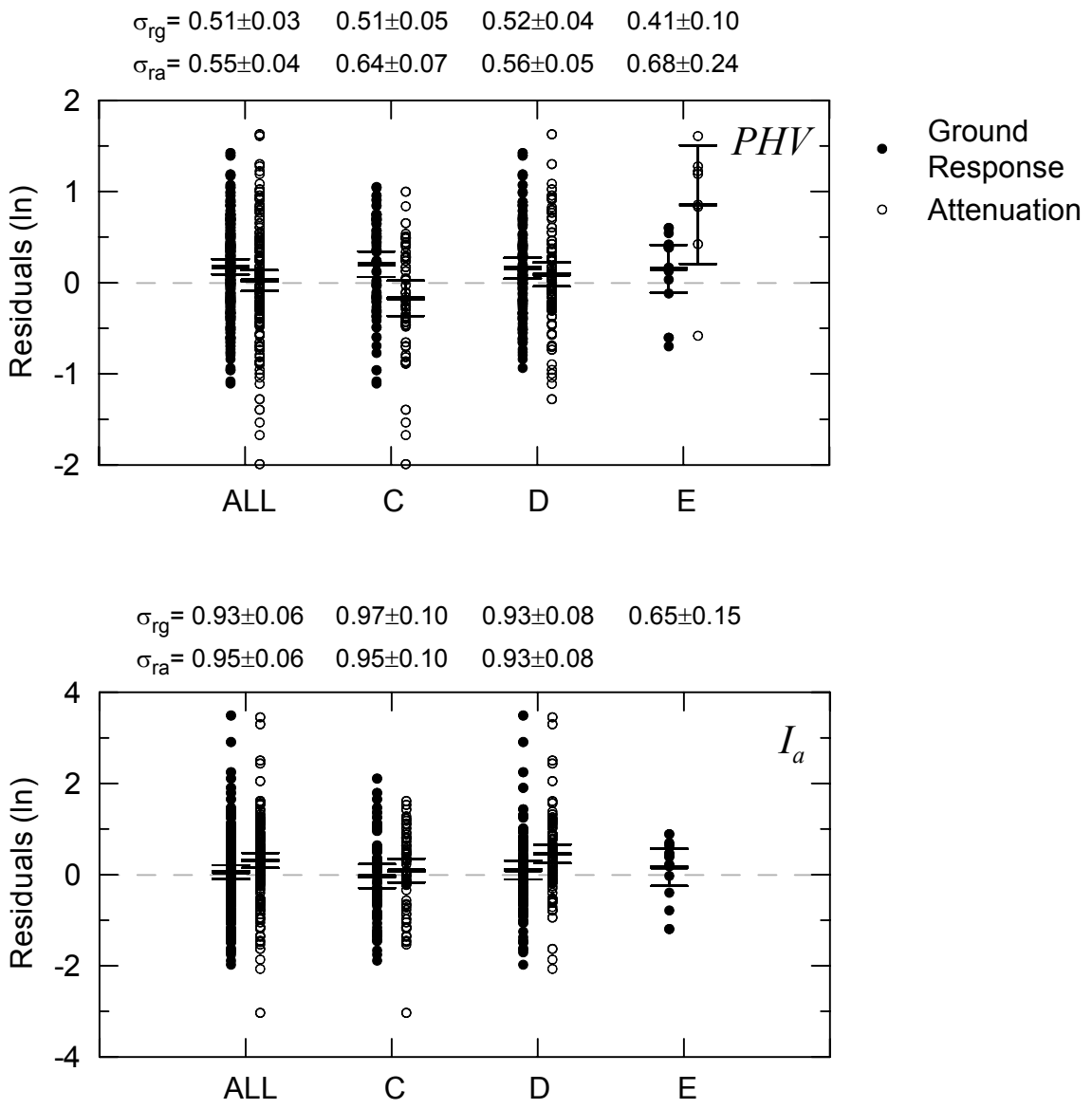

Fig. 6.30. Individual prediction residuals for the *IM*s of peak horizontal velocity (*PHV*) and Arias Intensity (I_a), along with category medians and 95% confidence intervals around the medians

Figure 6.31 shows results for *IM*s related to duration ($D_{a,5\text{-}75}$, $D_{a,5\text{-}95}$, $D_{v,5\text{-}75}$, $D_{v,5\text{-}95}$). We generally observe larger positive bias (indicating underprediction) in ground response predictions for Category D than for C. The bias for C is generally not significantly different from zero; for D the positive bias is insignificant for the 5-75 parameters (i.e., $D_{a,5\text{-}95}$ and $D_{v,5\text{-}95}$), but is significant for the 5-95 parameters. Category D sites are often located within basins, and since basin effects (which increase duration) are not accounted for by ground response analyses, this underprediction bias is expected. We generally observe negative bias for Category E, indicating overprediction. We are uncertain about the cause of this overprediction. The attenuation model for D_a duration parameters generally shows no significant bias for Categories C to D, but overprediction bias for E. Ground response predictions reduce the overprediction bias from attenuation for Category E, but for C-D ground response does not significantly improve upon attenuation. Standard deviations from ground response and attenuation are generally not significantly different for the D_a parameters. There is no significant variation of dispersion across site categories. However, the dispersion for 5-95 duration parameters is significantly less than the dispersion for the 5-75 duration parameters.

Figure 6.32 shows results for T_m, the only *IM* considered here that is related directly to frequency content. Ground response predictions are biased slightly low for Categories C and D and high for E, with the exact opposite trends for the attenuation model. In terms of bias reduction, the ground response predictions significantly improve upon attenuation only for Category E. Standard deviations from ground response are comparable to those from attenuation for Categories C-D, but are significantly smaller than attenuation for Category E. Moreover, the ground response standard deviation for E is notably smaller than those for other categories, indicating that ground response is consistently capturing the frequency content of the motions from these sites.

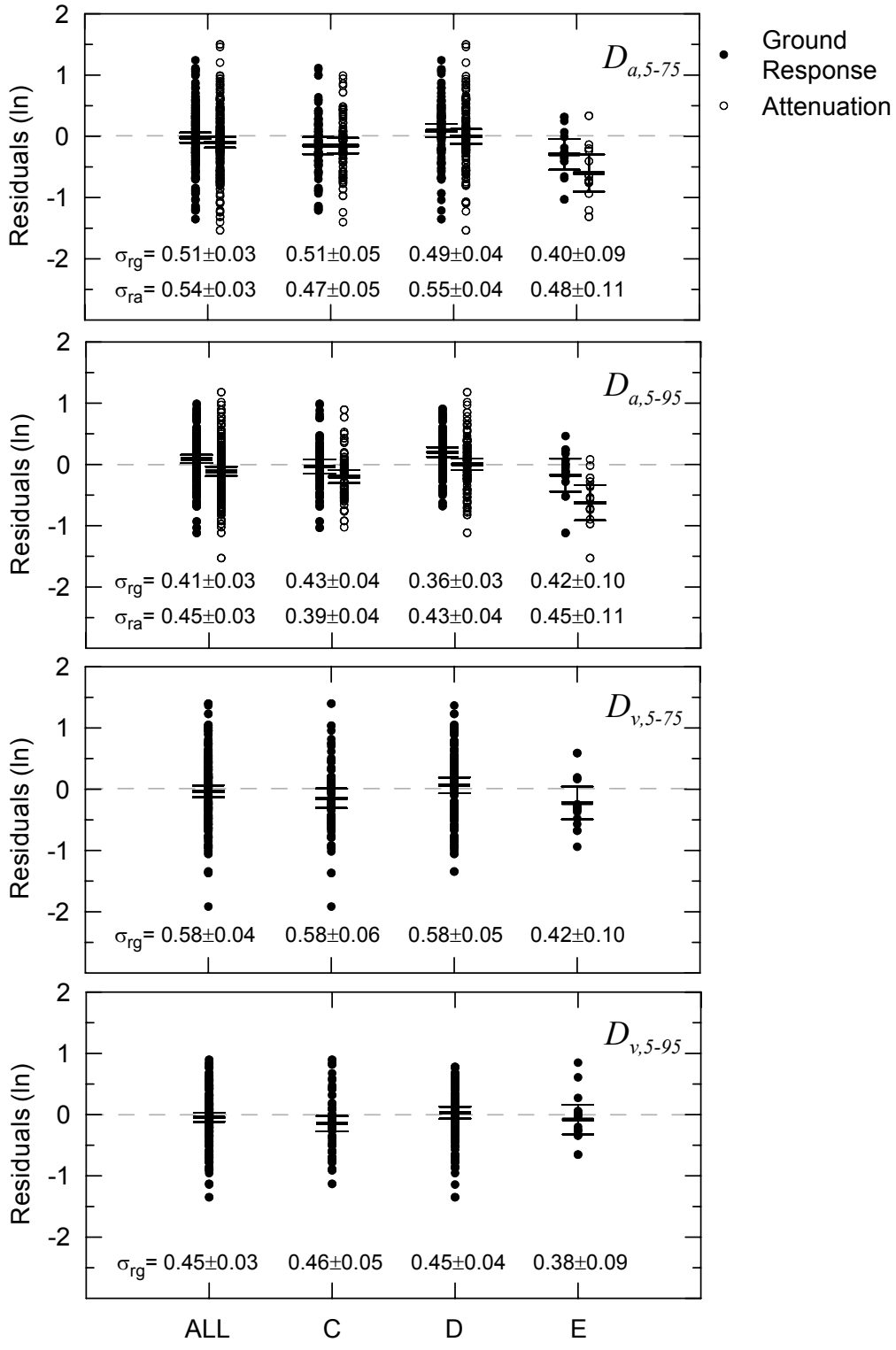

Fig. 6.31. Individual prediction residuals for duration *IM*s ($D_{a,5\text{-}75}$, $D_{a,5\text{-}95}$, $D_{v,5\text{-}75}$, $D_{v,5\text{-}95}$), along with category medians and 95% confidence intervals around the medians

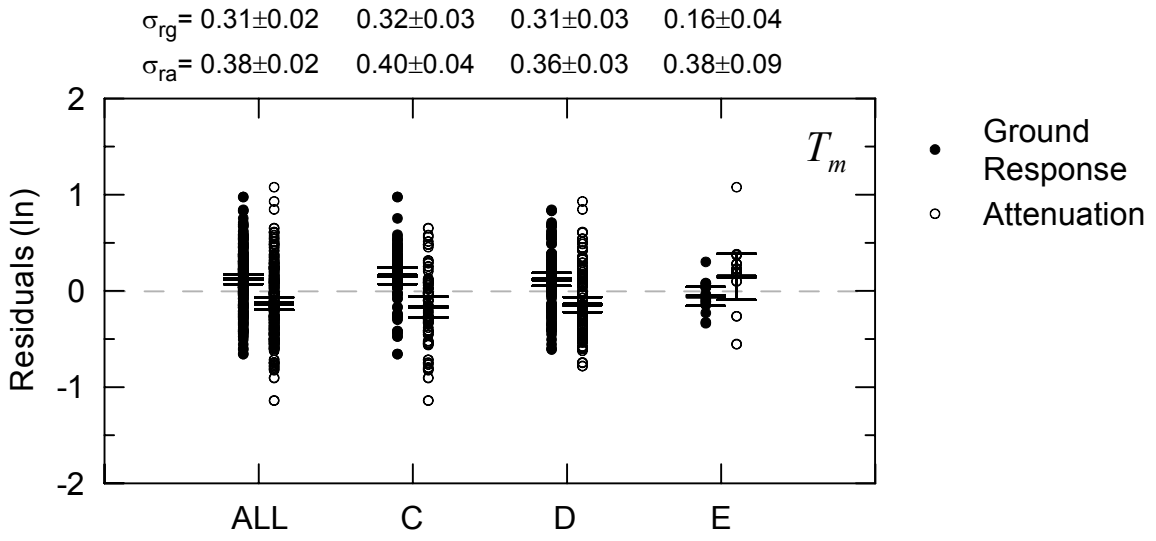

Fig. 6.32. Individual prediction residuals for T_m, along with category medians and 95% confidence intervals around the medians

Ground response analysis residuals for parameters *PHV*, $D_{a,5\text{-}95}$ and $D_{v,5\text{-}95}$ are examined with respect to parameter, z_1 (defined as depth to V_s= 1 km/s in m.). We expect these parameters to be influenced by basin effects, which in turn should be loosely related to z_1, thus a trend is anticipated. The residuals are plotted as a function of z_1 in Figure 6.33. Also plotted in figure 6.33 are the results of regression analyses performed according to the following equation:

$$\ln(\mu_{rg-IM})_j = g + h\ln(z_1)_j \qquad \textbf{(6.13)}$$

where $(\mu_{rg\text{-}IM})_j$ is the median residual from ground response for site *j*, $(z_1)_j$ is the depth to V_s= 1 km/s for that site, and *g* and *h* are regression coefficients. Confidence intervals (±95%) are also presented on the plots. The statistical significance of the slope of the regression lines is evaluated with hypothesis testing similar to that discussed in Section 6.3.5. Tabulated in Table 6.21 are the values of 1-α, which is here referred to as a "rejection confidence for an *h*=0 model". Large rejection confidence levels (i.e., >95%) suggest significant z_1 dependence of residuals.

As can be seen from Figure 6.33 and Table 6.21 there is a significant trend on the residuals with z_1. The trend of increasing residuals with depth suggests that the model is underestimating these parameters at sites that are underlain by deep sediments.

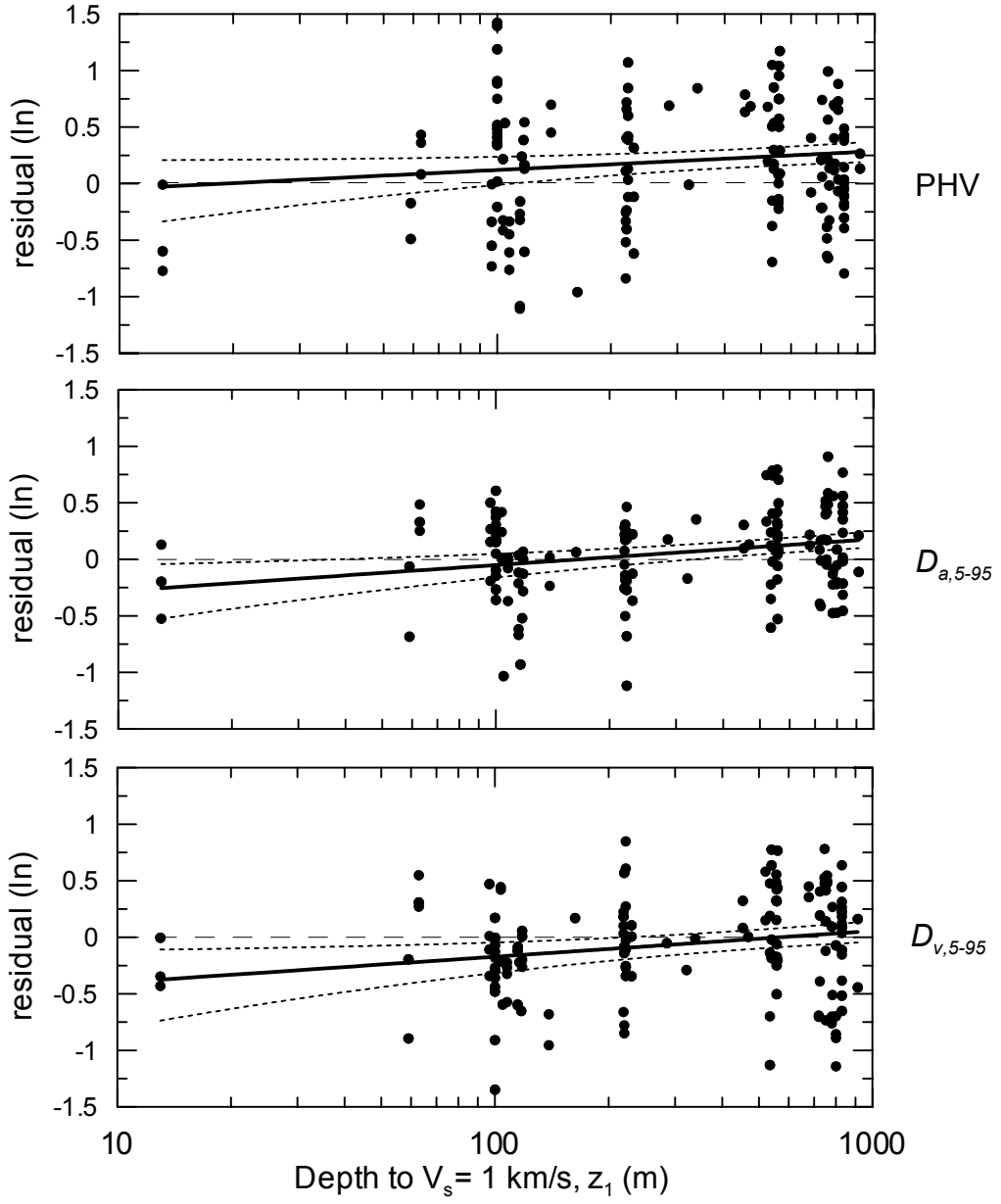

Fig. 6.33. The variation of selected *IM*s (PHV, $D_{a,5\text{-}95}$, $D_{v,5\text{-}95}$) with respect to z_1

Table 6.21. Regression coefficients for residuals of PHV, $D_{a,5\text{-}95}$ and $D_{v,5\text{-}95}$, vs. z_1

IMs	g	h	σ	Rejection confidence for h=0 model (%)
PHV	-0.21 ± 0.21	0.07 ± 0.04	0.53	94
$D_{5\text{-}95\%}$	-0.51 ± 0.15	0.10 ± 0.03	0.37	100
$DV_{5\text{-}95\%}$	-0.63 ± 0.17	0.10 ± 0.03	0.43	100

7 SUMMARY AND CONCLUSIONS

7.1 SCOPE OF RESEARCH

Probabilistic seismic hazard analyses require the use of Increasing amounts of strong motion data and detailed site characterization efforts have enabled the development of improved ground motion estimation models in recent years. The output of these engineering models that provide estimates of ground motion intensity measures (*IM*s) in terms of probability density functions (PDFs) that are is a probability density function (PDF) for a ground motion intensity measure (*IM*) conditioned on the occurrence of an earthquake with a particular magnitude at a particular distance from the site. The simplest way to estimate these PDFs is through the use of attenuation relationships that are derived for broadly defined site categories (e.g., rock and soil). If additional information is available that allows a site to be classified according to a detailed categorization scheme, the statistical moments (i.e., median, standard deviation) of PDFs from attenuation relations can be adjusted based on amplification factors for categories within the scheme. In either case (attenuation or attenuation with amplification factors), simple empirical models are used to account for the influence of site effects on *IM*s. In general, the physics underlying these site effects would be expected to include (1) the nonlinear response of shallow sediments to nearly vertically incident body waves (i.e., local ground response effects), (2) the effects of 2D or 3D deep basin structure on ground motions (basin response effects), and (3) the effects of irregular surface topography.

As an alternative to the use of attenuation relationships with or without amplification factors, *IM*s can be estimated through the use of site-specific analysis of local ground response effects. Since ground response analyses require detailed site characterization and significant engineering time, its use should improve the accuracy of predicted ground motions and decrease the level of uncertainty in these estimates relative to what would be obtained from simplified procedures, such as attenuation. However, the improvement in *IM* predictions from ground response analyses has not previously been quantified in a statistically robust manner. Moreover, due to the unknown uncertainty associated with *IM*s estimated from ground response analyses, it has not previously been possible to conveniently incorporate ground response analysis results into Probabilistic Seismic Hazard Analyses.

In this study, ground response analyses were performed for a large number of sites with strong motion recordings in order to identify the geologic/geotechnical conditions where ground response analyses significantly and consistently improve *IM* predictions relative to other models. A second objective was to identify the dispersion associated with ground response analysespredictions, so as to enable the results of such analyses to be utilized within Probabilistic Seismic Hazard Analyses of ground motion. The strong motion sites selected for use in this study have all been well characterized from a geotechnical and geophysical point of view, and also have at least one strong motion recording.

The ground response analyses were performed using equivalent linear modeling of nonlinear soil behavior. Input motions for analyses were compiled knowing the magnitude, distance, and site-source azimuth (rupture directivity effects) associated with the subject strong motion recording. A suite of input motions was selected from rock site recordings having similar source parameters as the subject recording, and the individual recordings were scaled to match a target soft rock response spectrum in an average sense. The target soft rock spectrum was estimated using the rock attenuation relationship by Abrahamson and Silva (1997), with modifications for weathering (to adjust the spectrum to that expected for a firm-rock site condition), event terms, and rupture directivity effects. Each of the scaled motions was used in ground response analyses, thus providing a suite of estimated motions at the soil surface. The "prediction" from ground response analyses was taken as the median of *IM*s computed from the suite.

In addition to ground response analyses, ground motion parameters were estimated by several alternative models such as attenuation relations and attenuation relations modified with amplification factors to enable the models' relative effectiveness of the models to be assessed. The models' performance was quantified in terms of prediction residuals, which are defined as the difference between the natural logarithm of the *IM* from the recording minus the predicted *IM*. These residuals were compiled across geological and geotechnical site categories, and as a function of real-valued site parameters such as $V_{s\text{-}30}$ (average 30 m shear wave velocity), z_1 (depth to V_s = 1 km/s isosurface), magnitude of causative earthquake, and calculated ground strains. The interpretation of benefits from ground response analysis was based on the reduction in the median and standard deviation of prediction residuals from ground response relative to those from other models, as well as the degree to which the various models were able to predict the observed response spectral shape.

7.2 RESEARCH FINDINGS AND RECOMMENDATIONS

7.2.1 Major Technical Findings

The results of this research can be broadly categorized as follows: (a) results providing insight into the conditions for which performing ground response analyses provides tangible benefits relative to alternative methods (i.e., attenuation only, attenuation with site amplification factors, and attenuation with basin amplification factors), (b) results relating to how ground response analyses should be used within the context of probabilistic seismic hazard analyses, and (c) assessments of possible bias in the nonlinear soil models used in ground response modeling. The major conclusions from the study are grouped according to these categories in the enumerated paragraphs that follow. This discussion is focused principally on the intensity measure of spectral acceleration, although there are similar findings for other *IM*s as well.

(a) *Benefits of Ground Response Analysis Relative to Other Methods*

1) Intra-Category Bias: Bias is defined as the difference between data and the median prediction of a ground motion estimation procedure, and can result from modeling errors or a ground motion calibration data set that exhibits unusually large or small ground motions. Empirical ground motion amplification factors will, by definition, not be biased for a given site category (as they are established from the data within the category). Accordingly, at issue is whether ground response procedures perform *worse differently* than amplification factors by introducing model-related bias. I We have generally found no evidence for statistically significant model-related bias in spectral accelerations computed from ground response analyses for periods $T \leq \sim 1$ s. For sites on deep soil, positive bias in ground response estimates was identified at long periods ($T \geq \approx 3$ 1 s), which is likely associated with ground motion amplification due to deep basin structure. An exception to the lack of short- to mid-period model bias reported above is positive model bias (indicating underprediction) for deep soil sites (identified in Section 67.3.3 for Geotechnical category D), which is discussed further below in Item 8.

2) Intra-Category Dispersion: The dispersion of a model prediction is calculated from an assemblage of residuals within a category, and represents in an average sense the degree to which a ground motion analysis model can track site-to-site variations in ground motion. An effective model would be expected to have lower intra-category dispersions than a relatively crude model. Hence, a comparison of dispersion values computed within site categories provides a metric for the relative effectiveness of the estimation procedures. For site conditions other than soft clay, I we generally found no statistically significant differences between prediction dispersions from the ground response and site amplification factor models. Conversely, for soft clay sites (e.g., NEHRP or Geotechnical category E, Surface Geology Hlm category), dispersions from ground response analyses are moderately to significantlynoticeably reduced for periods $T \leq < \sim 1$ s, although these reductions are generally of modest statistical significance..

3) Intra-Category Spectral Shape Misfit: The degree to which a ground motion prediction captures the shape of the observed response spectrum spectra is quantified with a shape misfit parameter. This misfit parameter is calculated evaluated for a given site by scaling the prediction to match the observed spectrum in an average sense over the period range $T = 0.05 - 2$ s, and then calculating the misfit parameter fromcalculating a normalized residual sum of squares (Eq. 67.2 __). Small misfit implies a good match of spectral shape. For site conditions other than soft clay, I we generally found no significant differences between shape misfit parameters from the ground response and attenuation models. Conversely, for soft clay sites, shape misfit parameters from ground response were significantly less than those from attenuation.

4) Trends of Residuals with Real-Valued Site/Earthquake Parameters: A robust ground motion estimation procedure should provide estimates that are not systematically unbiased with respect to real-valued parameters such as $V_{s\text{-}30}$, z_1, or magnitude. I We found that residuals from ground response analyses and from site amplification factors do not exhibit small to negligible a significant trends with $V_{s\text{-}30}$, no trend with or magnitude, and a statistically significant trend with but do exhibit a dependence on z_1 at long periods (1.0 s, 3.0 s).. The lack of a strong trend with $V_{s\text{-}30}$ is a desirable feature of these models, which is not shared by the attenuation or basin amplification models. The trend with z_1 can be explained by basin amplification effects, and is largely

removed also present with the attenuation and (surprisingly) the basin amplification models.

(b) *Application of Ground Response Analysis Results*

5) Median: If ground response analyses are to be used to estimate *IM*s, the median and standard deviation of the *IM* PDF is needed. Because ground response analyses do not appear to introduce bias at short periods (see Item 1 above), the median of the predicted motions can be taken as the true median. As discussed further in Section 67.2.2, median spectral ordinates can be calculated directly from the computed waveforms or calculated as the product of the median input spectrum and the median RRS (ratio of output/input response spectra). For deep soil sites at long periods, the median predictions from ground response are biased, and should be adjusted to match predictions from soil attenuation or attenuation with basin factors.

6) Standard Deviation: The dispersion in ground response results can be separated into two components - uncertainty about the location of the computed median *IM* ordinate (which can be readily quantified as part of the ground response analyses) and uncertainty due to various modeling errors (which cannot be readily quantified as part of an individual, site-specific analysis). The second uncertainty parameter was denoted as the net dispersion ($\sigma_{g\text{-}net}$), and was quantified in Section 67.4 from the difference between the total category variance from ground response results and the variance of the median ground response prediction. For $T < 1$ s, these $\sigma_{g\text{-}net}$ values range from about 0.38 for NEHRP Category E to 0.59 56 for NEHRP Category Categories C-D for $T < 1$ s. The overall dispersion for use in PSHA can be calculated from these values and the standard error of the median using Eq. 67.110. At longer periods, total dispersion can be estimated from attenuation or amplification factor models.

(c) *Assessment of Possible Bias in Nonlinear Soil Model*

7) Effect of Using Alternative Models: As described in Section 34.4.1, there is no consensus at present regarding appropriate nonlinear soil models for use in ground response analyses. The models utilized herein were derived from laboratory testing, and generally exhibit more nonlinearity than alternative models derived from the calibration of seismological simulation procedures (see Section 34.4.1 for details). As shown in Section 67.2.4, the difference between *IM*s predicted using lab-based and seismological nonlinear soil models can be significant when the shear strains in the ground exceed approximately 0.1-0.5%. More linear models will tend to produce larger amplitude spectral ordinates, and will shift the spectrum to shorter periods.

8) Bias in Results Derived from Lab-Based Nonlinear Soil Models: A significant bias in the nonlinear soil models utilized in ground response analyses would be expected to introduce a trend in prediction residuals with shear strain in the ground. The possible existence of such a trend was investigated in Section 67.5, and was not found to be consistently present at any spectral pfor $T \leq 1.0$ seriod. These results suggest the lack of a clear bias toward over- or under-prediction of soil nonlinearity. Conversely, the median ground response residuals for deep soil sites (Geotechnical Category D) were found in Section 67.3.3 to be larger than the median residuals from site amplification factors. This bias was not present for shallow sites. These results could be interpreted to imply that the nonlinear soil models provide excessive damping, which would reduce the amplitude of predicted motions on deep sites and hence increase residuals. Given these potentially conflicting results, the possible existence of a bias in the nonlinear soil models utilized in these studies cannot be ruled out.

7.2.2 Recommendations on the use of ground response analyses for ground motion hazard assessments

Ground response analyses were found to be beneficial for soft soil sites (NEHRP E, Geotechnical E, or Holocene-age lacustrine/marine) due to significant reductions of prediction dispersion at small periods and improved estimates of spectra shape relative to attenuation with or without amplification factors. Ground response analyses are not clearly beneficial for relatively stiff soil or soft rock sites such as NEHRP C-D or Quaternary alluvium/Tertiary.

Ground response analyses can be used to estimate the PDF of response spectral accelerations at a soil site for use in probabilistic seismic hazard analyses. The median and standard deviation of that PDF can be estimated using the recommendations provided above in Section 78.2.1(b).

Ground response analyses should be performed using a suite of input motions. The number of time histories in the suite should be large enough to provide a stable estimate of the median and to provide a sufficient representation of the aleatory uncertainty in the phasing of the input to properly quantify the RRS. It was generally found that 10-20 input time histories scaled according to the procedures developed in this research (see Section 56.1.3) is adequate to satisfy these criteria.

7.3

RECOMMENDATIONS FOR FUTURE RESEARCH

This research has identified several issues that should be considered in future work:

1) The ground response analyses performed in this research should be repeated with alternative nonlinear soil models and fully nonlinear computational routines to investigate the effects of these models and analysis routines on category median residuals and trends of residuals with shear strain. In particular, it will be of interest to find whether more linear models than those utilized herein reduce the underprediction of spectral accelerations at deep soil sites.
2) The strong motion sites considered in this research were selected on the basis of available geotechnical and geophysical data. This data is disproportionately available for sites with unusually strong ground motions, as reflected by the consistently positive median prediction residuals compiled for the amplification factor models in Section 67.3. Accordingly, there is a need to perform detailed site characterization at additional strong motion recording sites that do not have unusually large-amplitude recordings. This will reduce the inherent bias that is currently inherent to the present catalogue of well-characterized strong motion accelerograph sites.
3) The use of response spectral matching procedures for input motions used in ground response studies has not been investigated. This topic is of interest because input time histories for ground response analyses that are spectrally-matched to the target input spectrum would be expected to produce much less scatter in output time histories, thus enabling the median output to be estimated with a smaller number of computer runs. At issue is the number of spectrally matched time histories that is needed to establish a stable output median, and whether the output medians from "natural" time histories and spectrally matched time histories are the same.

REFERENCES

Abrahamson, N.A. (1998). "Non-stationary spectral matching program RSPMATCH," PG&E Internal Report, February.

Abrahamson, N.A. (2000). "Effects of rupture directivity on probabilistic seismic hazard analysis," *Proc. 6th Int. Conf. on Seismic Zonation*, Palm Springs.

Abrahamson, N.A. and Silva, W.J. (1996). "Empirical ground motion models," Report to Brookhaven National Laboratory.

Abrahamson, N.A. and Silva, W.J. (1997) "Empirical response spectral attenuation relations for shallow crustal earthquakes," *Seism. Research Letters*, 68(1), 94-127

Aki, K. and Richards, P.G. (1980). *Quantitative seismology*, Vol. 1, W.H. Freeman, San Francisco, CA.

Anderson, J.G., Trifunac, M.D., Teng, T.-L., Amini, A., and Moslem, K. (1981). "Los Angeles vicinity strong motion accelerograph network," *Report No. CE 81-04*, Univ. of Southern California.

Ang, A. H-S. and Tang, W.H. (1975). *Probability concepts in engineering planning and design: Volume I – Basic principles*, John Wiley & Sons, New York, NY.

Ayyub, B. M., and McCuen, R. H. (1997). *Probability, statistics, and reliability for engineers*, CRC Press, Boca Raton, NY.

Bazzuro, P. (1998). "Probabilistic seismic demand analysis," *Ph.D. Dissertation*, Civil Engineering Dept., Stanford University.

Boatwright, J., Thywissen, K. and Seekins, L. (2001). "Correlation of ground motion and intensity for the January 17, 1994 Northridge, California earthquake," *Bull. Seism. Soc. Am.*, 91, 739-752.

Boore, D.M., Joyner, W.B., and Fumal, T.E. (1997). "Equations for estimating horizontal response spectra and peak acceleration from western North American earthquakes: A summary of recent work," *Seism. Res. Letters*, 68(1), 128-153.

Borcherdt, R.D. (1994). "Estimates of site-dependent response spectra for design (methodology and justification)," *Earthquake Spectra*, 10(4), 617-653.

Borcherdt, R.D. (2002). "Empirical evidence for acceleration-dependent amplification factors," *Bull. Seism. Soc. Am*., 92, 761-782.

Borcherdt, R. D. and Glassmoyer, G. (1994). "Influences of local geology on strong and weak ground motions recorded in the San Francisco Bay region and their implications for site-specific

building-code provisions" The Loma Prieta, California Earthquake of October 17, 1989--Strong Ground Motion, U. S. Geological Survey Professional Paper 1551-A, A77-A108

Brocher, T. M. et al. (1998). “San Francisco Bay area 3D velocity model, revision 1,” USGS, Menlo Park, CA, unpublished manuscript.

Bullen, K.E. (1965). *An introduction to the theory of seismology*, Cambridge Univ. Press, Cambridge, U.K.

Campbell, K.W. (1997). “Empirical near-source attenuation relations for horizontal and vertical components of peak ground acceleration, peak ground velocity, and pseudo-absolute acceleration response spectra,” *Seism. Res. Letters*, 68(1), 154-179.

Campbell, K.W. (2000). Erratum to Campbell, 1997, *Seism. Res. Letters*, 71(3), 352-354.

Campbell, K.W. (2001). Erratum to Campbell, 2000, *Seism. Res. Letters*, 72(4), p 474.

Chang, S.W. (1996). “Seismic response of deep stiff soil deposits,” *Ph.D. Dissertation*, Univ. of California, Berkeley

Chang, S.W., Bray, J.D. and Seed, R.B. (1996) “Engineering implications of ground motions from the Northridge earthquake,” *Bull. Seism. Soc. Am*., 86 (1B), 270-288

Darragh, R.B. and Idriss, I.M. (1997) “A tale of two sites: Gilroy #2 and Treasure Island - Site response using and equivalent linear technique,” NEHRP Professional Fellowship Report, EERI, Oakland, CA

Dickenson, S.E. (1994). “The dynamic response of soft and deep cohesive soils during the Loma Prieta earthquake of October 17, 1989,” *Ph.D. Dissertation*, Univ. of California, Berkeley.

Doroudian, M. and Vucetic, M. (1995). “A direct simple shear device for measuring small-strain behavior,” *Geotech. Testing J.*, ASTM, 18(1), 69-85.

EPRI, Electrical Power Research Institute (1993). “Guidelines for determining design basis ground motions. Volume 1: Method and guidelines for estimating earthquake ground motion in eastern North America,” *Rpt. No. EPRI TR-102293*, Palo Alto, CA.

Field, E.H. (2000). “A modified ground motion attenuation relationship for southern California that accounts for detailed site classification and a basin depth effect,” *Bull. Seism. Soc. Am*., 90, S209-S221.

Frankel, A. and Stepheson, W. (2000). “Three dimensional simulation of ground motions in the Seattle region for earthquakes in the Seattle fault zone,” *Bull. Seism. Soc. Am*., 90, 1251-1265

Frankel, A., and Vidale, J. (1992). " A three-dimensional simulation of seismic waves in the Santa Clara Valley, California, from a Loma Prieta Aftershock," *Bull. Seism. Soc. Am.*, 82 (5), 2045-2074.

Fumal, T.E. (1991). "A compilation of the geology and measured and estimated shear-wave velocity profiles at strong-motion stations that recorded the Loma Prieta, California, earthquake," *OFR 91-311*, U.S. Geological Survey, Menlo Park, CA.

Fumal, T.E. and Tinsley, J.C. (1985). "Mapping shear-wave velocities of near-surface geologic materials," *U.S. Geological Survey Prof. Paper 1360*, 127-150

Geomatrix Consultants (1993). "Compilation of geotechnical data for strong motion stations in the Western United States." Report to Lawrence Livermore National Lab., Project No. 2256.

Gibbs, J.F., and Fumal, T.E. (1994). "Seismic velocities and geologic logs at seven strong-motion stations that recorded the 1989 Loma Prieta, California, earthquake, Part IV," *OFR 94-552*, U.S. Geological Survey, Menlo Park, CA.

Gibbs, J.F., Fumal, T.E., Boore, D.M., and Powers, T.J. (1992). "Seismic velocities and geologic logs from borehole measurements at seven strong motion stations that recorded the 1989 Loma Prieta, California, earthquake," *OFR 92-287*, U.S. Geological Survey, Menlo Park, CA.

Gibbs, J.F., Fumal, T.E., and Powers, T.J. (1993). "Seismic velocities and geologic logs from borehole measurements at eight strong motion stations that recorded the 1989 Loma Prieta, California, earthquake," *OFR 93-376*, U.S. Geological Survey, Menlo Park, CA.

Gibbs, J.F., Fumal, T.E., and Powers, T.J. (1994). "Seismic velocities and geologic logs from borehole measurements at eight strong motion stations that recorded the 1989 Loma Prieta, California, earthquake," *OFR 94-222*, U.S. Geological Survey, Menlo Park, CA.

Gibbs, J.F., Tinsley, J.C., Boore, D.M., and Joyner, W.B. (1999). "Seismic velocities and geological conditions at twelve sites subjected to strong ground motion in the 1994 Northridge, California, earthquake: A revision of OFR 96-740" *OFR 99-446*, U.S. Geological Survey, Menlo Park, CA.

Gibbs, J.F., Tinsley, J.C., Boore, D.M., and Joyner, W.B. (2000). "Borehole velocity measurements and geological conditions at thirteen sites in the Los Angeles, California region," *OFR 00-470*, U.S. Geological Survey, Menlo Park, CA.

Gibbs, J.F., Tinsley, J.C., and Joyner, W.B. (1996). "Seismic velocities and geologic conditions at twelve sites subjected to strong ground motion in the 1994 Northridge, California, earthquake," *OFR 96-740*, U.S. Geological Survey, Menlo Park, CA.

Graves, R.W., Pitarka, A., and Somerville, P.G. (1998) "Ground motion amplification in the Santa Monica area: effects of shallow basin edge structure," *Bull. Seism. Soc. Am*., 88, 1224-1242

Graves, R.W. (1993). "Modeling three-dimensional site response effects in the Marina District, San Francisco, California," *Bull. Seism. Soc. Am*., 83, 1042-1063

Guha, S., Bray, J.D. and Drnevich, V.P. (1993). "Characteristics of the deep old bay clay deposits in the east San Francisco bay area," *Rpt. No. UCB/GT/93-09*, Univ. of California, Berkeley.

Hsu, C.C. and Vucetic, M. (1999). "Results of cyclic and dynamic simple shear tests on soils from Tarzana and Rinaldi sites conducted for ROSRINE project and other research purposes," *Report No. UCLA/ENG-99-205*, Univ. of California, Los Angeles.

Idriss, I.M. (1990) "Response of soft soil sites during earthquakes*," Proc. H. Bolton Seed Memorial Symposium*, J.M. Duncan (ed.), Vol. 2, 273-290

Idriss, I.M. and Sun, J.I. (1992). "SHAKE91: A computer program for conducting equivalent linear seismic response analyses of horizontally layered soil deposits," Center for Geotech. Modeling, Univ. of California, Davis.

Idriss, I.M. (1999). "Quantitative geotechnical site characterization," PG&E/PEER Task 3.E Internal Report.

Iwasaki, Y., and M. Tai (1996). Strong motion records at Kobe Port Island, *Soils and Foundations* (special issue), 29-40

Joyner, W.B. (2000) "Strong motion from surface waves in deep sedimentary basins," *Bull. Seism. Soc. Am*., 90(6B), 95-112

Joyner, W.B., Warrick, R.E., and Fumal, T.E. (1981). "The effect of Quaternary alluvium on strong ground motion in the Coyote Lake, California earthquake of 1979," *Bull. Seism. Soc. Am.*, 71, 1333-1349.

KAJIMA Corporation (2000), *NFE project report*, Nuclear Power Department, Construction Group, Kajima Corporation

Kawase, H. and Nagato, K. (2000). "Structural damage impact of strong motions evaluated by the nonlinear analyses of a set of building models," *Proc. Sixth Int. Conf. Siesm. Zonation*, Palm Springs, CA.

Lee, Y. and Anderson, J. G. (2000) "Potential for improving ground-motion relations in southern California by incorporating various site parameters," *Bull. Seism. Soc. Am*., 90(6B), 170-186

Magistrale, H., Day, S., Clayton, R., and Graves, R. (2000). "The SCEC southern California reference three-dimensional seismic velocity model version 2," *Bull. Seism. Soc. Am.*, 90, S65-S76.

Martin, G.M. editor (1994). *Proceedings of the NCEER/SEAOC/BSSC Workshop on Site Response During Earthquakes and Seismic Code Revisions*, Univ. of Southern Calif.

Morton, D.M., Hauser, R.M., and Ruppert, K.R. (1999). “Preliminary Digital Geologic Map of the Santa Ana 30' x 60' Quadrangle, Southern California,” *Open-File Report 99-172*, U.S. Geological Survey, Menlo Park, CA.

Nigbor, R.L. and Steller, R.A. (1993). “Borehole geophysical measurements at 24 rock and soil sites,” *Report to EPRI, Rep#9225-6427*, Agbabian Assoc., March.

Park, S. and Elrick, S. (1998). “Prediction of shear wave velocities in southern California using surface geology,” *Bull. Seism. Soc. Am*., 88,677-685

Pitarka, A., Irikura, K., Iwata, T. and Sekiguchi, H. (1998) “Three dimensional simulation of the near-fault ground motion for the 1995 Hyogo-ken Nanbu (Kobe), Japan, earthquake,” *Bull. Seism. Soc. Am*., 89, 54-68

Porcella, R.L. (1984). "Geotechnical investigations at strong-motion stations in the Imperial Valley, California," *OFR 84-562*, U.S. Geological Survey, Menlo Park, CA.

Powers, T.J. and Fumal, T.E. (1993). “Geologic logs from 25 boreholes near strong motion accelerographs that recorded the 1989 Loma Prieta, California, earthquake,” *OFR 93-502*, U.S. Geological Survey, Menlo Park, CA.

Rathje, E.M., Abrahamson, N.A., and Bray, J.D. (1998). “Simplified frequency content estimates of earthquake ground motions,” *J. Geotech. & Geoenv. Engrg.*, ASCE, 124(2), 150-159.

Rathje, E., Idriss, I. M. and Somerville, P. (2000). Chapter 4: Strong Ground Motions and Site Effects. Kocaeli, Turkey Earthquake of August 17, 1999 Reconnaissance Report, T.L. Youd, J.P. Bardet, and J.D. Bray, eds., *Earthquake Spectra*, Supplement A to Vol. 16, 65-96.

Roblee, C.J., Silva, W.J., Toro, G.R., and Abrahamson, N.A. (1996). “Variability in site-specific seismic ground motion design predictions,” *ASCE Geotech. Special Publication No. 58*, Uncertainty in the Geologic Environment: From Theory to Practice, C.D. Shakelford, P.P. Nelson (eds.), Vol. 2, 1113-1133.

Rodriguez-Marek, A., Bray, J.D., and Abrahamson, N.A. (2001). “An empirical geotechnical seismic site response procedure,” *Earthquake Spectra*, 17(1), 65-87.

Rollins, K.M., Evans, M.D., Diehl, N.B., and Daily, W.D. (1998). “Shear modulus and damping relationships for gravels,” *J. Geotech. Geoenv. Engrg.*, ASCE, 124 (5).

ROSRINE, Resolution Of Site Response Issues from the Northridge Earthquake, http://geoinfo.usc.edu/rosrine/

Sadigh, K., Chang, C.-Y., Abrahamson, N.A., Chiou, S.J., and Power, M.S. (1993). “Specification of long-period ground motions: updated attenuation relationships for rock site conditions and adjustment factors for near-fault effects,” *Proc. Seminar on Seismic Isolation, Passive Energy Dissipation, and Active Control*, Applied Technology Council Publication No. 17-1, Vol. 1, 59-70.

Sadigh, K., Chang, C.-Y., Egan, J.A., Makdisi, F., and Youngs, R.R. (1997). "Attenuation relations for shallow crustal earthquakes based on California strong motion data," *Seism. Res. Letters*, 68(1), 180-189.

Sato, T., Graves, R. W. and Somerville, P. G. (1999). "3D finite difference simulations of long period strong motions in the Tokyo metropolitan are during the 1990 Odawara earthquake (Mj 5.1) and the Great 1923 Kanto earthquake (Ms 8.2) in Japan," *Bull. Seism. Soc. Am.*, 89, 579-598.

Schnabel, P.B., Lysmer, J. and Seed, H.B. (1972). "SHAKE: A computer program for earthquake response analysis of horizontally layered sites," *Rpt. No. EERC 72/12*, Earthquake Engineering Research Center, Univ. of California, Berkeley.

Schneider, J.F., Silva, W.J., and Wright, D. (2000). "Earthquake scenario ground motion hazard maps for the San Francisco Bay region," Report to U.S. Geological Survey, National Earthquake Hazards Reduction Program.

Seed, H.B. and Idriss, I. M. (1970). "Soil moduli and damping factors for dynamic response analyses," *Report EERC 70-10*, Earthquake Engineering Research Center, University of California, Berkeley.

Seed, H.B. and Idriss, I.M. (1971). "Influence of soil conditions on building damage potential during earthquakes," *J. Struct. Engrg*., ASCE, 97(2), 639-663.

Seed, H. B. and Idriss, I. M. (1982) "Ground motions and soil liquefaction during earthquakes" Monograph Series, Vol. 5, Earthquake Engineering Research Institute.

Seed, H. B., Whitman, R. V., Dezfulian, H., Dobry, R. and Idriss, I. M. (1972). "Soil conditions and building damage in 1967 Caracas earthquake" *J. Soil Mechanics and Foundations Div.*, ASCE, 98 (8), 787-806.

Seed, H.B., Romo, M.P., Sun, J.I., Jaime, A., and Lysmer, J. (1987) "Relationships between soil conditions and earthquake ground motions in Mexico City in the earthquake of September 19, 1985," *Rpt. No. UCB/EERC-87/15*, Earthquake Engineering Research Center, Univ. of California, Berkeley

Seed, H.B., Wong, R.T., Idriss, I.M., and Tokimatsu, K. (1984). "Moduli and damping factors for dynamic analyses of cohesionless soils," *Rpt. No. UCB/EERC-84/14*, Earthquake Engineering Research Center, Univ. of California, Berkeley.

Seed, H.B., Wong, R.T., Idriss, I.M., and Tokimatsu, K. (1986). "Moduli and damping factors for dynamic analyses of cohesionless soils," *J. Geotech. Engrg.*, ASCE, 112 (11), 1016-1032.

Seed, R. B. and Dickenson, S.E. (1996). "Nonlinear dynamic response of soft and deep cohesive soil deposits," Proceedings of the International Workshop on Site Response Subjected to Strong Earthquake Motions: Yokosuka, Japan, January 16-17, 1996, Japan Port and Harbour Research Inst., Yokosuka, Japan, Vol. 2, pages 67-81.

Seed, R. B., Dickenson, S. E., Riemer, M. F., Bray, J. D., Sitar, N., Mitchell, J. K., Idriss, I. M., Kayen, R. E., Kropp, A., Harder, L. F., Power, Jr. and M. S. (1990) "Preliminary report on the principal geotechnical aspects of the October 17, 1989 Loma Prieta earthquake" ***Rpt. No. UCB/EERC-90/05*****, Earthquake Engineering Research Center, Univ. of California, Berkeley**

Shannon & Wilson/Agbabian Associates, SW/AA (1980). "Geotechnical data from accelerograph stations investigated during the period 1975-1979, summary report," Report to U.S. Nuclear Regulatory Commission, Washington, D.C.

Silva, W.J., Abrahamson, N., Toro, G., and Costantino, C. (1997). "Description and validation of the stochastic ground motion model," Report to Brookhaven National Laboratory, Associated Universities, Inc., Upton, NY.

Silva, W.J., Darragh, R., Gregor, N., Martin, G., Abrahamson, N., and Kircher, C. (2000). "Reassessment of site coefficients and near-fault factors for building code provisions," Report to U.S. Geological Survey, National Earthquake Hazards Reduction Program.

Silva, W.J., Li, S., Darragh, R., and Gregor, N. (1999). "Surface geology based strong motion amplification factors for the San Francisco Bay and Los Angeles areas," Report to Pacific Earthquake Engineering Research Center.

Somerville, P.G., Smith, N.F., Graves, R.W. and Abrahamson, N.A. (1997). "Modification of empirical strong ground motion attenuation relations to include the amplitude and duration effects of rupture directivity," ***Seismological Research Letters*****, 68, 199-222.**

Spudich, P., Joyner, W.B., Lindh, A.G., Boore, D.M., Margaris, B.M., and Fletcher, J.B. (1999). "SEA99: A revised ground motion prediction relation for use in extensional tectonic regimes," ***Bull. Seism. Soc. Am.*****, 89, 1156-1170.**

Steidl, J.H. (2000). "Site response in southern California for probabilistic seismic hazard analysis," *Bull. Seism. Soc. Am.*, 90, S149-S169.

Steidl, J.H. and Lee, Y. (2000). "The SCEC Phase III strong-motion database," *Bull. Seism. Soc. Am.*, 90, S113-S135.

Stewart, J.P. (2000). "Variations between foundation-level and free-field earthquake ground motions," *Earthquake Spectra*, 16 (2), 511-532.

Stewart, J.P. and Stewart, A.F. (1997). " Analysis of soil-structure interaction effects on building response from earthquake strong motion recordings at 58 sites," *Rpt. No. UCB/EERC-97/01*, Earthquake Engineering Research Center, Univ. of California, Berkeley.

Stewart, J. P., Chiou, S. J., Bray, J. D., Graves, R. W., Somerville, P. G., and Abrahamson, N. A. (2001). "Ground motion evaluation procedures for performance based design" *Report No.*

PEER-2001/09, Pacific Earthquake Engineering Research Center, University of California, Berkeley, California.

Stewart, J.P., Liu, A.H., and Choi, Y. (2002-in press). "Amplification factors for spectral acceleration in tectonically active regions," *Bull. Seism. Soc. Am*.

Stokoe, K.H., Darendeli, M.B., Andrus, R.D., and Brown, L.T. (1999). "Dynamic soil properties: Laboratory, field and correlation studies," *Earthquake Geotechnical Engineering*, S. Pinto (ed.), Balkema, Rotterdam, Vol. 3, 811-845.

Sun, J.I., Golesorkhi, R., and Seed, H.B. (1988). "Dynamic moduli and damping ratios for cohesive soils," *Rpt. No. UCB/EERC-88/15*, Earthquake Engineering Research Center, Univ. of California, Berkeley.

Thiel, C.C. and Schneider, J.F. (1993). "Investigations of thirty-three Loma Prieta earthquake strong motion recording sites," Report to Building Contractors Society of Japan and Electical Power Research Institute, California Universities for Research in Earthquake Engineering, Stanford, CA.

Tinsley, J.C. and Fumal, T.E. (1985). "Mapping Quaternary sedimentary deposits for areal variations in shaking response," U.S. Geological Survey Prof. Paper 1360, 101-126.

Travasarou T., Bray, J.D., and Abrahamson, N.A. (2002-in review) "Empirical attenuation relationship for arias intensity," *Earthquake Spectra*

Trifunac, M.D. and Todorovska, M.I. (1996). "Nonlinear soil response – 1994 Northridge, California earthquake," *J. Geotech. & Geoenv. Engrg*., ASCE, 122 (9), 725-735.

Vucetic, M. and Dobry, R. (1991). "Effect of soil plasticity on cyclic response," *J. Geotech. Engrg.*, ASCE, 117(1), 89-107.

Vucetic, M., Hsu , C.C., and Doroudian, M. (1998). "Results of cyclic and dynamic simple shear tests on soils from La Cienega site conducted for ROSRINE project and other research purposes," *Report No. UCLA/ENG-98-200*, Univ. of California, Los Angeles

Weiler, W.A. (1988). "Small strain shear modulus of clay," *Proc. ASCE Conf. Earthquake Engineering & Soil Dynamics II: Recent Advances in Ground Motion Evaluation*, Geotechnical Special Publication 20, ASCE, New York, 331-335.

Wen, K-L. and Peng, H-Y. (1998). "Strong motion observations in the Taipei basin," The Effects of Surface Geology on Seismic Motion, Recent Progress and New Horizon on ESG Study, Proceedings of the Second International Symposium, A.A. Balkema, Rotterdam, Vol. 1, p. 263-270.

Wills, C.J. Petersen, M., Bryant, W.A., Reichle, M., Saucedo, G.J., Tan, S., Taylor, G., and Treiman, J. (2000). "A site conditions map for California based on geology and shear wave velocity," *Bull. Seism. Soc. Am.*, 90, S187-S208.

Wills, C.J. and Silva, W. (1998). “Shear wave velocity characteristics of geologic units in California,” *Earthquake Spectra*, 14(3), 533-556.

APPENDIX A: SELECTION OF CALIBRATION SITES FOR VALIDATION OF NONLINEAR GEOTECHNICAL MODELS

This work described in the main body of this report was funded in part by Grant 2G01 from the Lifelines Program of the Pacific Earthquake Engineering Research Center. The objective of the Lifelines 2G project series is to calibrate and further develop existing nonlinear geotechnical models for site response. The objective of the 2G01 project was to develop a collection of case histories (i.e., "calibration sites") that can be utilized in these studies. In this appendix, we identify a series of strong motion stations that can be utilized for such studies, describe the range of conditions present at the sites, and describe analyses performed for the sites beyond the analyses previously described in the main body of the report.

Detailed information on the full suite of sites considered in this research, including the selected calibration sites, is provided in Appendix B. In this appendix, the following information is provided for each site: (1) geotechnical data such as stratigraphy, soil types, and small-strain shear wave velocity profiles; (2) engineering models for dynamic soil properties; (3) existing strong motion recordings; and (4) a reference set of carefully chosen control motions for use as input in ground response analyses.

A.1 CRITERIA FOR SITE SELECTION

The first stage of the site selection process involved the development of the comprehensive site list that appears in Chapter 4 of this report (Table 4.1). Criteria utilized in the development of that list were as follows: (1) soil conditions at the sites must be well characterized, including in situ measurements of shear wave velocity and detailed descriptions of soil type, and (2) at least one strong motion recording must be available at each site. As described in Chapter 4, 68 sites were identified that meet those criteria, and 134 recordings are available from those sites.

Analysis of the ground motions at those sites was performed using the procedures in Chapter 5, with the results presented in Chapter 6.

The second stage of the site selection process involved the identification of calibration sites from the comprehensive site list of Table 4.1. The principal factors involved in the selection of these calibration sites are as follows:

1. The selected sites should span a broad, but representative, range of geotechnical site conditions. For example, we attempt to select roughly equivalent numbers of NEHRP C, D, and E sites, with diverse intra-category $V_{s\text{-}30}$ values (average shear wave velocity in upper 30 m) and z_1 values (depth to V_s = 1 km/s). In addition, some of the selected sites should have soil types that are predominantly cohesive, while others should be predominantly cohesionless.
2. The selected sites should have recorded motions of moderate to large amplitude and small amplitude. The "amplitude" of a motion is indexed by conventional parameters such as PHA and PHV, but also by the levels of strain expected to have occurred in the soil during strong shaking. This is assessed using procedures of the type discussed in Section 6.5.
3. Based on analyses of the type reported in Chapter 6, the recordings at the selected sites should span a range of amplitudes relative to what would generally be expected for the site category. For example, some recordings should be near the prediction from attenuation with a category-specific amplification factor, while others should be above and below these predictions.

The above criteria were used to select 20 sites, from which there are 41 recordings (Tables A.1-A.2). The tables also list three additional vertical array sites that will be considered in later work.

Table A.1. Station information for selected calibration sites

Station ID				Geology			30-m V_s and Geotechnical Data						
Location	**Station Name**	**Agency**	**Station #**	**Age**	**Dep. History**	**Reference[1]**	**V_{s-30} (m/s)**	**NEHRP**	**soil d. (m)[3]**	**Geot.**	**z_1 (m)**	**$z_{2.5}$ (m)**	**Reference[2]**
Corralitos	Eureka Canyon Road	CSMIP	57007	Tertiary	-	DOC, GEOM	458	C	28	C1	829	5066	USGS OFR 93-376
Los Angeles	Obregon Park	CSMIP	24400	Holocene	Alluvial Valley	GEOM	453	C	>65	D	557	3315	ROSRINE, USGS OFR 00-470
Los Angeles	Sepulveda VA	USGS	637	Pleistocene	Alluvial Fan	CDMG	370	C	>75	D2C	751	4100	USGS OFR 99-446
Pacoima	Pacoima Kagel Canyon	CSMIP	24088	Tertiary	-	CDMG, GEOM	502	C	7	C1	100	1349	ROSRINE
Santa Clara	IBM Alm., Santa Teresa Hill	CDMG	57563	Mesozoic	-	DOC	629	C	6	C1	115	2400	ROSRINE
Santa Cruz	UCSC Lick Observatory	CSMIP	58135	Mesozoic	-	DOC	700	C	8	C2	59	853	N&S(1993), USGS OFR 93-502
Simi Valley	Knolls School	USC	90055	Holocene	Alluvial Fan	CDMG	579	C	13	C2	100	100	USGS OFR 99-446
Sylmar	Jensen Gen. Bldg.	USGS	655	Pleistocene	Alluvial Fan	CDMG, boring	519	C	7	C1	780	5405	USGS OFR 99-446
El Centro	El Centro Array #7	USGS	5028	Holocene	Lacustrine	DOC, GEOM	216	D	>104	DC	-	-	KAJIMA
Gilroy	Gilroy Array #2	CSMIP	47380	Holocene	Alluvium	DOC	274	D	165	D1C	219	2400	USGS OFR 92-287, EPRI (1993)
Halls Valley	Halls Valley	CSMIP	57191	Holocene	-	DOC, GEOM	268	D	46	C3	97	3000	USGS OFR 93-502, N&S(1993)
Los Angeles	Epiphany	USC	90053	Holocene	Alluvial Fan	CDMG	287	D	73	D2C	453	2840	USGS OFR 99-446
Los Angeles	Rinaldi Receiving Stn.	LADWP	77, 5968	Pleistocene	Alluvial Fan	CDMG	327	D	13	C2	139	4537	USGS OFR 99-446
Newhall	Fire Station	CSMIP	24279	Holocene	Alluvial Fan	CDMG	273	D	35-55	C3	725	1365	ROSRINE
Oakland	Outer Harbor Wharf	CSMIP	58472	Holocene	Marine	DOC, GEOM	248	D	150	D1C	222	2400	USGS OFR 92-287
Sylmar	Olive View Hospital	CDMG	24514	Holocene	Fill	CDMG, GEOM	357	D	80	D2	800	8945	USGS OFR 99-446
El Centro	Meloland Overcrossing	CSMIP	5155	Holocene	Lacustrine	DOC, GEOM	195	E	>240	E1	-	-	ROSRINE
Emeryville	Pacific Park Plaza	USGS	1662	Holocene	Marine	DOC, GEOM	198	E	150	E1	222	2400	USGS OFR 94-222
Redwood City	Apeel #2	USGS	1002	Holocene	Marine	DOC, GEOM	136	E	86	E1	118	2400	USGS OFR 93-376
San Francisco	International Airport	CSMIP	58223	Holocene	Marine	DOC	227	E	152	E1	118	2400	USGS OFR 92-287
El Centro[4]	Meloland - Vertical Array	CSMIP	5155	Holocene	Lacustrine	DOC, GEOM	195	E	>240	E1	-	-	ROSRINE
Eureka[4]	Somoa Bridge - Vertical Array	CSMIP	89734	Holocene	Alluvium	DOC	188	D	218	D3	-	-	Roblee (personal communication)
Kobe[4]	Port Island - Vertical Array	CEOR	-	Holocene	Fill	F (2000)	196	D	>85	D	-	-	Iw asaki and Tai (1996)
Los Angeles[4]	La Cienega - Vertical Array	CDMG	24703	Holocene	Alluvium	CDMG	257	D	>287	D3	885	3423	ROSRINE

[1] GEOM : Geomatrix (1993)
DOC : 1:500 000 scale geology maps by California Department of Mines and Geology
CDMG : Geology maps by Calilfornia Department of Mines and Geology
F (2000) : Fukushima et al. (2000)

[2] N&S(1993) : Nigbor and Steller (1993)

[3] soil d.(m) : Soil depth to competent bedrock, the depth to a layer with Vs > 760 m/s, or the depth to a significant impedance contrast between surficial soil deposits and underlying harder material (Rodriguez-Marek et al., 2001)

[4] Vertical Array sites that were not analyzed in the study described in the main body of the text

Table A.2 Recordings and their intensity measures at calibration sites

Location	Station Name	Earthquake	m	r (km)	PHA (g)	S_a 0.3s (g)	S_a 1.0s (g)	S_a 3.0s (g)	PHV (cm/s)	I_a (cm/s)	D_{5-75} (s)	D_{5-95} (s)	T_m (s)
Corralitos	Eureka Canyon Road	Morgan Hill 1984	6.2	22.7	0.10	0.19	0.147	0.008	1.5	7.8	4.1	10.2	0.58
		Loma Prieta 1989	6.9	5.1	0.50	1.65	0.515	0.071	10.1	288.4	3.6	7.4	0.53
Los Angeles	Obregon Park	Whittier Narrows 1987, Aftershock	5.3	14.9	0.31	0.67	0.116	0.008	18.7	42.0	1.3	5.7	0.28
		Northridge 1994, Aftershock	5.9	39.9	0.06	0.07	0.007	0.000	1.7	1.7	2.7	6.9	0.19
		Whittier Narrows 1987	6	13.9	0.42	0.63	0.239	0.014	19.2	115.3	2.8	7.6	0.26
		Northridge 1994	6.7	37.9	0.45	0.93	0.173	0.010	20.2	124.6	5.6	11.1	0.29
		Hector Mine 1999	7.1	186.4	0.03	0.09	0.046	0.015	6.2	3.0	17.3	43.8	0.94
		Landers 1992	7.3	151.4	0.05	0.12	0.076	0.041	10.9	11.5	21.7	40.3	0.94
Los Angeles	Sepulveda VA	Northridge 1994	6.7	8.9	0.84	2.05	0.812	0.184	80.6	564.0	4.4	7.9	0.51
Pacoima	Pacoima Kagel Canyon	Whittier Narrows 1987	6	37.9	0.16	0.40	0.074	0.005	0.8	16.1	4.0	10.6	0.37
		Northridge 1994	6.7	8.2	0.44	0.95	0.423	0.085	16.9	257.3	4.6	9.2	0.79
		Northridge 1994, Aftershock	5.2	14.1	0.19	0.52	0.059	0.005	0.9	18.9	2.5	7.6	0.37
		Northridge 1994, Aftershock	5.9	9.4	0.07	0.20	0.015	0.001	0.2	2.3	1.3	6.4	0.27
		Hector Mine 1999	7.1	196.5	0.03	0.07	0.081	0.012	3.7	3.0	28.1	41.7	0.82
Santa Clara	IBM Almaden, Santa Teresa H.	Loma Prieta 1989	6.9	14.4	0.24	0.41	0.224	0.029	5.9	114.5	6.2	10.1	0.33
Santa Cruz	UCSC Lick Observatory	Loma Prieta 1989	6.9	17.9	0.46	1.10	0.203	0.022	4.5	221.8	6.0	9.5	0.26
		Morgan Hill 1984	6.2	44.1	0.05	0.16	0.028	0.003	0.4	4.4	4.5	7.7	0.30
Simi Valley	Knolls School	Northridge 1994	6.7	14.6	0.75	1.28	0.714	0.032	39.3	381.1	3.4	6.3	0.49
Sylmar	Jensen Gen. Bldg.	Hector Mine 1999	7.1	207.7	0.04	0.09	0.097	0.024	7.8	4.1	9.0	20.8	1.02
		Northridge 1994	6.7	6.24	0.74	1.69	0.826	0.233	35.9	436.7	3.9	6.7	0.68
El Centro	El Centro Array #7	Imperial Valley 1979, Aftershock	5.2	13.1	0.16	0.32	0.061	0.004	7.8	7.0	0.5	5.7	0.32
		Imperial Valley 1979	6.5	0.6	0.39	0.67	0.650	0.269	72.1	121.7	1.9	5.7	1.11
Gilroy	Gilroy Array #2	Coyote Lake 1979	5.7	7.5	0.27	0.67	0.243	0.025	16.5	38.4	1.4	5.6	0.44
		Loma Prieta 1989	6.9	12.7	0.19	1.01	0.395	0.061	35.9	116.4	2.5	10.7	0.60
		Morgan Hill 1984	6.2	15.1	0.34	0.39	0.088	0.011	8.0	20.1	6.0	13.9	0.38
Halls Valley	Halls Valley	Coyote Lake 1979	5.7	31.2	0.04	0.11	0.041	0.004	3.3	1.9	7.7	19.5	0.47
		Morgan Hill 1984	6.2	3.4	0.22	0.49	0.263	0.025	22.2	60.9	8.8	12.8	0.56
		Loma Prieta 1989	6.9	31.6	0.12	0.24	0.140	0.030	14.4	25.3	7.9	14.9	0.68
Los Angeles	Epiphany	Whittier Narrows 1987	6	47.4	0.13	0.50	0.055	0.005	8.0	20.1	5.3	12.9	0.34
		Northridge 1994	6.7	15.8	0.39	0.96	0.397	0.118	44.2	233.4	6.3	11.2	0.59
Los Angeles	Rinaldi Receiving Stn.	Northridge 1994	6.7	7.1	0.63	1.86	1.399	0.227	110.1	564.3	3.8	7.2	0.68
Newhall	Fire Station	Whittier Narrows 1987	6	55.2	0.05	0.15	0.037	0.002	2.9	3.8	7.2	15.8	0.40
		Northridge 1994	6.7	7.1	0.59	2.19	0.781	0.154	85.7	479.7	3.0	5.9	0.57
Oakland	Outer Harbor Wharf	Loma Prieta 1989	6.9	72.1	0.28	0.53	0.585	0.080	41.5	84.5	3.4	7.8	0.86
Sylmar	Olive View Hospital	Whittier Narrows 1987	6	47.7	0.06	0.14	0.033	0.004	3.8	5.8	6.3	14.3	0.37
		Northridge 1994	6.7	6.4	0.71	1.97	0.764	0.179	100.7	380.9	3.3	5.9	0.73
El Centro	Meloland Overcrossing	Imperial Valley 1979	6.5	0.5	0.30	0.68	0.349	0.237	80.6	85.7	2.7	8.2	1.17
Emeryville	Pacific Park Plaza	Loma Prieta 1989	6.9	76.9	0.23	0.48	0.500	0.043	29.4	68.1	5.1	11.7	0.98
Redwood City	Apeel #2	Loma Prieta 1989	6.9	47.9	0.25	0.33	0.777	0.065	42.9	92.5	3.3	9.9	0.95
San Francisco	International Airport	Morgan Hill 1984	6.2	71..2	0.05	0.18	0.050	0.003	2.9	3.2	10.7	14.3	0.39
		Loma Prieta 1989	6.9	64.4	0.28	1.05	0.368	0.041	26.7	87.9	4.6	11.0	0.55
El Centro	Meloland - Vertical Array	4/9/00	4.3	-	0.04	0.10	0.013	0.001	2.5	0.6	3.7	9.3	0.30
Eureka	Somoa Bridge - Vertical Array	9/22/00	4.4	-	0.01	0.02	0.003	0.000	0.4	0.1	5.0	14.9	0.31
Kobe	Port Island - Vertical Array	Kobe 1995	6.9	2.5	0.30	0.51	0.859	0.237	63.7	137.7	3.6	8.6	1.34
Los Angeles	La Cienega - Vertical Array	8/1/01	4.2	-	0.33	0.36	0.041	0.003	13.7	24.8	0.4	2.0	0.20

A.2 CHARACTERISTICS OF SELECTED SITES

The recording sites selected for use in this study are presented in Table A.1. The recordings and corresponding intensity measure (*IM*) parameters from those sites are listed in Table A.2. Histograms showing the breakdown of sites and recordings into various classification schemes are provided in Figure A.1. The *IM* parameter spaces covered by these recordings are shown in Figures A.2 (spectral accelerations), A.3 (peak horizontal velocity) and A.4 (Arias intensity, significant duration, and mean period).

The 5- and 95-percentile limits on various *IM*s from the recordings at selected sites are as follows:

PHA:	0.03g – 0.75g
S_a at 0.3s:	0.07g – 2.0g
S_a at 1.0s:	0.02g – 0.8g
S_a at 3.0s:	0.001g – 0.24g
PHV:	0.4 cm/s - 100 cm/s
Arias Intensity, I_a:	2 – 560 cm/s
5-75% significant duration, $D_{5\text{-}75}$:	1 – 22 s
5-95% significant duration, $D_{5\text{-}95}$:	6 – 42 s
Mean period, T_m:	0.3 – 1.1 s

These ranges of IM parameters for the calibration sites nearly match the ranges for the database as a whole, as provided in Section 4.2.

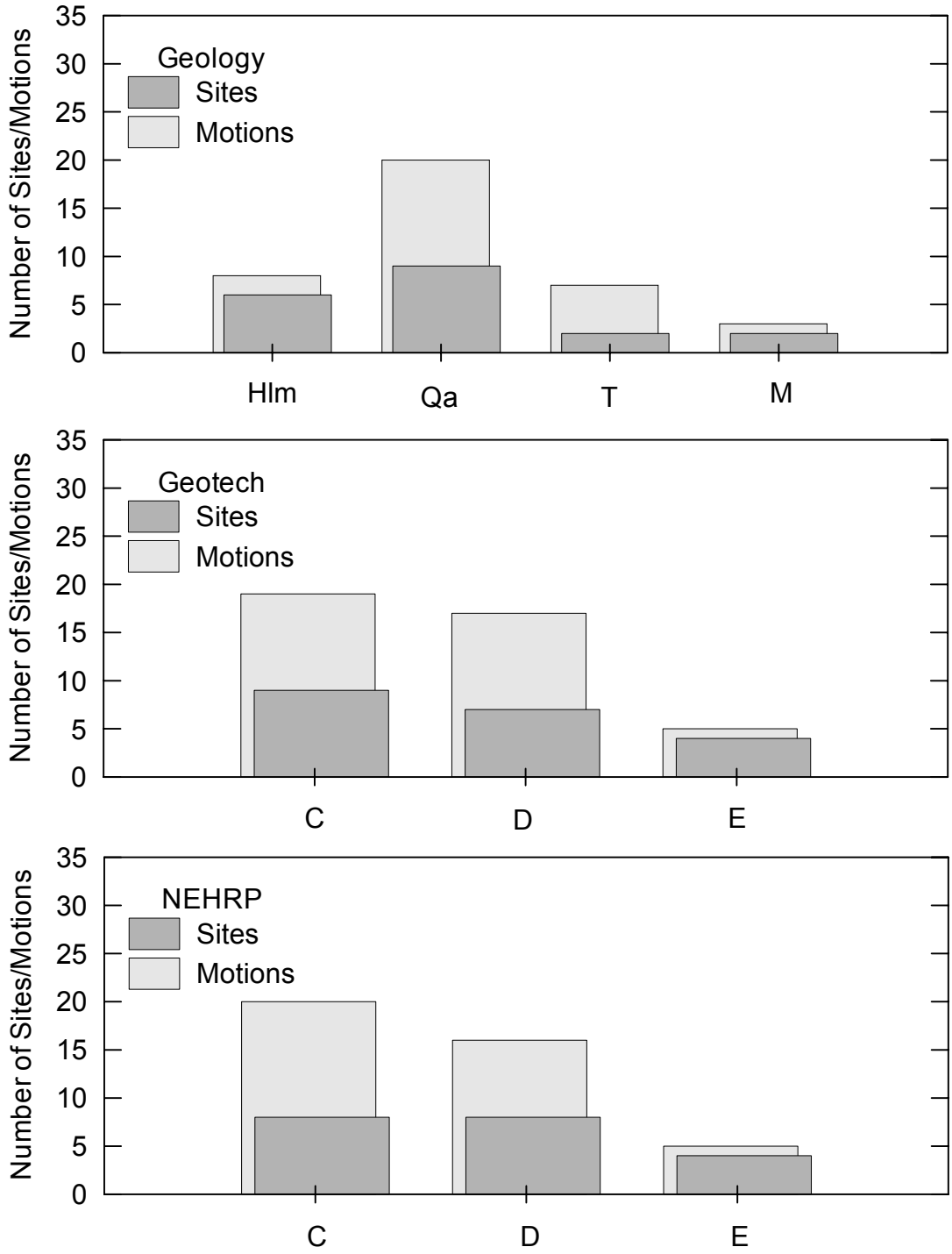

Fig. A.1. Data breakdown for Geology, Geotechnical (Rodriguez-Marek et al.,2001) and $V_{s\text{-}30}$ (NEHRP) classification schemes

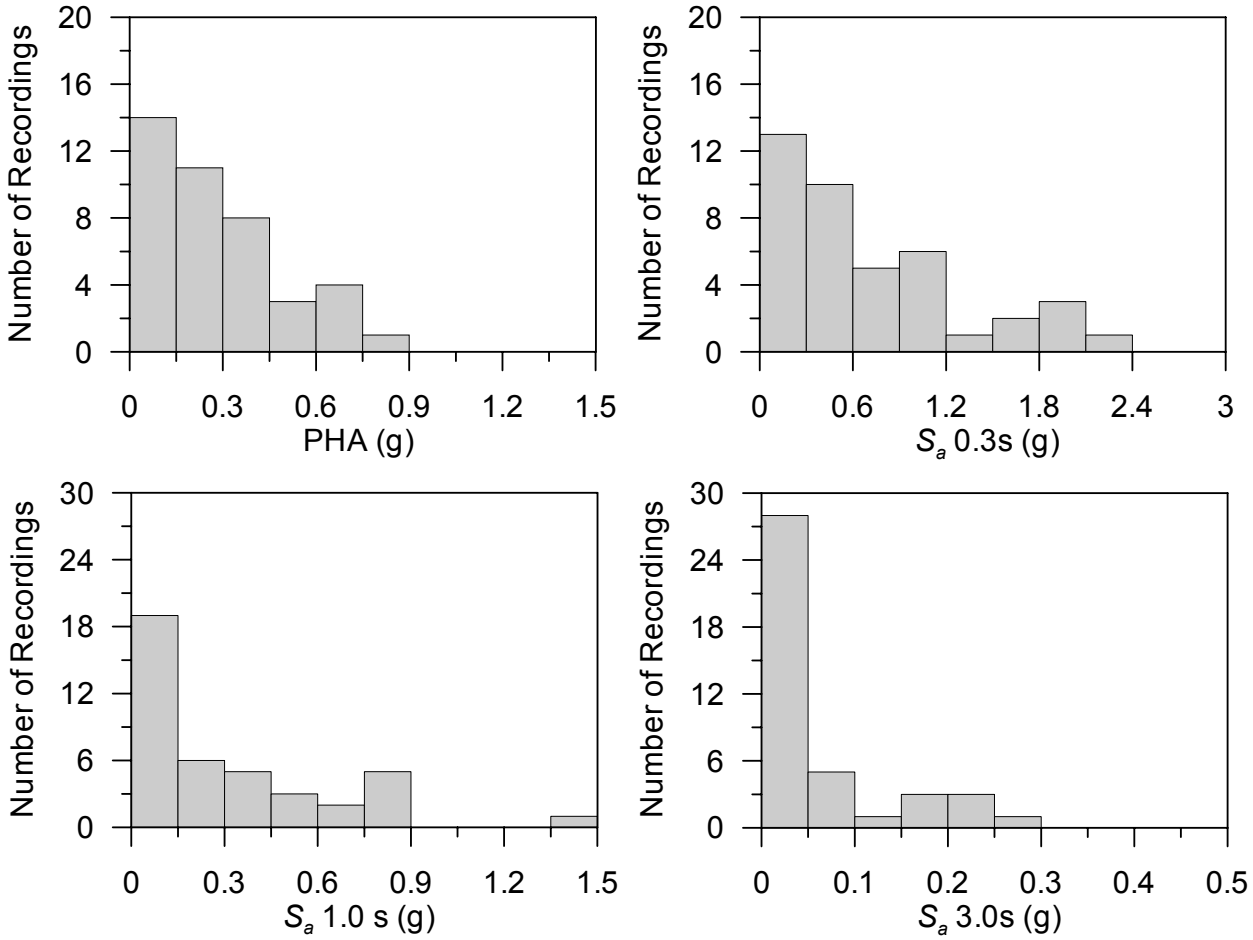

Fig. A.2. Histograms of 5% damped spectral acceleration at various periods for recordings at selected sites

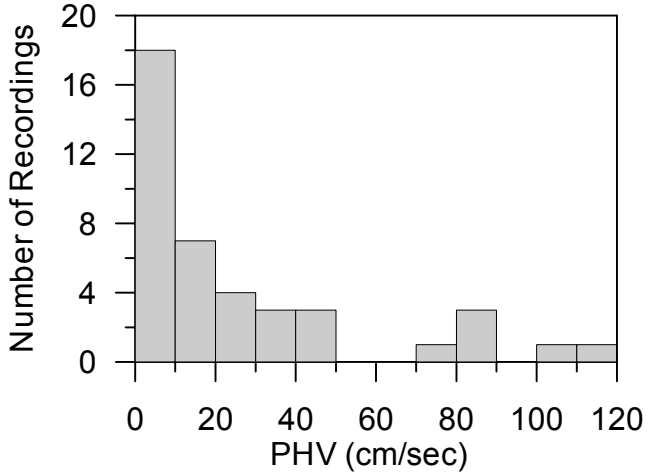

Fig. A.3. Histogram of peak horizontal velocities (*PHV*s) for recordings at selected sites

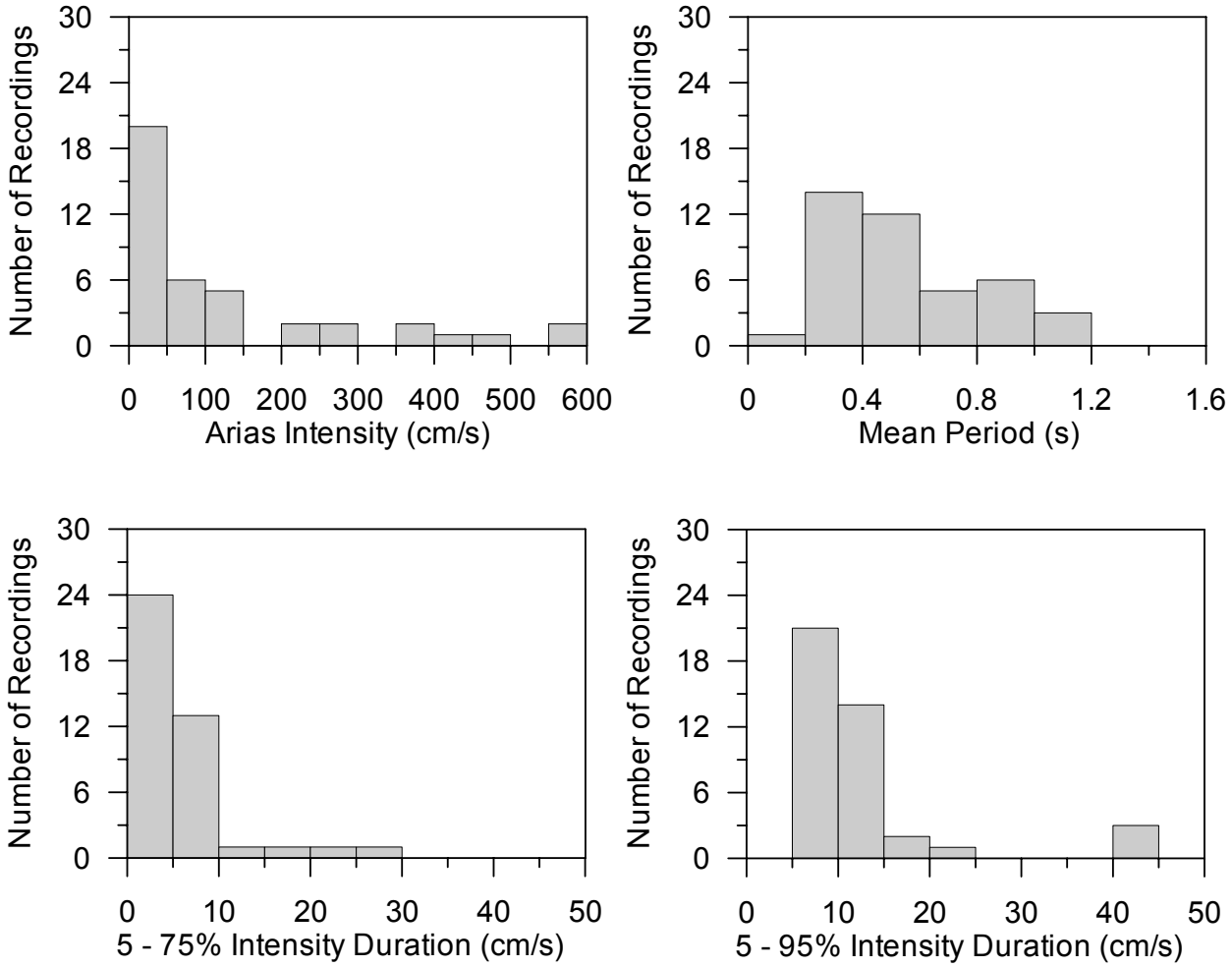

Fig. A.4. Histograms of various *IM* parameters for recordings at selected sites

As shown in the histograms, many of the recordings correspond to relatively weak shaking conditions. For example, only 27% have peak horizontal accelerations (PHA) in excess of 0.4 g. Calculated ground strains from ground response analyses are shown in Figures A.5 for both the selected calibrations sites (shown with dots) and the non-selected sites (open circles). The strain parameters plotted are the median + one-half standard deviation values of ε_1, ε_3, and ε_5 in Figures A.5 (a)-(c), respectively. These strain parameters are defined in Section 6.5. The selected sites generally span the full range of calculated ground strains, and in particular, the site/motion pair producing the largest strains within each NEHRP category are generally represented within the set of calibration sites.

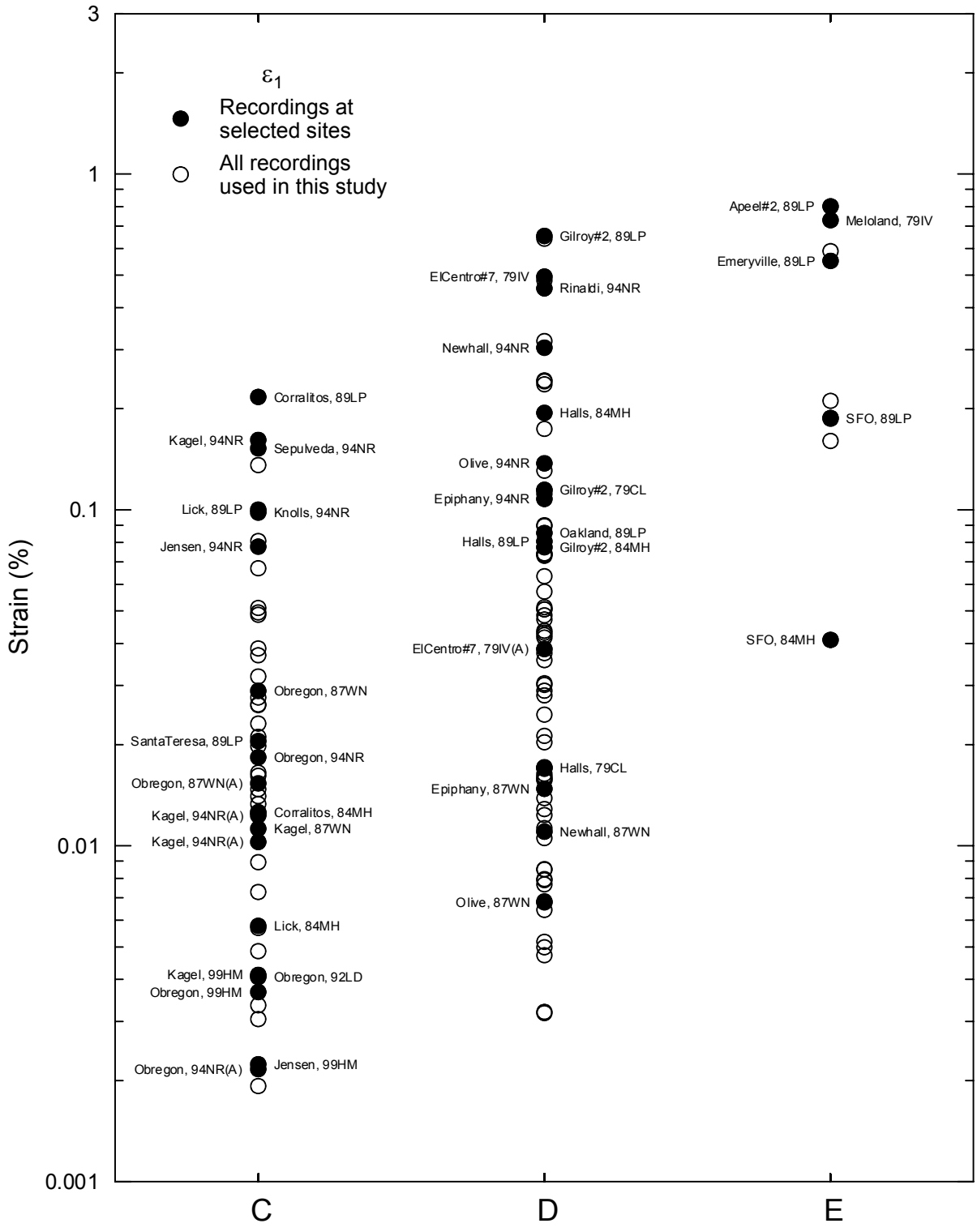

Fig. A.5 (a). Distributions of median + one-half standard deviation values of strain parameter ε_1 for NEHRP Categories C-E

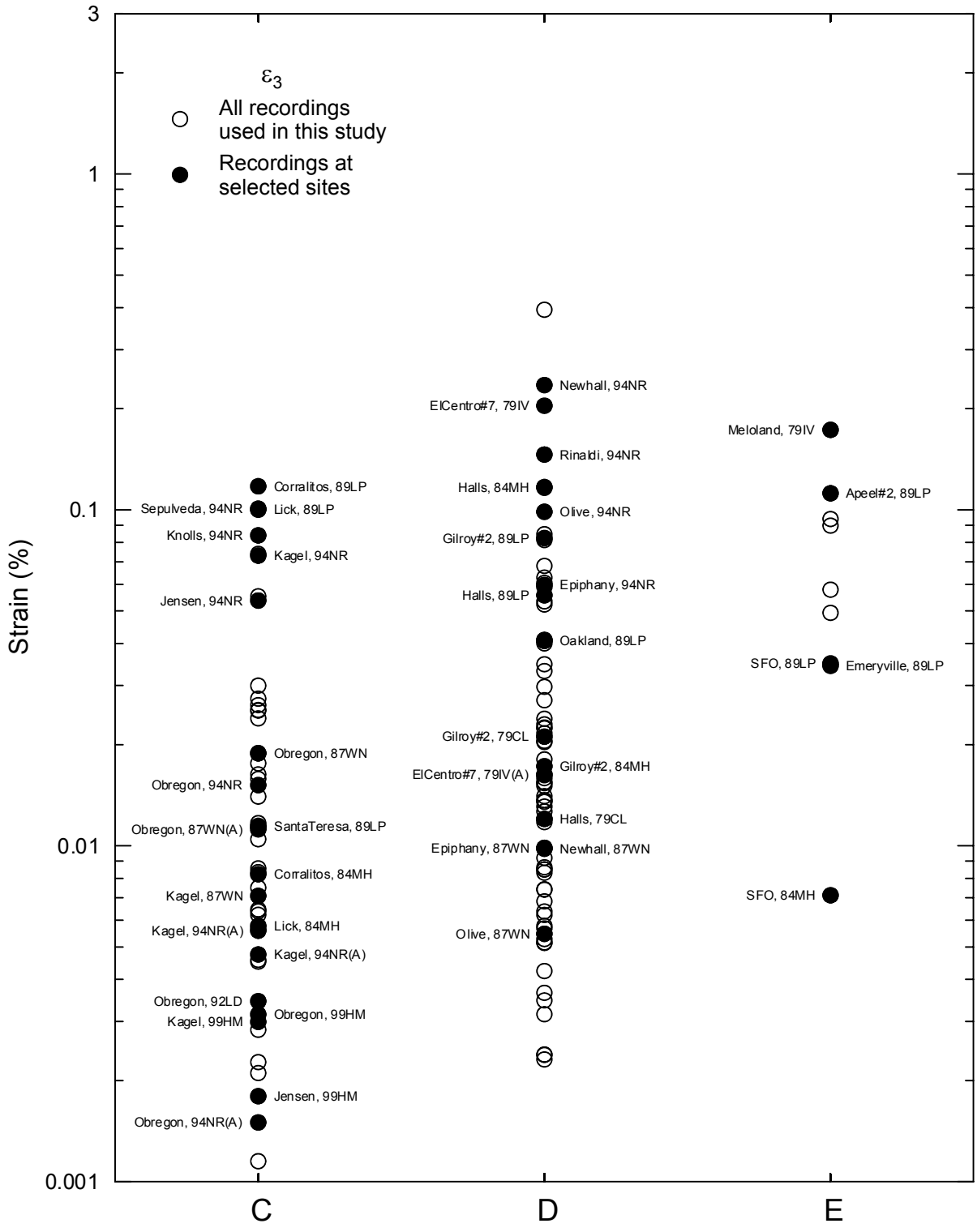

Fig. A.5 (b). Distributions of median + one-half standard deviation values of strain parameter ε_3 for NEHRP Categories C-E

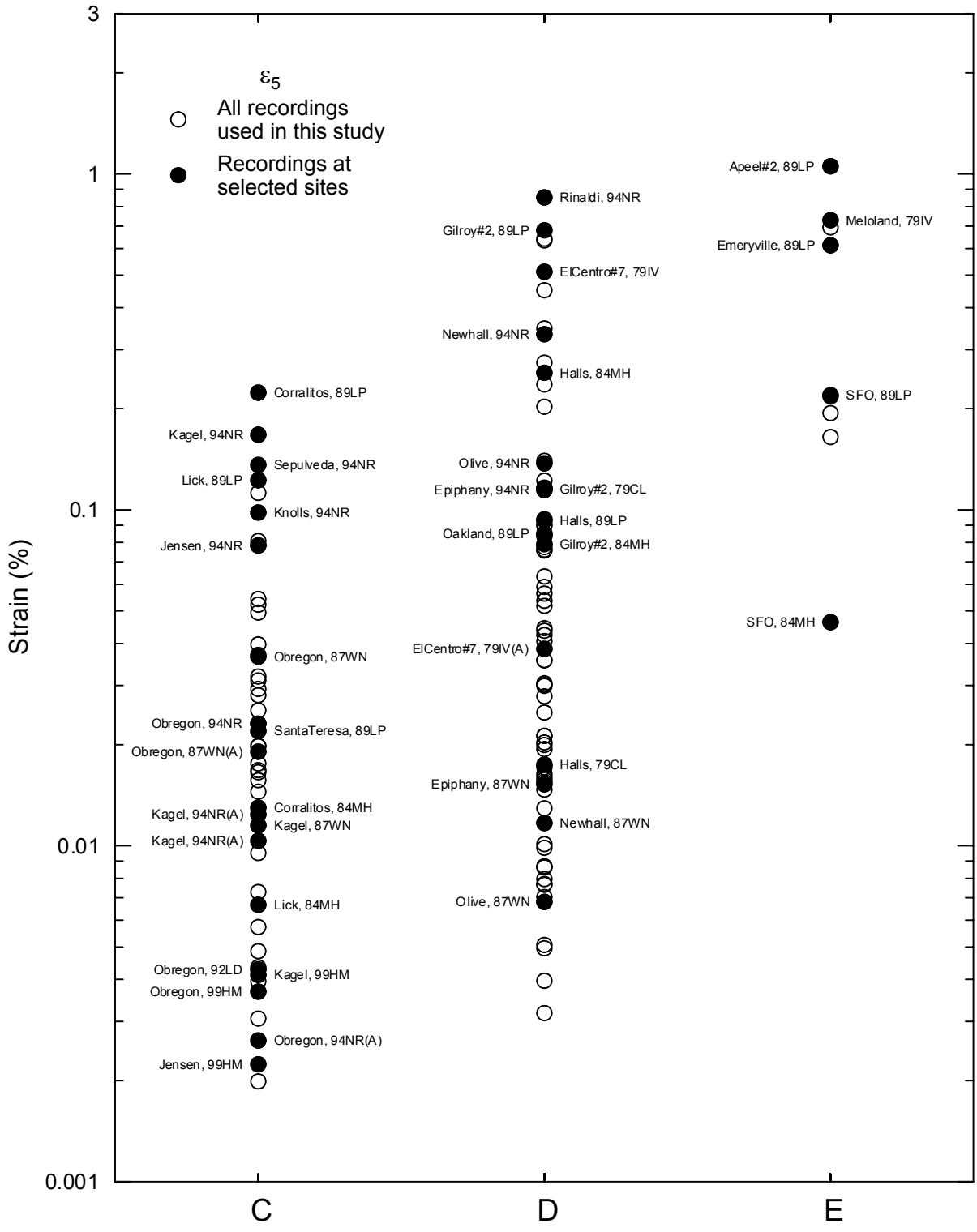

Fig. A.5 (c). Distributions of median + one-half standard deviation values of strain parameter ε_5 for NEHRP Categories C-E

A.3 GROUND RESPONSE CALCULATIONS WITH LARGE-AMPLITUDE INPUT MOTIONS

In order to provide a set of equivalent-linear ground response results corresponding to design-level input shaking levels, a suite of large-amplitude input motions was passed through each of the calibration sites. There are no surface recordings for such conditions against which the analysis results can be compared. Nonetheless, these results are compiled so that they can be compared to subsequent results from nonlinear ground response calculations.

The time histories used for these response calculations were generated by Dr. Walter Silva, who used a stochastic ground motion model. Four sets of three-component accelerograms were provided. The four sets can be described as follows:

D7.5 FC7.5: Time histories having durations consistent with a 7.5 magnitude source size and the phasing (frequency content) of an *m* 7.5 source.

D7.5 FC5.5: Time histories having durations consistent with a 7.5 magnitude source size, but scaled through response spectral matching to the frequency content of an *m* 5.5 source.

D5.5 FC5.5: Time histories having durations consistent with a 5.5 magnitude source size and the frequency content of an *m* 5.5 source.

D5.5 FC7.5: Time histories having durations consistent with a 7.5 magnitude source size, but scaled through response spectral matching to the frequency content of an *m* 7.5 source.

We use artificially adjusted frequency contents incompatible with the time history duration in order to investigate in subsequent work the effects of duration on ground response analysis results.

Response calculations were performed using two horizontal records for each of the above four sets of motions. The acceleration time histories utilized in the calculations are plotted in Figure A.6, and their 5%-damped response spectra are presented in Figure A.7. Other intensity measures for these input motions are summarized in Table A.3. Calculated response spectra from the ground response analyses are provided in Appendix B for each of the calibration sites. Calculated geometric mean intensity measures and ground strains from these analyses are summarized in Table A.4. For each site, the calculated strains from these analyses are generally greater than the upper-bound strain parameters for the site from Figure A.5.

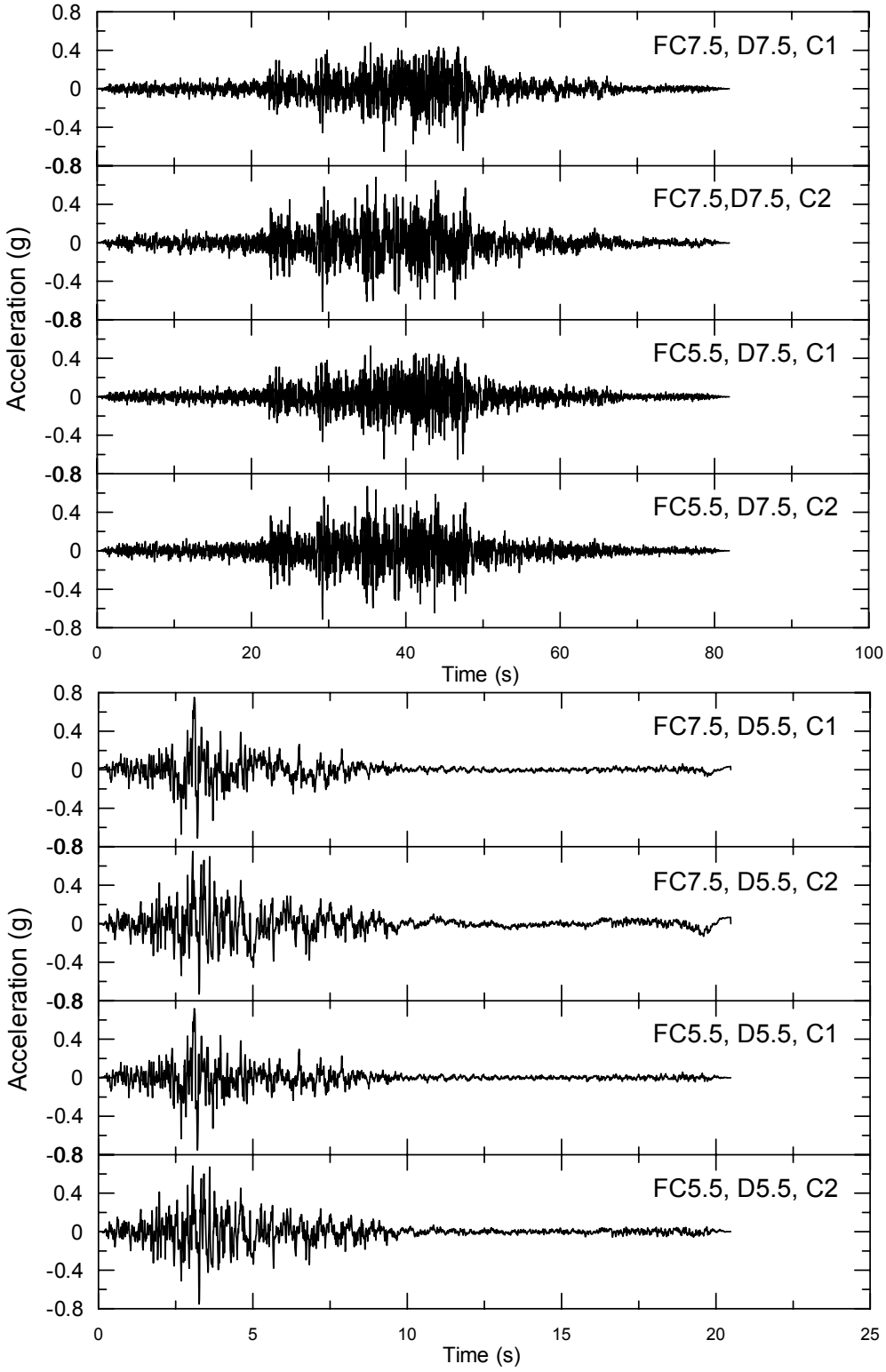

Fig. A.6. Synthetic large amplitude acceleration time histories used for ground response analyses

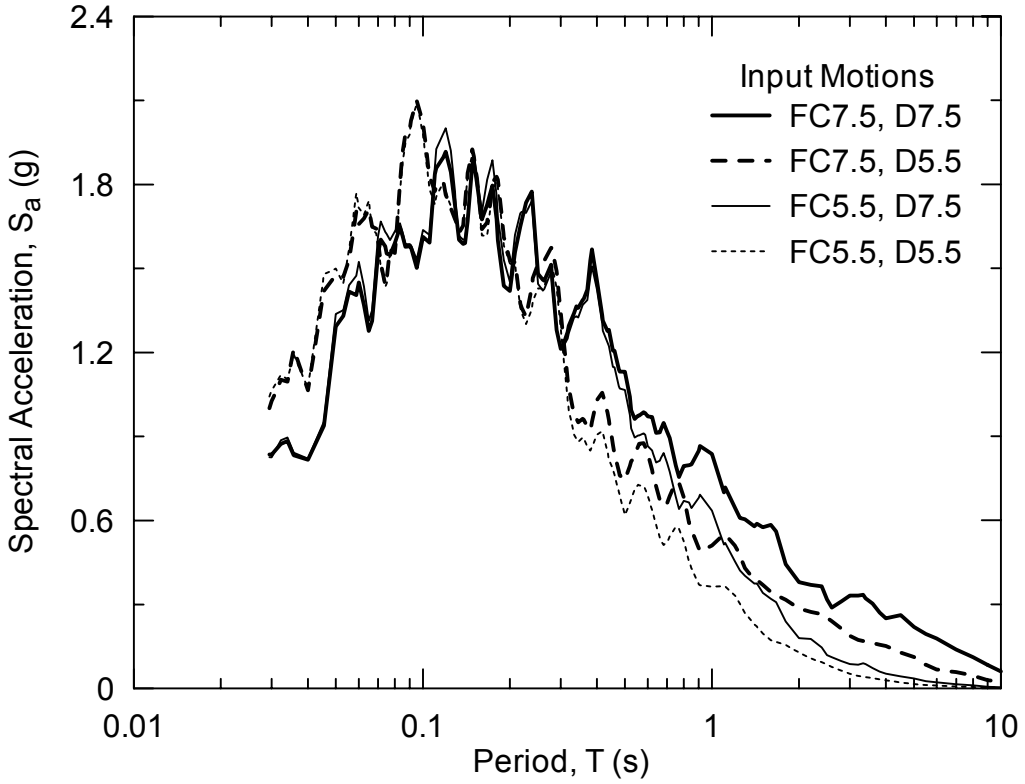

Fig. A.7. Response spectra at 5% damping for synthetic large amplitude acceleration time histories used for ground response analyses

Table A.3. Intensity measures for synthetic time histories used for ground response analyses

	PHA (g)	PHV (cm/s)	I_a (cm/s)	D_a,5-75 (s)	D_a,5-95 (s)	D_v, 5-75 (s)	D_v, 5-95 (s)	T_m (s)
FC7.5, D7.5	0.681	88.7	1451	22.1	29.8	25.2	34.6	0.41
FC7.5, D5.5	0.752	53.4	319	2.7	6.5	6.8	13.1	0.44
FC5.5, D7.5	0.680	42.6	1372	21.6	28.7	22.2	34.0	0.28
FC5.5, D5.5	0.752	31.3	277	2.7	5.9	2.9	6.8	0.27

Table A.4. Intensity measures and median + one-half standard deviation strain parameters of surface motions calculated from ground response analyses using large-amplitude synthetic time histories as input

		PHA (g)	PHV (cm/s)	I_a (cm/s)	D_a,5-75 (s)	D_a,5-95 (s)	D_v, 5-75 (s)	D_v, 5-95 (s)	T_m (s)	ε_1 (%)	ε_3 (%)	ε_5 (%)
Corralitos	FC7.5, D7.5	0.756	87.7	1419	21.6	29.9	23.2	36.1	0.55	0.218	0.125	0.226
	FC7.5, D5.5	0.730	55.5	318	2.3	6.2	5.5	16.6	0.48	0.134	0.087	0.136
	FC5.5, D7.5	0.745	49.7	1495	21.3	28.8	21.9	33.4	0.35	0.166	0.097	0.170
	FC5.5, D5.5	0.856	38.1	308	2.4	6.0	2.6	6.4	0.32	0.104	0.067	0.104
Obregon Park	FC7.5, D7.5	0.579	90.1	860	22.1	31.0	23.3	35.9	0.74	0.180	0.120	0.244
	FC7.5, D5.5	0.562	52.6	191	2.5	6.4	6.1	16.6	0.65	0.148	0.092	0.200
	FC5.5, D7.5	0.574	47.7	898	21.8	29.1	22.0	33.7	0.43	0.124	0.080	0.163
	FC5.5, D5.5	0.594	35.7	180	2.4	5.7	2.7	6.5	0.40	0.109	0.061	0.141
Sepulveda VA	FC7.5, D7.5	0.618	95.7	973	22.1	31.5	23.5	36.6	0.78	0.241	0.153	0.241
	FC7.5, D5.5	0.599	59.9	231	2.4	6.4	5.4	15.9	0.65	0.158	0.110	0.167
	FC5.5, D7.5	0.668	53.6	1151	22.1	29.1	21.9	33.5	0.42	0.149	0.099	0.149
	FC5.5, D5.5	0.720	38.9	246	2.2	5.6	2.4	6.3	0.38	0.097	0.072	0.097
Kagel Canyon	FC7.5, D7.5	0.525	93.0	750	22.3	32.2	23.3	36.4	0.81	0.307	0.149	0.317
	FC7.5, D5.5	0.549	53.9	188	2.6	6.7	6.3	16.7	0.63	0.242	0.103	0.246
	FC5.5, D7.5	0.569	45.3	1020	21.6	28.9	21.7	33.6	0.36	0.180	0.095	0.184
	FC5.5, D5.5	0.665	35.3	235	2.6	5.9	2.4	6.3	0.31	0.129	0.065	0.130
Santa Teresa Hill	FC7.5, D7.5	1.198	87.5	4360	21.5	28.7	23.5	36.1	0.24	0.065	0.035	0.088
	FC7.5, D5.5	1.372	52.1	908	2.5	5.9	5.4	16.5	0.23	0.061	0.035	0.131
	FC5.5, D7.5	1.293	53.8	4885	21.5	28.3	22.5	33.4	0.17	0.051	0.029	0.075
	FC5.5, D5.5	1.455	41.8	929	2.5	5.9	2.5	6.2	0.17	0.052	0.031	0.104
UCSC Lick Obs.	FC7.5, D7.5	1.066	88.0	3178	22.0	29.4	23.3	36.1	0.32	0.400	0.400	0.527
	FC7.5, D5.5	1.253	51.2	670	2.0	5.5	5.0	16.3	0.30	0.363	0.363	0.490
	FC5.5, D7.5	1.109	54.3	3970	21.6	28.5	22.6	33.3	0.22	0.264	0.264	0.330
	FC5.5, D5.5	1.372	40.9	696	2.1	5.3	2.4	6.2	0.23	0.335	0.335	0.442
Knolls School	FC7.5, D7.5	0.960	89.4	2070	20.9	29.7	23.8	37.0	0.49	0.533	0.110	0.616
	FC7.5, D5.5	1.032	54.9	542	2.6	6.2	4.9	16.1	0.40	0.300	0.069	0.335
	FC5.5, D7.5	1.038	55.4	3074	21.7	29.0	22.2	32.1	0.30	0.265	0.062	0.305
	FC5.5, D5.5	1.172	44.8	596	2.2	5.8	2.4	6.3	0.29	0.241	0.059	0.273
Jensen Gen. Bldg.	FC7.5, D7.5	0.705	87.8	1434	22.3	30.1	23.3	35.9	0.50	0.096	0.073	0.098
	FC7.5, D5.5	0.745	51.7	322	2.4	6.1	6.1	16.7	0.44	0.072	0.051	0.073
	FC5.5, D7.5	0.754	50.4	1683	21.8	28.8	22.0	33.7	0.29	0.071	0.047	0.072
	FC5.5, D5.5	0.804	35.6	337	2.4	5.7	2.6	6.4	0.27	0.049	0.036	0.049

Table A.4 (continued)

		PHA (g)	PHV (cm/s)	I_a (cm/s)	D_a,5-75 (s)	D_a,5-95 (s)	D_v, 5-75 (s)	D_v, 5-95 (s)	T_m (s)	ε_1 (%)	ε_3 (%)	ε_5 (%)
El Centro#7	FC7.5, D7.5	0.465	97.1	615	22.3	34.3	23.4	36.6	1.14	0.354	0.187	0.356
	FC7.5, D5.5	0.429	61.3	153	2.8	7.2	7.4	16.9	0.93	0.238	0.133	0.250
	FC5.5, D7.5	0.538	49.8	669	21.5	30.0	22.4	34.4	0.61	0.238	0.131	0.252
	FC5.5, D5.5	0.492	40.4	164	2.0	5.5	2.3	6.2	0.52	0.183	0.091	0.189
Gilroy #2	FC7.5, D7.5	0.482	110.8	846	24.3	36.0	24.5	38.5	1.36	1.660	0.168	1.712
	FC7.5, D5.5	0.556	85.1	235	2.8	7.5	5.5	16.7	1.06	0.813	0.104	0.847
	FC5.5, D7.5	0.539	71.5	841	22.1	30.8	23.3	35.3	0.74	0.775	0.103	0.827
	FC5.5, D5.5	0.627	54.4	208	1.9	5.6	2.2	5.8	0.62	0.470	0.069	0.477
Halls Valley	FC7.5, D7.5	0.746	109.2	1455	21.9	31.7	23.2	36.6	0.84	0.645	0.213	0.983
	FC7.5, D5.5	0.728	77.8	339	2.1	6.5	3.9	15.0	0.74	0.508	0.164	0.739
	FC5.5, D7.5	0.745	76.1	1527	22.2	29.6	21.3	31.9	0.55	0.404	0.149	0.556
	FC5.5, D5.5	0.766	55.2	312	2.3	5.7	2.2	6.0	0.51	0.321	0.121	0.432
Epiphany	FC7.5, D7.5	0.516	99.0	743	22.4	34.0	24.4	37.1	1.10	0.744	0.219	0.805
	FC7.5, D5.5	0.488	65.8	189	2.2	6.6	5.3	16.4	0.88	0.429	0.146	0.459
	FC5.5, D7.5	0.637	59.5	907	22.2	30.0	21.8	33.4	0.56	0.360	0.136	0.382
	FC5.5, D5.5	0.634	42.1	213	2.0	5.7	2.3	6.2	0.48	0.213	0.091	0.214
Rinaldi Rec. Stn.	FC7.5, D7.5	0.888	104.1	1750	21.9	30.7	23.5	36.8	0.68	0.502	0.180	0.929
	FC7.5, D5.5	0.749	72.9	446	2.1	6.1	4.4	15.4	0.57	0.293	0.126	0.507
	FC5.5, D7.5	0.921	67.3	2365	22.1	29.4	21.9	31.9	0.40	0.300	0.115	0.519
	FC5.5, D5.5	0.971	54.1	498	2.3	5.6	2.6	6.3	0.37	0.257	0.091	0.426
Newhall FS	FC7.5, D7.5	0.688	105.6	1241	21.9	31.7	23.1	36.4	0.86	0.640	0.149	0.699
	FC7.5, D5.5	0.676	76.0	301	2.1	6.2	4.4	15.6	0.73	0.530	0.110	0.607
	FC5.5, D7.5	0.693	70.8	1549	22.3	29.3	21.5	31.7	0.49	0.338	0.093	0.381
	FC5.5, D5.5	0.765	52.1	335	2.4	5.6	2.8	6.2	0.44	0.241	0.073	0.258
Oakland O. H.	FC7.5, D7.5	0.548	139.7	1014	25.3	37.9	23.9	38.1	1.63	0.766	0.326	0.767
	FC7.5, D5.5	0.510	82.4	292	3.6	8.8	6.4	15.3	1.23	0.525	0.203	0.529
	FC5.5, D7.5	0.637	72.7	1008	22.2	31.8	23.6	36.1	0.79	0.514	0.193	0.514
	FC5.5, D5.5	0.553	53.8	253	2.7	5.6	3.4	6.7	0.67	0.278	0.123	0.279
Olive View Hospital	FC7.5, D7.5	0.688	98.5	1214	22.3	31.0	23.5	36.6	0.71	0.183	0.124	0.185
	FC7.5, D5.5	0.743	63.6	284	2.3	6.4	4.8	15.8	0.61	0.138	0.093	0.140
	FC5.5, D7.5	0.712	59.5	1389	22.1	29.2	21.4	33.0	0.41	0.122	0.086	0.122
	FC5.5, D5.5	0.779	42.7	294	2.3	5.6	2.3	6.2	0.37	0.090	0.061	0.091

Table A.4 (continued)

		PHA (g)	PHV (cm/s)	I_a (cm/s)	D_a,5-75 (s)	D_a,5-95 (s)	D_v, 5-75 (s)	D_v, 5-95 (s)	T_m (s)	ε_1 (%)	ε_3 (%)	ε_5 (%)
Meloland	FC7.5, D7.5	0.360	113.9	518	24.3	36.5	22.7	36.3	1.61	0.511	0.191	0.511
	FC7.5, D5.5	0.382	64.4	146	3.3	8.2	6.4	15.0	1.17	0.408	0.113	0.416
	FC5.5, D7.5	0.501	55.2	608	21.1	30.7	23.5	36.7	0.76	0.379	0.110	0.387
	FC5.5, D5.5	0.424	44.4	159	2.1	5.3	2.8	6.6	0.64	0.248	0.074	0.249
Emeryville	FC7.5, D7.5	0.496	126.3	1201	26.0	39.9	25.6	39.5	1.76	6.388	0.338	6.840
	FC7.5, D5.5	0.391	96.0	319	3.6	7.9	5.7	12.9	1.46	4.237	0.232	5.602
	FC5.5, D7.5	0.509	89.4	858	21.3	33.0	25.0	36.0	1.16	3.949	0.215	4.788
	FC5.5, D5.5	0.512	70.5	243	2.3	5.2	2.3	4.6	0.97	2.373	0.139	2.510
Apeel#2	FC7.5, D7.5	0.525	136.4	1215	25.1	38.7	25.0	39.0	1.71	4.389	0.580	5.492
	FC7.5, D5.5	0.460	97.9	320	4.0	8.7	6.0	14.1	1.40	2.666	0.405	4.531
	FC5.5, D7.5	0.600	93.4	984	21.1	32.4	23.3	34.6	1.07	2.777	0.381	4.606
	FC5.5, D5.5	0.514	68.2	271	2.3	5.3	3.1	4.7	0.93	1.775	0.243	2.794
SFO	FC7.5, D7.5	0.787	137.2	1991	21.8	33.1	24.2	38.5	1.26	1.492	0.305	1.773
	FC7.5, D5.5	0.793	127.8	595	3.0	6.6	4.3	13.8	1.02	1.203	0.201	1.442
	FC5.5, D7.5	0.880	121.0	2362	21.7	30.4	23.6	35.2	0.75	1.079	0.197	1.275
	FC5.5, D5.5	0.785	93.6	599	2.1	5.7	2.4	5.9	0.67	0.982	0.137	1.158
El Centro Vert. Ar.	FC7.5, D7.5	0.360	113.9	518	24.3	36.5	22.7	36.3	1.61	0.511	0.191	0.511
	FC7.5, D5.5	0.382	64.4	146	3.3	8.2	6.4	15.0	1.17	0.408	0.113	0.416
	FC5.5, D7.5	0.501	55.2	608	21.1	30.7	23.5	36.7	0.76	0.379	0.110	0.387
	FC5.5, D5.5	0.424	44.4	159	2.1	5.3	2.8	6.6	0.64	0.248	0.074	0.249
Eureka Vert. Ar.	FC7.5, D7.5	0.499	141.3	1149	26.1	38.8	24.1	38.2	1.82	2.771	0.281	3.53
	FC7.5, D5.5	0.465	379.2	1202	16.1	32.7	23.3	53.5	3.00	2.036	0.179	2.59
	FC5.5, D7.5	0.524	88.0	876	21.7	32.7	25.2	37.2	1.08	2.204	0.161	3.14
	FC5.5, D5.5	0.528	289.2	921	9.0	22.9	9.4	23.8	2.72	1.620	0.104	2.23
Port Island Vert. Ar.	FC7.5, D7.5	0.282	98.5	329	24.6	37.3	22.9	37.0	1.72	0.969	0.350	0.99
	FC7.5, D5.5	0.292	224.2	353	12.5	36.6	30.7	66.9	2.35	0.755	0.198	0.79
	FC5.5, D7.5	0.371	39.8	304	22.1	31.6	23.2	36.1	0.79	0.732	0.183	0.74
	FC5.5, D5.5	0.381	131.2	329	8.0	22.8	9.5	25.7	1.89	0.387	0.114	0.39
La Cienega Vert. A.	FC7.5, D7.5	0.919	201.7	3213	28.6	41.8	34.7	43.6	1.75	1.536	0.290	2.041
	FC7.5, D5.5	0.848	125.0	980	6.3	11.3	8.9	13.7	1.41	0.927	0.177	1.169
	FC5.5, D7.5	1.102	135.7	3076	23.3	35.8	28.0	40.9	0.94	0.872	0.174	1.168
	FC5.5, D5.5	0.993	95.1	895	3.9	9.7	7.3	14.2	0.82	0.510	0.111	0.651